Technical University of Crete

Doctoral Thesis

Motorway Traffic Control with Connected Automated Vehicles

Author:
Vasileios Markantonakis

Supervisor:
Prof. Ioannis Papamichail

A thesis submitted in fulfillment of the requirements for the degree of Doctor of Philosophy

in the

Dynamic Systems & Simulation Laboratory
School of Production, Engineering & Management

December, 2024

The present thesis is approved by the following jury:

Advisory Committee:

Ioannis Papamichail (Supervisor)
Professor, School of Production Engineering and Management
Technical University of Crete, Chania, Greece

Markos Papageorgiou (Member of committee in charge)
Professor Emeritus, School of Production Engineering and Management
Technical University of Crete, Chania, Greece

Anargyros Delis (Member of committee in charge)
Professor, School of Production Engineering and Management
Technical University of Crete, Chania, Greece

Thesis Committee:

Eleftherios Doitsidis
Associate Professor, School of Production Engineering and Management
Technical University of Crete, Chania, Greece

Dimitrios Ipsakis
Assistant Professor, School of Production Engineering and Management
Technical University of Crete, Chania, Greece

Iasson Karafyllis
Professor, School of Applied Mathematical and Physical Sciences
National Technical University of Athens, Athens, Greece

Eleni Christofa
Professor, Civil and Environmental Engineering
University of Massachusetts, Amherst, USA

ΕΠΤΑΜΕΛΗΣ ΕΞΕΤΑΣΤΙΚΗ ΕΠΙΤΡΟΠΗ

Τίτλος (ελληνικά/αγγλικά):

Έλεγχος Κυκλοφορίας Αυτοκινητοδρόμων με Χρήση Συνδεδεμένων Αυτόματων Οχημάτων

Motorway Traffic Control with Connected Automated Vehicles

ΔΙΔΑΚΤΟΡΙΚΗ ΔΙΑΤΡΙΒΗ

(Ονοματεπώνυμο διδάκτορα)

ΒΑΣΙΛΕΙΟΣ ΜΑΡΚΑΝΤΩΝΑΚΗΣ

ΤΡΙΜΕΛΗΣ ΣΥΜΒΟΥΛΕΥΤΙΚΗ ΕΠΙΤΡΟΠΗ:

1. **Καθ. Ιωάννης Παπαμιχαήλ (Επιβλέπων)**
2. **Ομοτ. Καθ. Μάρκος Παπαγεωργίου**
3. **Καθ. Ανάργυρος Δελής**

Εγκρίθηκε από την επταμελή εξεταστική επιτροπή την: 02 / 12 / 2024

1. **Καθ. Ιωάννης Παπαμιχαήλ**
2. **Ομοτ. Καθ. Μάρκος Παπαγεωργίου**
3. **Καθ. Ανάργυρος Δελής**
4. **Αν. Καθ. Ελευθέριος Δοϊτσίδης**
5. **Επ. Καθ. Δημήτρης Ιψάκης**
6. **Καθ. Ιάσων Καραφύλλης, ΕΜΠ** Ι.Καραφύλλης
7. **Prof. Eleni Christofa, University of Massachusetts, Amherst** Christofa

TECHNICAL UNIVERSITY OF CRETE

Abstract

School of Production, Engineering & Management

Doctor of Philosophy

Motorway Traffic Control with Connected Automated Vehicles

by Vasileios MARKANTONAKIS

The Connected Automated Vehicle (CAV) revolution has begun, offering new benefits and mobility solutions to the society. The ability of CAVs to collect multiple types of data from the infrastructure and also exchange information with other connected vehicles (CV), promises to revolutionise the individual mobility within the upcoming years. Vehicle manufacturers experience the transition of becoming providers of innovative mobility solutions (IMS), replacing their up to now role of just producing conventional vehicles. Such technological advances and solutions usually come in the form of Advanced Drivers Assistance Systems (ADAS), already included at the majority of vehicles produced nowadays. These systems may contribute to improve safety and increase traffic flow efficiency on motorways, so as to develop a less congested and environmental friendly transportation network for all road users.

The development, testing and validation of traffic control strategies for ADAS systems, is an interesting topic that gathered momentum in the research and industrial community during the last decade. The development of these strategies sorely lies on the CAVs ability to react in a controlled manner according to the prevailing traffic conditions, utilizing their own sensing technology. These strategies may suggest a new speed limit, a lane change maneuvre, a new time-gap value or a dedicated lane advice that needs to be applied by CAVs. In the current work, a series of local level traffic control strategies for mixed traffic are evaluated through microscopic simulations, on two real calibrated test-beds utilizing different penetration rates (PR) of CAVs, that act both as sensors and as actuators. The control strategies receive in real-time density, flow or speed measurements and deliver a series of actions to be enabled with the use of CAVs according to the policy adopted. Taking into account their simplicity in terms of control design, the control strategies showcase a satisfactory control behaviour to all the control scenarios examined.

Analysing and optimising a multidestination network is typically considered a highly complex task. One destination may have more than one alternative routes, which are typically longer in distance and time. In most cases, road users select their route (i.e. which corresponds to the shortest route) based on travel time, in order to reach their destination as early as possible. This implies that during peak hours, the capacity of the route may attain or exceed its maximum value, leading to congested traffic conditions. Numerous studies in the literature address the problem of rerouting vehicles in order to prevent the formation of congestion at both urban and motorway environments, by proposing dynamic traffic assignment strategies using feedback strategies or optimal control problem formulations. In the current work, a first-order multi-lane macroscopic traffic flow model for motorway networks, incorporating capacity drop features, is utilized within an optimal control problem, to demonstrate the integrated use of various traffic control measures. Among these measures are mainstream traffic flow control, lane change control, ramp metering control and dynamic traffic assignment control.

The optimal control solutions derived from the Quadratic Programming (QP) problem formulation are cast in a Model Predictive Control (MPC) framework for testing via application of the control actions for various PR of CAVs, within a microsimulation environment. A real motorway network with multiple destinations and routes was identified as the system for the needs of the microscopic evaluations. The results proved beneficial at all PR examined reaching the main goal of each one of the traffic control strategies involved. The lane changing actions offered a twofold contribution; that is to achieve an appropriate distribution of vehicles among all lanes and redirect the traffic using all the alternative routes. Furthermore, even at low PR, CAVs were able to drive the average speed of all vehicles close to the speed limit ordered; thus, applying MTFC actions on the mainstream motorway. Moreover, the use of RM actions at specific on-ramp merges were necessary to keep the merging area at an under critical density regime and avoid the formation of congestion on the motorway corridor.

ΠΟΛΥΤΕΧΝΕΙΟ ΚΡΗΤΗΣ

Περίληψη

Σχολή Μηχανικών Παραγωγής και Διοίκησης

Doctor of Philosophy

΄Ελεγχος Κυκλοφορίας Αυτοκινητοδρόμων με Χρήση Συνδεδεμένων Αυτόματων Οχημάτων

Βασίλειος Μαρκαντωνάκης

Η επανάσταση του Συνδεδεμένου Αυτόματου Οχήματος (CAV) έχει ήδη ξεκινήσει, προσφέροντας νέα οφέλη και λύσεις κινητικότητας στην κοινωνία. Τα αυτόματα οχήματα έχουν τη δυνατότητα να συλλέγουν πολλαπλούς τύπους δεδομένων από την εκάστοτε υποδομή αλλά και να ανταλάσσουν δεδομένα με άλλα συνδεδεμένα οχήματα, φέρνοντας έτσι την επανάσταση στην ατομική κινητικότητα μέσα στα επόμενα χρόνια. Οι κατασκευαστές οχημάτων βιώνουν τη μετάβαση και γίνονται πάροχοι καινοτόμων λύσεων κινητικότητας (IMS), αντικαθιστώντας τον μέχρι τώρα ρόλο της απλής παραγωγής συμβατικών οχημάτων. Τέτοιες τεχνολογικές εξελίξεις και λύσεις έρχονται με τη μορφή Προηγμένων Συστημάτων Υποβοήθησης Οδηγού (ADAS), που ήδη περιλαμβάνονται στην πλειοψηφία των οχημάτων που παράγονται σήμερα. Αυτά τα συστήματα μπορούν να συμβάλλουν στη βελτίωση της ασφάλειας και στην αύξηση της απόδοσης της ροής της κυκλοφορίας στους αυτοκινητόδρομους, παράγοντας ένα φιλικό προς το περιβάλλον δίκτυο μεταφορών για όλους τους χρήστες του δρόμου.

Η ανάπτυξη, δοκιμή και αξιολόγηση στρατηγικών ελέγχου κυκλοφορίας για συστήματα ADAS, είναι ένα ενδιαφέρον θέμα που έχει συγκεντρώσει μεγάλη δυναμική στην ερευνητική και βιομηχανική κοινότητα την τελευταία δεκαετία. Η ανάπτυξη αυτών των στρατηγικών έγκειται πολύ στην ικανότητα των αυτόματων οχημάτων CAV να αντιδρούν με ελεγχόμενο τρόπο σύμφωνα με τις επικρατούσες κυκλοφοριακές συνθήκες, χρησιμοποιώντας τη δική τους τεχνολογία ανίχνευσης. Αυτές οι στρατηγικές μπορεί να προτείνουν ένα νέο όριο ταχύτητας, έναν ελιγμό αλλαγής λωρίδας, μια νέα τιμή χρονικού διαστήματος ή μια ειδική συμβουλή λωρίδας που πρέπει να εφαρμοστεί από τα αυτόματα οχήματα. Στην τρέχουσα εργασία, μια σειρά στρατηγικών ελέγχου κυκλοφορίας σε τοπικό επίπεδο για μικτή κυκλοφορία αξιολογούνται μέσω μικροσκοπικών προσομοιώσεων, σε δύο πραγματικά δίκτυα αυτοκινητοδρόμων που χρησιμοποιούν διάφορα ποσοστά αυτομάτων οχημάτων που λειτουργούν τόσο ως συλλέκτες δεδομένων όσο και ως ενεργοποιητές αποφάσεων. Οι στρατηγικές ελέγχου λαμβάνουν μετρήσεις πυκνότητας, ροής ή ταχύτητας σε πραγματικό χρόνο και παρέχουν μια σειρά ενεργειών που πρέπει να ενεργοποιηθούν με τη χρήση αυτόματων οχημάτων σύμφωνα με την πολιτική που έχει υιοθετηθεί. Λαμβάνοντας υπόψη την απλότητά τους ως προς τον σχεδιασμό ελέγχου, οι στρατηγικές ελέγχου παρουσιάζουν μια ικανοποιητική συμπεριφορά ελέγχου σε όλα τα σενάρια ελέγχου που εξετάστηκαν.

Η ανάλυση και η βελτιστοποίηση ενός δικτύου πολλαπλών προορισμών θεωρείται συνήθως μια πολύπλοκη εργασία. Ένας προορισμός μπορεί να έχει περισσότερες από μία εναλλακτικές διαδρομές, οι οποίες είναι συνήθως μεγαλύτερες τόσο σε απόσταση όσο και σε χρόνο. Στις περισσότερες περιπτώσεις, οι χρήστες του δρόμου επιλέγουν τη διαδρομή τους (η οποία συνήθως αντιστοιχεί στη συντομότερη διαδρομή) με βάση τον χρόνο ταξιδιού, προκειμένου να φτάσουν στον προορισμό τους όσο το δυνατόν νωρίτερα. Αυτό σημαίνει ότι κατά τις ώρες αιχμής, η χωρητικότητα της διαδρομής μπορεί να φτάσει ή να υπερβεί τη μέγιστη τιμή της, οδηγώντας σε συνθήκες κυκλοφοριακής συμφόρησης. Πολυάριθμες μελέτες στη βιβλιογραφία αντιμετωπίζουν το πρόβλημα της αναδρομολόγησης οχημάτων προκειμένου να αποτραπεί ο σχηματισμός συμφόρησης τόσο σε αστικά δίκτυα όσο και σε αυτοκινητόδρομους, προτείνοντας στρατηγικές δυναμικής εκχώρησης κυκλοφορίας χρησιμοποιώντας στρατηγικές με ανατροφοδότηση ή βέλτιστα προβλήματα ελέγχου. Στην τρέχουσα εργασία, ένα μακροσκοπικό μοντέλο κυκλοφοριακής ροής πρώτης τάξης πολλαπλών λωρίδων για δίκτυα αυτοκινητοδρόμων που ενσωματώνει χαρακτηριστικά πτώσης χωρητικότητας, χρησιμοποιείται σε ένα βέλτιστο πρόβλημα ελέγχου, για να καταδείξει την ολοκληρωμένη χρήση διαφόρων μέτρων ελέγχου της κυκλοφορίας. Μεταξύ αυτών των μέτρων είναι ο κύριος έλεγχος ροής κυκλοφορίας, ο έλεγχος αλλαγής λωρίδας, ο έλεγχος μέτρησης ράμπας και ο δυναμικός έλεγχος ανάθεσης κυκλοφορίας. Οι βέλτιστες λύσεις ελέγχου που προκύπτουν από τη διατύπωση του προβλήματος Τετραγωνικού Προγραμματισμού (QP), τοποθετούνται σε ένα πλαίσιο Προγνωστικού Ελέγχου Μοντέλου (MPC) για δοκιμή μέσω εφαρμογής των ενεργειών ελέγχου για διάφορα ποσοστά αυτόματων οχημάτων, μέσα σε ένα περιβάλλον μικροπροσομοίωσης. Ένα πραγματικό δίκτυο αυτοκινητοδρόμων με πολλαπλούς προορισμούς και διαδρομές, προσδιορίστηκε ως το δίκτυο για τις ανάγκες των αξιολογήσεων βελτιστοποίησης του επιπέδου του δικτύου. Τα αποτελέσματα αποδείχθηκαν ωφέλιμα για όλα τα ποσοστά CAV που εξετάστηκαν για την επίτευξη του κύριου στόχου καθεμιάς από τις εμπλεκόμενες στρατηγικές ελέγχου της κυκλοφορίας. Οι ενέργειες αλλαγής λωρίδας προσέφεραν διπλή συμβολή· δηλαδή να επιτευχθεί κατάλληλη κατανομή των οχημάτων σε όλες τις λωρίδες και να ανακατευθύνει την κυκλοφορία χρησιμοποιώντας όλες τις εναλλακτικές διαδρομές. Επιπλέον, ακόμη και σε χαμηλές τιμές αυτόνομων οχημάτων, τα CAV ήταν σε θέση να οδηγήσουν τη μέση ταχύτητα όλων των οχημάτων κοντά στο όριο ταχύτητας που είχε προταθεί, εφαρμόζοντας έλεγχο στην ροή κυκλοφορίας MTFC στον κύριο αυτοκινητόδρομο. Επιπλέον, η χρήση ενεργειών μετρήσεων ράμπας RM σε συγκεκριμένες ράμπες εισόδου ήταν απαραίτητη για να διατηρηθεί η περιοχή συγχώνευσης σε καθεστώς κάτω από κρίσιμη πυκνότητα και να αποφευχθεί ο σχηματισμός συμφόρησης στον αυτοκινητόδρομο.

Acknowledgements

My PhD journey has finally come to an end. This journey began almost 6 years ago and it was not meant to be an easy task. From beginning to the end, it was full of good and bad moments. Having reached the end of this journey, I would like to thank and express my sincere gratitude and appreciation to a group of people who have accompanied me along the way.

I would like to start with my advisors Prof. Papamichail and Prof. Papageorgiou. I am very grateful and fortunate to have these two excellent advisors. Their academic excellence, wisdom, guidance and patience, have been the most valuable ingredients for both my scientific work and my development as a researcher and as a person.

I would also like to thank all the exam committee members, Prof. Delis, Prof. Doitsidis, Prof. Ipsakis, Prof. Karafyllis and Prof. Christofa, for accepting to participate in the defense of my dissertation and for their fruitful and insightful comments on various parts of my dissertation. Of course, I would also like to thank my colleagues and members of the Dynamic Systems and Simulation Laboratory (DSSL) for their support and for the many interesting discussions over several topics and issues during this time. Last but not least, I would like to thank my family, my wife Iro for her endless support, understanding and encouragement. This accomplishment would not have been possible without each one of you.

I dedicate this thesis to Iro and my daughter Marilena.

This research received funding partially from the European Research Council under the European Union's Seventh Framework Programme (FP/2007-2013) / ERC Grant Agreement n. [321132], project TRAMAN21; partially from the European Commission under the European Union's Horizon 2020 Research and Innovation programme / Grant Agreement n. [723016], project INFRAMIX; and partially from the European Commission under the European Union's Horizon 2020 Research and Innovation programme / Grant Agreement n. [955317], project FRONTIER.

Contents

List of Figures

List of Tables

List of Abbreviations

ACC	**A**daptive **C**ruise **C**ontroller
ADAS	**A**dvanced **D**river **A**ssistance **S**ystems
AMOC	**A**dvanced **M**otorway **O**ptimal **C**ontrol
API	**A**pplication **P**rogramming **I**nterface
AV	**A**utomated **V**ehicle
AVD	**A**verage **V**ehicle **D**elay
CACC	**C**ooperative **A**daptive **C**ruise **C**ontrol
C-ITS	**C**ooperative **I**ntelligent **T**ransportation **S**ystems
CAV	**C**onnected **A**utomated **V**ehicle
CCV	**C**onventional **C**onnected **V**ehicle
CV	**C**onnected **V**ehicle
DLA	**D**ynamic **L**ane **A**ssignment
DTA	**D**ynamic **T**raffic **A**ssignment
EC	**E**uropean **C**ommission
EU	**E**uropean **U**nion
FD	**F**undamental **D**iagram
HLA	**H**igh **L**evel **A**rchitecture
ICOS	**I**ndependent **C**o-**S**imulation framework
IMS	**I**nnovative **M**obility **S**olutions
ITS	**I**ntelligent **T**ransportation **S**ystems
ITS-G5	**I**ntelligent **T**ransportation **S**ystems **G**5
IVI	**I**n **V**ehicle **I**nformation
KPI	**K**ey **P**erformance **I**ndicator
LCA	**L**ane **C**hange **A**dvice
LCC	**L**ane **C**hange **C**ontrol
LTE	**L**ong **T**erm **E**volution
LTI	**L**inear **T**ime **I**nvariant
MPC	**M**odel **P**redictive **C**ontrol
MTFC	**M**ainstream **T**raffic **F**low **C**ontrol
OC	**O**ptimal **C**ontrol
OV	**O**ptimal **V**elocity
P	**P**roportional
PI	**P**roportional **I**ntegral
PID	**P**roportional **I**ntegral **D**erivative
PR	**P**enetration **R**ate
QP	**Q**uadratic **P**rogramming
RG	**R**oute **G**uidance
RM	**R**amp **M**etering
RSU	**R**oad **S**ide **U**nit
SAE	**S**ociety of **A**utomotive **E**ngineers
TD	**T**otal **D**elay
TMC	**T**raffic **M**anagement **C**entre

TTS	**T**otal **T**ime **S**pent
TTT	**T**otal **T**ravel **T**ime
UI	**U**ser **I**nterface
VMS	**V**ariable **M**essage **S**igns
VSL	**V**ariable **S**peed **L**imits
VSimRTI	**V**2X **S**imulation **R**untime **I**nfrastructure
V2I	**V**ehicle **2** **I**nfrastructure
V2V	**V**ehicle **2** **V**ehicle
V2X	**V**ehicle **2** **E**verything

Dedicated to Iro and Marilena

Chapter 1

Introduction

The arteries of modern transportation infrastructure, known as motorways, play a crucial role in society's mobility. Motorways serve a very important means for vehicles and civilians to travel from one place to another, connecting in this manner cities, towns and countries among each other. Characterised by high speeds, increased number of lanes, on-ramps and off-ramps, they are meant for travelling long distances quickly with efficiency, safety and comfort. According to the European Commission (EC) safety report (European Commission, 2018), motorways exhibit much lower accident rates (injury accidents per million vehicle kilometres) than other road types. The latest available European Union (EU) traffic data from 2022 indicate that 52% of road traffic fatalities occurred on rural roads, versus 38% in urban areas and 9% on motorways (European Commission, 2024).

Apart from the undoubtedly positive effects motorways have on the social community, the use of motorways unfortunately brings along negative impacts as well, including congestion. Traffic congestion is the major cause of traffic overloading, i.e. when too many vehicles attempt to use a common transportation infrastructure with limited storage capacity (Papageorgiou et al., 2003). This type of congestion, known as recurring congestion, usually appears every day during the week (i.e. working peak hours) as a result of the increased high volumes of traffic travelling on motorways close to the infrastructure capacity. On the other hand, another type of congestion, known as non-recurring congestion, is the result of an unexpected/unplanned event (i.e. traffic incidents, adverse weather conditions) and/or special activities (i.e. road construction and maintenance). Both types of traffic congestion result in excessive delays, reduced safety, strong economic costs and increased environmental pollution. According to the most recent report of the European Court of Auditors (ECA), inefficiencies in urban mobility, and motorway congestion in particular, cost the EU an estimated 110 billion € per year, which is more than 1% of the EU's GDP (European Court, 2019).

Elimination of recurring congestion is not an easy task. It is well known over the years, that the root cause of recurring congestion is in fact bottlenecks. Either fixed (e.g. due to their particular infrastructure layout) or moving (e.g. a slow vehicle or truck), bottlenecks can occur at lane drop areas, merging areas, areas with tunnels or underpasses as well as areas with specific traffic conditions (e.g. strong weaving of traffic streams) or areas with strong grade or curvature. Once a fixed bottleneck is activated (e.g. when the arriving demand is higher than the nominal capacity of the bottleneck), vehicles are getting trapped in the mainstream causing two kinds of detrimental effects that have a major impact on the motorway capacity and throughput (Markantonakis et al., 2019):

- Motorway capacity drop: The condition at which the maximum outflow that passes through the bottleneck location is substantially lower than the nominal capacity of the bottleneck. Representative work analysing the effects of the capacity drop phenomenon can be found accordingly in the literature, e.g. by Leclercq et al. (2011); Srivastava and Geroliminis (2013); Yuan et al. (2015); Kontorinaki et al. (2017); Wang et al. (2020).

- Congestion tail blocks pairs of on/off-ramps: Due to the congestion formed on the mainstream motorway, the congestion tail propagates several kilometres upstream of the bottleneck location blocking a number of on/off ramps. See for instance, related work presented by Spiliopoulou et al. (2013); Spiliopoulou et al. (2014a); Spiliopoulou et al. (2014b); Wang et al. (2016); Guo et al. (2019), among many others addressing the case of on/off-ramp blocking.

On the other hand, non-recurring congestion reduces the available capacity and reliability of the entire transportation system. These temporary disruptions in traffic flow usually cause unreliable travel times and huge delays, that decrease passenger safety and comfort. In the worst case scenario, a non-recurring bottleneck may occur at the same time when a recurring bottleneck is activated (Falcocchio et al., 2015). The amount of delay caused in this case, paralyses the infrastructure that reveals poor practices and procedures as well as management miscalculations. Early studies in the literature measure recurrent and non-recurrent congeston in terms of incident-related delays. It is proved that a percentage between 13% to 30% of the total congestion delay during peak periods is caused by non-recurring congestion (Skabardonis et al., 2003). This is a non-negligible percentage given the fact that estimates of non-recurring congestion are difficult and not as reliable as the estimates of recurring congestion (Arnold et al., 1988). The available research found in literature lacks compared to recurrent congestion but some representative work can be found accordingly in (Kwoczek et al., 2014; Tympakianaki et al., 2014; Wang et al., 2013; Weng and Meng, 2013) addressing approaches on how to alleviate non-recurring congestion phenomena.

Over the years, a substantial effort has been devoted to develop traffic control strategies for both urban and motorway traffic optimization using mathematical models and techniques. As mentioned in (Papageorgiou et al., 2003), the presence of traffic and subsequently traffic congestion, creates this necessity which brings in new perspectives and ways to alleviate or even eliminate traffic congestion. When designing a traffic control strategy, there are several aspects that should be taken into consideration. One of the key aspects is safety. In order to ensure safety for all road users (e.g. light goods vehicles, heavy goods vehicles, passenger vehicles and trucks), the available traffic control measure(s) involved in the strategy should be utilised in an optimal way taking into consideration the infrastructure capabilities and all the potential risks that may appear during the control operation. For example, in terms of controlling the speed of a vehicle using VSLs as an actuator, the difference between two consecutive speed limits received by the strategy, should be less than or equal to an upper threshold bound, so as to avoid abrupt speed changes. In the case of controlling the inflow coming from an on-ramp (e.g. ramp metering), the controlled queue should remain within the available (maximum) queue storage length so as to avoid overspilling into upstream intersections (e.g. urban environment) (Papageorgiou and Papamichail, 2008). The traffic control measures mentioned above including also route guidance are a few of the most common ones that aim to distribute and control the road traffic using variable message signs (VMSs) and traffic signals as control actuators.

This thesis aims to investigate the use of traditional and novel traffic control strategies at a local and network level utilising CAVs that will contribute on a safer and less congested driving experience on motorways. CAVs are in fact intelligent vehicles, designed to help drivers perform specific driving tasks in an automated manner improving safety and comfort. The great evolvement of the automotive industry led to the development of ADAS systems that enhance the CAV functionalities (Ziebinski et al., 2017). Some of the key features include adaptive cruise control (ACC), cooperative adaptive cruise control (CACC), forward collision warning or avoidance, lane departure warning, lane-keeping assist as well as reverse brake assist. This implies that the automotive industry mainly focuses on designing systems that optimise the related actions and performance of individual vehicles, instead of

optimising traffic efficiency in the network as a whole. This approach may have no direct impact on traffic flow, as it aims to improve safety and driver comfort. Nevertheless, this is an issue that needs further investigation, especially for high penetration rates for which the impact may also be negative. In our view, there is a need to change or appropriately extend the algorithms used, especially for mixed traffic conditions, in order to make sure that traffic flow capacity and efficiency are not deteriorating, particularly in case of heavy traffic conditions.

CAVs are equipped with various types of sensors that perceive the environment; thus, providing real-time information of the current traffic state. In this manner, they replace traditional methods of collecting real-time information, that make use of road traffic sensors (e.g. inductive loop sensors, radar sensors) placed at measuring points across the motorway network. This is achieved in a vehicle-to-everything (V2X) environment where CAVs use vehicle-to-vehicle (V2V) and vehicle-to infrastructure (V2I) communication protocols, able to ensure fast and accurate exchange of information (Papamichail et al., 2019). Moreover, they also have the potential to act as control actuators, useful enough for the traffic management centre (TMC) to control the road traffic. At the moment, the market penetration rate of CAVs remains low, creating difficulties in exploiting these novel opportunities that may improve traffic control performance. However, as these penetration rates are expected to increase rapidly within the coming years, there is a pressing need to develop and test appropriate traffic control strategies which will allow the exploitation of existing or emerging CAV capabilities towards increased traffic flow efficiency.

1.1 Problem statement

A summary of the exposition concludes the following:

- A motorway system becomes stressed when either the demand (e.g. the potential road commuters) exceeds the supply (i.e. serving capacity of the infrastructure) or a series of events (e.g. crashes) occur in an unpredictive manner.
- On an everyday basis, thousands of vehicles make use of the motorway network having both positive and negative impacts on traffic flow. The occurence of traffic congestion, and in fact its negative impact, emphasizes the need for proper traffic management.
- Either in the case of recurring or non-recurring congestion, there are disruptions of traffic flow that cause underutilization of the available infrastructure.
- Identifying bottlenecks as a regular source of capacity loss, novel control techniques utilizing modern technologies on CAVs, fill in the gaps at which the current traffic state performance faces limitations.

1.2 Objectives and motivation for research

Considering the aforementioned difficulties and limitations, this thesis aims to explore possible advantages and disadvantages of Intelligent Transportation Systems (ITS) using CAVs as control actuators. For each one of the traffic control strategies investigated, different CAV configurations were examined on a mixed traffic environment so as to derive useful conclusions in terms of traffic flow efficiency. These strategies include dynamic lane assignment (DLA), dynamic traffic assignment (DTA), lane change advice (LCA), as well as adaptive cruise control (ACC) and mainstream traffic flow control (MTFC). A brief overview on the control actions of each strategy follows:

- DLA delivers dedicated lane advices via In-Vehicle-Infotainment (IVI) messages utilizing V2X communication.
- DTA delivers destination-based lane advices via IVI messages utilizing V2X communication.
- LCA tries to prevent congestion by advising individual vehicles to move to other lanes by delivering out lane change advices via IVI messages utilizing V2X communication.
- ACC with time-gap adaptation advices autonomous vehicles to reduce or increase their time headway to increase capacity on the motorway. Appropriate IVI messages are delivered utilizing V2X communication.
- MTFC delivers speed-limit advices via IVI messages utilizing V2X communication.

1.3 Contributions

In this thesis we can outline 4 main contributions:

1. **Extensive evaluations of a series of local-level controllers:** The conducted experiments were carried out using microscopic traffic simulations to obtain a deeper understanding of the conduct of mixed traffic on motorways and how mixed traffic can be enhanced using novel control techniques. Using different local/network level traffic controllers with more and more CAVs on the motorways offers multiple opportunities to increase traffic flow efficiency. Hence, an extensive evaluation of a series of local-level feedback controllers is carried out using CAVs as control actuators.
2. **Testing and evaluation on real motorway test-beds:** The most important aspects of the real motorway test-beds used in this thesis for the needs of the demonstrations, were modelled according to the evaluation focus on the individual simulation methods and traffic control strategies. Both motorway test-beds were calibrated utilizing real and synthetic traffic data in order to reproduce capacity drop phenomena as they appear in real-world infrastructures.
3. **A series of communication technologies are assumed:** Whereas conventional vehicles can only be handled conventionally with advice, e.g. by introducing and monitoring VMSs, CAVs can receive unique advice through Intelligent Transport Systems G5 (ITS-G5) or cellular communication technologies (e.g. Long Term Evolution (LTE) or 4G/5G), which are the technologies assumed in the experiments of this thesis.
4. **Use versatile programming languages to deliver a library of software tools:** The programming languages C and C++ were used to develop from scratch a library of software tools that includes a series of local-level controllers developed in the past as well as a new one for dynamic lane assignment. In addition, they were also used to develop a tool that includes a network-level controller used to derive the optimal solutions of a QP optimization problem when cast on an open-loop control and MPC scheme. INFRAMIX project the C programming language was used and for the FRONTIER project the C++ programming language was used. Both languages were selected for their great speed and memory efficiency that they offer.

Note that, part of this work (i.e. two of the local-level controllers, LCA and MTFC) were intially evaluated for a hypothetical motorway stretch in the Master Thesis of Markantonakis (Markantonakis, 2018), however in the present thesis additional and more extensive microscopic evaluations and investigations were conducted over more realistic scenarios in real motorway test-beds.

1.4 Thesis outline

Chapter 2 begins with a brief overview of traffic control schemes designed for vehicle/local level application. This group of traffic control schemes consist of a MTFC controller, a LCA controller, an ACC controller and a DLA controller. The controllers were developed in the frame of FP7 TRAMAN21 project (http://www.traman21.tuc.gr/) and extended, tested and used in microscopic evaluations in the H2020 INFRAMIX and FRONTIER projects (http://www.inframix.eu, https://www.frontier-project.eu). The INFRAMIX microscopic simulations were carried out on a large-scale calibrated simulation model along the motorway AP7 in Girona, Spain. On the other hand, the FRONTIER microscopic simulations were carried out on a cropped calibrated simulation model along the Attiki Odos corridor, Athens, Greece. Both motorways feature on/off-ramp merge areas as well as lane-drop areas and were calibrated using real and artificial traffic data. The simulation investigations, under various penetration rates of CAVs, demonstrate the effectiveness of the aforementioned traffic control strategies.

Chapter 3 presents a novel first-order multi-lane macroscopic traffic flow model for mixed vehicle traffic. The model is utilised within an optimal control problem in the form of a convex QP problem, developed, tested and used in microscopic evaluations in the frame of the H2020 FRONTIER project. The model specifications, methodology, design and implementation of the network level traffic control scheme is analysed in detail. Macroscopic investigations on a hypothetical motorway network with multiple destinations and routes demonstrate the efficiency of the open-loop solutions. Then, a new series of microscopic investigations for a calibrated simulation model along the Attiki Odos corridor, Athens, Greece, are performed for the evaluation of the QP solutions when cast in a MPC framework. Different penetration rates of CAVs were examined, indicating the overall performance achieved.

Finally, Chapter 4 concludes this thesis with some final remarks and future work.

1.5 Scientific work directly related to the PhD

The scientific work that is directly related to the PhD is listed as follows:

1.5.1 Journal Papers

- Markantonakis, V. and Papamichail, I., Model predictive control for integrated control of multi-lane motorway networks. (Submitted).

1.5.2 Conference Papers

- Markantonakis, V., Doko, A., Papamichail, I., Papageorgiou, M., Schrab, K., Neubauer, M., Protzmann R. (2021). "Traffic control algorithms for mixed vehicle traffic - A simulation-based investigation". *The 23rd Euro Working Group on Transportation (EWGT 2020), Paphos, Cyprus. Transportation Research Procedia* 52, pp. 356-363.

- Markantonakis, V., Papamichail I. (2023). "Integrated optimal control for multi-lane motorway networks". *31st Mediterranean Conference on Control and Automation (MED)*. IEEE, pp. 464-471.

1.5.3 Conference Presentations

- Markantonakis, V., Skoufoulas, D.I., Papamichail, I. and Papageorgiou, M. (2019). "Integrated traffic control for freeways using variable speed limits and lane change

control actions". *98th Annual Meeting of the Transportation Research Board*, Washington, DC, USA, January 13-17, 2019, paper No. 19-3865.

- Doko A., Markantonakis V., Papamichail I., Papageorgiou M., Schrab K., Neubauer M. and Protzmann R., A dynamic lane assignment strategy for mixed vehicle traffic – A simulation-based investigation. 3rd Symposium on Management of Future Motorway and Urban Traffic Systems (MFTS 2020), Luxemburg, July 6-8, 2020. (held virtually).

- Markantonakis V., Doko A., Papamichail I., Papageorgiou M., Schrab K., Neubauer M. and Protzmann R., Traffic control algorithms for mixed vehicle traffic – A simulation-based investigation. 3rd Symposium on Management of Future Motorway and Urban Traffic Systems (MFTS 2020), Luxemburg, July 6-8, 2020. (held virtually).

- Papamichail I., Markantonakis V., Doko A., Papageorgiou M., Schrab K., Neubauer M. and Protzmann R., Traffic control algorithms for mixed vehicle traffic. Invited talk, Tutorial Session on "Innovative topics and future challenges in traffic control", 1st Virtual IFAC World Congress (IFAC-V 2020), July 13-17, 2020.

1.6 Scientific work indirectly related to the PhD

The scientific work that is indirectly related to the PhD is listed as follows:

1.6.1 Conference Presentations/Papers

- Markantonakis V., Skoufoulas D., Papamichail I. and Papageorgiou M., Integrated motorway traffic control using variable speed limits and lane change control. 2nd Symposium on Management of Future motorway and urban Traffic Systems (MFTS 2018), Ispra, Italy, June 11-12, 2018.

- Martínez I., Markantonakis V., Papamichail I., Papageorgiou M. and Jin, W. L., Stationary States and Capacity Drop at Lane-Drop Bottlenecks with the Intelligent Driver Model. 101st Annual Meeting of the Transportation Research Board, Washington, DC, USA, January 9-13, 2022.

- Papamichail I., Schoenn-Anchling N., Malekzadeh M., Markantonakis V. and Papageorgiou, M., Macroscopic traffic flow model calibration for lane-free automated vehicle traffic. 26th IEEE International Conference on Intelligent Transportation Systems (ITSC 2023), Bilbao, Bizkaia, Spain, September 24-28, 2023.

1.6.2 Journal Papers

- Markantonakis V., Skoufoulas D.I., Papamichail I. and Papageorgiou M., Integrated traffic control for freeways using variable speed limits and lane change control actions. Transportation Research Record: Journal of the Transportation Research Board, Vol. 2673(9), pp. 602-613, 2019.

1.6.3 European project deliverables

- Markantonakis V., Mountakis K.S., Papageorgiou M. and Papamichail I., Traffic state estimation and traffic control algorithms for mixed vehicle traffic. Deliverable 2.5, Report of Project INFRAMIX (H2020-723016), Brussels, Belgium, December 2018.

- Markantonakis V., Papageorgiou M., Papamichail I., and partners of the EC Research Project, Implementation of traffic management strategies. Deliverable 3.4, Report of Project INFRAMIX (H2020-723016), Brussels, Belgium, November 2019.
- Markantonakis V., Papageorgiou M., Papamichail I., and partners of the EC Research Project, Evaluation results, impact analysis and new safety performance criteria for the road infrastructure. Deliverable 5.3, Report of Project INFRAMIX (H2020-723016), Brussels, Belgium, May 2020.
- Markantonakis V. and partners of the EC Research Project, Data Fusion, Harmonisation and Processing Pipeline - Initial version. Deliverable 3.2, Report of Project FRONTIER (H2020- 955317), Brussels, Belgium, October 2022.
- Markantonakis V., Papamichail I., Papageorgiou M. and partners of the EC Research Project, Traffic management schemes and control - Initial version. Deliverable 4.2, Report of Project FRONTIER (H2020-955317), Brussels, Belgium, October 2022.
- Markantonakis V., Papamichail I. and partners of the EC Research Project, Frontier Simulation Framework - Initial version. Deliverable 4.3, Report of Project FRONTIER (H2020-955317), Brussels, Belgium, October 2022.
- Markantonakis V. and partners of the EC Research Project, Data Fusion, Harmonisation and Processing Pipeline - Final version. Deliverable 3.4, Report of Project FRONTIER (H2020- 955317), Brussels, Belgium, December 2023.
- Markantonakis V., Papamichail I., Papageorgiou M. and partners of the EC Research Project, Traffic management schemes and control - Final version. Deliverable 4.5, Report of Project FRONTIER (H2020-955317), Brussels, Belgium, June 2024.
- Markantonakis V., Papamichail I. and partners of the EC Research Project, Frontier Simulation Framework - Final version. Deliverable 4.6, Report of Project FRONTIER (H2020-955317), Brussels, Belgium, December 2023.

Chapter 2

Simulation investigations using local-level controllers for CAVs

2.1 Introduction

Traffic congestion has become one of the most challenging problems in modern societies causing severe infrastructure degradation and underutilization. Longer travel times, lower speeds and extended congestion in the network, are only a few of the direct consequences. As mentioned by Markantonakis et al. (2019), an efficient way to influence traffic performance and alleviate traffic congestion on motorways is the development and implementation of appropriate traffic control strategies utilizing vehicle automation and communication systems. In the near future, vehicles equipped with such systems are expected to revolutionise the ordinary features and capabilities of conventional vehicles (Diakaki et al., 2015). Vehicle original equipment manufacturers (OEMs) are investing heavily in automation, while software is becoming a critical component of vehicles. At the same time, traffic and road authorities are seeking new technology solutions to increase safety and to reduce traffic congestion, fuel consumption and emissions. These solutions are often dependent on the vehicle's potential to recommend, support or even execute appropriately designed traffic control tasks and the ability of the infrastructure to provide various types of support for drivers and vehicles. Therefore, there is a need to prepare the road infrastructure to support the coexistence of conventional and automated vehicles, targeting the transition period when the penetration rate of CAVs will gradually increase. A number of control strategies, targeting maximum throughput at motorway bottleneck locations, was developed by the DSSL group within the FP7 ERC project TRAMAN21 (http://www.traman21.tuc.gr). These include a strategy that changes in real time the driving behaviour (specifically the employed time-gap and possibly also the acceleration strength) of ACC-equipped vehicles in motorway sections according to the prevailing traffic conditions in order to improve traffic flow efficiency (Spiliopoulou et al., 2018; Manolis et al., 2020); a strategy that employs mainstream traffic flow control using variable speed limits as an actuator (Markantonakis et al., 2019), when approaching areas with a particular infrastructure layout, e.g. a lane drop or an on-ramp merge area, in order to establish optimal traffic conditions; and a strategy that delivers appropriate lane-changing actions to selected connected vehicles using a feedback-feedforward control law (Roncoli et al., 2016, 2017; Markantonakis et al., 2019). Note that, these algorithms are presented below for completeness.

A library of software tools, that implements the aforementioned traffic control algorithms in a generic way for any network topology given by the user as well as a strategy that activates or deactivates in real-time the use of dedicated lanes for AVs according to the traffic flow conditions, has been developed within the H2020 project INFRAMIX (http://www.inframix.eu) using the C programming language. For the H2020 project FRONTIER (https://www.frontier-project.eu) the C++ programming language was used. Moreover, for the INFRAMIX project the advanced simulation environment VSimRTI

(Protzmann et al., 2017b) was used while for the FRONTIER project the commercial simulation platform AIMSUN (Aimsun, 2023) was used. The control algorithms have been integrated on both simulation environments and have been thoroughly assessed via comprehensive investigations involving a large variety of penetration rates for CAVs, infrastructure types and capabilities, and traffic conditions (free flow, critical, congested).

2.1.1 Literature review

Feedback control strategies early presented during the 90s were commonly based on the theories of proportional, integral and derivative control (PID). One of the fundamental advantages of feedback control strategies is the ability to react directly to tracking errors. In traffic control this implies to directly adjust the control actions based on the current traffic flow conditions. The system takes in real-time measurements of density, flow or speed and makes corrections according to the reference input (i.e. a set-point of density, flow or speed), so as to optimize performance and increase the systems efficiency i.e. achieve optimal traffic flow conditions by reducing the average Total Time Spent (TTS), reducing the Total Delay (TD) or even maximizing throughput. Due to their robustness and simplicity in design, they gained popularity which is reflected in the abounding literature existing in this field.

One of the pioneer studies using feedback control for ramp-metering applications was presented by Papageorgiou et al. (1991). The control strategy named ALINEA uses detectors to measure occupancy downstream of an on-ramp and determines the metering rate based on a pre-specified set-point for occupancy. The results of the real-life application of ALINEA on an on-ramp located at the Boulevard Pèriphèrique in Paris, demonstrated the robustness and flexibility of the strategy. Another early advancement using different feedback-control laws was presented by Pavlis and Papageorgiou (1999). A series of scenarios utilizing different demand profiles and incident conditions, were simulated so as to infer conclusions on the different types of feedback laws tested, e.g. bang bang, Proportional (P) or Proportional-Integral (PI) for route guidance. The reported results demonstrated the efficiency of each one of the proposed strategies investigated. Diakaki et al. (2000) presented an urban corridor traffic control strategy that incorporates three feedback control strategies, one for signal control, one for ramp metering control and one for route guidance control. The development and testing of the aforementioned traffic control scheme was applied on a real urban corridor in Glasgow, Scotland. Useful conclusions were derived from the simulation investigations adopted as well as the real-field applications of the strategy. A comparative study among the optimal control tool Advanced Motorway Optimal Control (AMOC) previously proposed by Kotsialos and Papageorgiou (2001) and the ramp metering feedback control strategy ALINEA previously proposed by Papageorgiou et al. (1991) was presented by Kotsialos et al. (2005). The idea of using hierarchical coordinated ramp metering control to configure the feedback regulator ALINEA, proved beneficial at all cases investigated. As a reference case for comparison, the ALINEA strategy was used as a stand-alone strategy. The results demonstrated the combined use of AMOC with ALINEA.

Another interesting feedback control strategy designed to control traffic jams was proposed by Zhao and Gao (2005). The strategy introduces a feedback signal acting on the traffic system in the optimal velocity (OV) model. Under known circumstances (i.e. when the state of the system is inhomogeneous), the signal will act moving the traffic system towards a homogeneous traffic state. Simulation investigations using different levels of noise validate the aforementioned. Carlson et al. (2011) presented a simple local feedfack controller for MTFC enabled via VSLs. The control strategy is based on a PI-type controller whose gains were tuned with the aid of the METANET model. The strategy was evaluated on a series of simulation investigations and compared to other optimal control approaches. Based on the results, useful conclusions were derived which are related to the robustness and

real-field application of the strategy. An ad-hoc combined LCA and VSL control scheme was presented by Zhang and Ioannou (2016), demonstrating the significant benefits of the strategy both at a macroscopic and microscopic level. The VSL controller uses a feedback linearization apporach based on the CTM model and the LCA strategy delivers lane-change recommendations upstream of a bottleneck location based on a rule-based strategy. The simulated data derived from the microscopic investigations for the I-710 highway utilizing the combined ad-hoc strategy, were then used to validate the macroscopic model CTM and evaluate the performance of the VSL controller itself. Both the microscopic and macroscopic simulations showed the percentage of improvement in travel time and other related KPIs.

Up to this point, this section presented a series of feedback control strategies published in the literature using conventional actuators (i.e. traffic lights and VMSs) to control the road traffic. Since the main target of this thesis is to highlight the potential benefits of utilizing CAVs as control actuators instead of using conventional actuators like the ones mentioned above, we choose to include some representative work in what follows.

A comparative study using different network topologies in a feedback-based platoon control strategy for CAVs was presented by Li et al. (2016). During the study a stability analysis of the feedback-based strategy was performed using a Lyapunov technique and the effects of the different communication network topologies on the convergence and robustness of the strategy were also investigated. Simulation experiments on two different scenarios demonstrated the effectiveness of the proposed strategy. Wei et al. (2019) designed a linear feedforward and feedback controller using the on-board radar sensors of a CAV and the V2V communication protocols, to follow a preceding vehicle while ensuring string stability. Simulation experiments under several traffic conditions, validate the robustness and adaptability of the proposed control strategy on realizing the longitudinal and lateral vehicle following behavior using the radar technology and communication protocols mentioned above. Another interesting approach of combining a VSL control algorithm and a fully connected microscopic environment for CVs within a feedback control framework was proposed by Wu et al. (2020). The strategy was implemented and validated on a hypothetical motorway stretch featuring a bottleneck using the software tool of VISSIM (Fellendorf and Vortisch, 2010) and the car-following model of IDM (Treiber et al., 2000). The study mainly focused to reduce the rear-end crash risks close to the bottleneck location in the presence of fog conditions. The related KPIs used to evaluate the effectiveness of the proposed traffic control strategy was the Total Travel Time (TTT) and the Time-to-Collision (TTC). The results demonstrated that the strategy was able to reduce both KPIs on a series of tests that included numerous relationships among vehicle gaps and visibility distances. Chen et al. (2021) developed a linear feedback-feedforward rotation-based CAV control strategy taking into account speed differences and spacing errors as the feedback component and the acceleration of preceding vehicles as the feedforward component to regulate the longitudinal and steering motion of CAVs at critical merging areas i.e. on-ramp merges. Moreover, a V2V communication topology is also developed and used in this work. Simulation experiments validate that the aforementioned control strategy can alleviate the distrurbances on the gap generation and merging procedures.

A lane-change controller for balancing traffic flows close to motorway merging areas was developed by Kim et al. (2023) using a PID controller. The feedback-based traffic control strategy used traffic data collected from CAVs upstream of a bottleneck location using V2I communication protocols with zero delays. The aggregated data per lane contained information of speed and flow which was then used as an input to the controller for deriving a number of lane-changes to be executed from CAVs. A hypothetical motorway network featuring a bottleneck and a real-world network featuring a pair of on/off ramps were simulated on the traffic simulation software VISSIM (Fellendorf and Vortisch, 2010) on a series of experiments using different demand profiles. The comparison among the scenarios of no-control,

control without feedback and control with feedback indicates the effectiveness of the feedback control strategy to decrease the disturbance among the lanes and significantly reduce the capacity drop phenomenon. A merging control strategy for motorway work zones that combines a short-term prediction model with a PID controller was recently presented by Kim et al. (2024). The control strategy uses real-time measurements of the system to dynamically adjust the merging behavior of CAVs in a mixed traffic environment with manually-driven vehicles. The employed traffic control strategy was evaluated through microscopic simulations using the software tool of VISSIM (Fellendorf and Vortisch, 2010) on a calibrated real-world network under mixed traffic flow conditions. The results proved that the strategy successfully distributes traffic among the lanes upstream of the work-zone maintaining both higher speeds and under-critical density values per lane.

A substantial amount of literature on feedback control strategies utilizing conventional and non-conventional traffic control actuators was presented in this section. The aforementioned studies explored the effects of MTFC control, RM control and RG control using both types of actuators while on the other hand studies exploring the effects of LCA control used only non-conventional traffic control actuators. In the following sections we provide an overview of a series of local-level traffic control strategies using feedback control and CAVs as control actuators serving as as a supplementary part of the literature review presented in this section. We focuse our attention on the potential benefits CAVs can offer within the next decades in reducing TTS, TD and maximizing throughput at bottleneck locations performing extended evaluations through microscopic simulations.

2.1.2 Contribution

Based on the simulation evaluations conducted within INFRAMIX, the following contributions arise:

- A library of tools delivered in the form of a Dynamic Link Library (DLL), was developed using the C programming language.
- The library was integrated with VSimRTI using an Application Programming Interface (API) based on the Java programming language.
- A new microscopic simulation environment (SUMO) was adopted with a more realistic mixture of traffic for the microscopic simulations.
- A more realistic model for the required communication between vehicles and the infrastructure, and different options were utilised to examine the minimum requirements from an infrastructure point of view.

Based on the simulation evaluations conducted within FRONTIER, the following contributions arise:

- A library of tools delivered in the form of a DLL, was developed using the C++ programming language.
- The library was integrated with AIMSUN using an extension that was developed from the AIMSUN group for the needs of the project.
- Microscopic investigations were carried out on a realistic microscopic model utilizing real and aritificial traffic data.

2.2 Mainstream traffic flow control

VSLs displayed on roadside or overhead VMSs in response to prevailing traffic conditions is an increasingly popular motorway traffic control measure that is used to enhance traffic safety for nearly two decades. When VSLs are applied, a homogenisation of speeds across different motorway lanes is observed, which reduces the accident of risk. In early studies (Papageorgiou et al., 2008), it was shown that VSL can be used to create a temporal or even a permanent flow decrease. As a result, VSLs can be used by a control strategy to regulate the mainstream traffic flow at critical motorway areas, for example at bottleneck areas where recurrent congestion phenomena appear during peak demand periods.

2.2.1 An overview of the MTFC concept

The basic idea of MTFC is to enable the mainstream traffic flow that is approaching areas with particular infrastructure layout, for example, on-ramp merges, mainstream lane-drops or other bottlenecks, to take values that will allow the establishment of optimal traffic conditions for any appearing demand (Carlson et al., 2010a,b). This can be achieved using VSLs that act as actuators and a feedback control strategy that maintains the density at the bottleneck area around a set-point that can be set equal to the critical density, i.e. the density at which capacity flow is achieved at the bottleneck area. The MTFC concept investigated in this thesis is illustrated in Fig. 2.1. MTFC actions are employed at an area upstream of the bottleneck location, leaving enough space for the vehicles to accelerate within the acceleration area and reach the bottleneck with an increased speed avoiding the capacity drop phenomenon; thus higher outflow is achieved (see Fig. 2.1). Of course a controlled congestion is formed at the MTFC application area that spills back further upstream. Appropriate VSLs can be also applied there (Safety area) in order to ensure a smooth reduction of speed and a safer vehicle approach to the MTFC application area. This controlled congestion is significantly reduced in space and time compared to the congestion created when no control actions are applied and has higher internal speeds due to the increased outflow (capacity) values. This also leads to less blocking of off-ramps and hence further improvements on the motorway. VSLs can be broadcasted on appropriately located VMSs and/or can be communicated to CAVs according to their current location on the motorway. Such a VSL message can be used either as on-board information (advise or order) to be applied manually by the driver or as a setting (order) to be applied automatically by CAVs. It is expected that, for a sufficient penetration of CAVs, this will be sufficient to impose the speed limit to non-equipped vehicles as well; hence, no VMSs would be necessary. Nevertheless, in case of mixed traffic the use of VMSs is suggested in order to properly inform the drivers of vehicles that are not connected.

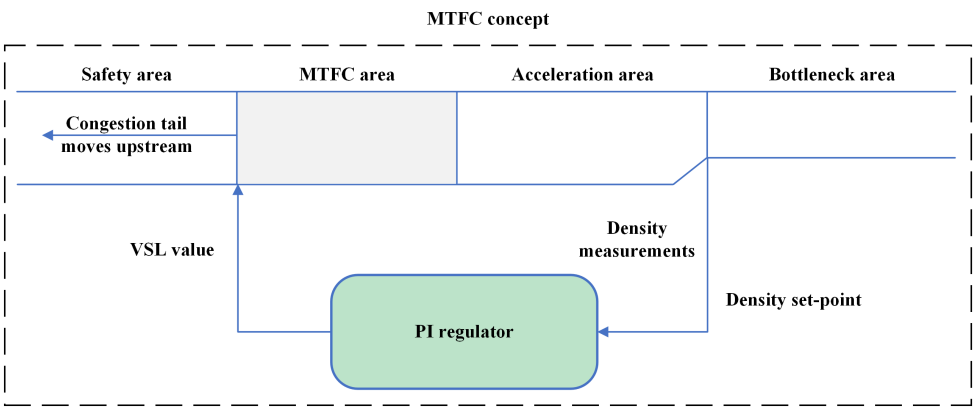

Figure 2.1: The MTFC concept.

2.2.2 A feedback regulator for MTFC

In this section, we present a feedback regulator for MTFC initially proposed by Carlson et al. (2013). The MTFC controller is a PI feedback regulator which is designed to maintain the bottleneck density ρ close to a selected set-point $\hat{\rho}$ using real-time measurements (or estimates) of density ρ. In the majority of cases, the set-point is selected around the critical density value, at which maximum outflow (capacity) is achieved at the bottleneck location. The following equation describes the PI-type feedback regulator:

$$vsl(k) = vsl(k-1) + K_I(\hat{\rho} - \rho(k)) + K_P(\rho(k-1) - \rho(k)) \tag{2.1}$$

with $k = 1, 2, 3, ...$ defined as the discrete time index. The control interval T for updating the decisions according to (2.1) is usually set between 30s-60s. The dynamics of the controller depend on the Proportional and Integral gains denoted by K_P and K_I , respectively. The $vsl(k)$ value delivered by the control strategy is truncated to remain within a range of admissible VSL values $[vsl_{min}, vsl_{max}]$ and the truncated value is used at the next time period as $vsl(k-1)$ in order to avoid the windup phenomenon (Shinskey, 1996).

As discussed above in Section 2.2.1, the VSL value is broadcasted at a VMS located at the beginning of the MTFC application area/segment and/or is sent for application to all CAVs that are located in the same area/segment. Upstream of the MTFC application area there is a VSL Safety area (divided into one or more subareas/segments) where speed limits are also applied (gradually increasing from a segment to the upstream one) to ensure a smooth reduction of speed and a safer vehicle approach to the MTFC application area. Furthermore, downstream of the MTFC application area, an acceleration area follows where an increased VSL is employed in order to allow a quick recovery of higher speeds by the vehicles so as to avoid the capacity drop and maximize the bottleneck throughput.

In order to settle the proper VSL value, some practical implementation aspects are taken into account. The VSL obtained from the PI regulator (2.1) is rounded to the closest value of a set of predefined discrete values (e.g. 90, 80, 70, 60,... km/h). Furthermore, the difference between two consecutive VSL values received by VMSs and/or connected vehicles in an area of the motorway is limited (e.g. to ± 20 km/h), so as to avoid abrupt speed changes. Also, the difference between two VSL values at consecutive areas/segments at the same control period is limited (e.g. to 20 km/h), as often required in practice, in order to achieve a safe approach of vehicles within the safety area.

2.3 Lane change advice

As previously mentioned in Section 2.2, bottleneck locations can be on-ramp merge areas, lane-drop areas, infrastructure layouts with a strong curvature, areas where strong weaving of traffic streams exists due to on/off-ramps that are located nearby, or areas with external capacity-reducing events (e.g. work-zones). In most of the cases, when the arriving demand is higher than the bottleneck capacity, the bottleneck is activated and congestion is formed upstream of this location. However, based on empirical investigations (Knoop et al., 2010), capacity flow in conventional traffic (manually driven vehicles) is not reached simultaneously at all lanes. Traffic breakdown may occur on a lane, while capacity has not yet been achieved on the other lanes. This means that the potentially achievable capacity over all lanes is usually not fully exploited. Once congestion appears on one lane, drivers on this lane try to avoid the speed drop by moving to adjacent lanes. This increased lateral movement of vehicles causes congestion over all lanes. After congestion has occurred, the discharge flow is reduced. This is mainly due to different vehicle accelerations at the congestion head that is causing the

so-called capacity drop phenomenon, and as a result an even faster congestion formation upstream of the bottleneck location (Papageorgiou et al., 2007).

Without proper traffic management techniques, delays, accidents and infrastructure costs will further increase providing more negative impacts on the everyday life. To fill in the gap, effective and proper traffic management techniques should arise that take into account all road users. To this end, a novel new traffic control strategy providing lane change advice was proposed by Roncoli et al. (2016, 2017) and is used in the upcoming investigations of this thesis.

2.3.1 An overview of the LCA concept

The main goal of the LCA strategy is to achieve a desired lane-based distribution of vehicles just upstream of a bottleneck area to exploit the capacity of each lane, in an attempt to increase the overall (cross-lane) capacity. For this reason, a linear state-feedback control law, resulting from an appropriate linear-quadratic regulator (LQR) problem formulation is utilized. The considered system under control comprises a number of interacting segment-lanes upstream of the bottleneck; while the feedback control law computes adequate lateral (lane-changing) flows for each segment-lane to be implemented by CAVs, thus enabling an opportune, pre-specified lane-based distribution of traffic flow. The feedback control law is fed with real-time measurements (or estimates) of the state of the system, i.e. of all segment-lane densities, and is targeting appropriate pre-specified set-points of lane-based traffic densities.

2.3.2 A linear quadratic regulator for LCA

The problem of manipulating the lateral flows upstream of a bottleneck location in order to increase capacity and hence retard or avoid the creation of congestion, is formulated as a Linear Quadratic (LQ) optimal control problem. Based on a linear multi-lane traffic flow model proposed by Roncoli et al. (2016, 2017), we consider a multi-lane motorway stretch subdivided into $i = 1, ..., N$ segments of length L_i, while each segment is composed of $j = m_i$,..., M_i lanes, where m_i and M_i are the minimum and maximum indexes of lanes for segment i. Each segment i is composed of M_i - $m_i + 1$ cells; while each motorway cell is indexed by (i, j). According to this definition, the total number of cells from the origin to segment i is $H_i = \sum_{r=1}^{i}(M_r - m_r + 1)$. The total number of cells for the whole stretch is $\overline{H} = H_N$. It is assumed that $j = 1$ corresponds to the right most lane of the motorway. The model is formulated in discrete time, considering the discrete time step T with a typical value of 10s. Each motorway cell (i, j) illustrated in Fig. 2.2 is characterized by traffic density, which is dynamically evolving following the conservation equation:

$$\rho_{i,j}(k+1) = \rho_{i,j}(k) + \frac{T}{L_i}\Big[q_{i-1,j}(k) - q_{i,j}(k)\Big] + \frac{T}{L_i}\Big[f_{i,j-1}(k) - f_{i,j}(k)\Big] + \frac{T}{L_i}d_{i,j}(k) \quad (2.2)$$

where each entity appearing in (2.2) is described as follows:

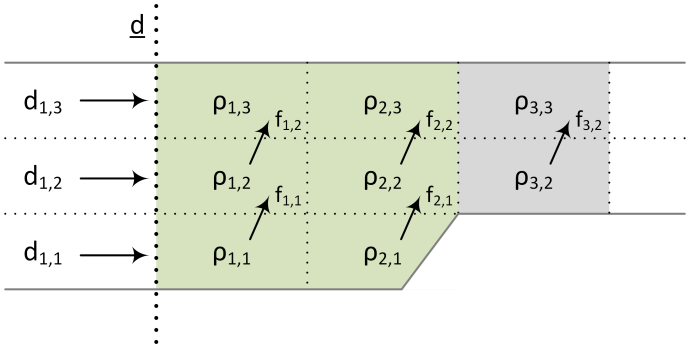

Figure 2.2: The LQR model formulation.

Variable	Definition
$\rho_{i,j}(k)$	is the density, i.e. the number of vehicles in cell (i, j) at time k divided by the segment length L_i
$q_{i,j}(k)$	is the longitudinal flow, i.e. the number of vehicles leaving segment i and entering segment $i+1$ remaining at lane j during time interval $(k, k+1]$
$f_{i,j}(k)$	is the lateral flow, i.e. the number of vehicles moving from lane j to lane $j+1$ during time interval $(k, k+1]$ (veh/h) when positive, or the number of vehicles moving from lane $j+1$ to lane j during time interval $(k, k+1]$ (veh/h) when negative
$d_{i,j}(k)$	is the external demand flow, i.e. the number of vehicles entering the control area in cell (i, j) during time interval $(k, k+1]$

For a different network geometry and topology, some terms of equation (2.2) may not be present. In particular, the inflow $q_{i-1,j}(k)$ for segment i does not exist if segment i is the first segment of the control area. Similarly, the outflow $q_{i,j}(k)$ of segment i does not exist if segment i is the last segment before a lane drop, while the lateral flow term $f_{i,j}(k)$ exists only for $m_i \leq j < M_i$. The external flow $d_{i,j}(k)$ exists only for a subset of cells (the upstream-most segment depicted in Fig. 2.2) Considering all the above, the total number of lateral flows is equal to $\overline{F} = \overline{H} - N$.

Let us consider the well-known relationship of density, flow and speed:

$$q_{i,j}(k) = \rho_{ij}(k) v_{i,j}(k) \tag{2.3}$$

Replacing some terms of equation (2.2) with equation (2.3), the following is obtained:

$$\begin{aligned} \rho_{i,j}(k+1) = {} & \frac{T}{L_i} v_{i-1,j}(k) \rho_{i-1,j}(k) + \left[1 - \frac{T}{L_i} v_{i,j}(k)\right] \rho_{i,j}(k) \\ & + \frac{T}{L_i} \left[f_{i,j-1}(k) - f_{i,j}(k) \right] + \frac{T}{L_i} d_{ij}(k) \end{aligned} \tag{2.4}$$

Speeds $v_{i,j}(k)$ are treated as known parameters and as a result a Linear Parameter Varying (LPV) system is obtained in the following form:

$$\mathbf{x}(k+1) = \mathbf{A}(k)\mathbf{x}(k) + \mathbf{B}\mathbf{u}(k) + \mathbf{d}(k) \tag{2.5}$$

In (2.5), we have the vectors of state, control and disturbance, respectively as follows:

$$\mathbf{x}(k) = \begin{bmatrix} \rho_{1,m_1} \dots \rho_{1,M_1} & \rho_{2,m_2} \dots \rho_{N,M_N} \end{bmatrix}^T \in \mathbb{R}^{\overline{H}} \tag{2.6}$$

$$\mathbf{u}(k) = \begin{bmatrix} f_{1,m_1} \dots f_{1,(M_1-1)} & f_{2,m_2} \dots f_{N,(M_N-1)} \end{bmatrix}^T \in \mathbb{R}^{\overline{F}} \tag{2.7}$$

$$\mathbf{d}(k) = \begin{bmatrix} \frac{T}{L_1} d_{1,m_1} \dots \frac{T}{L_1} d_{1,M_1} & \frac{T}{L_2} d_{2,m_2} \dots \frac{T}{L_N} d_{N,M_N} \end{bmatrix}^T \in \mathbb{R}^{\overline{H}} \tag{2.8}$$

and matrices **A**, **B**. Maxtrix **A** reflects the inter-connection between pairs of subsequent cells connected by a longitudinal flow $q_{i,j}(k)$ and matrix **B** reflects the inter-connection of adjacent cells connected by lateral flows $f_{i,j}(k)$. Matrix **A** is composed of elements:

$$a_{r,s} = \begin{cases} 1, & \text{if } r = s \text{ and } (j < m_{i+1} \text{ or } j > M_{i+1}) \\ 1 - \frac{T}{L_i} v_{i,j}(k), & \text{if } r = s \text{ and } (i = N \text{ or } m_{i+1} \le j \le M_{i+1}) \\ \frac{T}{L_i} v_{i-1,j}(k), & \text{if } r > H_1 \text{ and } s = r - M_{i-1} + m_i - 1 \\ 0, & \text{otherwise} \end{cases} \tag{2.9}$$

and matrix **B** of elements:

$$b_{r,s} = \begin{cases} \frac{T}{L_i}, & \text{if } j > m_i \text{ and } s = r - i \\ -\frac{T}{L_i}, & \text{if } j < M_i \text{ and } s = r - i + 1 \\ 0, & \text{otherwise} \end{cases} \tag{2.10}$$

where $r = H_{i-1} + j + m_i + 1$.

Assuming that the inflow arriving upstream of the bottleneck location is not exceeding the maximum capacity of the bottleneck (e.g. thanks to MTFC measures), and hence any formation of congestion can be avoided, our system can be treated as a Linear Time Invariant (LTI) system. Specifically, in free flow conditions, it is assumed that speed $v_{i,j}(k)$ in all cells (i, j) remains constant and equal to a speed value v^* ($v_{i,j}(k) \equiv v^*$) close to the critical speed. Thus, matrix **A**(k) is now treated as a constant matrix **A**. Also, external flows **d**(k) are assumed constant to enable an LTI system and hence a time-invariant feedback controller. Note, however, that the external flows **d** will be allowed to be time-varying according to measurements and will be explained later. Based on the aforementioned, the obtained LTI system reads:

$$\mathbf{x}(k+1) = \mathbf{A}\mathbf{x}(k) + \mathbf{B}\mathbf{u}(k) + \mathbf{d} \tag{2.11}$$

A quadratic cost function is defined that penalises the difference between the segment-lane densities and pre-specified (constant) density set-point values, at the area downstream of the lane-drop area (see grey area in Fig. 2.2). A penalty term is also included aiming at maintaining small control inputs, i.e. small lateral flows (Roncoli et al., 2016, 2017). The matrix form of the quadratic cost function reads:

$$J = \sum_{k=0}^{\infty} \left\{ \left[\mathbf{C}\mathbf{x}(k) - \hat{\mathbf{y}} \right]^T \mathbf{Q} \left[\mathbf{C}\mathbf{x}(k) - \hat{\mathbf{y}} \right] + \mathbf{u}^T(k)\mathbf{u}(k) \right\} \tag{2.12}$$

where:

- $\mathbf{C}$ is a matrix reflecting the cells that are tracked.
- $\mathbf{Q}$ is a weighting matrix associated to the magnitude of the state tracking error.
- $\hat{\mathbf{y}} \in \mathbb{R}^{\overline{Y}}$ is a vector containing the $\overline{Y}$ selected desired set-point density values at the bottleneck area.
- the time-horizon is infinite to enable a time-invariant feedback controller.

Note that $\mathbf{Q} = \mathbf{Q}^T$ is a positive definite matrix and matrix $\mathbf{C}$ is composed of elements $c_{r,s}$ ($1 \leq r \leq \overline{Y}$ rows and $1 \leq s \leq \overline{H}$ columns). Each row of matrix $\mathbf{C}$ contains elements equal to zero and a single element equal to 1 that corresponds to the element of vector $\mathbf{x}$ that is tracked.

2.3.3 Feedback-Feedforward Control Law

The solution to the formulated optimal control problem is given through a Linear Quadratic Regulator (LQR) in the form of a linear state feedback-feedforward control law. To ensure a stabilizing feedback-feedforward control law, our system must be at least stabilisable and detectable, see (Roncoli et al., 2016, 2017) for all the related details. The linear feedback-feedforward control law is given by:

$$\mathbf{u}^*(k) = -\mathbf{K}\mathbf{x}(k) + \mathbf{u}_{ff} \tag{2.13}$$

where:

$$\mathbf{K} = (\mathbf{I} + \mathbf{B}^T\mathbf{P}\mathbf{B})^{-1}\mathbf{B}^T\mathbf{P}\mathbf{A} \tag{2.14}$$

$$\mathbf{P} = \mathbf{C}^T\mathbf{Q}\mathbf{C} + \mathbf{A}^T\mathbf{P}\mathbf{A} - \mathbf{A}^T\mathbf{P}\mathbf{B}(\mathbf{I} + \mathbf{B}^T\mathbf{P}\mathbf{B})^{-1}\mathbf{B}^T\mathbf{P}\mathbf{A} \tag{2.15}$$

$$\mathbf{u}_{ff} = (\mathbf{I} + \mathbf{B}^T\mathbf{P}\mathbf{B})^{-1}\mathbf{B}^T\mathbf{F}(\mathbf{C}^T\mathbf{Q}\hat{\mathbf{y}} - \mathbf{P}\mathbf{d}) \tag{2.16}$$

$$\mathbf{F} = (\mathbf{I} - (\mathbf{A} - \mathbf{B}\mathbf{K})^T)^{-1} \tag{2.17}$$

Note that the feedback gain matrix $\mathbf{K}$ is calculated via (2.14) only once offline (time invariant controller) after solving the Ricatti equation (2.15) iteratively starting from $\mathbf{P} = \mathbf{I}$. Subsequently, equation (2.16) with $\mathbf{F}$ from (2.17), represents the feedforward term that may be calculated offline. However, for practical implementation, one may measure the external flow $\mathbf{d}$, in which case the feedforward term becomes time-varying (online), with equations (2.13, 2.16) rewritten as:

$$\mathbf{u}^*(k) = -\mathbf{K}\mathbf{x}(k) + \mathbf{u}_{ff}(k) \tag{2.18}$$

$$\mathbf{u}_{ff}(k) = \mathbf{\Phi} - \mathbf{\Delta}\mathbf{d}(k) \tag{2.19}$$

where $\mathbf{\Phi} = (\mathbf{I} + \mathbf{B}^T\mathbf{P}\mathbf{B})^{-1}\mathbf{B}^T\mathbf{F}\mathbf{C}^T\mathbf{Q}\hat{\mathbf{y}}$ and $\mathbf{\Delta} = (\mathbf{I} + \mathbf{B}^T\mathbf{P}\mathbf{B})^{-1}\mathbf{B}^T\mathbf{F}\mathbf{P}$ may be calculated offline.

The feedback-feedforward control law delivers "macroscopic" lane-changing flows for each cell. These lateral flows are translated to corresponding vehicle numbers that should change lane in each cell, and related messages are submitted to a corresponding number of CAVs. Note that the control design model is only used for deriving the feedback-feedforward control law, which is robust, i.e. similarly efficient for changing speed values (corresponding to different "parameter" values in the control design model). Thus, although these assumptions of course do not hold true in a microscopic simulation model, the investigations reported in 2.7.4 verify and demonstrate the effectiveness of the strategy with the controller being robust enough.

2.4 Adaptive cruise control

The existence of vehicles equipped with ACC systems is now a reality, and their use will be expanded in the near future. ACC systems enable drivers to adjust their speed and time-gap to the preceding vehicle when following slower vehicles. These systems apply automatically the appropriate acceleration or deceleration of the vehicle, based on real time measurements and driver's parameterisation. They are mainly designed to increase safety and comfort, thus some conservative values for the ACC system parameters may be used, i.e. comparatively large time-gaps. However, such conservative parameter values may eventually lead to degradation of the static and dynamic road capacity compared to conventional manual-driving vehicle traffic. The higher the penetration rate of ACC-equipped vehicles, the more pronounced will be the influence of their driving style on the overall traffic flow.

In contrast to the vast literature on ACC and CACC systems, which focuses on the design, functionality or architecture of these systems, there is a comparatively small number of investigations related to the impact of these systems on traffic flow. These works aim to capture this impact under different settings (mainly different time-gaps) and penetration rates, using either microscopic simulation or macroscopic approaches. See for instance, related work presented in microscopic simulations by Ioannou and Stefanovic (2005); Shladover et al. (2012) and in macroscopic approaches presented by Ngoduy (2013); Delis et al. (2016). However, these studies do not systematically examine how the ACC settings should be specified to improve the overall traffic performance. For a more comprehensive literature review, as well as for a discussion on studies that advance towards the direction of specifying the ACC settings either offline or online, see the novel work presented by Manolis et al. (2020).

2.4.1 An overview of the ACC concept

A simple but effective ACC-based control strategy, which aims to adjust in real time the ACC parameters of equipped and connected vehicles based on the prevailing traffic conditions was presented by Manolis et al. (2020). The main philosophy behind the proposed concept is to:

- leave the ACC parameters at their driver-selected values if traffic flow is clearly under-critical so as to limit interventions only to traffic situations that call for efficiency increase.
- change the ACC parameters gradually as appropriate to improve the flow efficiency when critical traffic states are imminent or present.

The proposed control strategy depends only on real-time measurements of mean speed and flow. It is actually activated only when, where and to the extent needed. For the sake of understanding and completeness, the control strategy is presented in what follows.

2.4.2 A real-time time-gap adaptation strategy

Consider a motorway with both manually-driven and ACC-equipped vehicles. The ACC-equipped vehicle drivers may introduce their desired ACC system parameters, i.e. desired speed, v_d, and minimum time-gap, T_d, but the time-gap is subject to change if the control strategy orders different values. The motorway is considered to be divided into segments, and the traffic management centre (TMC) applies the proposed control strategy at every motorway segment i. In particular, at every control interval t_c, the strategy receives real-time measurements of the exiting flow q_i and mean speed v_i of every segment i . This information may be obtained through conventional spot detectors. The proposed strategy has two goals which are presented below.

The first goal is to determine in real time the time-gaps of the ACC-equipped vehicles that lead to the increase of the static and dynamic road capacity, only where and when it is needed. To achieve this, the strategy calculates the suggested time-gap as a function of the current segment flow, $T_i[q_i(k)]$, as shown in Fig. 2.3. As long as the segment flow is low (i.e. $q_i \leq Q_1$), the maximum time-gap, T_{max}, is suggested, since traffic is not critical. Beyond this lower limit, as the flow increases, the strategy gradually decreases the suggested time-gap value, while for high flow values (i.e. $q_i \geq Q_2$) the strategy suggests the minimum time-gap T_{min}. Note that the suggested time-gap value is reduced to the minimum value before the flow reaches the nominal capacity of the segment, Q_{cap}. In this way, the strategy aims to delay, or even prevent, the formation of congestion, by maximizing timely the segment's capacity. It should be also noted that the adopted function $T_i[q_i(k)]$ of time-gap versus flow must be non-increasing, but can have any form deemed appropriate, e.g. deliver only a (high or low) number of discrete time-gap values, rather than being continuous (see Fig. 2.3a), as the stepwise function shown in Fig. 2.3b. This will be, in fact, the form to be used in the simulation investigations presented below. If, despite the intended capacity increase, the segment becomes congested (e.g. due to even higher arriving demand or due to a shockwave arriving from downstream), then the strategy releases its operation at the congested segments, by suggesting the maximum time-gap T_{max} for safety reasons. The suggested time-gap will be applied only if it is lower than the individual time gap setting. The above control decisions are summarized by the following relation that determines the suggested time-gap,

$$T_{stg,i} = \begin{cases} T_i[q_i(k)] & \text{if } v_i(k) > v_{cong} \\ T_{max} & \text{else} \end{cases} \tag{2.20}$$

where $k = 1, 2, ...$, is the discrete time index, and v_{cong} indicates the congestion limit. The control strategy decisions are calculated at the TMC and are disseminated to the ACC-equipped vehicles, e.g. via V2I communication. To avoid possible oscillations, the flow and speed measurements are sufficiently smoothed before being used, e.g. using an exponential filter.

The second goal of the proposed control strategy is the maximization of the discharge flow during congestion at the location of active bottlenecks (dynamic capacity). It is empirically known that the discharge flow at the head of a congested area is lower than capacity, and the second goal is to mitigate this capacity drop. The strategy first identifies the location of active bottlenecks. More specifically, if two consecutive segments $i-1$ and i, have a speed difference higher than a threshold Δv, and the mean speed $v_i(k)$ of the downstream segment i is higher than the congestion speed v_{cong}, while the mean speed of the upstream segment, $v_{i-1}(k)$, is lower than v_{cong}, this indicates that these two segments are located just upstream and just downstream of the head of a congested area, i.e. that an active bottleneck has been identified. The discharge flow at the congestion head can be increased by suggesting the minimum time-gap T_{min} applied by ACC-equipped vehicles driving within the two

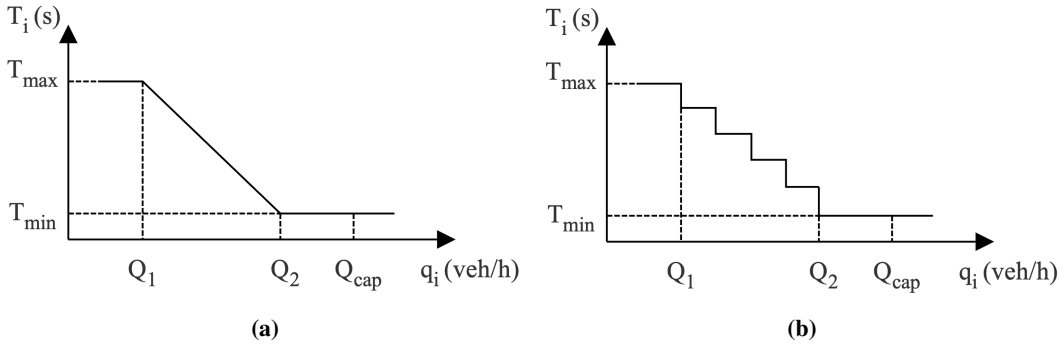

Figure 2.3: Time-gap value calculation using: a linear (a) and stepwise function (b).

mentioned segments. These extended control decisions are implemented via the following relations:

$$\begin{aligned} &\text{If } v_i(k) > v_{cong} \text{ and } v_{i-1}(k) < v_{cong} \text{ and } \left[v_i(k) - v_{i-1}(k)\right] > \Delta v \\ &\text{then } T_{stg,i}(k) = T_{min} \text{ and } T_{stg,i-1}(k) = T_{min} \end{aligned} \tag{2.21}$$

Again, speed measurements are sufficiently smoothed before being used in order to avoid possible oscillations or false alarms, e.g. due to moving shock waves. The suggested time-gap $T_{stg,i}$ for each control interval t_c is determined by (2.20) and (2.21). The ACC-equipped vehicles receive the suggested time-gap, but they apply it only if their individual time-gap setting is higher than the time-gap suggested by the controller. Note that ACC-equipped vehicles update their time-gap settings with a frequency that may be higher than at every control interval due to crossing of segment boundaries. Based on extensive simulation investigations, it has been found that the Q_1 and Q_2 values, as well as the size of the motorway segments and the control interval t_c have minor impact on the performance of the strategy.

2.5 Dynamic lane assignment

The impact of setting (permanent) dedicated lanes for CAVs on traffic flow throughput has been investigated recently using appropriate modelling techniques of CAVs in heterogeneous traffic flow (Vander Laan and Sadabadi, 2017; Ye and Yamamoto, 2018; Rad et al., 2020; Chakraborty et al., 2021; He et al., 2022; Yao et al., 2023; Sha et al., 2024). Simulation results from these studies indicate that at low CAV penetration rates, setting CAV dedicated lanes deteriorates the performance of the overall traffic flow throughput, particularly under a low density level. When CAVs reach a dominant role in the mixed flow, the merits of setting dedicated lanes also decrease. The benefit of setting CAV dedicated lanes can only be obtained within a medium density range. CAV penetration rate and individual CAV performance are significant factors that decide the performance of CAV dedicated lanes. The higher level of performance the CAVs could achieve, the greater benefit will be attained through the deployment of CAV dedicated lane. Of course, the level of performance of CAVs depends on the various settings, e.g. time-gap, maximum acceleration, reaction time. Besides, the performance of CAV dedicated lanes can be improved through setting higher speed limits for CAVs on the dedicated lanes than vehicles on other normal lanes. Some other papers found in literature, study the impact of deploying permanent dedicated lanes for CAVs on a network level assuming various penetration rates; see for instance Cohen (2011); Ivanchev et al. (2017); Fakhrmoosavi et al. (2023). These studies are using macroscopic models and a lot of related assumptions and reach similar conclusions. In a mixed traffic environment with

a penetration rate varying within the day, a dynamic assignment of a dedicated lane to CAVs sounds more appropriate than a permanent one. The main aim should be to maintain traffic throughput at least at the same level as in case of today's traffic consisted of only conventional vehicles.

2.5.1 An overview of the DLA concept

The main goal of the DLA strategy is to achieve in real-time the activation of a set or one dedicated lane(s) for CAVs in a mixed traffic environment, as long as some conditions are met. For this reason, a threshold-based strategy fed with real-time measurements (or estimates) of the state of the system, i.e. of all segment densities, is developed. The considered system under control comprises a number of interacting segment-lanes across the network; while the strategy computes adequate activation/deactivation lane intervals to be implemented by CAVs, thus enabling an opportune, pre-specified dedicated lane-based distribution of traffic flow.

2.5.2 A real-time lane assignment strategy for CAVs

A simple threshold-based control strategy has been developed for dynamic lane assignment to CAVs. Of course, connectivity is a prerequisite in order to communicate related DLA activation and deactivation messages to CAVs. Although the concept can be generalised, we will consider a motorway stretch divided into n segments with the same homogeneous characteristics such as the number of lanes m, for each segment i and a flow capacity Q_{cap} that is obtained around a critical density ρ_{cr}. Only one specific lane can be assigned to CAVs, as long as some conditions are met. The location of the lane (e.g. right or left lane) and the minimum number of consecutive segments ($\leq n$) that are required for the activation of a dedicated lane are preselected by the operator considering traffic management goals as well as safety parameters.

Considering the aforementioned features and characteristics of the DLA strategy, the following conditions are checked at every control period for all segments $i = 1, 2, ..., n$ on which a dedicated lane is not already active:

$$\rho_{act}^{min} < \rho_i(k) < \rho_{act}^{max} \tag{2.22}$$

$$\frac{1}{m}\rho_{act}^{min} < \rho_i^{CAV}(k) < \frac{1}{m}\rho_{act}^{max} \tag{2.23}$$

$$\frac{m-1}{m}\rho_{act}^{min} < \rho_i(k) - \rho_i^{CAV}(k) < \frac{m-1}{m}\rho_{act}^{max} \tag{2.24}$$

where $k = 1, 2, 3, ...$ is defined as the discrete time index, ρ_i being the density measurement (or estimate) of all vehicles on segment i, ρ_i^{CAV} being the density measurement (or estimate) of CAVs on segment i, while $\rho_{act}^{min} < \rho_{act}^{max} < \rho_{cr}$ are appropriately selected thresholds. If all inequalities (2.22) - (2.24) are met for a segment, then this segment becomes a candidate for application of the dedicated lane for CAVs. Conditions (2.22) - (2.24) take into account the penetration rate of CAVs, which is in fact ρ_i^{CAV}/ρ_i, and make sure that the logic is applied only for densities that are above some thresholds. They also take into account the capacity of the segments, the capacity of the dedicated lane and the capacity of the rest of the lanes left for conventional traffic.

If a segment $i = 1, 2, ..., n$ was a candidate in the previous control period, then the following conditions are checked:

$$\rho_i(k) < \rho_{deact}^{min} \tag{2.25}$$

$$\rho_{deact}^{max} < \rho_i(k) \tag{2.26}$$

$$\rho_i^{CAV}(k) < \frac{1}{m}\rho_{deact}^{min} \tag{2.27}$$

$$\frac{1}{m}\rho_{deact}^{max} < \rho_i^{CAV}(k) \tag{2.28}$$

$$\rho_i(k) - \rho_i^{CAV}(k) < \frac{m-1}{m}\rho_{deact}^{min} \tag{2.29}$$

$$\frac{m-1}{m}\rho_{deact}^{max} < \rho_i(k) - \rho_i^{CAV}(k) \tag{2.30}$$

with ρ_{deact}^{min} and ρ_{deact}^{max} being appropriately selected thresholds such that $\rho_{deact}^{min} < \rho_{act}^{min} < \rho_{act}^{max} < \rho_{deact}^{max} < \rho_{cr}$ holds in order to add some hysteresis. If any of the inequalities (2.25) - (2.30) are true for a segment, then this segment is not any more a candidate segment for application of the dedicated lane for CAVs and it will be included in the subset of segments for which conditions (2.22) - (2.24) will be checked in the next control step.

If a number of consecutive segments are candidates and this number is greater than or equal to the minimum number of segments required for the activation of a dedicated lane, then these segments become active. Otherwise they are not active. Consecutive active segments form a cluster that is used to assign a lane to CAVs. These segments remain part of the cluster as long as they are active and for a period that is at least equal to a predefined minimum period in order to avoid weaving phenomena that are expected during activation and deactivation of the dedicated lane on the segments. Every time that a new candidate segment is attached to a cluster of active segments, the timer used to count the active period is reset for all segments that are necessary to form a dedicated lane with at least the minimum number of segments required in a cluster that contains the new candidate.

The time period T for updating decisions according to the above can be set equal to a period that is suggested to be within the range of 1 to 5 minutes. It is also suggested to use smoothed measurements (or estimates) in order to avoid possible oscillations or false alarms. Of course, adequate physical infrastructure adaptations have to be considered as well as the type and kind of V2X communication, in order to achieve availability and consistency of information for all types of vehicles. Conventional vehicles can be informed using VMSs while CAVs will receive the information as well as specific lane-change advices. A speed limit value that differs from the default speed limit can be used if deemed necessary whenever a dedicated lane is active on some segments.

2.6 Microscopic investigations for the INFRAMIX project

Microscopic investigations were carried out using the microscopic traffic simulator SUMO (Lopez et al., 2018). SUMO is an open source, highly portable, microscopic and continuous traffic simulation package designed to handle large-scale networks. It provides realistic mobility pattern for a multitude of vehicles and generates the overall traffic flow in the investigated scenarios. Each vehicle in the simulation is modelled as an individual agent using simplified car-following models e.g. the Gipps model (Gipps, 1981) or the IDMM model (Treiber and Helbing, 2003) which is the one used in the upcoming investigations. All simulated vehicles in the Traffic Simulator, such as SUMO, have a corresponding agent in the application simulator and could be equipped with models to provide the dedicated functionality of e.g. behaviour of conventional vehicles or communication capabilities of CAVs. Furthermore, this approach allows the modelling of different vehicle types such as trucks and passenger cars.

2.6.1 VSimRTI and ICOS microscopic simulation frameworks

The V2X Simulation Runtime Infrastructure (VSimRTI) is a comprehensive framework for the assessment of new solutions for Cooperative Intelligent Transportation Systems (C-ITS). It covers the simulation of microscopic traffic, communication, applications, and road infrastructure. VSimRTI uses an ambassador concept inspired by some fundamental concepts of the High Level Architecture (HLA); thus, it has the ability to couple different simulators e.g. SUMO (Lopez et al., 2018) is used in this thesis, so as to allow the simulation of the various aspects of future Intelligent Transportation Systems (ITS) (Protzmann et al., 2017a).

On the other hand, the Independent Co-Simulation framework (ICOS) models the submicroscopic behaviour of automated vehicles and vehicles with human drivers in detail. It uses new and innovative coupling algorithms to successfully bridge all the available models which are developed in different simulation environments. ICOS enables a simultaneous simulation of all models and manages the synchronisation of the inputs and outputs between the models (Protzmann et al., 2017b).

For the needs of the INFRAMIX project, both VSimRTI and ICOS are coupled with each other. This is established by integrating ICOS into VSimRTI by following its ambassador concept. The models coupled within VSimRTI are the following:

- **Map**: The geometry of the road on a microscopic basis.
- **Road traffic**: Vehicle movements on the motorway resembling real traffic patterns.
- **Communication**: Different communication paths including ITS-G5 and cellular communication (LTE-V2X, 5G).
- **Road infrastructure**: Includes VMSs for speed limits and lane assignments for CAVs, various road detectors, as well as road side units (RSUs) used for the ITS-G5 communication with the vehicles.
- **Traffic management and services**: Collect position data from vehicles and distribute advices.
- **User behaviour**: Reacting on VMSs and advices via in-vehicle information (IVI) messages.
- **Vehicle applications**: Includes differentiation in driving behaviour of CAVs and conventional vehicles. CAVs can furthermore react to advices via IVI messages on their own.

Additionally the control algorithms have been directly integrated with the Traffic Management Center (TMC) in the microscopic simulation environment. Fig. 2.4 illustrates all the models included in the microscopic simulations. More detailed information about the models can be found in the public deliverable D2.2 (INFRAMIX, 2018). Apart from trailers and motorcycles, three types of vehicles (cars) are considered within VSimRTI with different Society of Automotive Engineers (SAE) levels:

- **Conventional Vehicle (CV)**: vehicle with SAE level of automation equal to 0, 1, or 2 which does not communicate with the TMC-model.
- **Connected Conventional Vehicle (CCV)**: vehicle with SAE level of automation equal to 0, 1, 2 or 3 which communicates through wireless messages with the TMC-model (via cellular or ITS-G5 communication).

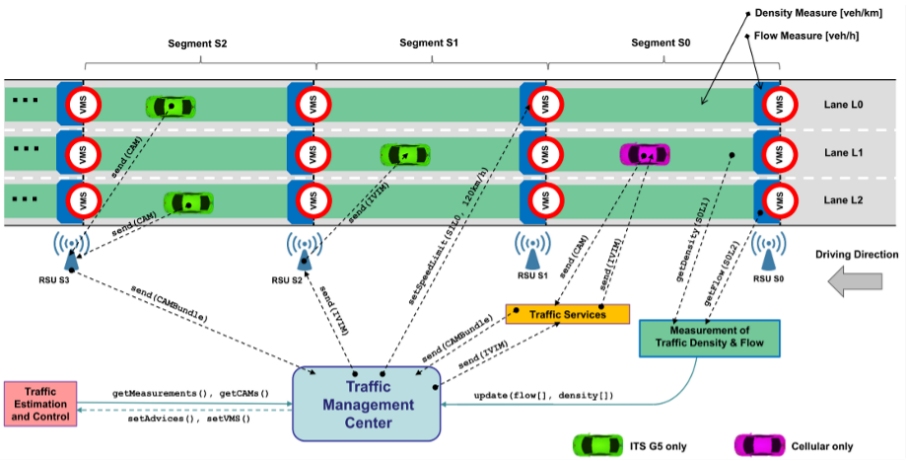

Figure 2.4: Overview of all models included in the microscopic simulation (INFRAMIX, 2020).

- **Connected Automated Vehicle (CAV)**: vehicle with SAE level of automation equal to 3, 4, or 5 which communicates through wireless messages with the TMC-model (via cellular or ITS-G5 communication).

2.6.1.1 Intelligent Driver Model with Memory (IDMM)

A car-following model describes all the necessary actions of a vehicle as a function of it's leader. These types of models require extensive calibration and validation in order to reproduce traffic flow phenomena as they appear in real traffic. For the needs of the upcoming investigations, the well-known car-following model IDMM is used. Compared to its predecessor, which is the IDM model (Treiber et al., 2000), the IDMM model incorporates the memory effects of speed to the IDM model. Like IDM, IDMM is also a time and space continuous car-following model, formulated as an ordinary differential equation.

In the IDM, the acceleration of each vehicle is derived from the continuous function of the vehicle's velocity v_a, the gap s_a and the velocity difference Δv_a to the leading vehicle:

$$\dot{v}_a(s_a, v_a, \Delta v_a) = a\left[1 - \left(\frac{v_a}{v_0}\right)^4 - \left(\frac{s^*(v_a, \Delta v_a)}{s_a}\right)^2\right] \tag{2.31}$$

where the tendency of the vehicle to accelerate is expressed from the term $a\left[1-(v_a/v_0)^4\right]$ and the tendency of the vehicle to decelerate from the term $-a\left(s^*(v_a,\Delta v_a)/s_a\right)^2$. When decelerating, the desired gap s^* as well as the actual gap s_a are considered in the term, where the desired gap s^* is derived from the following expression:

$$s^*(v_a, \Delta v_a) = s_0 + v_a T + \frac{v_a \Delta v_a}{2\sqrt{ab}} \tag{2.32}$$

In the IDMM, an internal dynamical variable $\lambda_a(t)$ that represents the subjective level of service, incorporates the memory effects in microscopic traffic flow models. For each driver, the instantaneous level of service $\lambda_0(v)$ is a function of the actual velocity $v(t)$:

$$\lambda_0(v) = \frac{v}{v_0} \tag{2.33}$$

Then, for each driver the subjective level of service is given by the exponential moving average of the instantaneous level of service exprerienced in the past:

$$\lambda_a(t) = \langle \lambda_{0a} \rangle_{EMA} = \int_0^t \lambda_0(v_a(t'))e^{-(t-t')/\tau}\, dt' \tag{2.34}$$

This internal variable clearly influences a set of parameters of the driving style. One of them is the time-gap T. Time-gap T corresponds to the minimum time needed when following the preceding vehicle and in the IDMM model is transformed according to the following expression:

$$T(\lambda) = T_0[\beta_T + \lambda(1-\beta_T)] \tag{2.35}$$

This implies that in steady state conditions, the following distance is given by:

$$s_e(v) = \frac{s_0 + vT_0\left(\beta_T + (1-\beta_T)\,\frac{v}{v_0}\right)}{\sqrt{1-\left(\frac{v}{v_0}\right)^4}} \tag{2.36}$$

2.6.1.2 Development in C

A software tool using the C programming language has been developed that implements all the control strategies in a generic way for performance evaluation in simulation experiments using VSimRTI. The software tool is delivered in the form of a DLL which is used as a software component in VSimRTI. The library has been developed using the Visual Studio IDE that allows you to view, edit and build code into a DLL file.

2.6.1.3 Project integration using C and Java

A collaboration with a group of software developers from Franuhofer FOKUS (https://www.fokus.fraunhofer.de), took place during the INFRAMIX project. The group was in charge of delivering the microscopic simulator (along with the test-beds) that was used for the needs of the project as well as providing a proper interface that integrates Java with C. Since VSimRTI is written in Java, the integration of ICOS (responsible for the models coupled within VSimRTI) is implemented using the Java Native Interface API. In this way we can include the DLL where all the control strategies are implemented directly in VSimRTI. In detail, among many subroutines and functions, the integration was implemented using three core functions:

- **Initialise function:** This is the first function to be called. For each control strategy, the configuration parameters are selected and the appropriate files for storing the output of each strategy during run-time are created.
- **Main function:** This is the second function to be called. It includes seperate function-calls for each control strategy, activated when a control strategy is selected or not. It is called every control step until the end of the simulation horizon.
- **Teardown function:** This function is the last function to be called at the end of the simulation. It frees up the memory for each control strategy and terminates the process.

2.6.2 The AP7 motorway test-bed

The INFRAMIX test site at Girona (Spain), along the motorway AP7, was the basis of the microscopic simulation evaluations for traffic efficiency. In order to simulate vehicle traffic on highways, VSimRTI uses the microscopic traffic simulator SUMO v1.5.0 (sumo.dlr.

de/docs). Modelling the road traffic for the microscopic simulations was one of the main challenges that has been accomplished following a two-step process. On the basis of real toll data provided by Autopistas (www.autopistas.com), a large-scale simulation scenario along the highway AP7 has been created with more than half a million vehicles during a 24 h period. This scenario has been calibrated to match the real traffic as close as possible utilising the IDMM car-following model (Treiber and Helbing, 2003). Since the Spanish test site at Girona covers only a small part of AP7, the large-scale scenario has been cropped to a 19 km stretch using novel techniques implemented in the simulation framework. This final simulation scenario allows focusing the experiments and evaluation on the test site only and enables simulations faster than real time for a simulation period of three hours (8am to 11am). The considered highway stretch, shown in Fig. 2.5, includes 3 on-ramps and 2 off-ramps and is divided into 38 segments with a length of about 0.5 km each. Segments 1 to 4 have 3 lanes, while all other segments have 4 lanes.

2.6.3 Microscopic simulation setup for ACC

The penetration rate of CVs, CCVs and CAVs (CV-CCV-CAV) can be parametrized individually. The following six configurations have been considered to reflect typical and future market penetrations (100-0-0, 94-4-2, 85-10-5, 70-20-10, 55-30-15, 30-45-25). CVs are selected to have SAE level 0, CCVs are selected to have SAE level 3, while CAVs are selected to have SAE level 5. Communication between vehicles and the TMC is modelled with ITS-G5 via RSUs which are located along the road. Messages are sent to the vehicles in a range of about 200 m from the RSUs every 5 sec. These messages contain advices for 10 downstream segments. In order to investigate what are the minimum requirements from an infrastructure point of view, three different cases have been considered for RSU coverage for both ACC and DLA investigations as follows:

- **Full RSU coverage:** RSUs are placed at the entry of each segment, i.e. every 500 m.
- **Mid RSU coverage:** RSUs are placed every 4th segment, i.e. every 2 km.
- **Low RSU coverage:** RSUs are placed every 10th segment, i.e. every 5 km.

For each one of the RSU investigated cases, all six CV-CCV-CAV configurations are considered, while for each configuration, ten simulation replications with different seeds were carried out and the respective average value of delay (AVD) encountered by the vehicles is reported and compared. The simulation step for SUMO is set to 0.5 sec and the whole simulation horizon is set to 180 min. For the control strategy, the configuration parameters are set as follows: $t_c = 30$ sec, $v_{cong} = 50$ km/h, $Q_1 = 1200$ veh/h/lane, $Q_2 = 1800$ veh/h/lane, $T_{max} = 1.6$ sec, while three different cases of (1.2, 1.0 and 0.8 sec) are considered for the value of the minimum suggested time-gap, T_{min}. The strategy suggests discrete time-gap values with increments of 0.2 sec according to the stepwise function presented in 2.4.2.

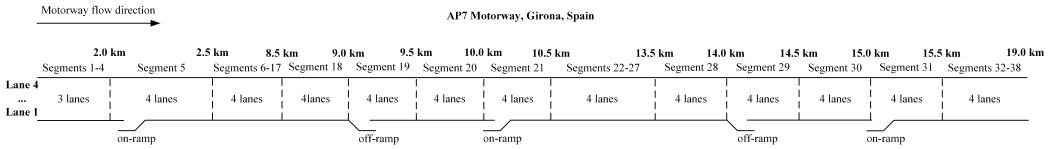

Figure 2.5: Test site at Girona (Spain), along the motorway AP7.

2.6.4 ACC investigations

In this section we present the simulation results obtained for the no-control scenario as well as for the control scenario where the ACC-parameter adaptation strategy is applied. Vehicles are using a range of different default time-gap values, sampled from a normal distribution with a mean value μ and a standard deviation σ equal to 0.05 μ, while any values out of the $[\mu - 2\sigma, \mu + 2\sigma]$ range are truncated. The mean value μ is different per category of vehicle. More specifically, the mean value is selected to be equal to 1.1 sec for slow CVs and CCVs, 0.9 sec for fast CVs and CCVs, and 1.4 sec for slow and fast CAVs. CAVs (SAE level 5) are supposed to be equipped with ACC systems and apply automatically any advice for the time-gap setting if it is lower than their default setting, while CCVs (SAE level 3) are equipped with ACC systems that are activated manually (with a probability of 50% and a delay of 5 seconds) by the drivers if the time-gap advice received through communication is lower than the one applied manually.

2.6.4.1 ACC: No-control scenario

A replication close to the average AVD value is selected for illustration purposes on all the scenarios investigated. The resulting speed contour plots for the no-control scenario and for all six CV-CCV-CAV configurations are presented in Fig. 2.6. Due to the conservative parameter values used by CAVs, the static and dynamic road capacity is degraded when their penetration rate is increasing. As a result, a strong congestion is created at the merge area of the most downstream on-ramp located at segment 31 (Fig. 2.5) and the average vehicle delay increases. The congestion duration and extend are increasing with the increase of the penetration rate of CAVs. Additional figures related to the no-control scenario can be found accordingly in Appendix A.1.

2.6.4.2 ACC: Control scenario

Similar to the no-control scenario, the replication close to the respective average AVD value is selected for illustration purposes. The resulting speed contour plots for the control scenario, for all six CV-CCV-CAV configurations and for the Full RSU case are presented in Figs. 2.7, 2.8, 2.9. For the case of $T_{min} = 1.2$ sec, the percentage of improvement reported over the no-control scenario, lies within the range of $[0.9\% - 31.2\%]$. The lowest improvement is reported for the case of 94-4-2 and the highest improvement for the case of 30-45-25. Looking at Fig. 2.7, one can easily observe that for all six CV-CCV-CAV configurations, congestion is reduced significantly both in space and time.

On the other hand, when the minimum time-gap T_{min} suggested by the controller is either 1.0 or 0.8 sec, i.e. lower than the one applied on average by CVs, the AVD achieved per CV-CCV-CAV configuration is lower than the no-control scenario for the 100-0-0 configuration (i.e. only CVs). In fact, looking at Figs. 2.8, 2.9 no congestion phenomena are appearing on the motorway; hence, free-flow conditions are prevailing throughout the simulation horizon and for all CV-CCV-CAV configurations investigated. For the cases of $T_{min} = 1.0$ sec and $T_{min} = 0.8$ sec, the percentage of improvement reported over the no-control case, lies within the range of $[3.6\% - 45.0\%]$ and $[5.7\% - 54.4\%]$ respectively.

Table 2.1 includes the results for all control cases. Specifically, the values of AVD compared with the ones derived from the no-control case are presented. One can easily observe that for all RSU coverage cases and all minimum suggested time-gap values considered, improvements are reported over the no-control case for all CV-CCV-CAV configurations. See also the bar-chart presented in Fig. 2.10 for the improvements reported as a percentage over the no control case. Additional figures related to the control scenario can be found accordingly in Appendix A.2.

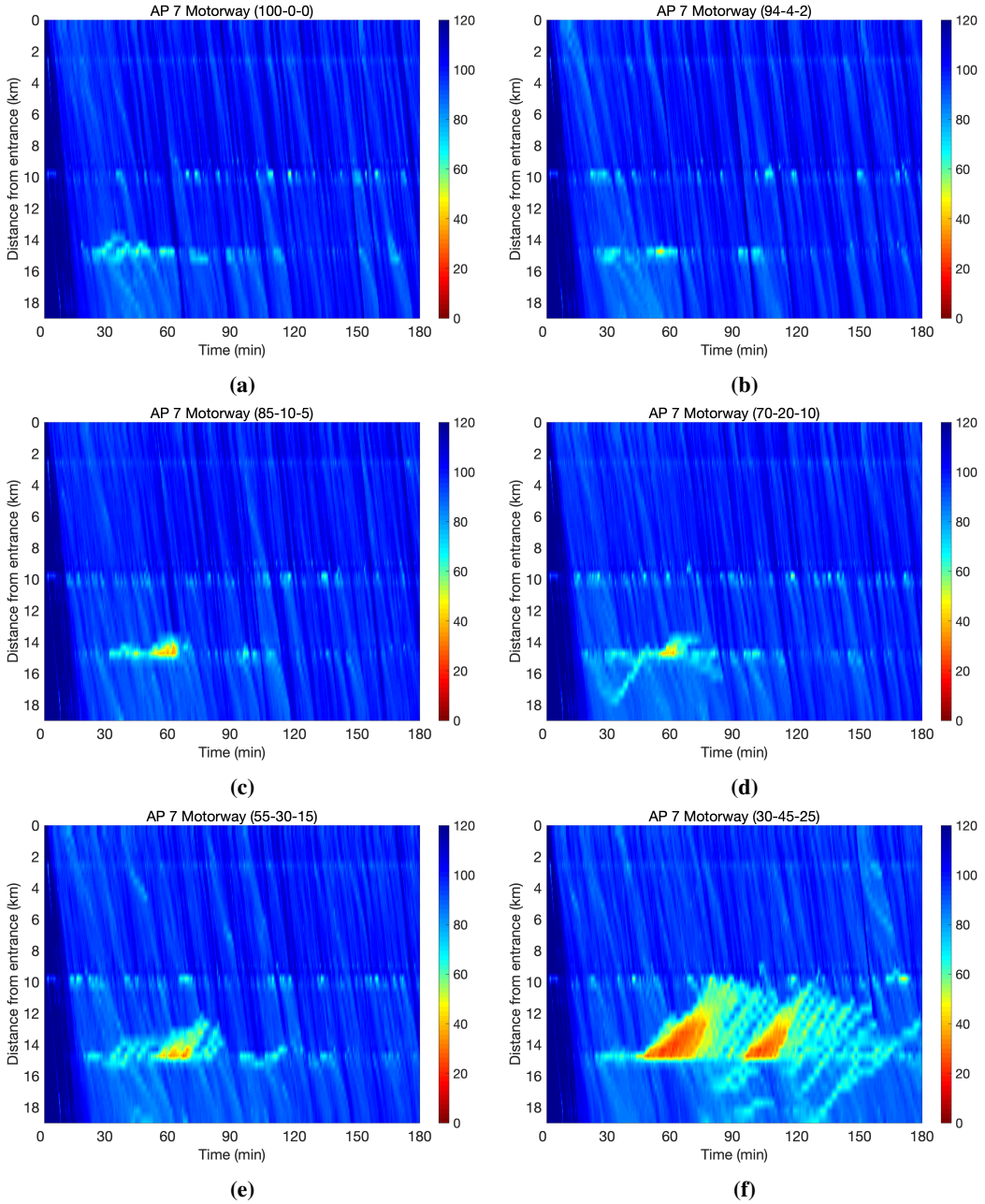

Figure 2.6: Speed (km/h) plots for the no-control case and for all six CV-CCV-CAV configurations investigated; 100-0-0 (a), 94-4-2 (b), 85-10-5 (c), 70-20-10 (d), 55-30-15 (e) and 30-45-25 (f).

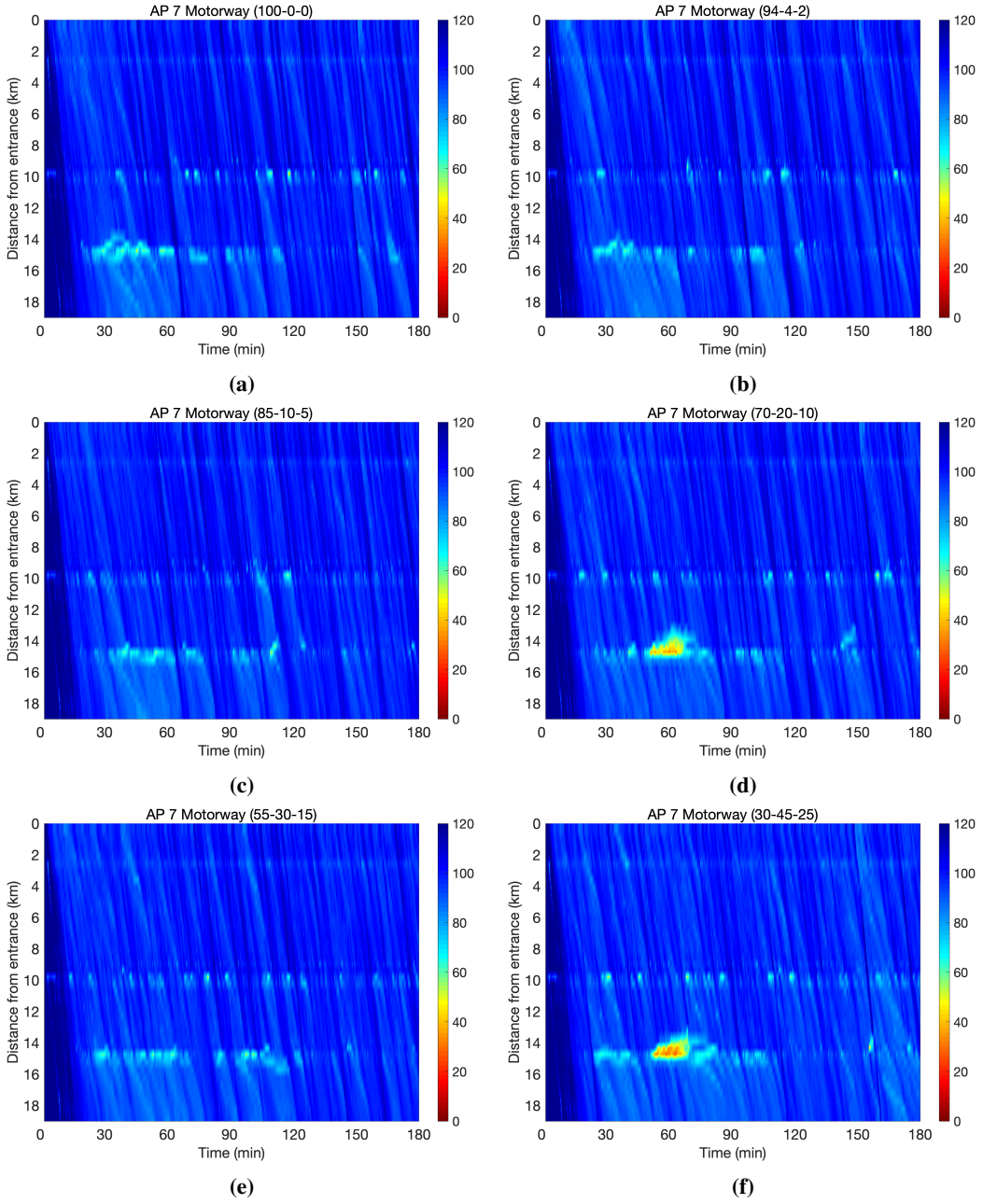

Figure 2.7: Speed (km/h) plots for the control case with Full RSU coverage and $T_{min} = 1.2$ sec, for all six CV-CCV-CAV configurations investigated; 100-0-0 (a), 94-4-2 (b), 85-10-5 (c), 70-20-10 (d), 55-30-15 (e) and 30-45-25 (f).

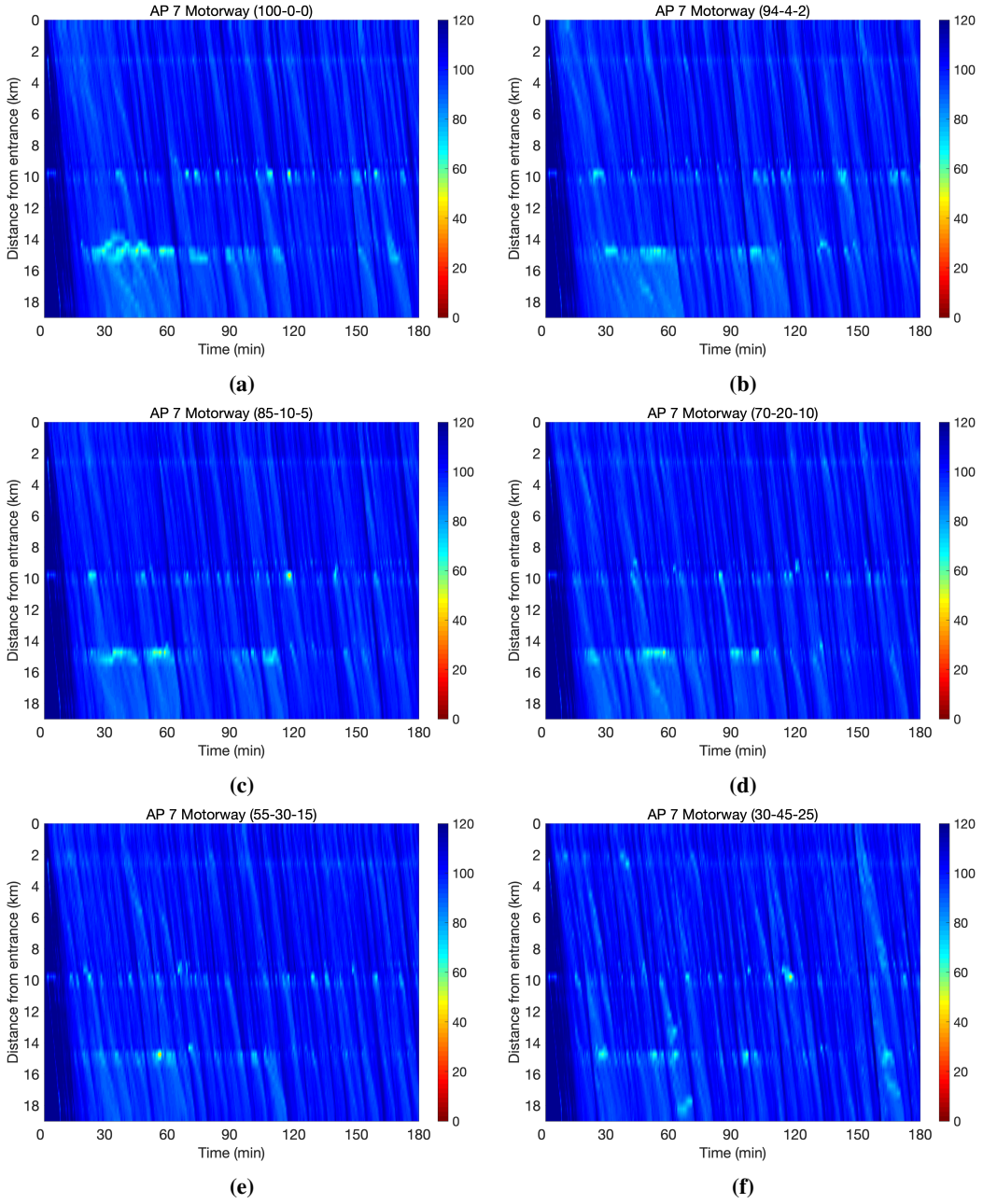

Figure 2.8: Speed (km/h) plots for the control case with Full RSU coverage and $T_{min} = 1.0$ sec, for all six CV-CCV-CAV configurations investigated; 100-0-0 (a), 94-4-2 (b), 85-10-5 (c), 70-20-10 (d), 55-30-15 (e) and 30-45-25 (f).

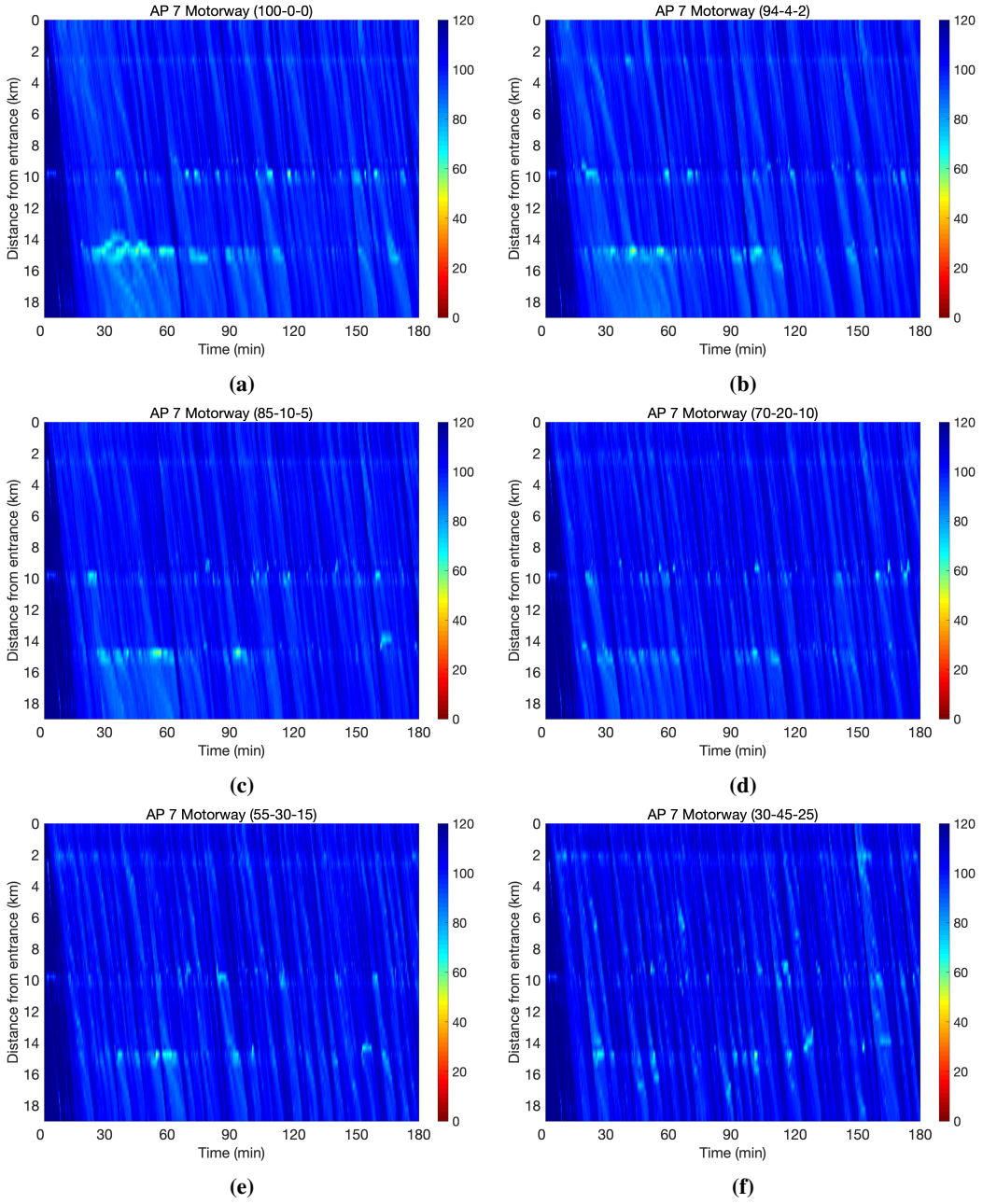

Figure 2.9: Speed (km/h) plots for the control case with Full RSU coverage and $T_{min} = 0.8$ sec, for all six CV-CCV-CAV configurations investigated; 100-0-0 (a), 94-4-2 (b), 85-10-5 (c), 70-20-10 (d), 55-30-15 (e) and 30-45-25 (f).

Table 2.1: Average Vehicle Delay (sec)

CV-CCV-CAV	100-0-0	94-4-2	85-10-5	70-20-10	55-30-15	30-45-25
No-control case	133.0	134.2	140.7	150.8	168.4	214.7
Full RSU coverage						
T_{min} = 1.2 sec	133.0	133.0	133.0	137.1	144.3	147.6
T_{min} = 1.0 sec	133.0	129.4	128.7	124.4	119.7	118.0
T_{min} = 0.8 sec	133.0	126.6	119.3	109.8	103.2	97.9
Mid RSU coverage						
T_{min} = 1.2 sec	133.0	133.1	137.3	138.7	143.4	147.4
T_{min} = 1.0 sec	133.0	129.4	127.8	122.3	120.7	118.6
T_{min} = 0.8 sec	133.0	126.2	119.6	109.6	103.9	98.6
Low RSU coverage						
T_{min} = 1.2 sec	133.0	133.8	136.4	137.7	143.2	147.5
T_{min} = 1.0 sec	133.0	129.8	127.6	123.8	120.9	120.8
T_{min} = 0.8 sec	133.0	125.9	119.8	111.4	106.4	100.8

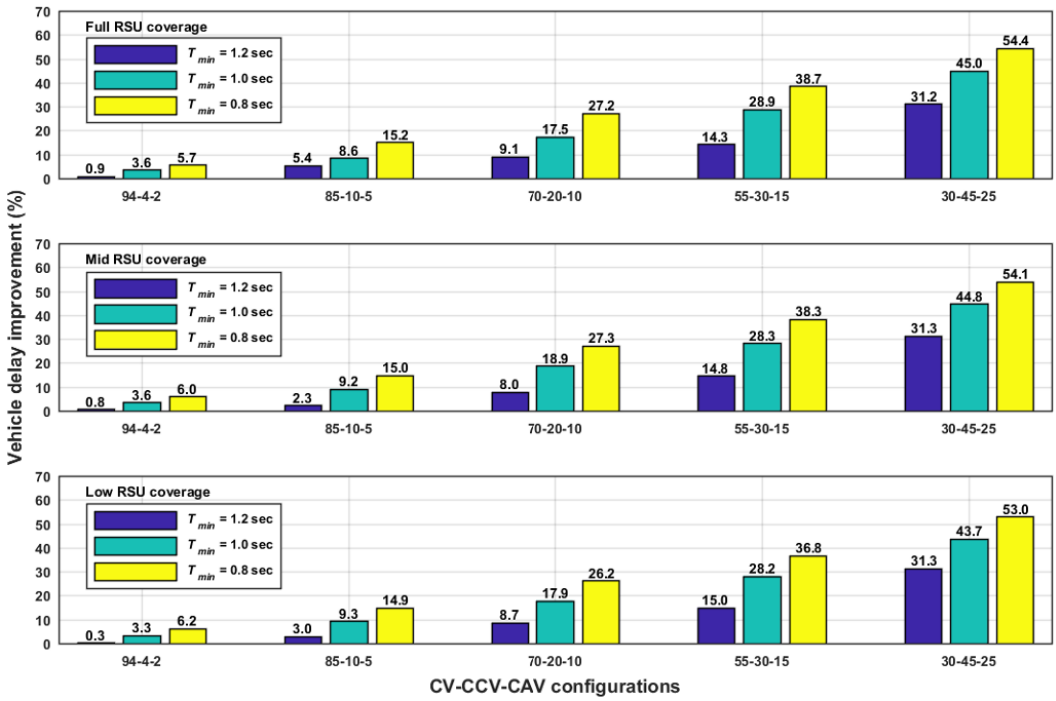

Figure 2.10: Bar chart for the vehicle delay improvements (%) over the no control case for all control cases and all CV-CCV-CAV configurations.

2.6.5 Microscopic simulation setup for DLA

For the DLA simulation investigations, only two types of vehicles (CVs and CAVs) for two different configurations were considered. Specifically, the penetration rate of CAVs among vehicles has been set initially equal to 25% and 30%, as 34 out of the 38 segments of the motorway stretch considered have 4 lanes. Of course, this is expected to be very beneficial for CAVs and less beneficial to the rest of the traffic that will have to occupy the rest of the lanes. Based on the aforementioned, the following 75-0-25 and 70-0-30 (CV-CCV-CAV) configurations were investigated.

Adequate physical infrastructure adaptations have been considered by the co-simulation environment in order to achieve availability and consistency of information for all types of vehicles. CVs can be informed using VMSs at the beginning of each segment, while CAVs receive the information as well as specific lane-change advices via communication (RSUs) well in advance. As discussed already above, weaving phenomena are expected during activation and deactivation of the dedicated lane on the segments. These weaving phenomena are due to the reshuffling that is necessary in order to get all vehicles on the lanes that have been assigned to them. As a result, when density values are high these weaving phenomena lead to congestion and increase of density values even more. The dedicated lane is deactivated if the whole phenomenon is observable by the controller. However, there are cases where congestion is created upstream of the already assigned lane and, as a result, the phenomenon is not observed by the controller in order to terminate the assignment.

Based on the above findings, the testing of the DLA controller using reduced (scaled-down) demand profiles was necessary. The scaling factors utilized where either equal to 0.6 or equal to 0.7. While assigning the fast lane (lane 4, Fig. 2.5) to CAVs, two different cases have been considered with respect to the areas around pairs of on/off-ramps, i.e. segments 18-21 and segments 28-31. In the first case, assignment of the fast lane is possible on all segments. In the second case considered, assignment is not possible on the above mentioned segments.

Additionally, for the dynamic lane assignment strategy all configuration parameters are set as follows:

- the time period (T) for updating decisions according to 2.5.2 has been set equal to 1 min.
- exponentially smoothed measurements have been used in order to avoid possible oscillations or false alarms.
- the minimum number of consecutive segments required for activation has been set to 5 segments.
- the minimum number of active control steps has been set to 5 steps that correspond to 5 min.
- the min threshold values for activation/deactivation $(\rho_{act}^{min}, \rho_{deact}^{min})$ have been set equal to 4 veh/km/lane and 6 veh/km/lane respectively.
- the max threshold values for activation/deactivation $(\rho_{act}^{max}, \rho_{deact}^{max})$ have been set equal to 15 veh/km/lane and 17 veh/km/lane (for the first set of simulations) respectively.

Note that, the lane that is assigned to CAVs is always the fast lane (lane 4) for the network studied (see Fig. 2.5). This decision was taken due to the high penetration of trailers that occupy a big portion of the slow lane (lane 1). Similarly to the ACC investigations, the simulation step for SUMO is set to 0.5 sec and the whole simulation horizon is set to 180 min.

A comprehensive analysis and testing, to derive useful conclusions for the proposed dynamic lane assignment strategy, is presented in the following section. As already discussed in Section 2.5, the benefit of setting a CAV dedicated lane can only be obtained within a medium density range. This is why we chose to run two sets of simulations by changing the max threshold values for activation/deactivation $(\rho_{act}^{max}, \rho_{deact}^{max})$. For the second set of simulations, the values were increased by 2 veh/km/lane. The above mentioned 4 dimensions of different parameters used, i.e. scaling of traffic demand, penetration of CAVs, inclusion or not of the areas around pairs of on/off-ramps, and the min/max values used for the density thresholds, lead to 16 different sets of simulations.

2.6.6 DLA investigations

For each one of the aforementioned sets defined in the previous Section 2.6.5, 10 replications with different seeds have been performed and lead to the results (weighted means over 10 replications) presented in Figs. 2.11, 2.12, 2.13, 2.14.

The results well support the conclusion that in most of the simulations the situation is beneficial for CAVs, especially when traffic demand is scaled-down to 60% and the penetration of CAVs is 25%, but it is not for the rest of the traffic. This leads to a deterioration of the calculated KPI (i.e. Total Travel Time) for the whole population. The results are not really sensitive with respect to the values used for the max $(\rho_{act}^{max}, \rho_{deact}^{max})$ thresholds. As expected, whenever areas around pairs of on/off-ramps are included in the assignment logic the results are a bit better compared to the opposite case. Of course, this is due to the fact that the lane assigned is always the fast one and inclusion of these areas leads to assignments that continue through the network without interruptions that may lead to strong weaving phenomena. The DLA controller is able to deactivate these segments on its own based on the density thresholds used.

In Fig. 2.15, corresponding DLA flag activation and speed plots for traffic demand scaling down to 60% are presented. Specifically, only the case of 25% of CAVs is presented on both cases where areas around pairs of on/off-ramps are included in the assignment logic or not. As mentioned at the beginning of this section, the level of performance of CAVs depends on the various settings, e.g. time-gap, maximum acceleration, reaction time, speed limits. On the top, in case of even higher penetration of CAVs, one could consider testing the dynamic assignment of 2 lanes. This is expected to improve performance even more because it will allow to the fast CAVs to overtake any slow CAVs, something that is not possible with just a single lane assigned. However, any improvement on the performance of CAVs will not lead to improvements for the rest of the traffic.

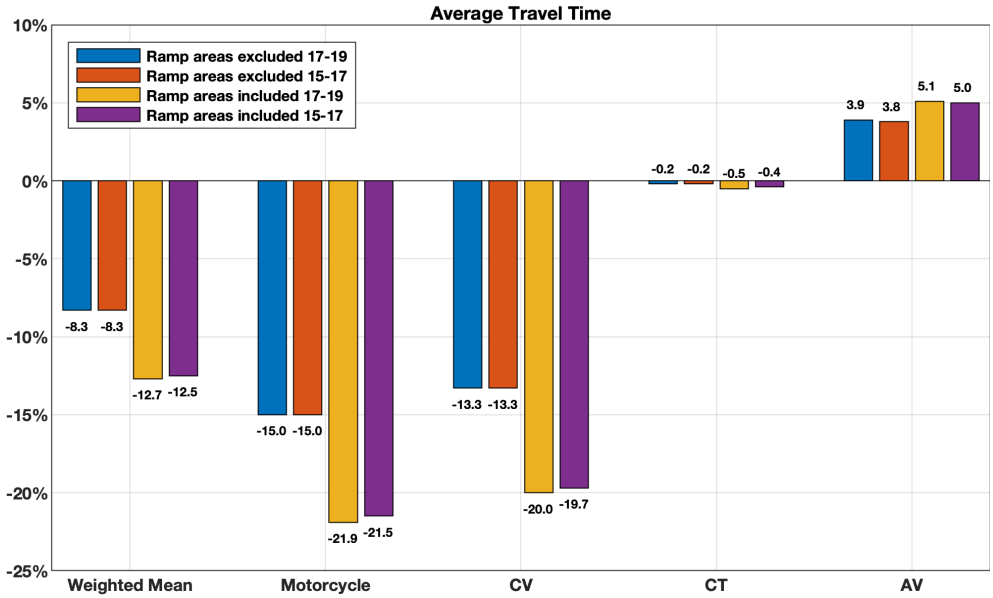

Figure 2.11: Total Travel Time in DLA scenario with scaling 0.6 and penetration rate 25% of CAVs

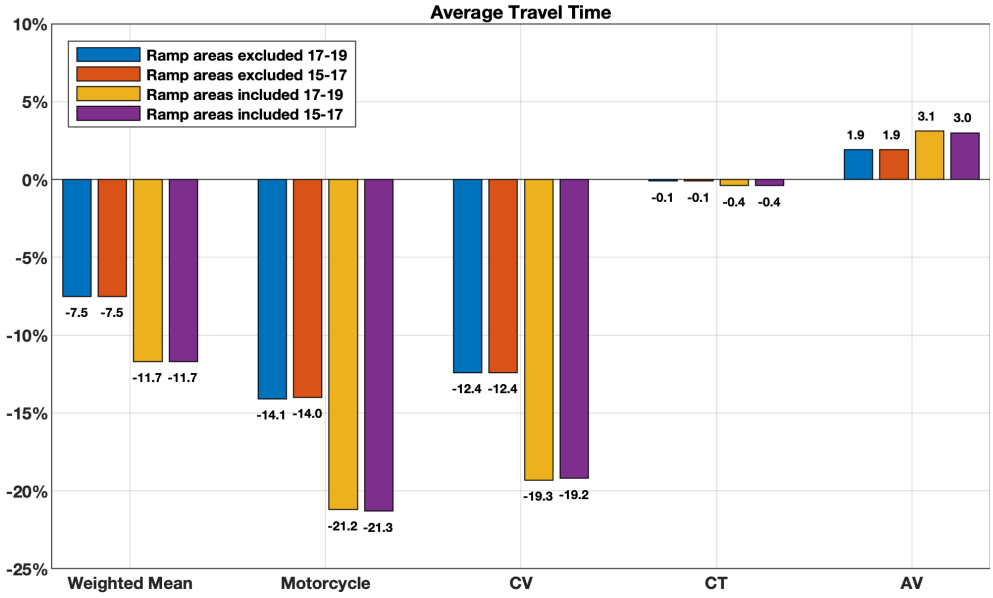

Figure 2.12: Total Travel Time in DLA scenario with scaling 0.6 and penetration rate 30% of CAVs

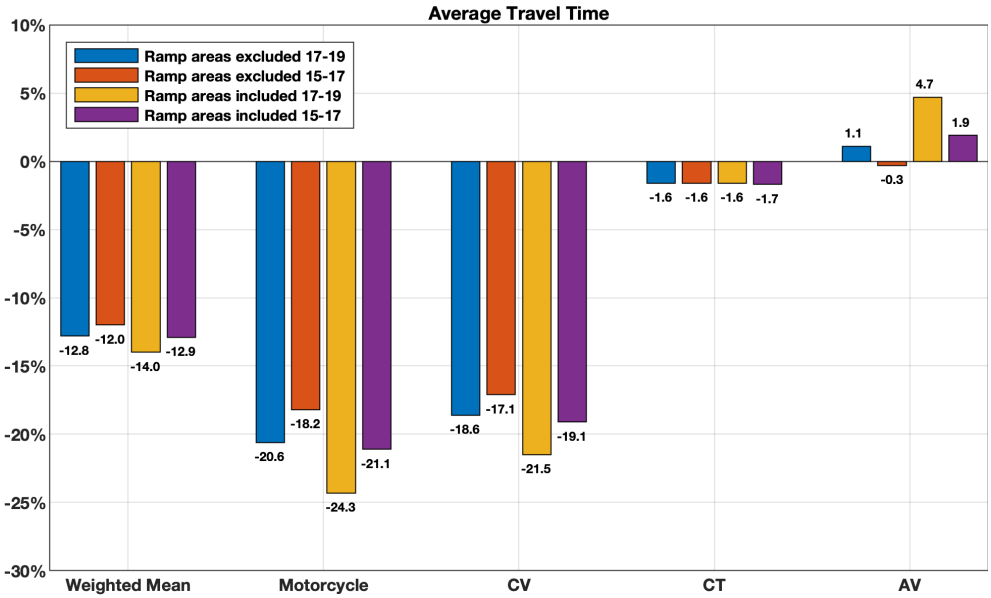

Figure 2.13: Total Travel Time in DLA scenario with scaling 0.7 and penetration rate 25% of CAVs

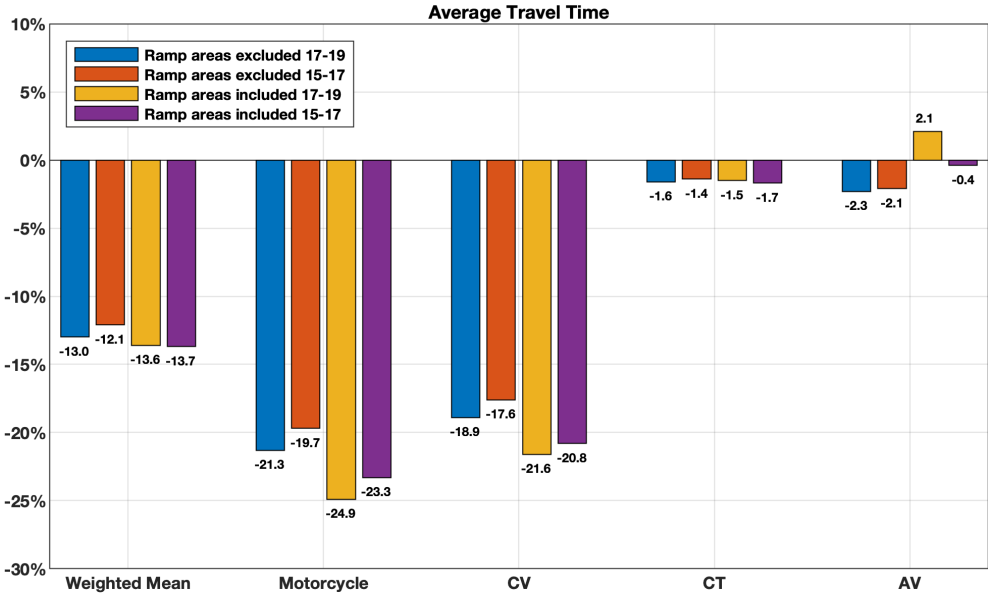

Figure 2.14: Total Travel Time in DLA scenario with scaling 0.7 and penetration rate 30% of CAVs

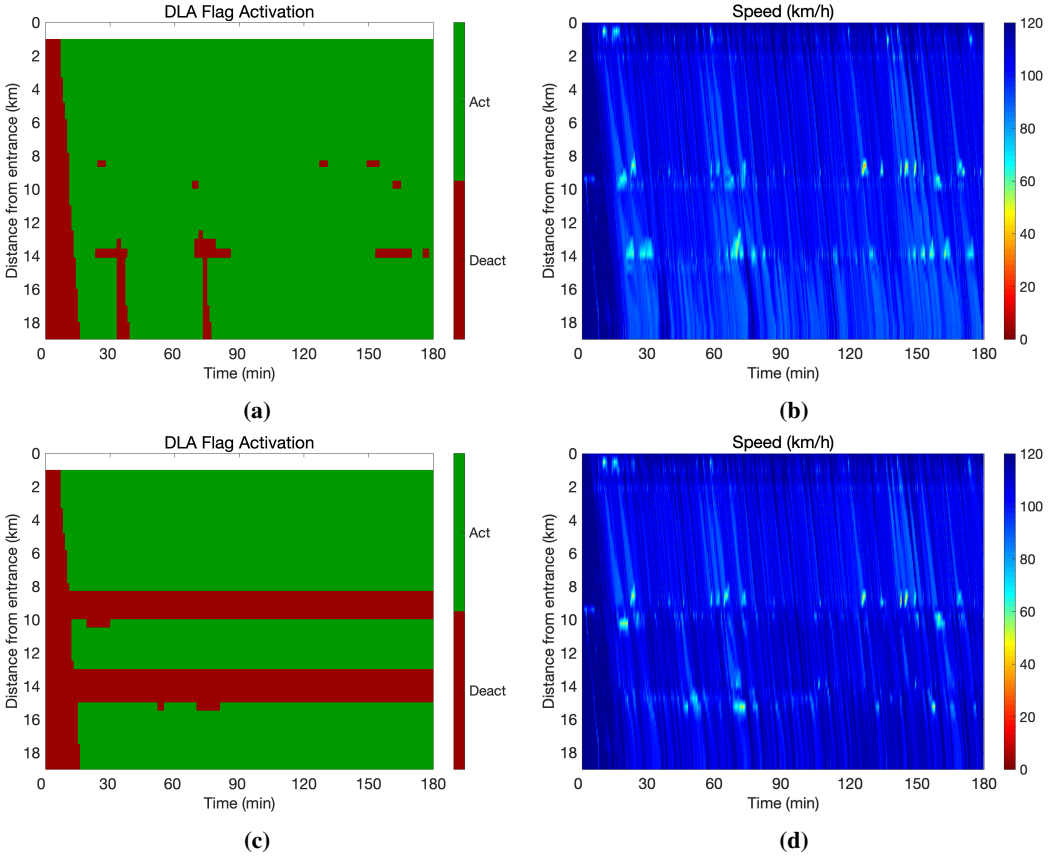

Figure 2.15: DLA flag activation and speed (km/h) plots for traffic demand scaling down to 60% and penetration rate 25% of CAVs with areas around pairs of on/off-ramps included in the assignment logic (a,b) or not (c,d)

2.7 Microscopic investigations for the FRONTIER project

Microscopic investigations were carried out for the needs of the FRONTIER project, utilizing a group of traffic control strategies and schemes at a vehicle/local level application. In detail, a simulation framework that integrates the previously presented traffic control strategies in Sections 2.2, 2.3, 2.4 was delivered, providing the infrastructure to test the FRONTIER scenarios and infer conclusion on the impact of different response plans for operations as well as understand the network performance for planning decisions.

These vehicle/local level application strategies act on mitigating congestion at motorway bottlenecks (on-ramp merge areas, lane-drop areas, tunnels, bridges, etc.), using CAVs as actuators. These strategies include an Adaptive Cruise Control (ACC) time-gap adaptation strategy, a strategy for lane-change advice (LCA) and a Mainstream Traffic Flow Controller (MTFC) that is applied using VSLs. All traffic control strategies were tested in a microscopic simulation environment using the AIMSUN software (Aimsun, 2023) for the test-bed of "Attiki Odos" corridor Athens, Greece.

2.7.1 Aimsun microscopic simulation environment

Any microscopic model relies on car-following and lane-changing models. AIMSUN by default uses the Gipps models for both the car-following and lane-changing (Gipps, 1981, 1986). It is well-known that using the car-following model of Gipps, is very difficult to reproduce the capacity drop phenomena in critical areas, e.g. at a lane-drop or at an on-ramp merge area (Wang et al., 2005). For this reason, some proper modifications (in collaboration with the AIMSUN group) were added to the model so as to reflect in a better way the traffic flow dynamics. For the lateral movements, similar limitations are known. The model is not always able to represent in a realistic way the merging behaviour of vehicles in a lane-drop or an on-ramp merge area, especially when high flows are present (Chevallier and Leclercq, 2009). Therefore, the model is used as is for most parts of the motorway, but at important merging points, it is altered by incorporating certain heuristic rules at specific regions of the network using the microSDK tool of AIMSUN (Roncoli et al., 2014).

2.7.1.1 Development in C++

A software tool has been developed that implements all control strategies in a generic way for performance evaluation in simulation experiments using the AIMSUN software. The software tool is delivered in the form of a DLL which is used as a software component in the AIMSUN micro-simulator. The library has been developed using the C++ programming language that allows for an object-oriented implementation. Among many subroutines and functions, the tool itself has three core functions:

- **Initialise function:** This is the first function to be called. All the configuration parameters of each control strategy are initialised and the appropriate file for storing the output of each control strategy during run-time is created.
- **Main function:** This is the function to be called after the initialise function. It includes seperate function-calls for each control strategy, activated when a control strategy is selected or not. It is called every control step until the end of the simulation horizon.
- **Teardown function:** This function is the last function to be called at the end of the simulation horizon. It frees up the memory of each control strategy and terminates the process.

2.7.1.2 Project integration using AIMSUN APIs

A collaboration with a group of software developers from AIMSUN, took place during the FRONTIER project. The group was in charge of developing an extension (the AIMSUN FRONTIER extension), that integrates all the local-level controllers using the dll file mentioned in Section 2.7.1.1. The extension itself includes a new UI (User Interface) for the configuration parameters needed for the proper use of each local controller, replacing the up to now use of input files. This is, in fact, making faster and more user-friendly the set-up and use of the controller. The input and output functionalities of each local controller are also addressed within the FRONTIER extension, utilizing subroutines and functions (created for the context of FRONTIER) of the AIMSUN software.

To elaborate further, for the input functionality, all the necessary traffic data (e.g. flow, speed, or density) are passed from the AIMSUN database to the selected (activated) controller when and to the extent needed. In a similar manner, for the output functionality, all the decisions delivered by the selected (activated) controller are passed to the AIMSUN database utilizing functions developed for the needs of each local controller, to ensure proper implementation. It is worth mentioning that the above integration required a considerable amount of time to develop the necessary code and perform the required tests for debugging.

The novelty of this extension is not only the UI that replaces the more traditional way of having input files for each controller. It also has the ability to run each local controller within the same simulation, in multiple areas on the network. Before the simulation starts, the areas are appropriately defined using the UI and the necessary information is passed from the UI to the local controller for creating as many instances of itself as the number of areas. This novelty covers the necessity of running the same local controller in bigger networks multiple times, like the one used in the following simulation investigations.

2.7.2 The Attiki Odos motorway test-bed

For the purpose of FRONTIER, the software tool integrated with the FRONTIER extension is tested in the microscopic model of Attiki Odos. In particular, a cropped version of the Attiki Odos corridor (a modern motorway extending along 70 km and constituting a ring road of the greater metropolitan area of Athens) including on-ramp merge areas as well as lane-drop areas, was identified as the network for the needs of the demonstrations. The network illustrated in Fig. 2.16 covers both directions of the corridor, from Metamorphosi to the Airport (eastbound direction) and vice versa.

The modelled eastbound direction has a length of 2.6 km while the modelled westbound direction has a length of 3.1 km. Both directions are subdivided to six segments, where each segment has a unique length between 0.3-0.6 km. For the eastbound direction, two on-ramps denoted by E_ON_1 and E_ON_2 and one off-ramp denoted by E_OFF_1 are included.

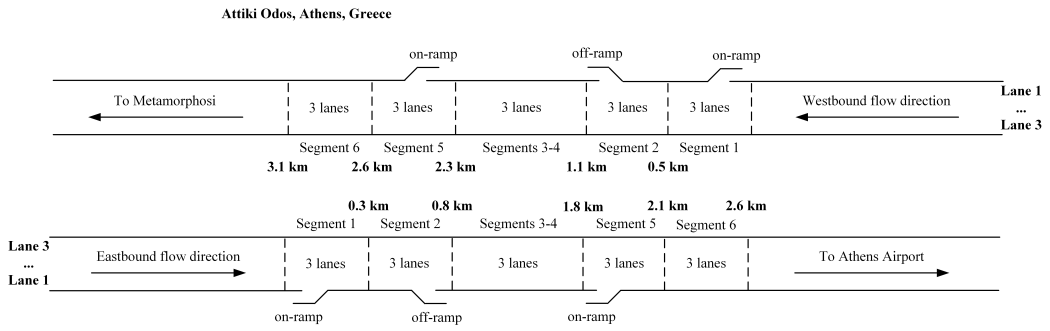

Figure 2.16: The Athens network used for the microscopic simulations.

Similarly, for the westbound direction two on-ramps denoted by W_ON_1 and W_ON_2 and one off-ramp denoted by W_OFF_1 are also included. In both directions all segments consider three lanes. For the remaining part of the motorway network which is not shown in Fig. 2.16, two more on-ramps and off-ramps are included on each direction. We choose to omit this part of the motorway network since it is not included in any local controller segmentation.

According to deliverable D2.3 (FRONTIER, 2022), the microscopic model of Attiki Odos has been calibrated to match the real-life traffic conditions as close as possible. However, congestion phenomena were not observed; hence, the use of any local level controller would make no major difference in the traffic flow. Therefore, it was necessary to create artificial traffic demand profiles, in order to apply any of the local level controllers in scenarios where congestion phenomena are observed.

2.7.3 Microscopic simulation setup for MTFC

Different penetration rates of CAVs were used in the upcoming investigations, carefully selected in order to reflect typical and future market penetrations (20%, 40%, 60%, 80% and 100%). All vehicles (CVs and CAVs) are using a range of different default parameters (e.g. acceleration, deceleration, desired speed etc.), sampled from a normal distribution with different mean μ and standard deviation σ values, truncated within a range of $[min, max]$ values for each one of the parameters. The simulation step used in AIMSUN is set to 1.0 sec and the whole simulation horizon is set to 120 min. Also, the configuration parameters for the MTFC control strategy are set as follows: critical density $\hat{\rho} = 70$ veh/km, control interval $T = 60$ sec, proportional gain $K_P = 4.0$ km^2/(veh·h) and integral gain $K_I = 6.0$ km^2/(veh·h). The control strategy delivers proper VSL values to be implemented with the use of CAVs (actuators).

2.7.4 MTFC investigations

For each one of the scenarios investigated, twenty AIMSUN replications are run for a simulation period of 2 hours, simultaneously for both directions. The same average demand profile is used for all replications with the accompanied results related to one of the replications with Key Performance Indicators (KPIs) close to the average values. The artificial traffic demand profiles for both directions, for the selected replication, are shown in Fig. 2.17. We can see that the mainstream demand (which is the same for both directions, Fig. 2.17a) is increasing for about 35 minutes reaching values ($\approx$ 6000 veh/h) close to the capacity of the bottleneck ($\approx$ 6200 veh/h) and the total on-ramp flow entering the network reaches values around 1500 veh/h, for the eastbound direction, and around 2200 veh/h, for the westbound direction (Fig. 2.17b). As the demand remains high for about 35 minutes, it is expected to activate the bottleneck and create congestion phenomena at the merging area (segment 5, Fig. 2.16) on both directions of the motorway, where the on-ramp with the highest entering flow merges. Then, the demand is falling and finally stays at quite low values for some 35 minutes, thus allowing for free-flow conditions at the end of the simulation period for all scenarios considered.

2.7.4.1 No-control scenario

When no control actions are applied, i.e. no VSL values are calculated to be communicated to CAVs. This scenario will be the main reference for comparison to the aforementioned traffic control strategies. The evaluation of the strategy is achieved using two KPIs. The first is the TTS, which is the actual time spent by vehicles to travel along the network and the waiting time at the queues (origins), and the second is the TD, which is the respective average value of delay encountered by the vehicles when travelling along the network.

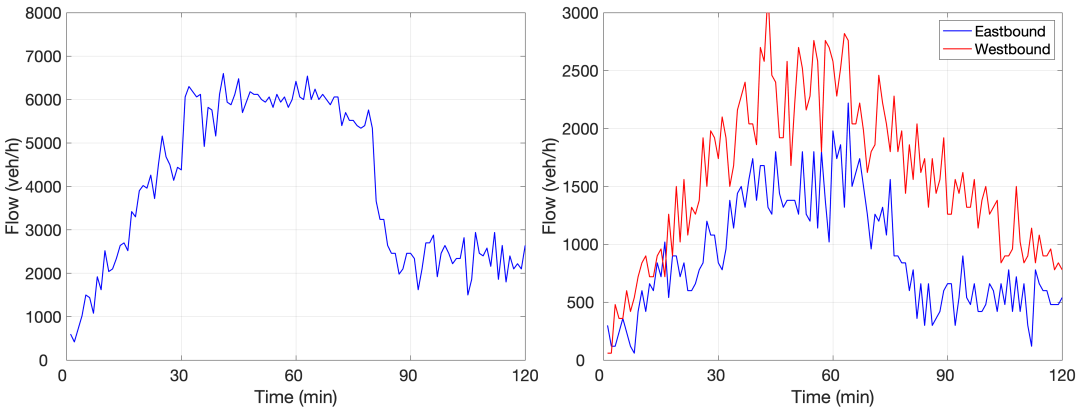

Figure 2.17: Mainstream (left) and on-ramps (right) demand profiles used in one of the replications for testing MTFC for both the eastbound and westbound direction.

Looking at Fig. 2.18, congestion starts around $t = 45$ min (on both directions) due to high values of the arriving demand and the lane-change manoeuvres that are taking place at the merging areas located at the 2.1 km on the eastbound direction and at the 2.6 km on the westbound direction of the motorway. The congestion created spillback phenomena and covers some 2 km upstream of the merging areas, as observed from the speed contour plot displayed in both Fig. 2.18a and Fig. 2.18b. In this case the average TTS obtained a value of 2,225.5 veh·h and the average TD obtained a value of 22.6 sec/km.

2.7.4.2 Control scenario

The MTFC strategy described in Section 2.2.2 is fed with density measurements from the merging area (segment 5, Fig. 2.16) and calculates the VSL values to be applied in the MTFC application area. VSLs are also applied in the acceleration area (downstream of the MTFC area) and the safety areas (upstream of the MTFC area). The MTFC strategy is applied with VSLs communicated to CAVs for various penetration rates. For all the results presented below, we assume full compliance to the suggested MTFC orders and no I2V communication delays.

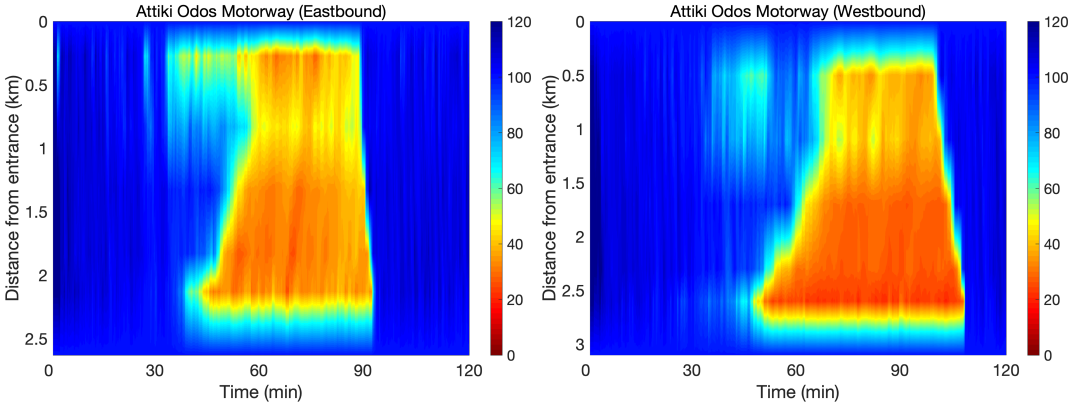

Figure 2.18: No-control – Speed contour plot for the eastbound direction (a) and westbound direction (b).

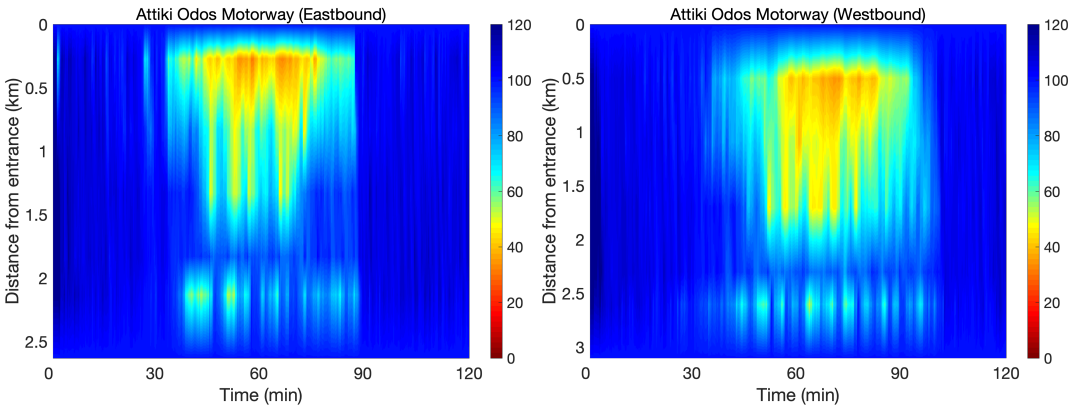

Figure 2.19: MTFC applied using VSLs communicated to 20% of CAVs – Speed contour plots for the eastbound (a) and westbound (b) direction.

The control interval for the PI controller (2.1) that provides the appropriate VSL to be applied, is set equal to 60 sec for both directions of the motorway where the controller is applied. This is done using a set-point equal to the critical density (70 veh/km), for which capacity flow is achieved in the no-control scenario. The VSL bounds are set to 40 km/h and 120 km/h, i.e. the controller is able to act within a broad range of values to accomplish its goal.

Looking at Fig. 2.19, speed contour plots are displayed for both directions when the MTFC strategy is implemented for a 20% penetration rate of CAVs. It is obvious from the plots that no MTFC actions are necessary for the first 35 min on both directions. Then, the density at the merging area is rising and is crossing the set-point (see Fig. 2.20, upper row). Therefore, the VSL values ordered by the controller are gradually decreasing, reaching the minimum admissible value of 40km/h on both the eastbound and westbound direction (see Fig. 2.20, bottom row).

In addition, density at the bottleneck area is kept close to the selected set-point and, as a result, a controlled congestion is created further upstream. Note that for the eastbound

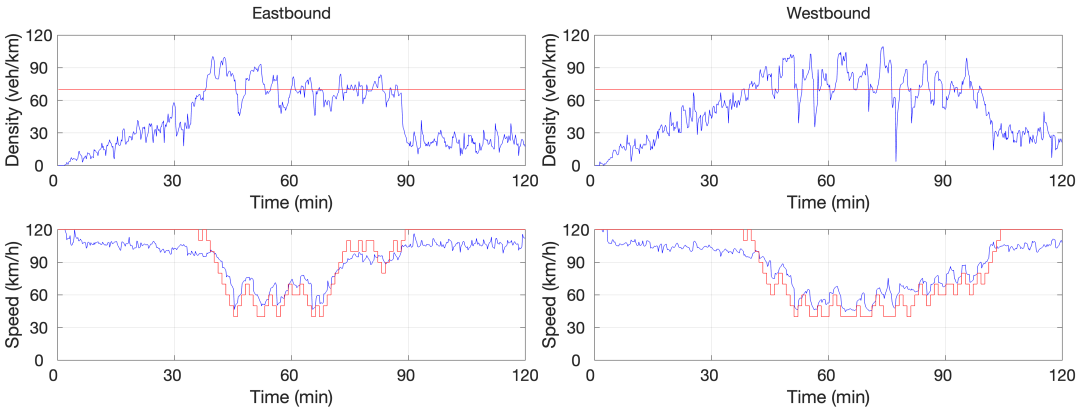

Figure 2.20: MTFC applied using VSLs communicated to 20% of CAVs – Density (blue line) at the lane-drop area with the corresponding critical density (red line) (upper row of (a) and (b)); and measured speed (blue line) at the MTFC application area with the corresponding speed limits (red line) (bottom row of (a) and (b).

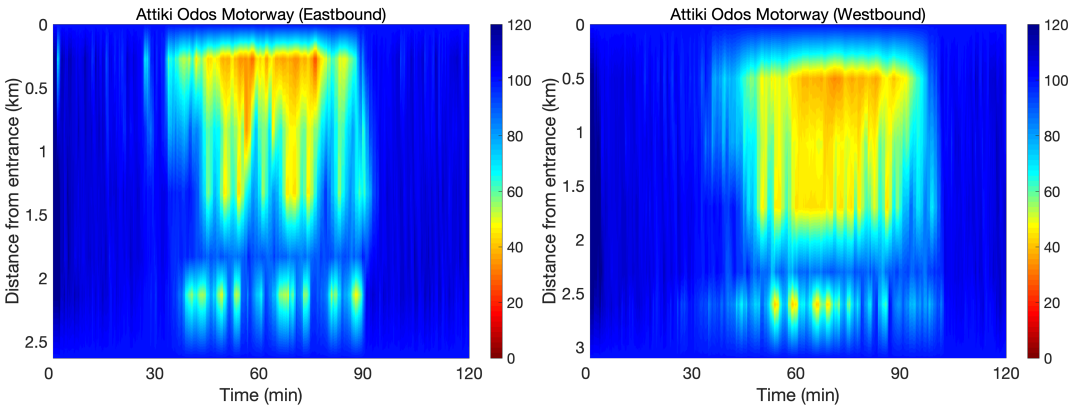

(a) **(b)**

Figure 2.21: MTFC applied using VSLs communicated to 40% of CAVs – Speed contour plots for the eastbound (a) and westbound (b) direction.

direction, the area at which the controller is operating is between the 0.5 km and the 1.5 km whereas for the westbound direction the area lies between the 0.5 km and the 2.0 km. Hence, the congestion observed at these areas is deemed normal. For this case, the percentages of improvement over the no-control case for both KPIs are 3.7% for TTS and 8.9% for TD. It is worth noting that a percentage of 20% of CAVs is able to drive the average speed of all vehicles close to the VSL value ordered by the PI controller. The MTFC strategy is now applied for a penetration rate of 40% of CAVs. The same setup is used for the PI controller as in the previous case and the resulting speed contour plots are presented in Fig. 2.21. As in the previous case, no MTFC actions are necessary for the first 35 min on both the eastbound and westbound direction. Consequently, as shown in Fig. 2.22 (upper row), the density at the merging area is exceeding the selected set-point on both directions.

As a result, the VSL values ordered by the controller are reduced gradually within bounds. All practical implementation aspects mentioned above are considered. The density at the merging area remains near the set-point until the controller reaches saturation. Speed measurements at the MTFC application area suggest that a penetration rate of 40% is adequate to

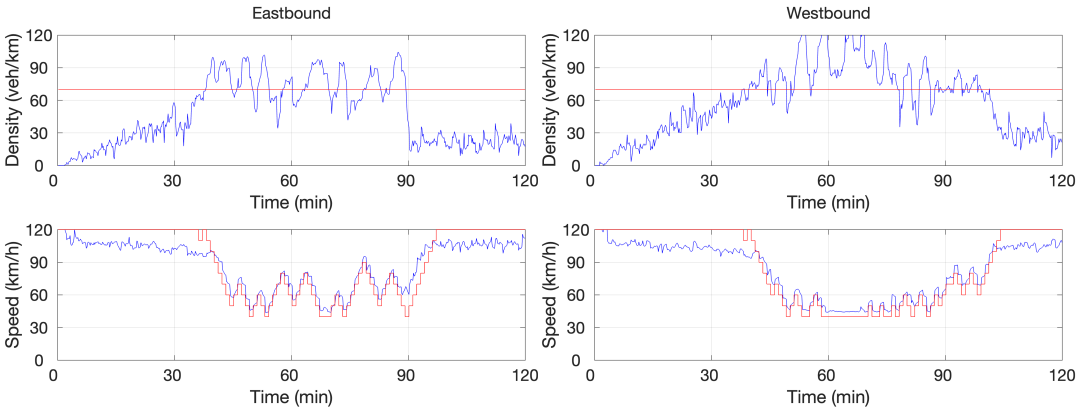

(a) **(b)**

Figure 2.22: MTFC applied using VSLs communicated to 40% of CAVs – Density (blue line) at the lane-drop area with the corresponding critical density (red line) (upper row of (a) and (b)); and measured speed (blue line) at the MTFC application area with the corresponding speed limits (red line) (bottom row of (a) and (b).

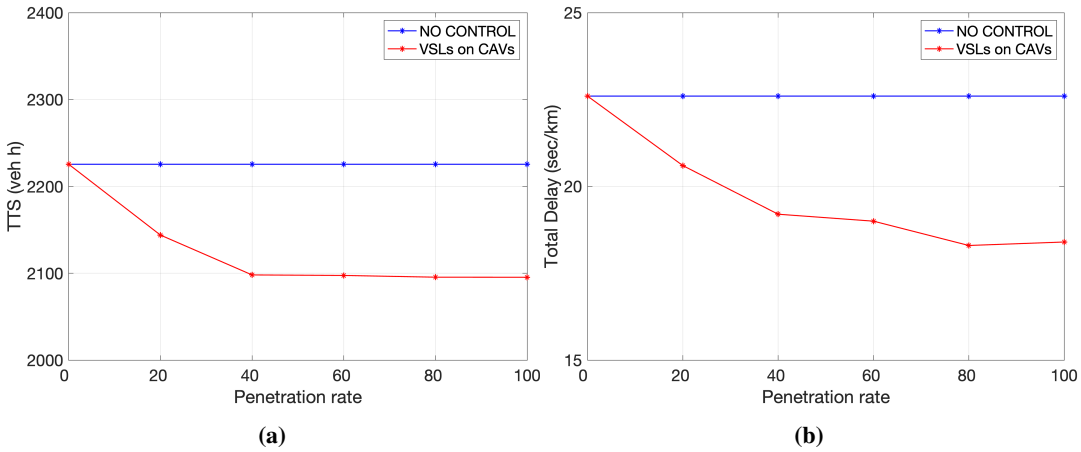

Figure 2.23: MTFC – Average Total Time Spent (TTS) and Total Delay (TD) per penetration rate of CAVs for the no-control and control case.

drive the average speed of all vehicles close to the VSL value ordered by the controller (Fig. 2.22, bottom row).

As a result of the VSL actions, a controlled artificial congestion is created further upstream. The average TTS obtained a value of 2,109.5 veh·h and the average TD obtained a value of 19.0 sec/km. The percentage of improvement over the no-control case is 5.2% for TTS and 16.1% for TD, respectively. As demonstrated in Fig. 2.23, a corresponding increase in the level of improvement achieved in the average TTS and TD values is observed as the penetration rates of CAVs is increasing. Additional figures related to the control scenario can be found in Appendix B.1.

2.7.5 Microscopic simulation setup for LCA

Following a similar manner as in the previous investigations of the MTFC control strategy, the penetration rates of CAVs were selected between the range of 20%-100%. This also implies that in the upcoming investigations the same setup was used for all vehicles (CVs and CAVs), the same simulation step was used in the AIMSUN simulator and the same traffic demand profiles were used to derive the no-control and control scenarios. For the configuration parameters of the LCA strategy, the control inverval T is set equal to 10 sec and the density set-points were carefully selected to achieve a desired distribution of vehicles across all lanes. Hence, the selected values for the eastbound direction were set as follows: 28 veh/km/lane for lane 1 and 40 veh/km/lane for lanes 2 and 3 downstream of the merging areas (bottleneck); for the westbound direction the selected values were set as follows: 25 veh/km/lane for lane 1 and 28 veh/km/lane for lanes 2 and 3. Note that the lane numbering is illustrated for both directions in Fig. 2.16.

2.7.6 LCA investigations

In order to investigate the use of the LCA strategy, a no-control scenario where no control actions are applied, will be the main reference for comparison. As already mentioned, the no-control scenario used for the evaluation of the strategy is the one previously presented in Section 2.7.4.

2.7.6.1 No-control scenario

Since the LCA strategy is a lane-based strategy, it is proper to investigate the level of capacity drop on each lane in the case where no control actions (lane changing orders) are applied to the motorway. Specifically, looking at Figs. 2.24c, 2.24d a corresponding capacity drop equal to 18% of the nominal capacity for the three lanes is observed for the eastbound direction and a capacity drop equal to 20% for the westbound direction. The congestion created on both directions spills back covering a few segments upstream (~2.5 km), as shown in the speed contour plots displayed in Fig. 2.18a for the eastbound and Fig. 2.18b for the westbound direction. In addition, density trajectories are displayed in Fig. 2.24a, 2.24b for each lane at the merging area for both directions. It is obvious from the plots that approximately at $t =$ 35 min a steep rise on density is observed in lanes 1, 2 and 3 which indicates a corresponding decrease in speed and the onset of congestion in all lanes.

Looking at the outflows per lane depicted in Fig. 2.24c, one can easily observe that for the eastbound direction lane 1 (which is the lane next to the merging lane, blue trajectory) attains its capacity below the nominal capacity (≈2200 veh/h) for a few minutes. Then, as soon as speed breaks down, lane 1 breaks down and congestion spreads rapidly to lane 2 and lane 3 that also break down at a lower flow level (around 2000 veh/h and 1800 veh/h respectively). For the westbound direction, similar conclusions can be drawn. Looking at Fig. 2.24d, as soon as lane 1 (which is the lane next to the merging lane, blue trajectory) reaches values close to (≈2000 veh/h) suddenly drops to 1800 veh/h due to speed break-down, that also affects the adjacent lanes 2 and 3. It is worth noting that after $t = 45$ min a flow value of ≈1800veh/h is observed at all lanes. In this no-control scenario, the average values for TTS and TD are the ones observed in Section 2.7.4.1 i.e. 2,225.5 veh·h for TTS and 22.6 sec/km for TD.

2.7.6.2 Control scenario

The main goal of the LCA controller is to achieve a desired (specified) distribution of densities across different lanes in the area downstream of the merging area (bottleneck). This enables each lane to utilise its full capacity when and to the extend needed. The controller is using real-time density measurements per lane for six segments, five upstream of the bottleneck (including the bottleneck) and one downstream of it. The control step for the lane change controller is set equal to 10 sec and lateral flows per lane are produced accordingly. These flows are then communicated to CAVs as lane change advices to be implemented, if other safety constraints allow it (i.e. safety constraints from the microscopic simulator).

For the case of 40% of CAVs, Fig. 2.25 illustrates the speed contour plots obtained by applying the controller on both directions of the motorway. The set-points for the eastbound and the westbound direction are the ones mentioned in Section 2.7.5. Looking at Fig. 2.26a one can easily observe that for the eastbound direction a higher outflow is now achieved for each lane close to the nominal capacity (~2200 veh/h) for about 30 min. After 60 min of simulation time, the lateral flows ordered by the controller cannot be fully executed because the penetration rate is insufficient and, as a result, the goal of the controller is not fully accomplished (see Fig. 2.27a). Congestion is not avoided, due to high demand, spilling back covering almost 1.2 km upstream of the bottleneck area. For the westbound direction, Fig. 2.26b indicates that a penetration rate of 40% of CAVs is able to keep the outflows per lane close to 2000 veh/h and Figs. 2.27b, 2.27d and 2.27f prove that the densities per lane are close to the set-point of the lane change controller. Compared to the reference scenario (the no-control scenario), the capacity of each lane is increased and congestion is reduced in space and time but not fully avoided. The percentages of improvement over the no-control scenario

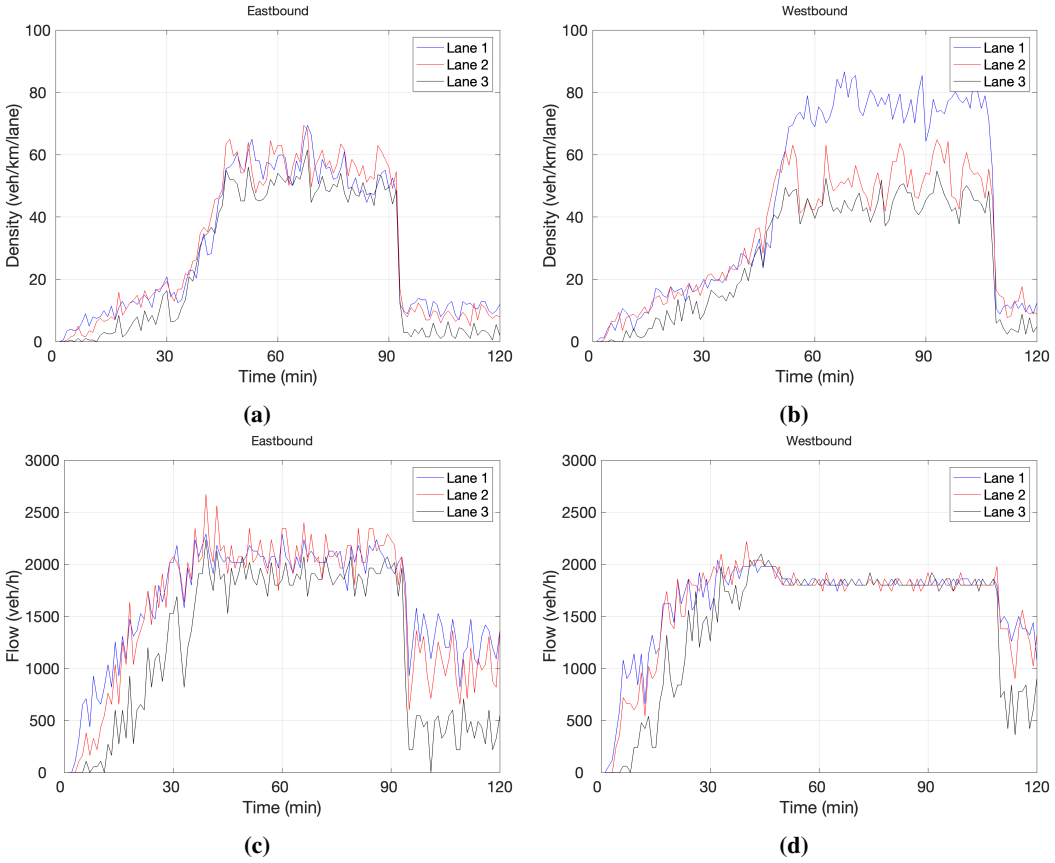

Figure 2.24: No-control – Per lane density trajectories (a) and (b); and per lane outflow trajectories at the merging area (c) and (d) for both directions

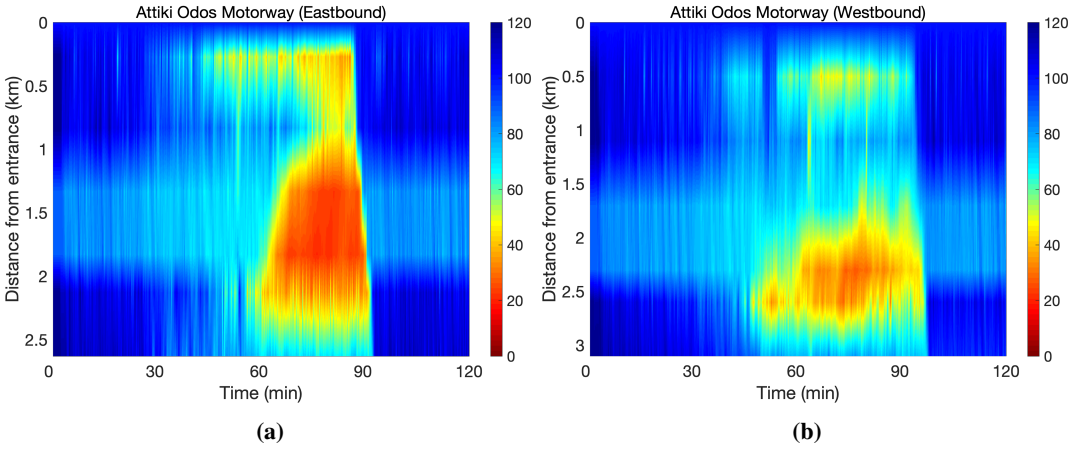

Figure 2.25: LCA – Speed contour plots for the eastbound direction (a) and westbound direction (b) for 40% of CAVs

for both directions and performance indices are 5.7% for the average TTS and 11.4% for the average TD.

For a higher penetration rate of CAVs (80%), the results depicted in Fig. 2.30a illustrate that for the eastbound direction all lanes can attain higher flow rates for an extended period of time until the demand reaches lower values after $t = 90$min. This is normal, since the lane changes recommended by the lane change controller are executed successfully and, as a result, the goal of the controller is virtually achieved (see also Figs. 2.28a, 2.28c, 2.28e).

Since the total capacity value is now higher (≈6900 veh/h), no congestion is observed (Fig. 2.29a). For the westbound direction, similar conclusions can be drawn. In comparison to the previous case of 40% of CAVs, the outflows for each of the lanes 1, 2 and 3 are even higher (Fig. 2.30b), reaching at short periods of time values close to 2500veh/h. On the other hand, density values for each of the lanes 1, 2 and 3 (see Figs. 2.28b, 2.28d and 2.28f) are in fully agreement with the selected set-points and as a result the goal of the controller is fully achieved.

For this penetration rate, the average value for TTS is 2,019.6 veh·h and the average TD obtained a value of 18.1 sec/km. As depicted in Fig. 2.31, the percentage of improvement both on TTS and TD becomes more significant in comparison to the reference scenario, eventually reaching a 9.3% on TTS and 19.8% on TD. Additional figures related to the control scenario can be found accordingly in Appendix C.

It is worth noting that even with high penetration rates, solely relying on LCC may not be sufficient in preventing breakdowns if the demand is further increased beyond the increased capacity. While LCC can increase the bottleneck capacity, it does not guarantee the prevention of congestion in such scenarios. In these cases, a potential solution could be to integrate LCC with MTFC actions.

2.7.7 Microscopic simulation setup for the Integrated MTFC and LCA

In order to see the effect of applying the MTFC control strategy in addition to the LCA control strategy, we choose to use the same setups as in the previous investigations (2.7.4, 2.7.6). Hence, for the MTFC control strategy we use the setup as described in Section 2.7.3 and for the LCA control strategy we use the setup as described in Section 2.7.5.

2.7.8 Integrated MTFC and LCA investigations

As already mentioned, the following investigations are derived when MTFC is applied in addition to LCA. This is to ensure that no congestion phenomena will appear at the bottleneck area and that the increased capacity due to lane change advices will maintain for longer periods during simulation. Similarly to all previous investigations, the same average traffic demand profiles (Fig. 2.17) are also used in this scenario.

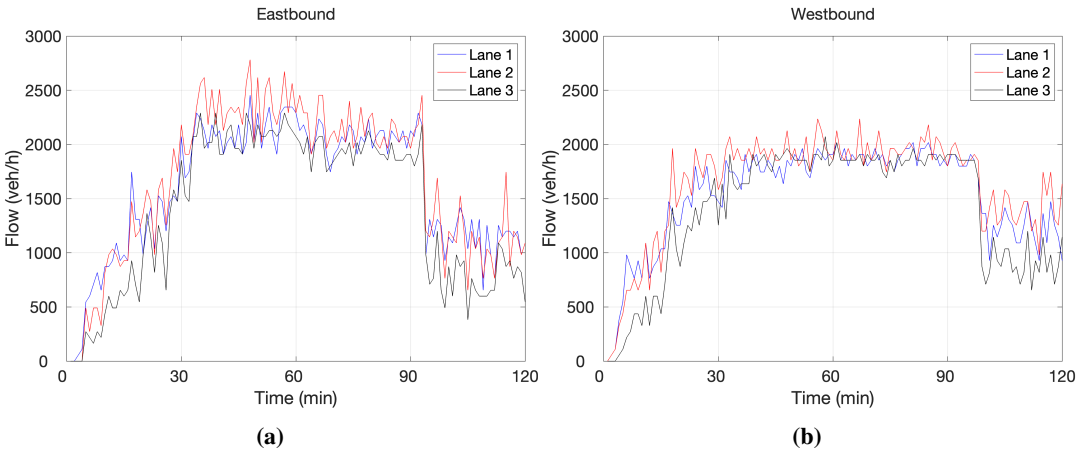

Figure 2.26: LCA – Per lane outflow trajectories at the merging area (bottleneck) for the eastbound direction (a) and westbound direction (b) for 40% of CAVs.

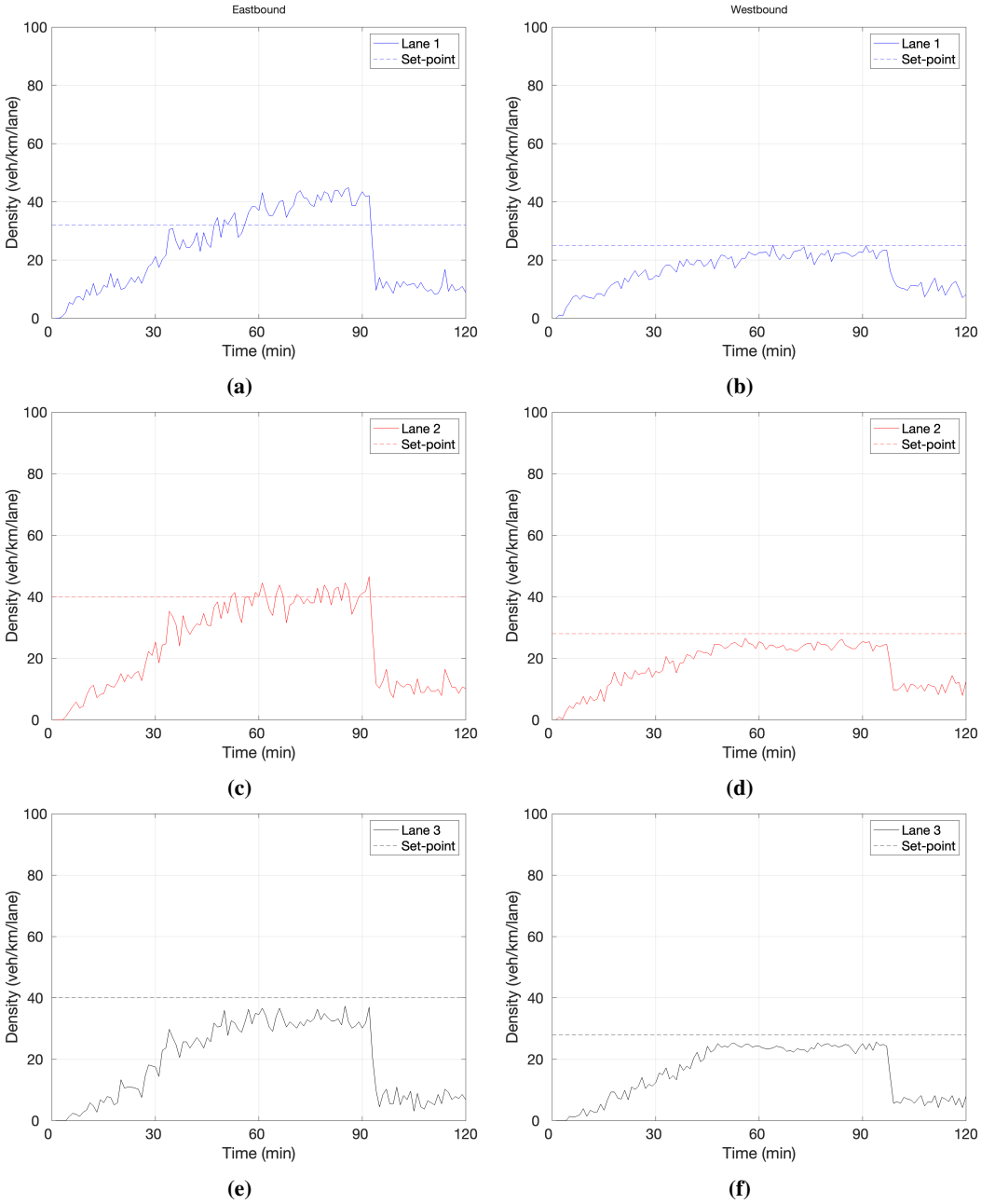

Figure 2.27: LCA – Per lane density trajectories (continuous lines) and corresponding set-points (dotted lines) downstream of the bottleneck area for 40% CAVs for both the eastbound (left) and westbound (right) direction.

2.7.8.1 Control scenario

Similarly to all previous investigations, in order to investigate the integrated use of both traffic control strategies in the control scenario, a no-control scenario will be the main reference for comparison. The no-control scenario is the one presented previously in Section 2.7.4.1.

For the integrated control scenario, we use the same setup for both the controllers, like the ones used in Sections 2.7.4.2 and 2.7.6.2. For the penetration rate of 20% of CAVs, one can easily observe that there is an increased improvement compared to the previous non-integrated scenarios of MTFC and LCA on both directions. For the eastbound direction, Fig. 2.32a indicates that the combined use of both control actions is able to eliminate any congestion phenomena close to the bottleneck area (segment 5, Fig. 2.16). The VSL actions

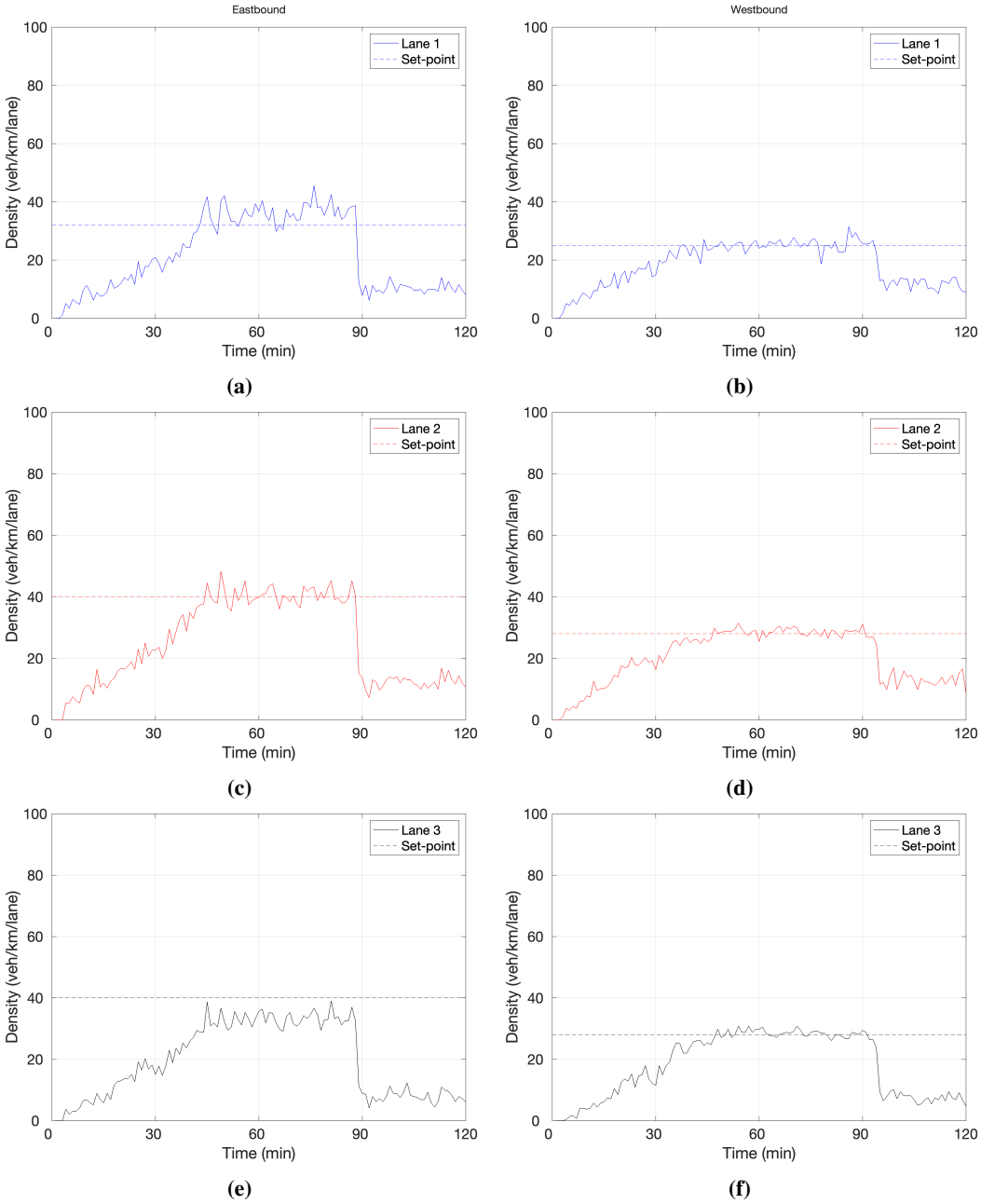

Figure 2.28: LCA – Per lane density trajectories (continuous lines) and corresponding set-points (dotted lines) downstream of the bottleneck area for 80% CAVs for both the eastbound (left) and westbound (right) direction.

appearing in Fig. 2.33a, prove that density at the merging area is always close to the set-point and the VSL values ordered by the controller are gradually decreasing, reaching shortly the minimum admissible value of 40km/h. On the other hand, density downstream of the bottleneck area is always close to the selected set-point per lane (Fig. 2.34a, 2.34c, 2.34e) as the controller exploits the per-lane capacity.

For the westbound direction, similar conclusions can be drawn. For this case, the average TTS observed a value of 2,048.2 veh·h and the average TD obtained a value of 17.4 sec/km. The percentage of improvement over the no-control scenario corresponds to 8.0% for TTS and 23.1% for TD. As demonstrated in Figs. 2.35a and 2.35b, higher penetration rates of CAVs, result in greater improvement on the average TTS and on the average TD. In addition,

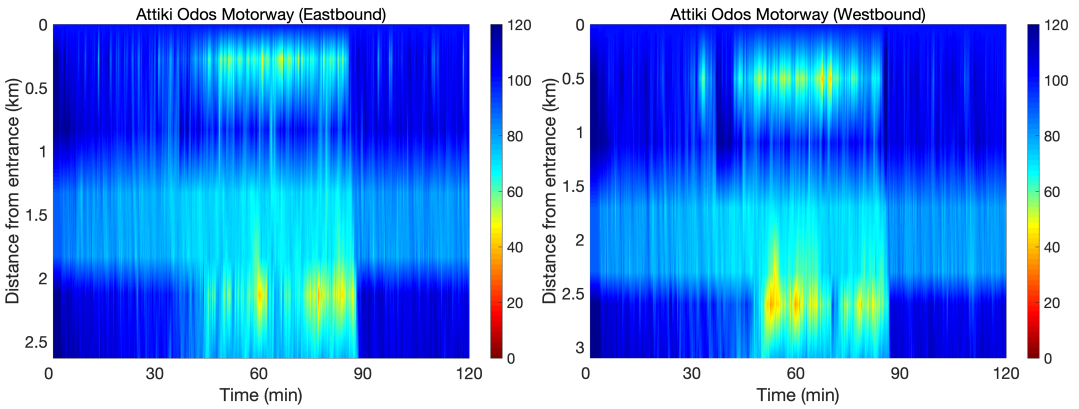

(a) **(b)**

Figure 2.29: LCA – Speed contour plots for the eastbound direction (a) and westbound direction (b) for 80% of CAVs

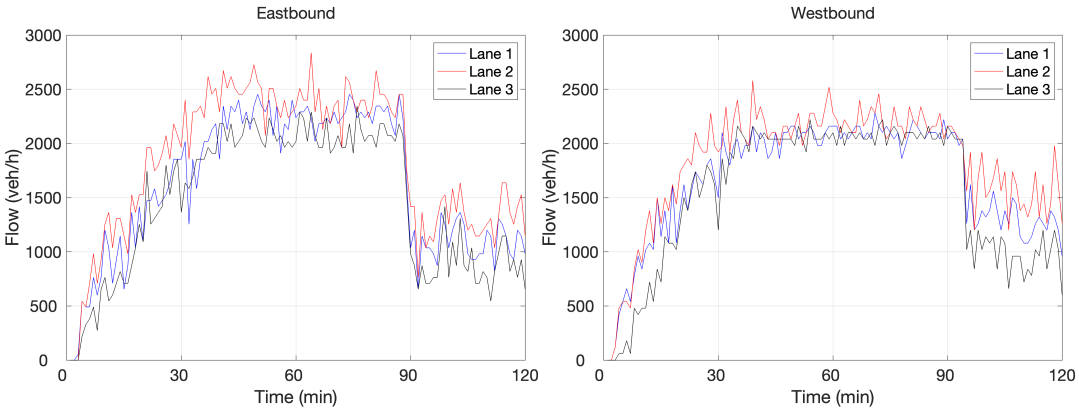

(a) **(b)**

Figure 2.30: LCA – Per lane outflow trajectories at the merging area (bottleneck) for the eastbound direction (a) and westbound direction (b) for 80% of CAVs.

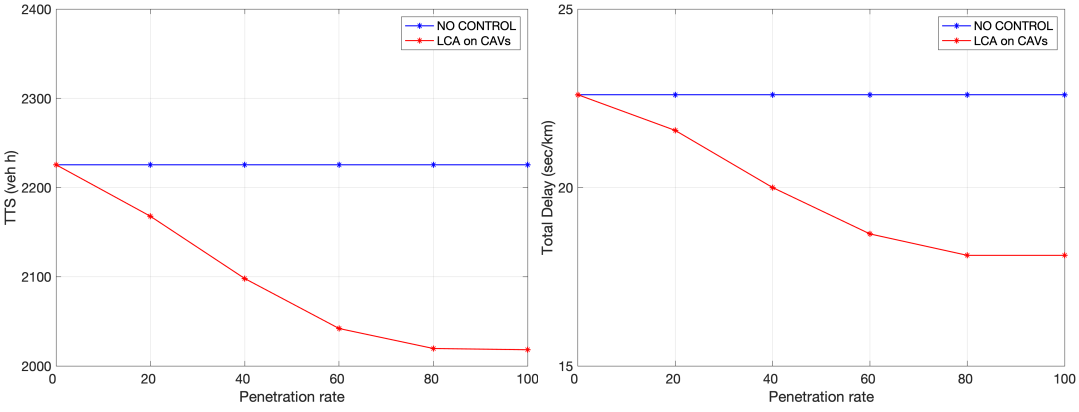

(a) **(b)**

Figure 2.31: LCA – Average Total Time Spent (TTS) and Total Delay (TD) per penetration rate of CAVs for the no-control and control scenario.

for all penetration rates the integration of the LCA and MTFC controllers (Fig. 2.35, magenta lines) leads to further improvement when compared to the MTFC scenario (Fig. 2.35, red

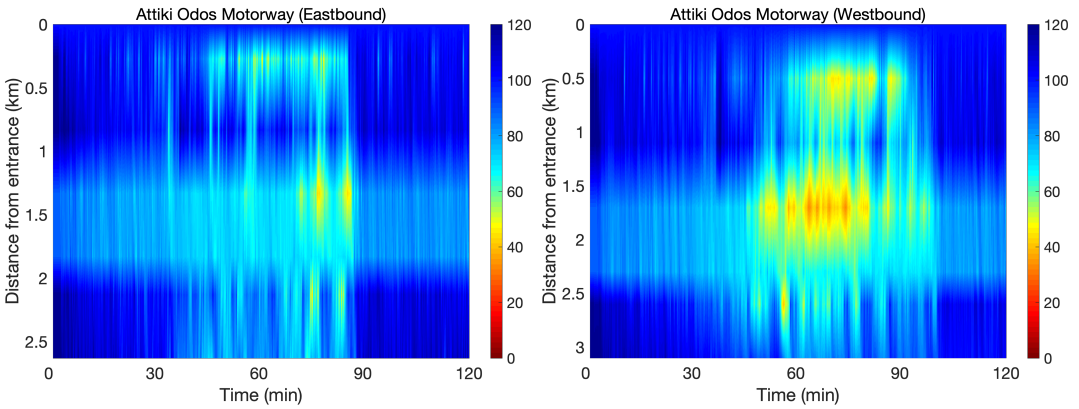

(a) **(b)**

Figure 2.32: Integrated – Speed contour plots for the eastbound direction (a) and westbound direction (b) for 20% of CAVs

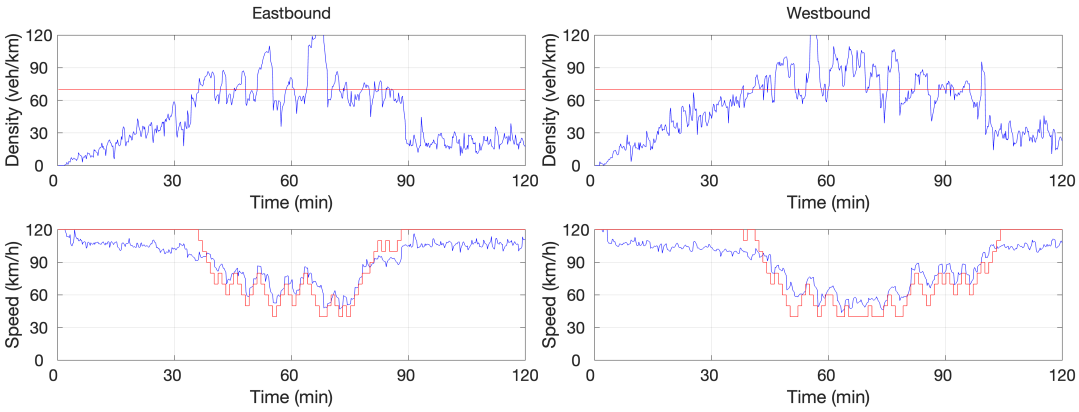

(a) **(b)**

Figure 2.33: MTFC applied using VSLs communicated to 20% of CAVs – Density (blue line) at the lane-drop area with the corresponding critical density (red line) (upper row of (a) and (b)); and measured speed (blue line) at the MTFC application area with the corresponding speed limits (red line) (bottom row of (a) and (b).

line) and LCA scenario (Fig. 2.35, black line). Additional figures related to the control scenario can be found accordingly in Appendix D.

2.7.9 Microscopic simulation setup for ACC

In this section, we briefly explain the microscopic simulation setup used for the time-gap adaptation controller. Following a similar manner as in Sections 2.7.3, 2.7.5, 2.7.7, two classes of vehicles are used in our experiments. The first one is the class of conventional vehicles and the second one is the class of vehicles equipped with ACC capabilities. In order to explore all the aspects of the controller, different penetration rates of ACC vehicles e.g. 20%, 40%, 60%, 80% and 100% were considered. In addition, for both classes of vehicles, a range of parameters (e.g. time-gap, acceleration, deceleration, desired speed etc.), sampled from a normal prespecified distribution with different mean μ and standard deviation σ values are considered. Before being assigned to each one of the vehicles, these parameters are also truncated to remain within a range of $[min, max]$ values.

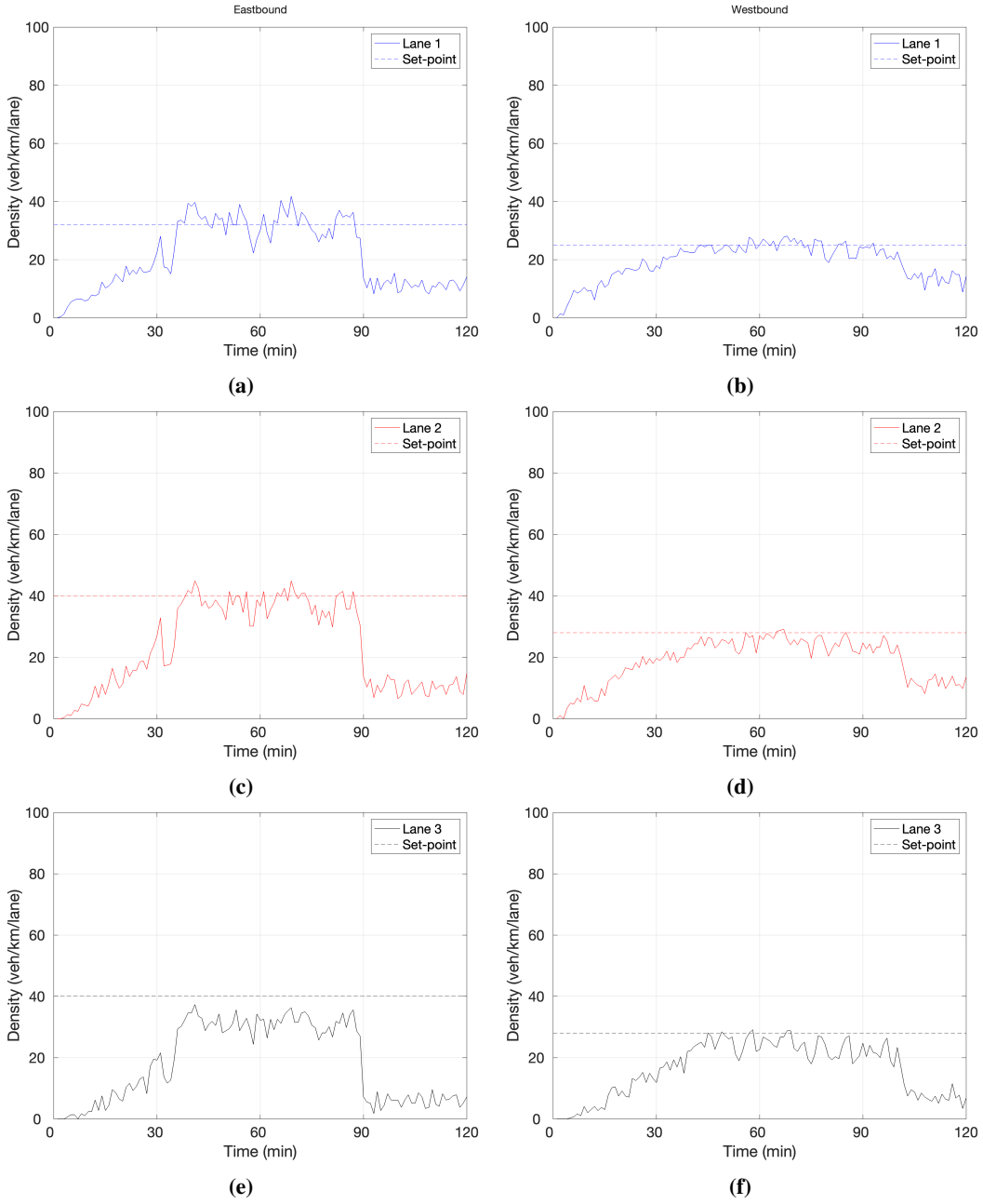

Figure 2.34: Integrated – Per lane density trajectories (continuous lines) and corresponding set-points (dotted lines) downstream of the bottleneck area for 20% CAVs for both the eastbound (left) and westbound (right) direction.

In order to see the effects of the ACC controller, the simulation step for the microscopic simulation is set equal to the reaction time used for the ACC vehicles. For the conventional vehicles this is not a prerequisite. Hence, the reaction time of ACC vehicles is set to 0.1 sec and the reaction time of conventional vehicles is set equal to 1.0 sec. Moreover, the configuration parameters for the time-gap adaptation strategy are set as follows: control step $t_c = 30$ sec, congestion speed $v_{cong} = 60$ km/h, minimum time-gap value $T_{min} = 0.8$ sec, maximum time-gap value $T_{max} = 2.2$ sec, minimum flow value per lane $Q_{min} = 1000$ veh/h, maximum flow value per lane $Q_{max} = 1500$ veh/h.

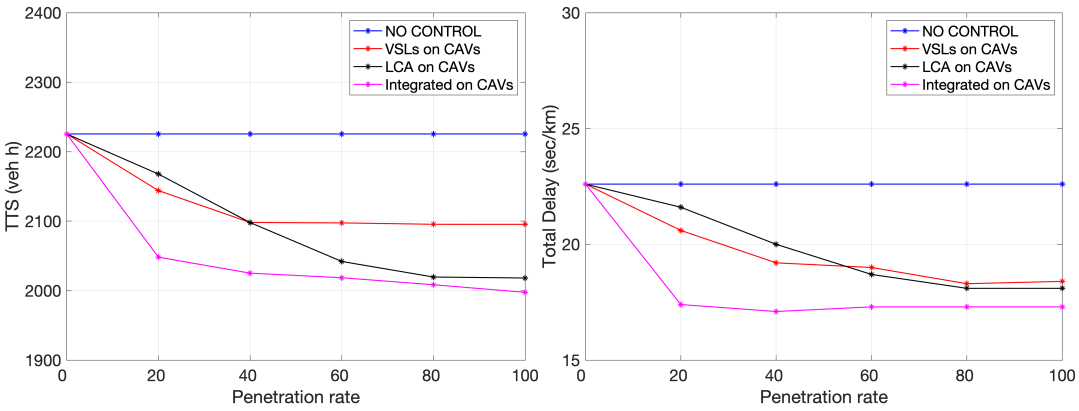

(a) **(b)**

Figure 2.35: Average Total Time Spent (TTS) and Total Delay (TD) per penetration rate of CAVs for all the control scenarios.

2.7.10 ACC investigations

Another traffic control strategy has been evaluated on the microscopic model of Attiki Odos using the artificial traffic demand profiles depicted in Fig. 2.36 for both directions. The same average demand profiles are used for all replications with the accompanied results related to one of the replications with KPIs close to the average values. We can see that the mainstream demand (which is the same for both directions, Fig. 2.36a) is increasing for about 30 minutes reaching values (≈5000 veh/h) and the total on-ramp flow entering the network for both directions reaches values close to 2000 veh/h. As the total demand remains at high values it is expected to activate the bottlenecks and cause congestion at the merging areas (segment 5, Fig. 2.16) on both directions of the motorway where the on-ramp with the highest entering flow merges. Then, the demand falls and finally stays at quite low values for some 35 minutes, thus allowing for free-flow conditions at the end of the simulation period for all scenarios considered.

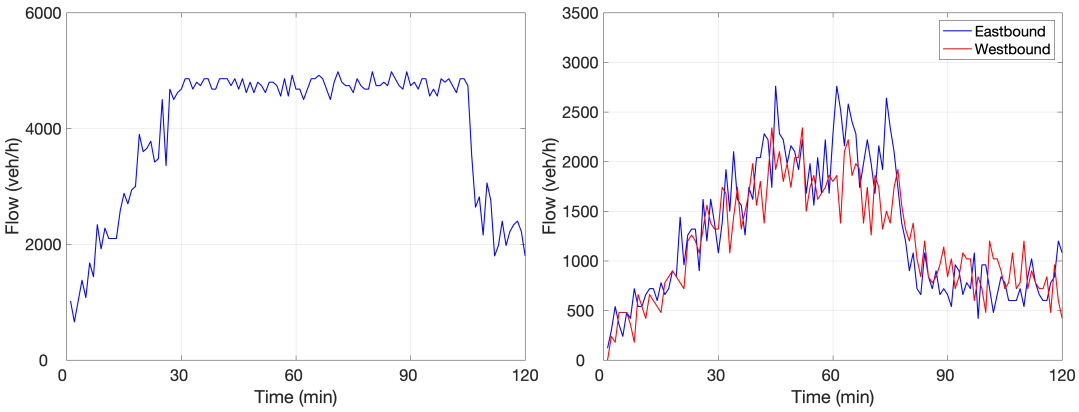

(a) **(b)**

Figure 2.36: ACC – Mainstream (a) and on-ramps (b) demand profiles used in one of the replications for testing the time-gap adaptation strategy for both the eastbound and westbound direction.

2.7.10.1 Scenario 1: ACC-based control without any time-gap adaptation

For this base-case scenario, the time-gap values for the ACC-equipped vehicles are selected from a range with a mean that is higher than that of the manually-driven vehicles. For the manually-driven vehicles a mean value of 1.3 sec is selected and for the ACC-equipped vehicles a value of 1.6 s is selected.

Table 2.2 presents the average (over the twenty replications) TD achieved, considering different penetration rates, for this scenario and the difference observed, compared to PR (0%). It can be observed that conservative (high) time-gap values lead, as expected, to higher TD values (longer delays) that increase with the increase of the PR. On the other hand, Table 2.2 also presents the average (over the twenty replications) TTS achieved, considering different penetration rates (PR), for this no-control adaptation scenario and the difference observed, compared to PR (0%). Similarly, to the TD values, conservative (high) time-gap values lead, as expected, to higher TTS values (longer travel time experience) that increase with the increase of the PR. It is worth mentioning that the values for both KPIs for all the scenarios investigated, are calculated from the available measurements of flow, density, and speed from all the segments used in the ACC controller.

Speed contour plots for the eastbound direction and for all penetration rates of CAVs including the case where only manual vehicles are considered, are displayed in Fig. 2.37. Looking at the plots, one can easily observe that as the penetration rate of ACC-equipped vehicles increases the congestion increases in space and time covering several kilometres upstream of the bottleneck area (due to an on-ramp merging), located at the 2.1 km of the motorway (segment 5, Fig. 2.16).

Similar conclusions are derived for the westbound direction. As depicted in Fig. 2.38, speed contour plots for all penetration rates of CAVs, including the case where only manual vehicles are considered, indicate the formation of congestion at all cases. Specifically, looking at Fig. 2.38a strong congestion initiates at the 2.6 km, spilling back covering almost 0.5 km of the motorway. As the penetration rate of ACC-equipped vehicles increases, a more pronounced congestion is observed on the motorway that covers several kilometres upstream of the bottleneck area (2.6 km), where an on-ramp merges to the motorway (segment 5, Fig. 2.16). Additional figures related to Scenario 1 can be found in Appendix A.3.

Table 2.2: Scenario 1: Total Delay (TD) and Total Time Spent (TTS) for various PR.

	Total Delay (veh·h)		Total Time Spent (veh·h)	
PR (%)	Scenario 1	Difference (%)	Scenario 1	Difference (%)
0	114.8	-	708.8	-
20	180.3	57.0	828.1	16.8
40	212.7	85.2	890.9	25.7
60	223.5	94.6	912.1	28.7
80	234.7	104.4	935.9	32.1
100	270.5	135.6	1017.0	43.5

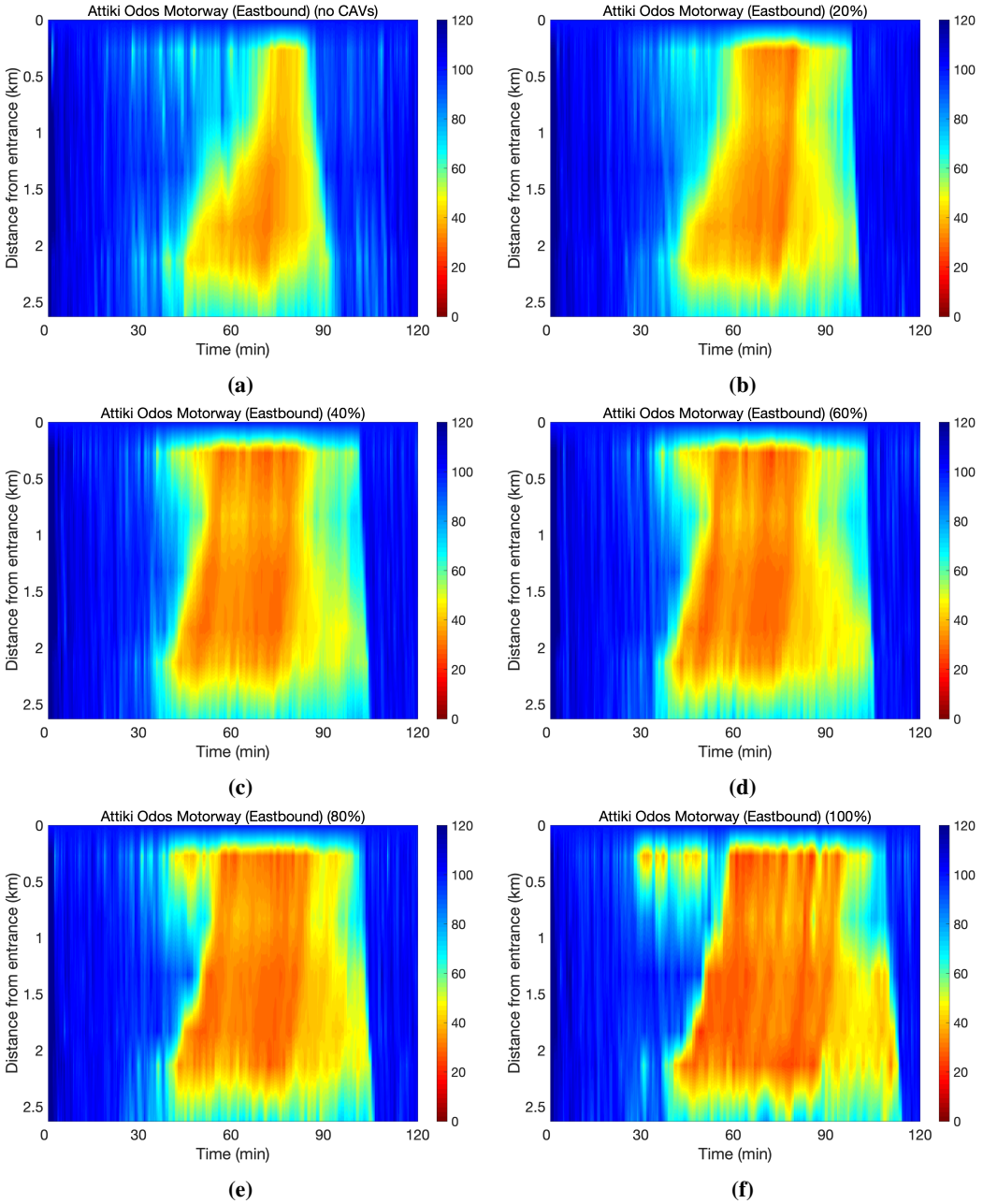

(a) **(b)** **(c)** **(d)** **(e)** **(f)**

Figure 2.37: ACC – Scenario 1: Speed contour plots for the eastbound direction and for all penetration rates of CAVS; no CAVs, 20% CAVs, 40% CAVs, 60% CAVs, 80% CAVs, 100% CAVs.

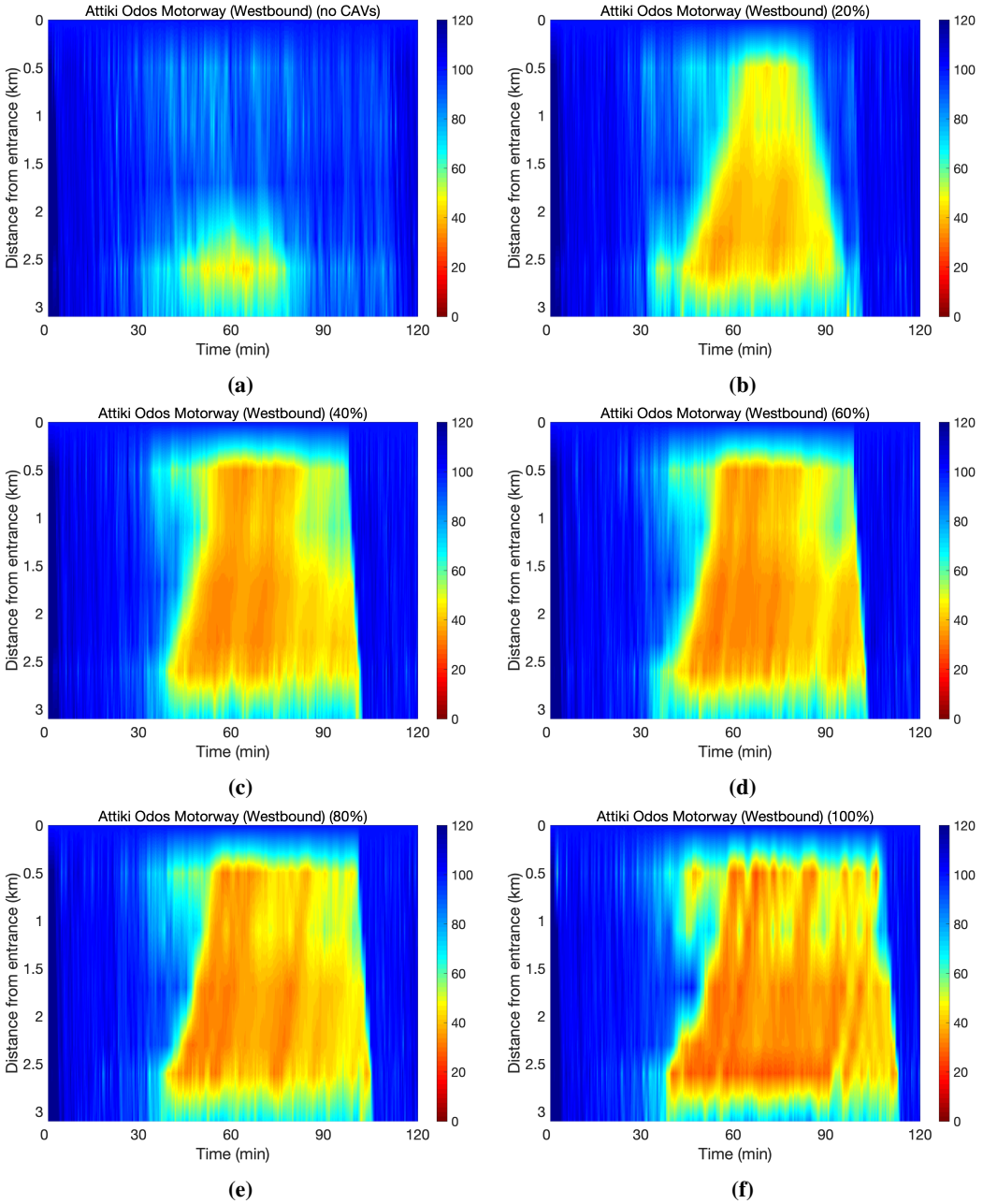

(a) **(b)** **(c)** **(d)** **(e)** **(f)**

Figure 2.38: ACC – Scenario 1: Speed contour plots for the westbound direction and for all penetration rates of CAVS; no CAVs, 20% CAVs, 40% CAVs, 60% CAVs, 80% CAVs, 100% CAVs.

2.7.10.2 Scenario 2: ACC-based control applying only capacity increase using time-gap adaptation

In the second scenario, we apply ACC-based control trying to achieve capacity increase for each segment using time-gap adaptation. The configuration parameters used in the time-gap adaptation strategy are the ones presented in Section 2.7.9. A stepwise function is used, as the one shown in Fig. 2.3b, with an increment for the flow that is equal to 125.0 veh/h/lane and an increment for the time-gap that is equal to 0.35 sec. The frequency used for updating the individual time-gap setting of ACC-equipped vehicles is set to once every simulation step (0.1 sec). This is done to make sure that ACC-equipped vehicles receive the correct information even when crossing segment boundaries. Table 2.3 presents the average TD achieved, considering different PR and the difference observed, compared to the same PR of the no-control scenario. The use of time-gap adaptation achieves significant improvements, especially for high PR. In addition, Table 2.4 presents the average TTS achieved, considering different PR and the difference observed, compared to the same PR of the no-control scenario. Also, for this performance key indicator similar conclusion are derived. The higher the PR of CAVs, the more improvement is observed.

The resulting speed contour plots for all PRs and both directions of the motorway are presented in Figs. 2.39 and 2.40. It is evident from the plots that even for a low PR of 40% of ACC vehicles, significant improvement is observed on the motorway for both directions, reaching a percentage of improvement close to 61% over the no-control case for TD and 24.8% for TTS. As the penetration rate increases, further improvement is observed, and congestion is eliminated even for 60% of CAVs. Nevertheless, the highest improvement is observed for the case of 100% of CAVs, reaching the value of 40.1% for TTS. Additional figures related to Scenario 2 can be found in Appendices A.3, A.4.

Table 2.3: Scenario 2: Total Delay (TD) for various PR.

Total Delay (veh·h)			
PR (%)	Scenario 1	Scenario 2	Difference (%)
0	114.8	-	-
20	180.3	103.1	-42.8
40	212.7	82.9	-61.0
60	223.5	42.5	-81.0
80	234.7	34.8	-85.2
100	270.5	46.5	-82.8

Table 2.4: Scenario 2: Total Time Spent (TTS) for various PR.

Total Time Spent (veh·h)			
PR (%)	Scenario 1	Scenario 2	Difference (%)
0	708.8	-	-
20	828.1	712.5	-14.0
40	890.9	670.3	-24.8
60	912.1	589.5	-35.4
80	935.9	575.7	-38.5
100	1017.0	609.3	-40.1

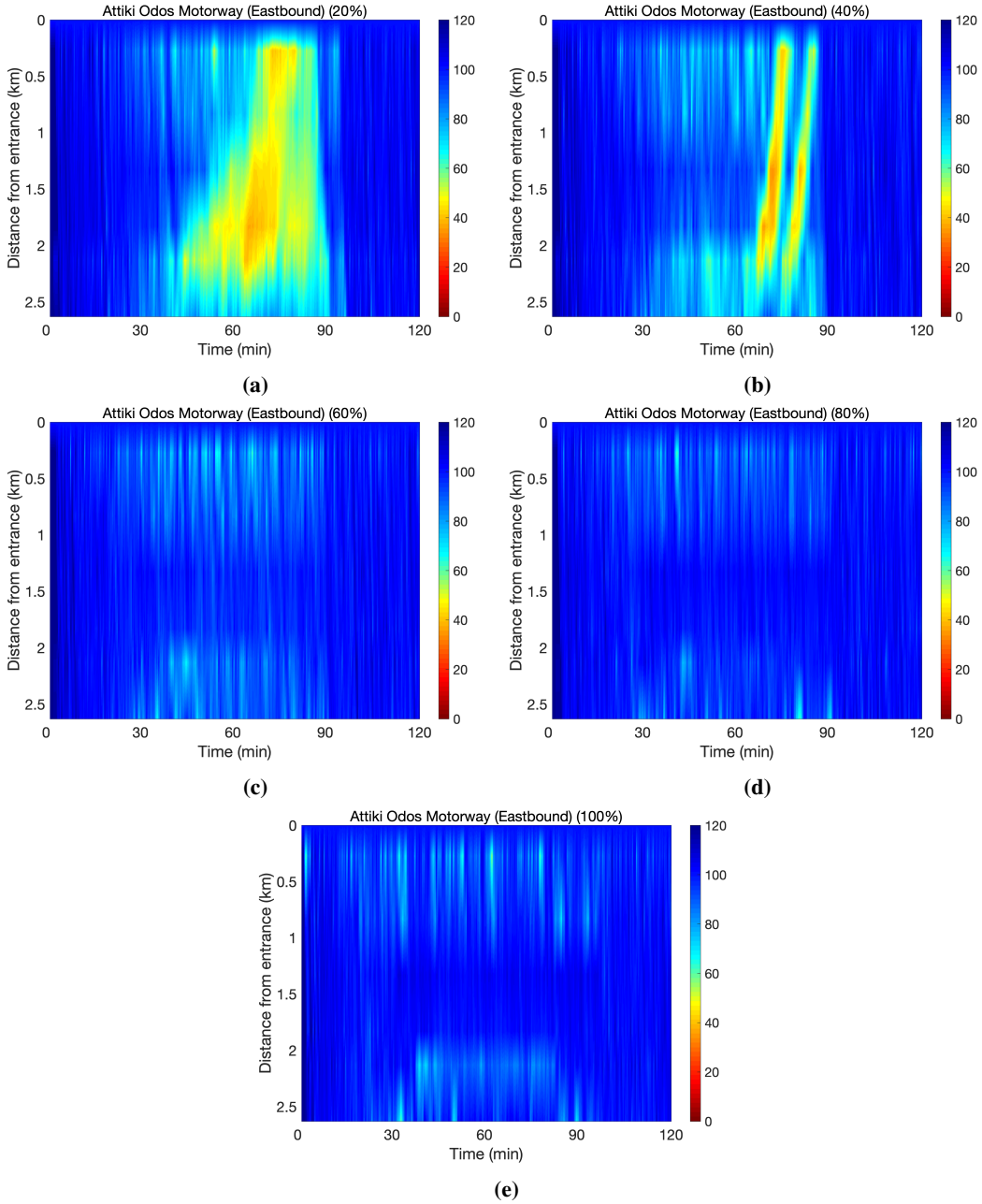

Figure 2.39: ACC – Scenario 2: Speed contour plots for the eastbound direction and for all penetration rates of CAVS; 20% CAVs, 40% CAVs, 60% CAVs, 80% CAVs, 100% CAVs.

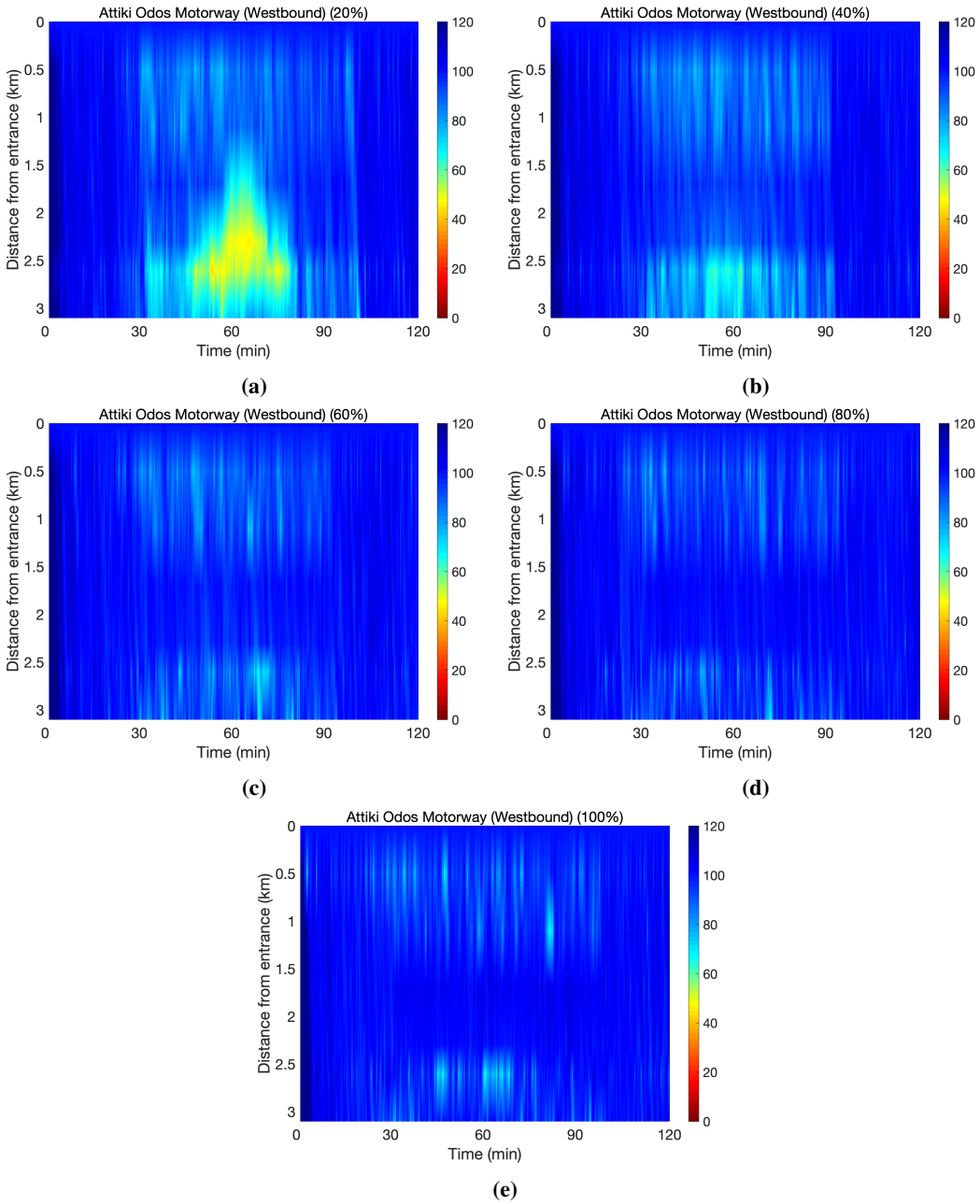

(a) **(b)** **(c)** **(d)** **(e)**

Figure 2.40: ACC – Scenario 2: Speed contour plots for the westbound direction and for all penetration rates of CAVS; 20% CAVs, 40% CAVs, 60% CAVs, 80% CAVs, 100% CAVs.

2.7.10.3 Scenario 3: ACC-based control applying capacity increase and discharge flow rate increase using time-gap adaptation

In this scenario, ACC-based control is applied in order to achieve both goals, i.e. capacity increase, and discharge flow rate increase. Similar to the previous Scenario (2.7.6.2), we use the same setup for the control time-step, the minimum and maximum time-gaps, the range for flow per lane and the function used to derive the discrete time-gap values.

Table 2.5 presents the average TD achieved and Table 2.6 presents the average TTS achieved, considering different PR and the corresponding differences observed, compared to the same PR of the no-control scenario (2.7.6.1). One can easily observe that the control strategy achieves significant improvements, even for lower PR (20%, 40% of CAVs) compared to the previous Scenario 2 (2.7.6.2).

Following a similar manner, speed contour plots for all PRs and both directions of the motorway are generated and presented in Figs. 2.41 and 2.42. It is evident from the plots that even for the lower PR of 20% of ACC-equipped vehicles, significant improvement is observed on the motorway for both directions. For this case, the percentages of improvement over the no-control adaptation case for both KPIs are 56% for TD and 20.0% for TTS. As the penetration rate increases, further improvement is observed, and congestion is eliminated even for 60% of CAVs. Nevertheless, the highest improvement is observed for the case of 100% of CAVs, reaching values of 87.4% for TD and 42.5% for TTS over the no-control adaptation scenario. Aggregated results for all the scenarios are illustrated in Fig. 2.43. It is obvious from the plots that as the penetration rate for CAVs increases, there is a corresponding increase in the level of improvement achieved in the average TTS and TD values, for both Scenarios 2 and 3 with the highest improvements observed in Scenario 3. Additional figures related to Scenario 3 can be found in Appendices A.3, A.4.

Table 2.5: Scenario 3: Total Delay (TD) for various PR.

Total Delay (veh·h)			
PR (%)	Scenario 1	Scenario 3	Difference (%)
0	114.8	-	-
20	180.3	79.1	-56.1
40	212.7	59.4	-72.1
60	223.5	41.3	-81.5
80	234.7	34.8	-85.2
100	270.5	34.2	-87.4

Table 2.6: Scenario 3: Total Time Spent (TTS) for various PR.

Total Time Spent (veh·h)			
PR (%)	Scenario 1	Scenario 3	Difference (%)
0	708.8	-	-
20	828.1	664.3	-19.8
40	890.9	623.3	-30.0
60	912.1	587.1	-35.6
80	935.9	575.7	-38.5
100	1017.0	584.7	-42.5

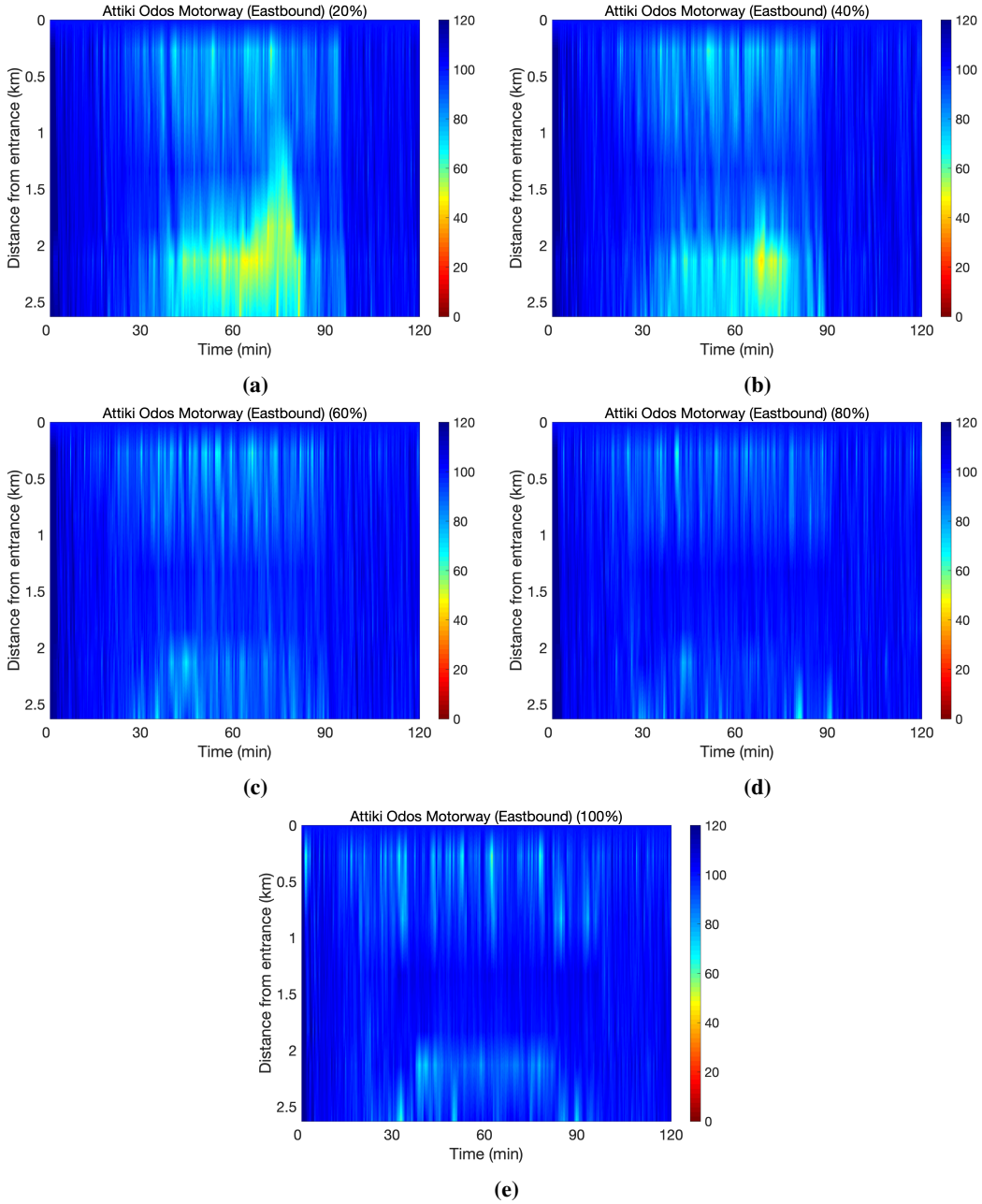

Figure 2.41: ACC – Scenario 3: Speed contour plots for the eastbound direction and for all penetration rates of CAVS; 20% CAVs, 40% CAVs, 60% CAVs, 80% CAVs, 100% CAVs.

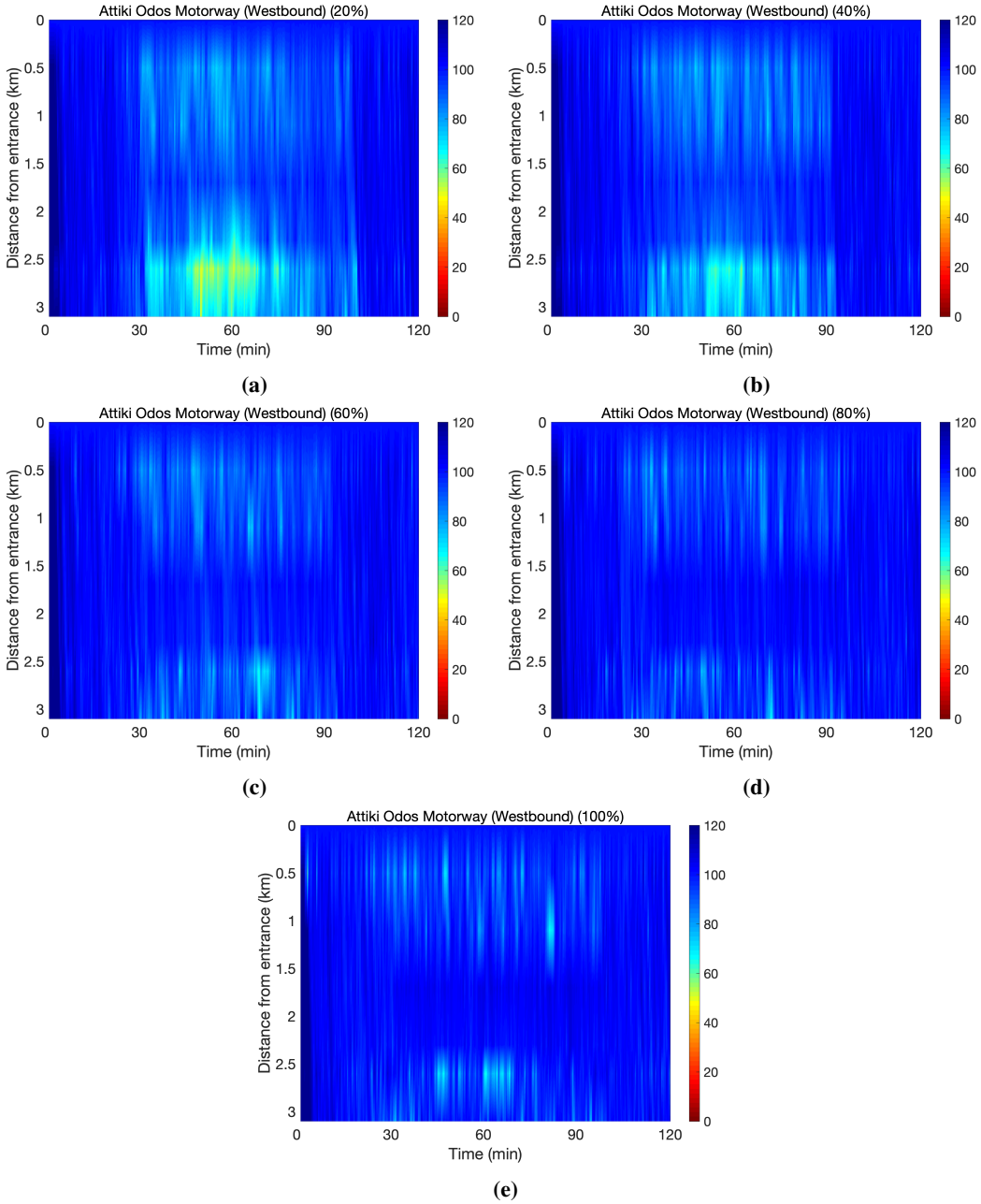

(a) **(b)** **(c)** **(d)** **(e)**

Figure 2.42: ACC – Scenario 3: Speed contour plots for the westbound direction and for all penetration rates of CAVS; 20% CAVs, 40% CAVs, 60% CAVs, 80% CAVs, 100% CAVs.

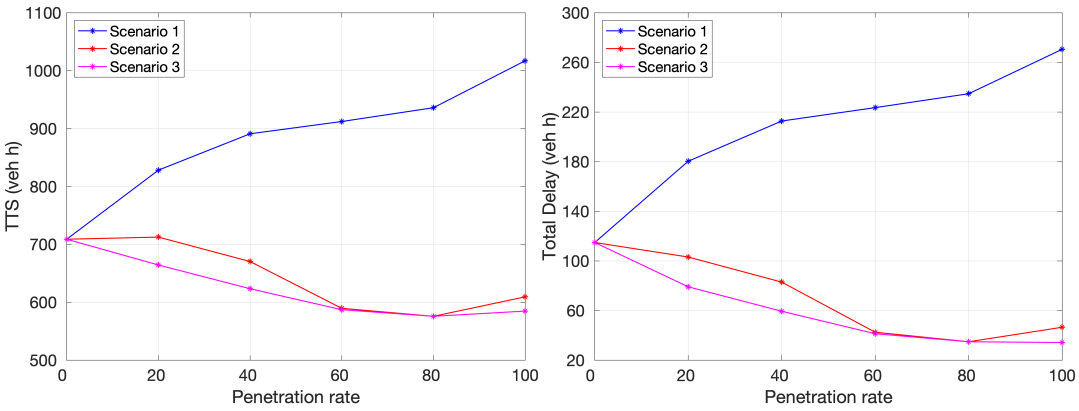

(a) **(b)**

Figure 2.43: Average Total Time Spent (TTS) and Total Delay (TD) per penetration rate of CAVs for the ACC time-gap adaptation Scenarios 1-3

Chapter 3

Network level traffic management control for CAVs

3.1 Introduction

The phenomenon of traffic congestion has always been a major issue for big cities. This condition is characterized by substantial delays, lower speeds and exhausted congestion phenomena, typically appearing due to geometrical changes (bottlenecks) of the motorway infrastructure (e.g., a lane-drop, a merging lane, a tunnel or a bridge) and rapid increase in the number of vehicles travelling. Moreover, weather conditions and incidents (e.g., accidents, construction work) can deteriorate the infrastructure capacity. The most straight forward way to overcome such difficulties is to further expand the existing infrastructure to accommodate higher traffic volumes. However, this is no longer an option, commonly due to high cost and environmental reasons. Hence, the most reasonable approach is to tackle congestion through traffic control measures. The latter can be distinguished among conventional and non-conventional measures. Both measures aim to distribute and control motorway traffic flows in time and space so as to avoid the onset of congestion. Conventional measures make use of traffic lights and VMSs to affect traffic while on the other hand, non-conventional measures use on-board vehicle systems to send recommendations that will affect the driving behavior of drivers. This work takes into account the potential presence of CAVs, for the purpose of supporting the formulation of an integrated optimal control problem for motorway networks under a mixture of conventional and novel traffic control measures.

3.1.1 Literature review

Traffic flow modelling and control has been of prime interest since the mid-20th century. The first macroscopic traffic flow model composed of a single conservation equation for the vehicles followed by a density-flow relationship referred to as the fundamental diagram (FD), was presented by Lighthill and Whitham (1955). A discrete approximation of this model in time and space, known as the CTM, was then presented for a single origin-destination highway stretch by Daganzo (1994) and was extended by the same author in (1995) simulating the propagation of traffic over complex networks of links and nodes using macroscopic variables (e.g., density, flow). An alternative modelling approach to calculate the evolution of densities and mean speeds on motorway networks was based on a second-order traffic flow model proposed by Messmer and Papageorgiou (1990). As presented by Kotsialos et al. (2002), the modelling tool METANET, in which the model is involved, allows for simulation of all kinds of traffic conditions (e.g., free flow conditions, dense or congested conditions), capacity-reducing events with prescribed characteristics (location, intensity, duration) and arbitrary network topology (bifurcations, on-ramps, off-ramps).

The aforementioned macroscopic traffic flow models as well as many others found in the literature, are utilized for developing a specific type of advanced controllers; the model-based

controllers. As mentioned by Burger et al. (2013), model-based controllers are controllers where the known dynamics of the system and its response to actuation is taken into account in determining control actions. Even though they consider all the traffic variables aggregated across all lanes; thus, providing less detail on experimental and observational details, proper traffic control measures such as route guidance, ramp metering and mainstream traffic flow control demonstrate the potential benefits of the models utilized. Representative work using macroscopic traffic flow models can be found accordingly in the literature, e.g. (Gomes and Horowitz, 2006; Carlson et al., 2010b; Han et al., 2015).

Another group of traffic controllers aiming to keep the control variables (e.g., flow, speed, density) to predefined selected values, are called feedback controllers. As mentioned by Burger et al. (2013), in feedback control, measurements or estimates of quantities are taken from the process to determine the current state of the control variables. Subsequently, using the system state, a controller determines the control actions that need to be applied to the system in order to force it towards some desired situation. Feedback control strategies can be used either in a local or in a coordinated scheme; they are easy to develop and very robust to uncertainties in the input, due to the feedback nature of the regulator. These schemes are very popular and widely used over the years in ramp metering, mainstream traffic flow control and lane changing control applications, with some of them applied in real-field applications. See for instance, related work presented by Papageorgiou et al. (1991), Spiliopoulou et al. (2013), Spiliopoulou et al. (2014a), Wang et al. (2014), Iordanidou et al. (2014), among many others addressing feedback control strategies by the use of conventional traffic control measures.

A great number of advancements have been proposed by many research institutions who have been developing and testing novel control approaches focused on macroscopic traffic flow models as well as feedback control strategies utilizing CAVs, in simulation as well as in real field applications. In this section, such novelties are reviewed, including VSL, LCC, DTA, RM as well as integrated control. An MPC architecture for platoons was proposed by Baskar et al. (2012), for regulating the lane change activity, speeds and on-ramp flows in a simple simulation example of a two-lane highway stretch featuring one origin-destination and two on-ramps. Specifically, the MCP approach leads to a non-convex optimization problem that requires proper optimization techniques in order to be solved fast in real-time, minimizing TTS. In a similar manner, a VSL control algorithm was presented by Khondaker and Kattan (2015) through the use of an MPC approach tested on microscopic simulations, via application of the control actions on CAVs. In detail, the authors emphasized the need for lane-based traffic data for the development of the strategy, since the majority of the control algorithms found in literature consider aggregated traffic data. Grumert et al. (2015) studied the potential benefits of using V2I and I2V communications, to enable variable speed limit control per lane. Specifically, a cooperative variable speed limit system is proposed and evaluated on microscopic simulations, demonstrating the benefits of traffic flow efficiency.

A first-order multi-lane macroscopic traffic flow model for motorways, was firstly introduced by Roncoli et al. (2015a) and utilized within an optimal control problem, in a companion (Part II) paper from the same authors in (2015b). A modified/extended version of the well-known CTM is used as a starting point, considering additional aspects of traffic dynamics, such as lane changes. Various control variables are used to incorporate different options for control, namely, MTFC via VSL, LCC and RM. A quadratic objective is considered, and the optimal control problem is formulated as a QP problem. This is then casted in an MPC mode for microscopic simulation testing using CAVs. The optimal control scheme has generated important and useful results, showing that the use of CAVs could enable strong benefits for the traffic conditions, alleviating congestion and consequently improving safety. An optimal feedback control strategy, formulated as a Linear Quadratic Regulator (LQR), was proposed by Roncoli et al. (2016, 2017). The strategy aims at regulating the lane assignment of vehicles upstream of a bottleneck location so as to maximize the bottleneck throughput,

targeting critical densities as set points.

Different VSL control strategies were developed and presented by Han et al. (2017) using V2V communication architectures, aiming to maximize throughput at bottleneck locations and reduce system time delays. It should be pointed out that the effect of lane changing was not considered for simplicity; aspect of major importance for controlling the lane change activity upstream of a bottleneck location. Zhang and Ioannou (2017) developed a combined lane-changing and VSL control strategy with the purpose of avoiding unnecessary lane-changing movements in the immediate proximity of a bottleneck. The VSL controller is developed using a feedback linearization approach based on the CTM and is shown analytically to guarantee exponential convergence to the optimum equilibrium point. Appropriate lane-changing commands are also delivered as recommendations to the drivers according to a set of case-specific rules.

Markantonakis et al. (2019) presented the combined deployment and evaluation of two feedback traffic control strategies, using a microscopic simulation model for a lane-drop infrastructure. The control strategies involved MTFC via VSL and LCC, previously proposed by Carlson et al. (2013) and Roncoli et al. (2016, 2017), respectively. The first control strategy employs mainstream traffic flow control using appropriate variable speed limits as an actuator. The second control strategy delivers appropriate lane-changing actions to selected connected vehicles using a feedback-feedforward control law. The VSL control strategy has proved successful in avoiding the capacity drop, even at low penetration rates. The LCC control strategy is able to achieve an appropriate lane assignment of vehicles upstream of the bottleneck and as a result to increase capacity. For low penetration rates of connected vehicles, the integrated use of the two strategies is demonstrated to be highly beneficial. The reported results were obtained assuming full compliance and no communication delays. A novel methodology for the integrated use of lane changing and ramp metering feedback control in the presence of connected vehicles is proposed by Tajdari et al. (2019) and extended by the same authors in (2022) to include an extremum seeking algorithm to compute the optimal set-points of the feedback strategy. The optimal feedback control strategy is formulated as a Linear Quadratic Integral (LQI) regulator, based on a simple linear time-invariant traffic flow model. The methodology is evaluated via simulation experiments on a first-order traffic flow model and compared in order to further investigate the potential benefits of ramp metering to the well-known feedback controller ALINEA, proposed by Papageorgiou et al. (1991). A series of simulation experiments demonstrate the effectiveness of the recently developed methodology.

Dynamic traffic assignment is long recognized as a key component for real-time traffic management. As mentioned by Wang et al. (2001), this proactive modelling approach refers to the distribution of traffic demand with the same origin and destination (O-D) among alternative routes of a traffic network, so that some optimality principles are satisfied. In one of the earlier works found in literature, Wardrop (1952) classified DTA based on two famous principles that describe the so-called user-optimal (UO)-DTA and system-optimal (SO)-DTA. In the former, each O-D pair is characterized by equal and minimum travel times along its alternative routes, meaning that no user can experience lower travel times by changing the route; hence, ensuring fairness to all users. In the latter, the sum of the travel times for all O-D pairs is the lowest possible. This implies that some users may experience longer travel times on alternative routes, compared to other users travelling for the same origin-destination. In order to approximate either UO-DTA or SO-DTA in a traffic network, different strategies are employed. These strategies include feedback control, reinforcement learning, shortest path algorithms, linear and quadratic programming techniques. According to the author's knowledge, the vast majority of the dynamic traffic assignment strategies found in literature consider the process of user-optimal DTA; only a limited number of studies consider the process

of system-optimal DTA in motorway networks. The work presented in Chapter 3 is concerned only with the latter. One of the early advancements addressing system-optimal DTA using the CTM model was presented by Ziliaskopoulos (2000). A single destination SO-DTA problem was formulated as a Linear Program (LP) using linear relationships of flow and occupancy to describe the traffic evolution over time. The model was limited to include only one destination, which could be too simplified to be used in practical ITS applications, although it is able to capture important traffic features as they are captured by the cell transmission model. This work inspired Li et al. (2003) to develop a Dantzig-Wolfe based solution algorithm to solve SO-DTA problems first on a single-origin single-destination pair, and then to more complex networks of single-origin multi-destination and multi-origin multi-destination pairs. The reported results on the single destination case, indicate substantial computational effort in comparison with the commercial LP solver introduced by Ziliaskopoulos (2000). For the extended case of multi origins and destinations, the computational performance was not studied.

A CTM-based single destination SO-DTA problem is investigated by Zheng et al. (2015), focusing on a case where the cell entities are time-invariant. Evidence shows that the upstream propagation of congestion does not affect the optimal arrival flow pattern of SO-DTA if the demand and supply parts of the FD are triangular. Inspired by Zheng and Chiu (2011), this work further investigates the earliest arrival flow (EAF) approach for time-invariant entities. A theoretical result was established, proving that EAF is a subset of SO-DTA when there is no cell division. A case study on a real-world network verifies the results and reports the computational benefits of the proposed method. Zhu and Ukkusuri (2015) presented a novel linear lane-based programming (LP) formulation for intersection control within a connected vehicle environment, stemming from the work addressed by Yperman (2007). A bi-level optimization model is introduced to propagate traffic flows in the network, accounting for dynamic route choice and control in the context of system optimum network model. The non-linear constraints are transformed to linear inequalities and incorporated to the linear programming (LP) formulation. Three case studies are conducted to demonstrate the properties and effectiveness of the novelty formulation to solve autonomous intersection control. Como et al. (2016) designed two optimal control problems utilizing a first-order macroscopic traffic flow model for freeway networks, for the use of system optimal dynamic traffic assignment. The well-known CTM is considered in continuous time to model the relationship among the densities and flows, assuming a concave Fundamental Diagram. In the first optimal control problem, the turning ratios (referred to as the driver's route choice) are used as control variables for (DTA); while in the second one, the turning ratios are assigned as exogenous parameters. Moreover, open loop variable speed limits, ramp metering and routing controllers are designed to ensure the feasibility of the optimal solutions. A series of experiments illustrate the proposed methodologies in the standard discrete time space version of CTM.

3.1.2 Contribution

In this work, we continue and extend our research on the validation of the traffic control scheme proposed by Markantonakis and Papamichail (2023), which is an extension of the work proposed by Roncoli et al. (2015a,b), for the integrated use of various traffic control measures. The contribution of this work is twofold:

- An MPC strategy is adopted to evaluate on a real traffic corridor infrastructure, the optimal control solutions derived from the network level optimization problem. The corridor of Attiki Odos, Athens, is simulated utilizing real traffic data, by the use of the AIMSUN microscopic simulator Aimsun (2023). The corridor includes several

on/off ramp merge areas as well as lane-drop areas, where congestion phenomena are prevailed during high-peak hours, that are suitable enough for the QP problem formulation, to derive appropriate traffic control actions to be enabled with the aid of CAVs.

- In order to demonstrate the adequacy of the traffic control actions which are exclusively performed by CAVs, different penetration rates are examined in a case (the control case), where all the available traffic control measures are enabled. This case is then compared to the reference case (the no-control case), where no control actions are applied to the motorway system.

3.2 Traffic Control Measures

In the following sections a description of the traffic control measures used in an optimal control problem formulation follows. Two of them are already defined previously in Sections 2.2 and 2.3 but applied from a different control perspective (i.e. local level traffic control). However, their cooperative use in this work with other traffic control measures (i.e. ramp metering and dynamic traffic assignment) is investigated from the network-level control perspective. Hence, we choose to briefly present in a similar manner the details of the traffic control measures mentioned above for completeness.

3.2.1 Mainstream Traffic Flow Control

The basic idea of this control measure is to apply mainstream traffic flow control upstream of areas with a particular infrastructure, e.g., lane-drops or bottlenecks in order to establish optimal traffic conditions for any appearing demand with the use of VSLs. VSL displayed on roadside or overhead VMS in response to prevailing traffic conditions is an increasingly popular freeway traffic control measure (Carlson et al., 2010b). One of the main targets of VSL is enhanced traffic safety as a result of the homogenization of speeds of individual vehicles and of the mean speeds of different freeway lanes which reduce the risk of accident (Papageorgiou et al., 2008). In this work, VSLs are applied using CAVs as actuators which may directly receive the value of the speed limit that is delivered by the control strategy, according to their current location in the network, and it is expected that, for a sufficient penetration of CAVs, this will be sufficient to impose the speed limit onto non-equipped vehicles as well; hence, replacing the use of VMS gantries. For this need, an integral (I-type) regulator uses the optimal density value of each segment-lane ordered by the QP optimization problem as a set-point, to derive the VSL values, so as to establish optimal traffic conditions for any appearing demand.

3.2.2 Lane Change Control

New and promising traffic control measures such as the LCC, aim to achieve a desired distribution of vehicles among the lanes, so as to exploit the capacity of each and every lane, thus increase the overall (cross-lane) capacity and improve traffic flow efficiency. LCC usually applied upstream or close to the proximity of a bottleneck provides lane change advice to be implemented by CAVs, thus enabling an opportune pre-specified distribution of traffic flow among the lanes. In this work, the optimal lateral flows delivered by the QP problem formulation are converted to a sufficient number of vehicles that are required to implement the lane-changing actions.

3.2.3 Ramp Metering Control

Ramp metering control is a popular traffic control measure that consists in regulating the number of vehicles entering from the origins (on-ramps) of a motorway network to the mainstream motorway. Since it is a conventional traffic control measure, which is applied directly at the on-ramps using ordinary traffic signals, it does not necessarily require any particular in-vehicle equipment. In this work we follow a similar manner as in the MTFC control application, using an integral (I-type) regulator that uses the optimal density value (derived from the QP optimization problem) of the segment-lane where the on-ramp is located, as a set-point, to derive the appropriate ramp-flow values.

3.2.4 Dynamic Traffic Assignment Control

This control measure aims to distribute the traffic demand with the same origin-destination (O-D) among alternative routes of the network, so that some optimality principles are satisfied. In our work, we focus on system-optimal DTA, where the sum of the travel times of all O-D pairs should be the lowest possible. The optimal lateral flows for each segment-lane and destination are the ones also used for the LCC control actions.

3.3 Optimal control problem formulation

In this section the optimal control problem formulation is analytically described. Specifically, in Section 3.3.1 we describe in detail the traffic flow model utilized along with the QP problem formulation, while in Sections 3.3.2 and 3.3.3 the linear equality/inequality constraints as well as the objective and penalty functions are presented.

3.3.1 CTM-based traffic flow modelling

Based on a linear multi-lane traffic flow model proposed by Roncoli et al. (2015a) and further utilized within an optimal control problem by the same authors in (2015b), we consider a multi-lane motorway network, which is divided in n segments, while each segment comprises a number of lanes. We use the indexes i, j, l_i, L_i to specify the segment, the lane, the total number of lanes in segment i and the length of segment i, respectively. Since our modelling scheme includes the destination notation, we denote as $D_{i,j}$ the set of all reachable destinations from segment-lane (i, j) and d a reachable destination from segment-lane (i, j). For each segment, we assume internally homogeneous characteristics, such as the number of lanes. The model is formulated in discrete time, considering the discrete time step T for a simulation horizon K indexed by $k = 1, 2, ..., K$ where the simulation time is $t = KT$. In addition, we denote as T^Q the MTFC control time step, as T^D the DTA and LCC control time step and as T^R the RM control time step. The corresponding discrete time indices for each control action are defined by:

$$k^Q = \left\lfloor \frac{kT}{T^Q} \right\rfloor, k^D = \left\lfloor \frac{kT}{T^D} \right\rfloor, k^R = \left\lfloor \frac{kT}{T^R} \right\rfloor$$

with $k = 1, 2, ..., K$ and $\lfloor . \rfloor$ denoting the integer part.

Consider a network discretized in space by defining segment-lane entities. These entities are characterized by non-negative variables and parameters. We adopt the following notation for the corresponding variables, that are used in the optimal control problem formulation:

Variable	Definition
$\rho^{d}_{i,j}(k)$	number of vehicles per destination d travelling in segment-lane (i,j), at time step k, divided by the segment length L_i, $d \in D_{i,j}$.
$q^{in}_{i,j,d}\left(k^{Q}\right)$	traffic flow per destination d entering segment-lane (i,j) during the time interval $\left(k^{Q}, k^{Q}+1\right]$, $d \in D_{i,j}$.
$q^{out}_{i,j,d}\left(k^{Q}\right)$	traffic flow per destination d exiting segment-lane (i,j) during the time interval $\left(k^{Q}, k^{Q}+1\right]$, $d \in D_{i,j}$.
$f^{d}_{i,j,\bar{j}}\left(k^{D}\right)$	lateral traffic flow per destination d moving from lane j to lane $\bar{j} = j \pm 1$, during time interval $\left(k^{D}, k^{D}+1\right]$, $d \in D_{i,j}$.
$f^{d}_{i,\bar{j},j}\left(k^{D}\right)$	lateral traffic flow per destination d entering lane j from lane $\bar{j} = j \pm 1$, during the time interval $\left(k^{D}, k^{D}+1\right]$, $d \in D_{i,j}$.
$r^{d}_{i,j}\left(k^{R}\right)$	traffic flow per destination d entering segment-lane (i,j) if an on-ramp is located at the corresponding segment-lane during the time interval $\left(k^{R}, k^{R}+1\right]$, $d \in D_{i,j}$.

The following conservation equation describes the traffic dynamics of the partial density $\rho^{d}_{i,j}(k)$ for each segment-lane (i,j) and reachable destination d (see Fig. 3.1):

$$\rho^{d}_{i,j}(k+1) = \rho^{d}_{i,j}(k) + \frac{T}{L_i}\left(q^{in}_{i,j,d}\left(k^{Q}\right) - q^{out}_{i,j,d}\left(k^{Q}\right) + f^{d}_{i,\bar{j},j}\left(k^{D}\right) - f^{d}_{i,j,\bar{j}}\left(k^{D}\right) + r^{d}_{i,j}\left(k^{R}\right)\right),$$
$$i = 1,2,...,n,\ \ j = 1,2,...,l_i, \bar{j} = j \pm 1, d \in D_{i,j} \tag{3.1}$$

The original CTM model as well as the extension of it used in this work, is a discrete approximation to the LWR traffic flow model proposed by Lighthill and Whitham (1955). All traffic flow models should be numerically stable. This implies that for each control action included in the problem formulation, a specific control time step is assigned, to ensure that the proper behavior of the control action is achieved in a given situation. Therefore, the control time-steps T^{Q}, T^{D}, T^{R} should be integer multiples of the traffic flow model time step T, where T must be in agreement with the Courant-Friedrichs-Lewy (CFL) condition. Given the above, the following inequality must hold:

$$T \leq \min_{i,j} \frac{L_i}{v^{free}_{i,j}} \tag{3.2}$$

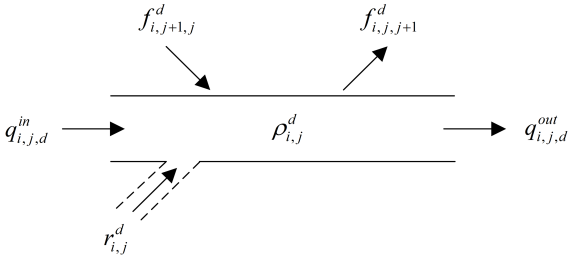

Figure 3.1: Conservation equation notion.

where $v_{i,j}^{free}$ is the free speed allowed in segment-lane (i, j).

When modelling ordinary networks, where there is no change in the geometry of the network, the partial inflow $q_{i,j,d}^{in}\left(k^{Q}\right)$ at time-step k consists of the longitudinal partial flow sent from the upstream segment-lane $(\bar{i}, \bar{j})$ to the downstream segment-lane (i, j). In situations where there is a radical change in the geometry of the network e.g., motorway to motorway connections or segments (parts of the motorway) that feature a lane-drop, a lane addition, or a bifurcation, strong lateral flows may appear close to the end of the segment. As a result, diagonal left/right lateral flows $q_{\bar{i},\bar{j}-1,d}^{left}(k)$, $q_{\bar{i},\bar{j}+1,d}^{right}(k)$ act as additional longitudinal inflow to the downstream segment-lane (i, j). In order to have a generic modelling development that considers any possible network layout, appropriate flags are used in the input files when and to the extent needed.

Based on the above analysis, we may yield the following for the inflows and outflows $q_{i,j,d}^{in}\left(k^{Q}\right)$, $q_{i,j,d}^{out}\left(k^{Q}\right)$ at time-step k (see Fig. 3.2):

$$q_{i,j,d}^{in}(k) = \begin{cases} q_{\bar{i},\bar{j},d}(k), \text{longitudinal movement from the upstream segment-lane} \\ q_{\bar{i},\bar{j},d}(k) + q_{\bar{i},\bar{j}-1,d}^{left}(k), \text{longitudinal and left diagonal movement} \\ q_{\bar{i},\bar{j},d}(k) + q_{\bar{i},\bar{j}+1,d}^{right}(k), \text{longitudinal and right diagonal movement} \\ q_{\bar{i},\bar{j},d}(k) + q_{\bar{i},\bar{j}-1,d}^{left}(k) + q_{\bar{i},\bar{j}+1,d}^{right}(k), \text{all the above} \end{cases} \tag{3.3}$$

$$q_{i,j,d}^{out}(k) = \begin{cases} q_{i,j,d}(k), \text{longitudinal movement to the downstream segment-lane} \\ q_{i,j,d}^{left}(k), \text{left movement to the downstream segment-lane} \\ q_{i,j,d}^{right}(k), \text{right movement to the downstream segment-lane} \\ q_{i,j,d}(k) + q_{i,j,d}^{left}(k), \text{combination of the above} \\ q_{i,j,d}(k) + q_{i,j,d}^{right}(k), \text{combination of the above} \end{cases} \tag{3.4}$$

As mentioned earlier, the motorway network is spatially subdivided introducing segment-lane entities that are characterized by a number of variables; the total density $\rho_{i,j}$, the total inflow $q_{i,j}^{in}$, the total outflow $q_{i,j}^{out}$ and the total ramp-flow $r_{i,j}$ which are given by the sum of all the corresponding partial entities. Hence, each variable is determined according to the following equations:

$$q_{i,j}^{out}(k) = \sum_{d \in D_{i,j}} q_{i,j,d}^{out}(k) \tag{3.5}$$

$$q_{i,j}^{in}(k) = \sum_{d \in D_{i,j}} q_{i,j,d}^{in}(k) \tag{3.6}$$

$$\rho_{i,j}(k) = \sum_{d \in D_{i,j}} \rho_{i,j}^{d}(k) \tag{3.7}$$

$$r_{i,j}(k) = \sum_{d \in D_{i,j}} r_{i,j}^{d}(k) \tag{3.8}$$

for $i = 1, 2, ..., n,\ \ j = 1, 2, ..., l_i$.

By design, on-ramp merge areas consist of a typical feature of almost every type of motorway. In most cases, ramp metering actions are necessary to control the traffic volume

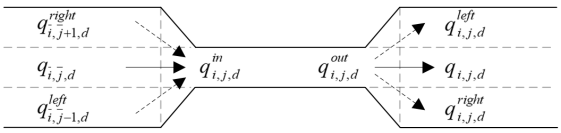

Figure 3.2: Entering and exiting flows of a segment-lane.

entering the mainstream using local or coordinated ramp metering strategies that make use of measurements of an entire region of the motorway network. In our modelling approach, the arriving demand $D^d_{i,j}$ for each destination d of an on-ramp located at segment-lane (i, j), is uncontrollable and feeds the motorway network with the corresponding ramp flow $r^d_{i,j}$. For controlling the respective ramp outflows, it is necessary to account also for the queues that are created due to the corresponding ramp metering actions. The formation of queues is limited since the motorway segments and on-ramps have finite storage capacities. These values are imposed as hard constraints to the optimal control problem formulation and are strictly respected during the optimization process. In cases when there is an excessive demand scenario, infeasible solutions cannot be avoided. In that case, no control action can accommodate the external demand without violating the storage capacity constraints. To address the need of avoiding such situations where the admissible control region is void, and enable the computation of optimal control for any arbitrary scenario, the following variables are introduced to the model:

- real ramp queue $w^d_{i,j}$ [veh]: the number of vehicles waiting at the queue without violating the storage capacity for each destination d
- virtual extra queue $W^d_{i,j}$ [veh]: the number of vehicles waiting virtually at the queue for each destination d
- internal demand $m^d_{i,j}$ [veh/h]: the demand flow that is capable to enter the real ramp queue $w^d_{i,j}$ for each destination d

while the dynamics of the queues formed at the on-ramps for each destination d due to the ramp metering actions read:

$$w^d_{i,j}(k+1) = w^d_{i,j}(k) + T\left[m^d_{i,j}(k) - r^d_{i,j}\left(k^R\right)\right] \tag{3.9}$$

$$W^d_{i,j}(k+1) = W^d_{i,j}(k) + T\left[D^d_{i,j}(k) - m^d_{i,j}(k)\right] \tag{3.10}$$

and the equations for the total real ramp queues and total virtual extra queues read as follows:

$$w_{i,j}(k) = \sum_{d \in D_{i,j}} w^d_{i,j}(k) \tag{3.11}$$

$$W_{i,j}(k) = \sum_{d \in D_{i,j}} W^d_{i,j}(k) \tag{3.12}$$

for $i = 1, 2, ..., n,\ j = 1, 2, ..., l_i,\ d \in D_{i,j}$.

The external demand $D^d_{i,j}$ for each destination d is feeding the extra-queue $W^d_{i,j}$, while the internal demand $m^d_{i,j}$ connects the extra-queue with the real ramp queue $w^d_{i,j}$. A strong penalty factor for the total extra queues $W_{i,j}$, is used in the objective function, to penalize extra queues and keep them equal to zero. In special cases, where there is an excessive demand scenario, the problem will remain within its feasible region by charging the extra queues $W_{i,j}$. The per-destination lane inflows entering the first segment of the network are formally treated as uncontrollable on-ramps. In simple terms, this derives that for each lane $j = 1, 2, ..., l_i$ the

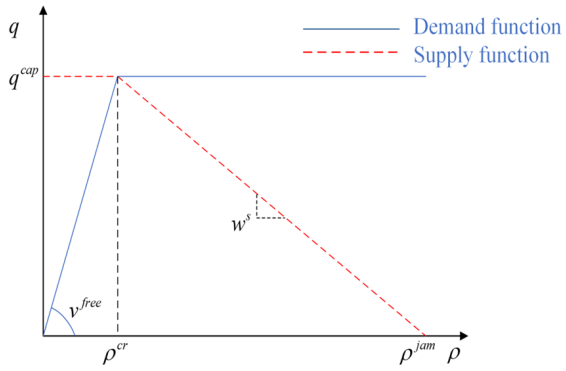

Figure 3.3: Triangular fundamental diagram.

total queues $w_{i,j}$ are set to zero, by setting the upper bound to zero, and the total extra queues $W_{i,j}$ are also weighted in the objective function, to avoid infeasible solutions.

In the original CTM formulation, traffic flow is computed as the minimum between an upstream demand function and a downstream supply function (see Fig. 3.3). In our approach, we adopt the same logic for computing the longitudinal flows $q_{i,j}(k)$ enhanced with additional terms in the min-operator when required from the geometry of the network. Thus, the longitudinal flow $q_{i,j}(k)$ at time-step k is derived as follows:

$$q_{i,j}(k) = \min\Bigg[Q^D_{i,j}(k) - \sum_{d\in D_{i,j}} q^{left}_{i,j,d}\left(k^Q\right) - \sum_{d\in D_{i,j}} q^{right}_{i,j,d}\left(k^Q\right), \\ Q^S_{\tilde{i},\tilde{j}}(k) - \lambda_r r_{\tilde{i},\tilde{j}}\left(k^R\right) - \sum_{d\in D_{i,j}} q^{left}_{i,j-1,d}\left(k^Q\right) - \sum_{d\in D_{i,j}} q^{right}_{i,j+1,j}\left(k^Q\right)\Bigg] \tag{3.13}$$

for $i = 1,2,...,n,\ j = 1,2,...,l_i$ and $\tilde{i} = 2,3,...,n,\ \tilde{j} = 1,2,...,l_{\tilde{i}}$, where (i,j) is the current segment-lane and $(\tilde{i},\tilde{j})$ is the downstream segment-lane, while the demand and supply functions are given by the following equations:

$$Q^D_{i,j}(k) = \min\left[v^{free}_{i,j}\rho_{i,j}(k), q^{cap}_{i,j} + \lambda_d q^{cap}_{i,j}\frac{\rho_{i,j}(k) - \rho^{cr}_{i,j}}{\rho^{cr}_{i,j} - \rho^{jam}_{i,j}}\right] \tag{3.14}$$

$$Q^S_{i,j}(k) = \min\left[q^{cap}_{i,j}, w^S_{i,j}\left(\rho^{jam}_{i,j} - \rho_{i,j}(k)\right)\right] \tag{3.15}$$

where $\rho^{jam}_{i,j}$ and $w^S_{i,j}$ are the total jam density and the back-wave speed, respectively.

It is well known that the original CTM does not reproduce capacity drop phenomena. To address the need and be able to investigate the impact of possible capacity drop, two additional terms are added in the model (appearing in (3.13) and (3.14) using parameters λ_r and λ_d). As mentioned by Kontorinaki et al. (2017), if these two parameters are set $\lambda_r = 1$ and $\lambda_d = 0$, by default no capacity drop is introduced as typical for CTM; if set between 0 and 1, a corresponding level of capacity drop is produced by the model. For our simulation investigations, both parameters are set as $\lambda_r = 1$ and $\lambda_d = 0$, since capacity drop phenomena are successfully reproduced by the microscopic simulation model.

For all first-order models described by one dynamic equation, speed (which is not a decision variable of the QP problem formulation) is calculated only a posteriori. Hence, using both equations (3.5) and (3.7) speed for each segment-lane (i,j) is calculated from the non-linear relation of flow and density as:

$$v_{i,j}(k) = \frac{q_{i,j}^{out}(k)}{\rho_{i,j}(k)},\ i = 1,2,...,n,\ j = 1,2,...,l_i \tag{3.16}$$

3.3.2 Linear inequality constraints

The computation of the lateral flows for each destination d, used to determine the LCC and DTA control actions, is fully delegated to the optimizer; only upper bounds are specified to the non-negative lateral flows as well to the on-ramp flows and real queues as follows:

$$\left[f_{i,j,j-1}^{d}\left(k^{D}\right) + f_{i,j,j+1}^{d}\left(k^{D}\right)\right] \leq \frac{L_i}{T}\rho_{i,j}^{d}(k) \tag{3.17}$$

$$\sum_{d\in D_{i,j}} f_{i,j-1,j}^{d}\left(k^{D}\right) + f_{i,j+1,j}^{d}\left(k^{D}\right) \leq \frac{L_i}{T}\left[\rho_{i,j}^{jam} - \rho_{i,j}(k)\right] \tag{3.18}$$

$$\sum_{d\in D_{i,j}} f_{i,j,j-1}^{d}\left(k^{D}\right) \leq f_{i,j,j-1}^{\max} \tag{3.19}$$

$$\sum_{d\in D_{i,j}} f_{i,j,j+1}^{d}\left(k^{D}\right) \leq f_{i,j,j+1}^{\max} \tag{3.20}$$

$$r_{i,j}\left(k^{R}\right) \leq r_{i,j}^{\max} \tag{3.21}$$

$$w_{i,j}(k) \leq w_{i,j}^{\max} \tag{3.22}$$

Equation (3.17) represents the upper-bound as a restriction for the lateral movements determined by the number of vehicles in the current segment-lane; (3.18) is the upper-bound for the lateral flows entering segment-lane from the adjacent lanes, considering the available space in the current segment-lane; whereas, equations (3.19) and (3.20) serve as hard constraints on both directions, to limit any unrealistic lateral movements. In addition, equations (3.21) and (3.22) represent the upper bounds for the total on-ramp flow and maximum queue allowed at the on-ramp, respectively.

The equations (3.1), (3.5), (3.6), (3.7) and (3.8) are linear but due to the presence of the min-operator the CTM flow equations presented previously, (3.13), (3.14) and (3.15), are non-linear. In this regard, such nonlinearities may be transformed to linear inequalities. This is achieved by requesting the left-hand side of the equation, where the min-operator appears to be smaller than or equal to each of the terms included in the min-operator. Hence, the following transformations are obtained for (3.13), (3.14) and (3.15):

$$q_{i,j}^{out}(k) \leq v_{i,j}^{free}\rho_{i,j}(k) \tag{3.23}$$

$$q_{i,j}^{out}(k) \leq q_{i,j}^{cap} + \lambda_d q_{i,j}^{cap}\frac{\rho_{i,j}(k) - \rho_{i,j}^{cr}}{\rho_{i,j}^{cr} - \rho_{i,j}^{jam}} \tag{3.24}$$

$$q_{i,j}^{in}(k) \leq q_{i,j}^{cap} - \lambda_r r_{i,j}\left(k^{R}\right) \tag{3.25}$$

$$q_{i,j}^{in}(k) \leq w_{i,j}^{S}\left(\rho_{i,j}^{jam} - \rho_{i,j}(k)\right) - \lambda_r r_{i,j}\left(k^{R}\right) \tag{3.26}$$

for $i = 1,2,...,n,\ j = 1,2,...,l_i$. Inequalities (3.23), (3.24) represent the demand part of the FD; while (3.25), (3.26) represent the supply part of the FD.

Each O-D pair in the network is described by use of the partial flow $q_{i,j,d}^{out}$ and the partial density $\rho_{i,j}^{d}$. For the optimizer both $q_{i,j,d}^{out}$ and $\rho_{i,j}^{d}$ are control variables; meaning that multiple pairs of $q_{i,j,d}^{out}$ and $\rho_{i,j}^{d}$ may satisfy the constraints of the optimal control problem. In order to

limit any unrealistic pairs, the following inequality must hold:

$$q_{i,j,d}^{out} \leq v_{i,j}^{free} \rho_{i,j}^{d}, i = 1, 2, ..., n, \ j = 1, 2, ..., l_i, \ d \in D_{i,j}. \tag{3.27}$$

3.3.3 Objective function

As already mentioned, our optimization problem for integrated motorway optimal control in the presence of CAVs, is based on the formulation and solution of a convex QP problem. In detail, a quadratic cost function that includes linear as well as quadratic penalty terms is appropriately defined so as to derive specific traffic control actions to be enabled with the aid of CAVs. For simplicity and demonstration purposes, due to the large number of terms used in the objective function, we choose to split the objective into two parts as shown below:

$$J_{QP} = J_{linear} + J_{quadratic} \tag{3.28}$$

The first part of (3.28) consists of the linear terms defined as:

$$\begin{aligned} J_{linear} = T \sum_{k=1}^{K} \sum_{i=1}^{n} \sum_{j=1}^{l_i} \left[L_i \rho_{i,j}(k) + w_{i,j}(k) \right] + \beta_1 \sum_{k=1}^{K} \sum_{i=1}^{n} \sum_{j=1}^{I_i} \left[W_{i,j}(k) \right] \\ + \sum_{k^D=1}^{K^D} \sum_{i=1}^{n} \sum_{j=1}^{l_i} \sum_{d \in D_{i,j}} \left[a_{i,j,j-1}^{d} f_{i,j,j-1}^{d}\left(k^D\right) + a_{i,j,j+1}^{d} f_{i,j,j+1}^{d}\left(k^D\right) \right] \end{aligned} \tag{3.29}$$

This is the most crucial part of the objective function since the first linear term represents the Total Time Spent, which is the time spent by vehicles to travel along the network and the waiting time at the queues formed at the on-ramps. Moreover, the second linear term weighted by β_1 is a penalty term for the extra queues. The value of the weight should be big enough to make sure that all variables $W_{i,j}$ are set equal to zero when $w_{i,j}$ remains within bounds. The third linear term weighted by coefficients $\alpha_{i,j,j-1}^{d}, \alpha_{i,j,j+1}^{d}$ aims at penalizing the partial lateral flows; it has the purpose of reducing the unnecessary lateral movements. However, the use of lower values for the coefficients at specific locations across the network (e.g., upstream of a bottleneck location) may facilitate reasonable and beneficial lateral movements. The second part of (3.28) consists of the quadratic terms defined as:

$$\begin{aligned} J_{quadratic} = \beta_2 \sum_{k^D=2}^{K^D} \sum_{i=1}^{n} \Bigg\{ \sum_{j=2}^{l_i} \sum_{d \in D_{i,j}} \left[f_{i,j,j-1}^{d}(k^D) - f_{i,j,j-1}^{d}(k^D - 1) \right]^2 \\ + \sum_{j=1}^{l_i - 1} \sum_{d \in D_{i,j}} \left[f_{i,j,j+1}^{d}\left(k^D\right) - f_{i,j,j+1}^{d}\left(k^D - 1\right) \right]^2 \Bigg\} \\ + \beta_3 \sum_{k^D=2}^{K^D} \sum_{i=1}^{n} \Bigg\{ \sum_{j=1}^{l_i} \sum_{d \in D_{i,j}} \left[r_{i,j}^{d}\left(k^R\right) - r_{i,j}^{d}\left(k^R - 1\right) \right]^2 \Bigg\} \\ + \beta_4 \sum_{k^D=2}^{K^D} \sum_{i=1}^{n} \Bigg\{ \sum_{j=1}^{l_i} \sum_{d \in D_{i,j}} \left[q_{i,j,d}^{out}\left(k^Q\right) - q_{i,j,d}^{out}\left(k^Q - 1\right) \right]^2 \Bigg\} \end{aligned}$$

$$
\begin{aligned}
&+\beta_5 \sum_{k=1}^{K} \sum_{i=1}^{n} \left\{ \sum_{j=1}^{l_i} \sum_{d \in D_{i,j}} \frac{\left[q_{i,j,d}^{out}\left(k^Q\right) - q_{i,j}^{out}\left(k^Q\right) - v_{i,j}^{*}\left(\rho_{i,j}^{d}\left(k\right) - \rho_{i,j}\left(k\right)\right)\right]^2}{\left(\rho_{i,j}^{*}\right)^2} \right\} \\
&+\beta_6 \sum_{k=2}^{K-1} \sum_{i=1}^{n} \left\{ \sum_{j=1}^{l_i} \sum_{d \in D_{i,j}} \frac{\left[q_{i,j,d}^{out}\left(k^Q\right) - q_{i,j,d}^{out}\left(k^Q - 1\right) - v_{i,j}^{*}\left(\rho_{i,j}^{d}\left(k\right) - \rho_{i,j}^{d}\left(k-1\right)\right)\right]^2}{\left(\rho_{i,j}^{*}\right)^2} \right\} \\
&+\beta_7 \sum_{k=1}^{K} \sum_{i=1}^{n} \left\{ \sum_{j=1}^{l_i} \sum_{d \in D_{i,j}} \frac{\left[r_{i,j}^{d}\left(k^R\right) - r_{i,j}\left(k^R\right) - \delta_{i,j}^{*}\left(w_{i,j}^{d}\left(k\right) - w_{i,j}\left(k\right)\right)\right]^2}{\left(w_{i,j}^{*}\right)^2} \right\} \\
&+\beta_8 \sum_{k=1}^{K} \sum_{i=1}^{n} \left\{ \sum_{j=1}^{l_i} \sum_{d \in D_{i,j}} \frac{\left[m_{i,j}^{d}\left(k\right) - m_{i,j}\left(k\right) - \varepsilon_{i,j}^{*}\left(W_{i,j}^{d}\left(k\right) - W_{i,j}\left(k\right)\right)\right]^2}{\left(W_{i,j}^{*}\right)^2} \right\}
\end{aligned} \tag{3.30}
$$

The quadratic terms play an important role in the objective function since they aim at penalizing the variation of the control variables from time step to time step and between destinations. To elaborate more on this, looking at (3.30) the first quadratic term weighted by β_2 is related to time-variations of the partial lateral flows; the second and third term (weighted by β_3, β_4) have the purpose of penalizing time-variations of the on-ramp flows and partial flows accordingly. The remaining quadratic terms weighted by β_5, β_6, β_7 and β_8, are derived using the procedure that is described in the following Section (3.3.4).

The formulated discrete-time optimal control problem can be written in matrix form as:

$$\min Z = \mathbf{c}^{\mathrm{T}}\mathbf{x} + \frac{1}{2}\mathbf{x}^{\mathrm{T}}\mathbf{H}\mathbf{x} \tag{3.31}$$

subject to

$$\mathbf{A}_i\mathbf{x} \leq \mathbf{b}_i \tag{3.32}$$

$$\mathbf{A}_e\mathbf{x} = \mathbf{b}_e \tag{3.33}$$

$$\mathbf{0} \leq \mathbf{x} \leq \mathbf{b}_{ub} \tag{3.34}$$

where $\mathbf{x}$ is the decision vector including all the states and control variables. In (3.31) the vector $\mathbf{c}^{\mathrm{T}}$ and the matrix $\mathbf{H}$ contain all the coefficients for the linear terms and the specifics of the quadratic terms of (3.28), respectively.

3.3.4 Penalty functions

Each O-D pair inside the network is described by the use of partial flows q_d^{out}, which express traffic flows per destination d reachable through the corresponding network. These flows can be described with the use of composition rates γ^d, which are portions of the traffic volume q^{out}. Since γ^d is not considered as a decision variable in the QP formulation, it can only be considered via the non-linear relation $\gamma^d = \rho^d/\rho$ to derive the partial flows q_d^{out} for segment-lane (i, j) as follows:

$$q_{i,j,d}^{out}\left(k\right) = \gamma_{i,j}^{d}\left(k\right) q_{i,j}^{out}\left(k\right) = \frac{\rho_{i,j}^{d}\left(k\right)}{\rho_{i,j}\left(k\right)} q_{i,j}^{out}\left(k\right) \tag{3.35}$$

Due to the fact that the relation among the decision variables in (3.35) is also non-linear, it cannot be included as a constraint. Therefore, the following procedure is used instead so as

to include a penalty term in the objective function:

$$\frac{q_{i,j,d}^{out}(k)}{\rho_{i,j}^{d}(k)} = \frac{q_{i,j}^{out}(k)}{\rho_{i,j}(k)} \Rightarrow \frac{q_{i,j}^{out}(k) + \Delta q_{i,j}}{\rho_{i,j}(k) + \Delta\rho_{i,j}} = \frac{q_{i,j}^{out}(k)}{\rho_{i,j}(k)} \tag{3.36}$$

where, $\Delta q_{i,j} = q_{i,j,d}^{out}(k) - q_{i,j}^{out}(k)$ and $\Delta\rho_{i,j} = \rho_{i,j}^{d}(k) - \rho_{i,j}(k)$. Subsequently,

$$\frac{\rho_{i,j}(k)\Delta q_{i,j} - q_{i,j}^{out}(k)\Delta\rho_{i,j}}{\rho_{i,j}(k)(\rho_{i,j}(k) + \Delta\rho_{i,j})} = 0 \Rightarrow \frac{\Delta q_{i,j} - \frac{q_{i,j}^{out}(k)}{\rho_{i,j}(k)}\Delta\rho_{i,j}}{\rho_{i,j}(k) + \Delta\rho_{i,j}} = 0 \Rightarrow \frac{\Delta q_{i,j} - v_{i,j}(k)\Delta\rho_{i,j}}{\rho_{i,j}^{d}(k)} = 0 \tag{3.37}$$

In order to suppress the undesired non-linearity, fixed values for $v_{i,j}(k)$ and $v_{i,j}(k)$ namely v^* (free speed) and ρ^* (critical density), may be considered in order to treat this penalty term as a linear approximation around nominal values:

$$\frac{\Delta q_{i,j} - v^*\Delta\rho_{i,j}}{\rho^*} = 0 \tag{3.38}$$

It should be pointed out that (3.38) corresponds to the quadratic term in the objective function weighted by β_5. For the term weighted by β_6 (time-variations), the penalty term is derived in the same way. Following a similar manner, analogous definitions r^d for the partial on-ramp flow and m^d for the partial internal demand are derived, using the non-linear relations w^d/w and W^d/W as follows:

$$r_{i,j}^{d}(k) = \frac{w_{i,j}^{d}(k)}{w_{i,j}(k)} r_{i,j}(k) \tag{3.39}$$

$$m_{i,j}^{d}(k) = \frac{W_{i,j}^{d}(k)}{W_{i,j}(k)} m_{i,j}(k) \tag{3.40}$$

The corresponding penalty terms for the on-ramp flows and internal demands are derived in the same way:

$$\frac{r_{i,j}^{d}(k)}{w_{i,j}^{d}(k)} = \frac{r_{i,j}(k)}{w_{i,j}(k)} \Rightarrow \frac{r_{i,j}(k) + \Delta r_{i,j}}{w_{i,j}(k) + \Delta w_{i,j}} = \frac{r_{i,j}(k)}{w_{i,j}(k)} \tag{3.41}$$

$$\frac{m_{i,j}^{d}(k)}{W_{i,j}^{d}(k)} = \frac{m_{i,j}(k)}{W_{i,j}(k)} \Rightarrow \frac{m_{i,j}(k) + \Delta m_{i,j}}{W_{i,j}(k) + \Delta W_{i,j}} = \frac{m_{i,j}(k)}{W_{i,j}(k)} \tag{3.42}$$

$$\frac{w_{i,j}(k)\Delta r_{i,j} - r_{i,j}(k)\Delta w_{i,j}}{w_{i,j}(k)(w_{i,j}(k) + \Delta w_{i,j})} = 0 \Rightarrow \frac{\Delta r_{i,j} - \frac{r_{i,j}(k)}{w_{i,j}(k)}\Delta w_{i,j}}{w_{i,j}(k) + \Delta w_{i,j}} = 0 \Rightarrow \frac{\Delta r_{i,j} - \delta_{i,j}(k)\Delta w_{i,j}}{w_{i,j}^{d}(k)} = 0 \tag{3.43}$$

$$\frac{W_{i,j}(k)\Delta m_{i,j} - m_{i,j}(k)\Delta W_{i,j}}{W_{i,j}(k)(W_{i,j}(k) + \Delta W_{i,j})} = 0 \Rightarrow \frac{\Delta m_{i,j} - \frac{m_{i,j}(k)}{W_{i,j}(k)}\Delta W_{i,j}}{W_{i,j}(k) + \Delta W_{i,j}} = 0 \Rightarrow \frac{\Delta m_{i,j} - \varepsilon_{i,j}(k)\Delta W_{i,j}}{W_{i,j}^{d}(k)} = 0 \tag{3.44}$$

Replacing $\delta_{i,j}(k), \varepsilon_{i,j}(k), w_{i,j}^{d}(k), W_{i,j}^{d}(k)$ with fixed values in order to treat these penalty terms as linear approximations, derive the following:

$$\frac{\Delta r_{i,j} - \delta^*\Delta w_{i,j}}{w^*} = 0 \tag{3.45}$$

$$\frac{\Delta m_{i,j} - \varepsilon^* \Delta W_{i,j}}{W^*} = 0 \tag{3.46}$$

3.4 Open-loop control framework

A description of the networks used for the macroscopic simulations, the configuration of the macroscopic traffic flow model presented in Section 3.3, the configuration of the QP model, the development of the software tool in C++ as well as the results of the corresponding QP problem, are presented in this section. Useful conclusions are derived regarding the adequacy of the four available traffic control measures in two open loop control scenarios, whose control actions are not updated during the process. The goal is to perform a coordinated exploitation of the available measures so as to enable the computation of optimal control for any arbitrary demand scenario.

3.4.1 Network description

The macroscopic traffic flow model presented in Section 3.3 has been derived with a view to adopt different network structures that include lane drop areas, merge areas as well as multiple origins and destinations for the DTA policy. Following that approach, in this work we explore the efficiency of the open-loop control strategy for a challenging and sizable hypothetical motorway network with multiple destinations and routes, on a realistic traffic demand scenario.

The considered motorway networks are illustrated in Fig. 3.4. Both networks are composed by a part of four lanes (segments 1-4), a part of three lanes (segment 12), parts with two lanes (segments 5-9), and parts with a single lane for segments 10, 11 and it presents one on-ramp at segment 8. They also feature two origins denoted by O_1 and O_2 as well as two reachable destinations denoted by D_1, D_2 for scenarios 1 and 2 and one more destination D_3 for scenarios 3 and 4. Starting from origin O_1, two alternative routes of 4.0 km and 4.6 km length exist to reach D_1, while a unique route of 3.5 km length exists for destination D_2 and of 1.0 km for destination D_3 accordingly. For those entering from origin O_2, both destinations D_1 and D_2 can be reached via unique routes of 2.0 km and 1.5 km, respectively. Note that in scenarios 1 and 2, only vehicles heading towards destination D_2 are entering from origin O_2 and in scenarios 3 and 4 vehicles towards destinations D_1 and D_2 are entering.

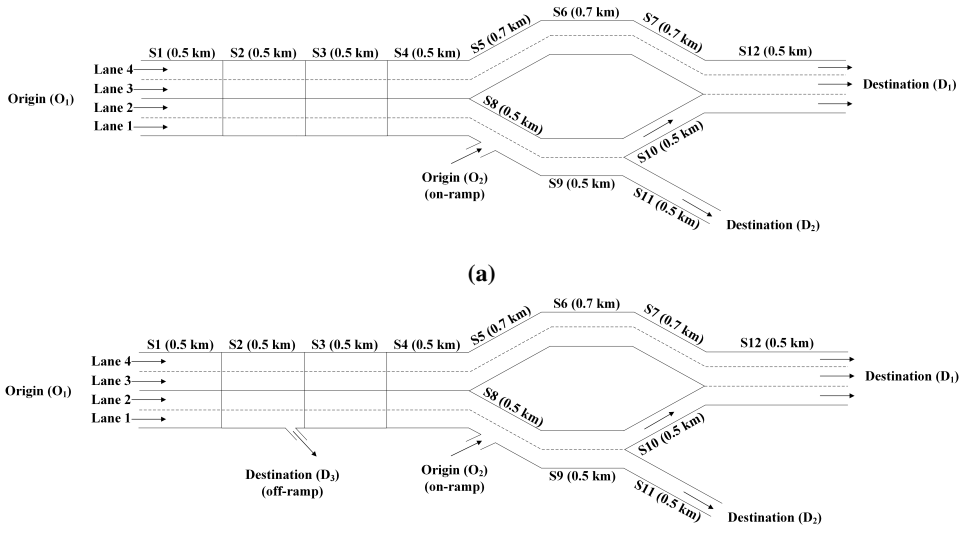

Figure 3.4: Motorway networks used for scenario 1 (a) and scenario 2 (b)

3.4.2 Configuration of the macroscopic traffic flow model and the QP model

The utilized CTM parameters are $v_{i,j}^{free} = 100$ km/h, $\rho_{i,j}^{cr} = 22$ veh/km, $\rho_{i,j}^{jam} = 120$ veh/km and $w_{i,j}^{s} = 22.4$ km/h. Also, the values used to enable the capacity drop are $\lambda_d = 0.3$, $\lambda_r = 0.7$. The choice of the simulation step T is a crucial aspect that must be carefully taken into account. In fact, a too long simulation step could allow vehicles to travel in more than one cell during its duration, causing numerical instability of the mathematical model; on the other hand, the size of the optimization problem is also affected by this choice. In this case, a value T =10 s is set, that satisfies the CFL condition (3.2) for model stability. Once the simulation step is chosen, the control steps are defined as a multiple of the simulation step. In our case, the control step for all the control variables is set equal to the simulation step. Hence, the control variables on both scenarios examined are updated synchronously with the state variables and have the highest degree of freedom. Based on the aforementioned, $T^Q = T^D = T^R = 10$ sec.

Moreover, the weighting parameters used in the objective function of the QP problem for the respective terms have been tuned and are $\beta_1 = 10^4$, $\beta_2 = 10^{-5}$, $\beta_3 = 10^{-5}$, $\beta_4 = 10^{-5}$, $\beta_5 = 10^{-2}$, $\beta_6 = 10^1$, $\beta_7 = 10^{-5}$, $\beta_8 = 10^{-5}$ on both scenarios examined. For the linear penalty terms related to the partial lateral flows, the weight $a_{i,j,\bar{j}}^{d}$ is set either equal to zero, to encourage vehicles to change lane if necessary, or equal to 10^2, when no lane changing movement is allowed. As a result, the QP problem is a convex optimization problem and has a unique solution. In addition, upper bounds are provided for the lateral movements (f^{max} = 400 veh/h for scenarios 1,2 and f^{max} = 300 veh/h for scenarios 3,4), for the on-ramp queues at segment 8 (w^{max} = 60 veh for scenario 1 and w^{max} = 50 veh for scenario 2) and for the maximum flow that is allowed to enter from the on-ramp at segment 8 (r^{max} = 1800 veh/h on both scenarios). Furthermore, the parameters for suppressing oscillations of the control variables have been chosen as $v_{i,j}^{*} = v_{i,j}^{free}$, $\rho_{i,j}^{*} = \rho_{i,j}^{cr}$, $\delta_{i,j}^{*} = 10^2$, $\epsilon_{i,j}^{*} = 10^2$, $w_{i,j}^{*} = w^{max}$, $W_{i,j}^{*} = w^{max}$.

3.4.3 Development in C++

A software tool using the C++ programming language has been developed that implements the control strategy in a generic way. More precisely, a stand-alone application is developed having also access to an external optimization tool GUROBI, Gurobi Optimization, L.L.C (2023), demonstrating the efficiency of open-loop solutions. The software tool is delivered in the form of an executable file (exe) that the system can execute directly under user request. Among many subroutines and functions, the tool itself has five core functions Fig. 3.5:

- **Initial function:** This is the first function to be called. All the initial conditions, configuration parameters of the QP optimization problem are initialised and the appropriate file for storing the output of the strategy during run-time is created.
- **Main function:** This function is called after the initial function and includes the main body of the control strategy. At this point the model is created and along with the Gurobi parameters is passed to the optimizer.
- **GUROBI optimizer:** This function calls the optimizer that creates an environment and starts the optimization process.
- **Optimize again:** This function is called after the optimization process is terminated. The output is stored and the user has the option to reoptimize the model by changing the initial conditions of the model and the parameters.
- **Ending function:** This function is the last function to be called at the end of the process after the user chooses not to reoptimize the model. It frees up the memory and the program exits.

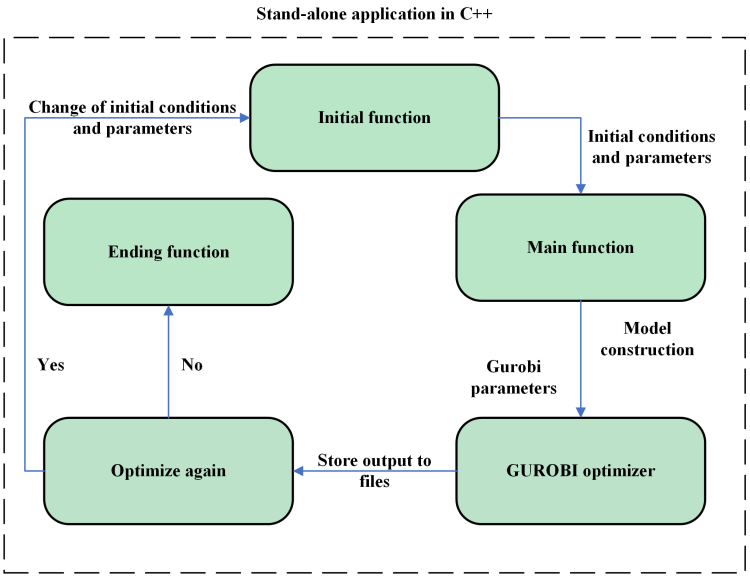

Figure 3.5: Open-loop framework

3.4.4 Macroscopic investigations

In the following Sections (3.4.4.1, 3.4.4.2, 3.4.4.3 and 3.4.4.4) we present the experimental results obtained from the use of the traffic flow model presented in Section 3.3.1 on a series of macroscopic simulation experiments. Sections 3.4.4.1 and 3.4.4.3 report the results of the no-control scenarios whereas Sections 3.4.4.2 and 3.4.4.4 report the results when the optimal control scheme is applied. For the development of the no-control scenarios a generic modelling framework was adopted similar to the one presented by Roncoli et al. (2015a). The details of the framework adopted are briefly listed as follows:

1. Equations (3.1), (3.14), (3.15) and (3.16) were used to describe the partial density, the demand function, the supply function and speed, respectively.

2. Since lateral flows are treated as control variables in the optimal control problem formulation, they should also be included in the no-control scenario for a fair evaluation. The main idea is to reproduce the natural lane-changing behavior of traffic among lanes in the best possible way. In our modelling approach, we adopt the scheme presented by Roncoli et al. (2015a) for computing lateral flows per segment-lane, and then deriving the lateral flows per destination according to the composition rate (i.e. portions of the traffic volume for each reachable destination).

3. As in the case of lateral flows, longitudinal flows are also treated as control variables in the optimal control problem formulation. In our modelling approach, equations (3.3), (3.4) were used to describe the inflows and outflows of a segment-lane that include the longitudinal and diagonal flows per destination, derived according to the composition rate for each destination.

Both scenarios were used as the main reference for comparison to the control scenarios.

3.4.4.1 Scenario 1: Results

In this scenario, a time-horizon equal to 60 min is considered and the corresponding trapezoidal traffic demand profiles for all O-D pairs are depicted in Fig. 3.6. Since no-control actions are applied in this scenario, congestion phenomena are observed. Specifically, a congestion starts at t =10 min, as the arriving demand for both destinations exceeds the capacity,

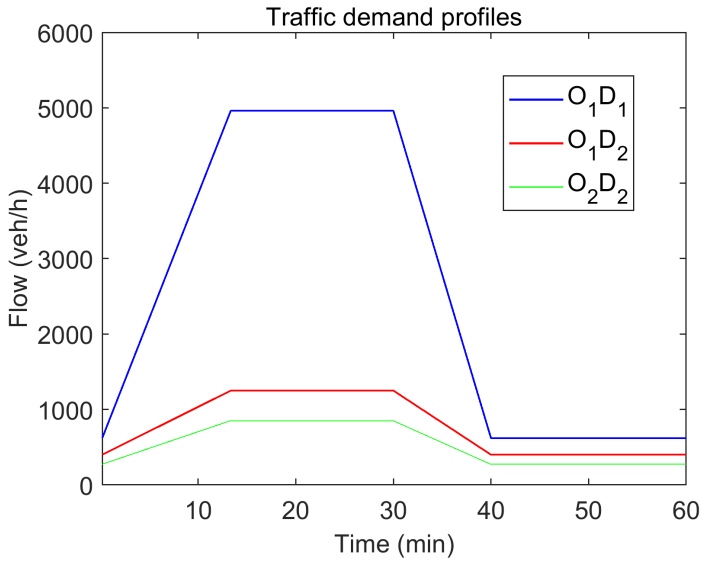

Figure 3.6: Traffic demand profiles for origin 1 destination 1 (blue line), origin 1 destination 2 (red line), origin 1 destination 3 (black line), on-ramp origin 2 destination 1, 2 (green line) for scenarios 1,2

and lasts for about 35 min. A spillback is observed covering several sections (1.5 km) upstream of segment 8 (on-ramp merge) as depicted in the speed contour plot (see Fig. 3.8). The outflows per lane at segment 8, displayed in Fig. 3.7, validate that both lane 1 and lane 2 (with lane 1 being the right-most lane as presented in Fig. 3.4) reach capacity (~2200 veh/h), after which speed breaks down on both lanes. A capacity drop of about 18% of the nominal capacity (~2200 veh/h) is observed in Fig. 3.7. For this scenario the average TTS observed a value of 259.5 veh·h and the TD observed a value of 100.8 veh·h. For a more detailed overview on the development of this scenario (used as the main reference for comparison to scenario 2) please refer to Roncoli et al. (2015a).

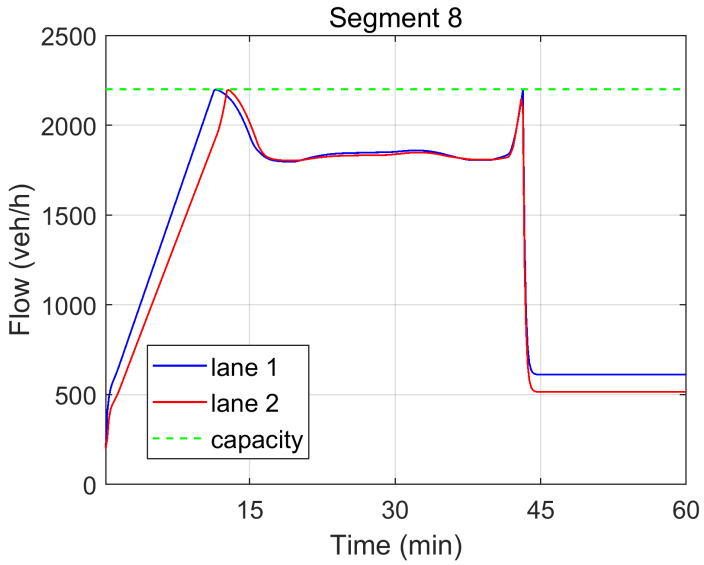

Figure 3.7: Per lane outflow trajectories at segment 8 (on-ramp merge) for lane 1 (blue line) and lane 2 (red line), respectively, for Scenario 1

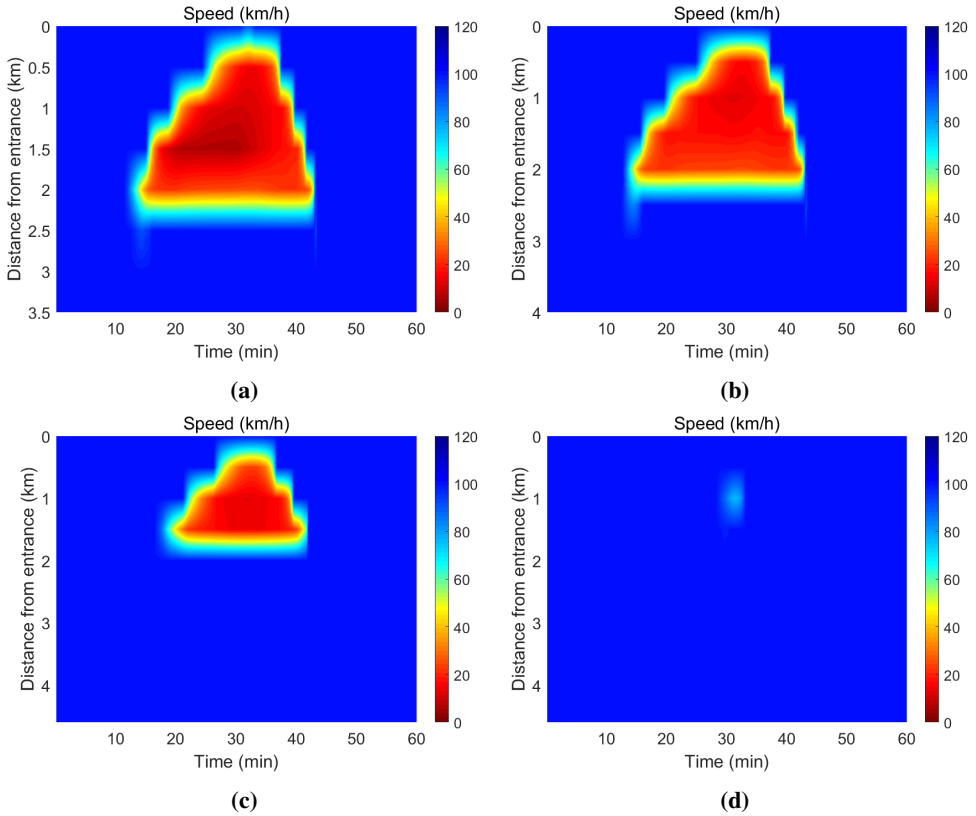

Figure 3.8: Speed contour plots for lane 1 (a), lane 2 (b), lane 3 (c) and lane 4 (d), respectively, for Scenario 1

3.4.4.2 Scenario 2: Results

In Scenario 2, appropriate control actions proved beneficial for the mitigation of congestion presented in Scenario 1. In detail, an algorithm based on the barrier method Dikin (1967) implemented in GUROBI GUROBI, Gurobi Optimization, L.L.C (2023) provides a fast solution of the QP problem in almost 48 sec [1]. The optimisation problem is applied to the same network (see Fig. 3.4a), using the same traffic demand profiles, shown in Fig. 3.6 and the parameters described in Section 3.4.2. The external input (demand) is feeding the mainstream entrance at segment 1 and the on-ramp located at segment 8. As in Scenario 1, no boundary conditions are specified for the network exits, allowing a fair comparison of the results. The TTS as well as the TD improvements compared to the no-control scenario (Scenario 1), are 36% and 79%, respectively. Due to the increased demand from the on-ramp located at segment 8 lane 1, an integrated use of all the traffic control measures is performed. Specifically, lateral movements are performed from lane 1 to lane 2 at segment 8 for the vehicles traveling towards destination D_1, so as to create the necessary space for those entering from the on-ramp (see Fig. 3.9d). In addition, strong and effective RM actions are performed at segment 8 lane 1 throughout the simulation horizon for all vehicles entering, enabling the use of the ramp queues (see Fig. 3.9b). Both control measures successfully maintain the density at the merging area below its critical value (see Fig. 3.9a); thus, capacity drop is avoided and the use of MTFC actions in the upstream segments is not necessary. In fact, as demonstrated in Fig. 3.9c, at segment 4 lane 1, this corresponds to VSL values ordered that are close to the value of 100 km/h, which corresponds to free-speed.

[1] Intel(R) Core(TM) i5-10500 CPU @ 3.10GHz, 8.00GB DDR4 RAM, 64-bit Operating System, x64-based processor

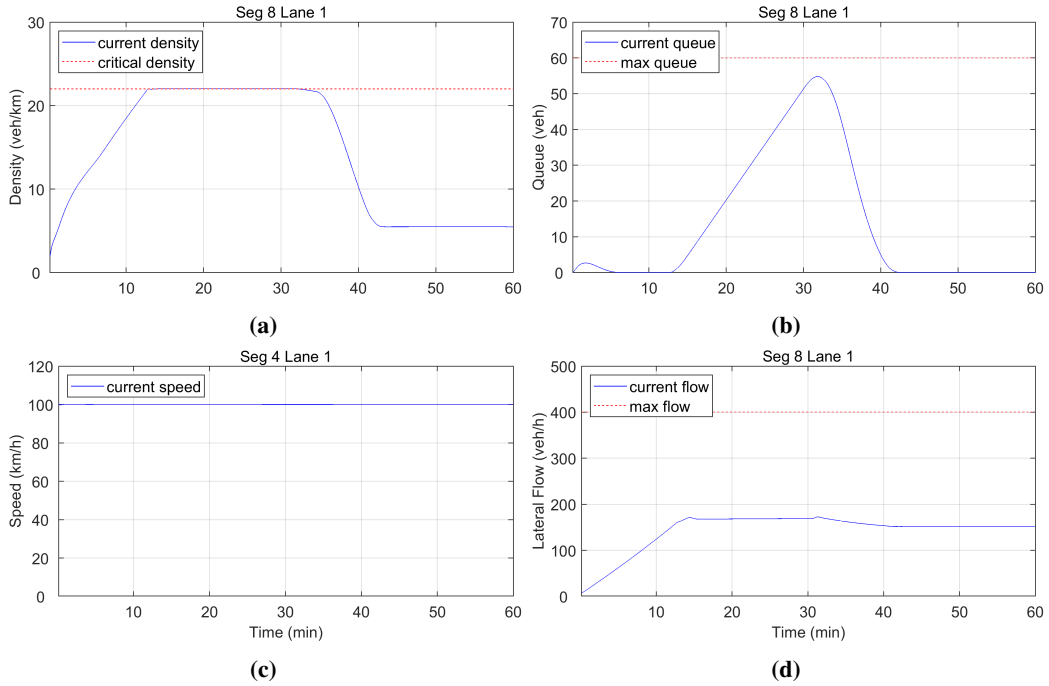

Figure 3.9: Total density value (in blue) (a), ramp queue (in blue) (b), speed value (in blue) (c), lateral flow of destination 1 (in blue) (d); and the corresponding critical, maximum, and speed limit values (in dashed red) for Scenario 2

As mentioned earlier in Section 3.4.1, destination D_1 can be reached using three alternative routes:

$$R1 : S1 \rightarrow S2 \rightarrow S3 \rightarrow S4 \rightarrow S5 \rightarrow S6 \rightarrow S7 \rightarrow S12$$
$$R2 : S1 \rightarrow S2 \rightarrow S3 \rightarrow S4 \rightarrow S8 \rightarrow S9 \rightarrow S10 \rightarrow S12$$
$$R3 : S8 \rightarrow S9 \rightarrow S10 \rightarrow S12$$

For those entering from origin O_1, routes $R1$ and $R2$ can be used while for those entering from origin O_2 , the unique route $R3$ is available. In a similar manner, destination D_2 can be reached using two alternative routes:

$$R4 : S1 \rightarrow S2 \rightarrow S3 \rightarrow S4 \rightarrow S8 \rightarrow S9 \rightarrow S11$$
$$R5 : S8 \rightarrow S9 \rightarrow S11$$

For those entering from origin O_1 the unique route $R4$ exists while for those entering from origin O_2, the unique route $R5$ exists.

It is reasonable that, when in free-flow conditions, all drivers travelling towards a destination want to use the shortest route as the best option to reduce their travel time. In our study, the optimality principle adopted for system optimal DTA implies that the travel times for each O-D pair along alternative routes are not equal, which means that some users may experience longer travel times on alternative routes compared to other users travelling for the same O-D. Starting from origin O_1, destination D_1 can be reached via the shortest route $R2$ and destination D_2 via the route $R4$. As expected, the displayed results in Fig. 3.10 confirm that densities (Fig. 3.10a, 3.10b) are always equal to the respective critical densities at both segments 10 and 11; hence, the outflows (Fig. 3.10c, 3.10d) are always close to the nominal capacity (2200 veh/h) for both segment 10 and segment 11. This implies that the optimizer

tackles the DTA problem effectively utilizing the maximum capacity of the shortest routes of the network for all destinations, so as to reduce the total travel time of the system. For the remaining vehicles travelling towards destination D_1, the longest route $R1$ is utilized. Fig. 3.11 depicts that densities at segment 5 (immediate segment after the routing diversion) never reach the respective critical values; hence, the outflows are always lower than the nominal capacity per lane (2200 veh/h). Furthermore, looking at the speed contour plots per lane in Fig. 3.12, one can easily observe that the speed reductions are totally avoided; hence, congestion is eliminated.

The results of the partial flows per destination in comparison to Scenario 1 are depicted in Fig. 3.13 and Fig. 3.14 for destination D_1 and destination D_2 , respectively. It is evident from the plots that for Scenario 2 (open-loop scenario) the shortest route for destination D_1 (see Fig. 3.13) is optimally utilized as in segment 10 lane 1 the partial flow reaches the capacity (2200 veh/h) while the remaining flow uses the longest route to reach the final destination at segment 12. On the other hand, for destination D_2 (see Fig. 3.14) the capacity drop is avoided due to the proper lane change assignment of vehicles and the effective ramp metering control actions; hence, the outflow of segment 11 also reaches the capacity (2200 veh/h).

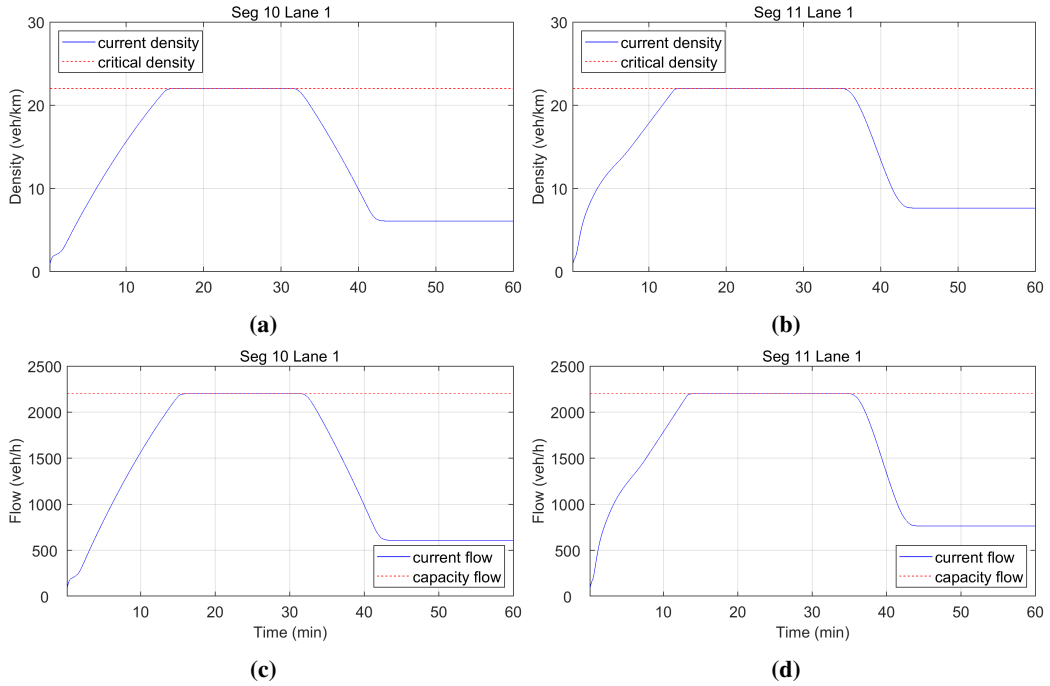

Figure 3.10: Density values (in blue) of destination 1 (a) and destination 2 (b); flow values (in blue) of destination 1 (c) and destination 2 (d); and the corresponding critical, and capacity values (in dashed red) of segments 10 and 11 for Scenario 2

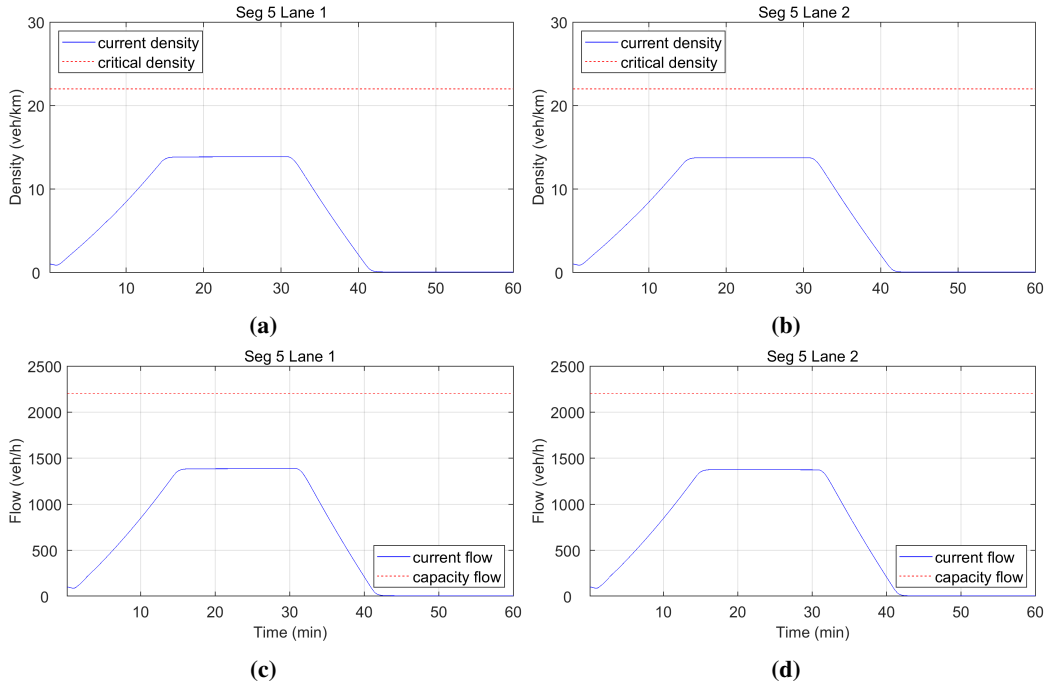

Figure 3.11: Density values (in blue) of destination 1 (a, b); flow values (in blue) of destination 1 (c, d); and the corresponding critical, and capacity values (in dashed red) of segment 5 lane 1 and lane 2 for Scenario 2

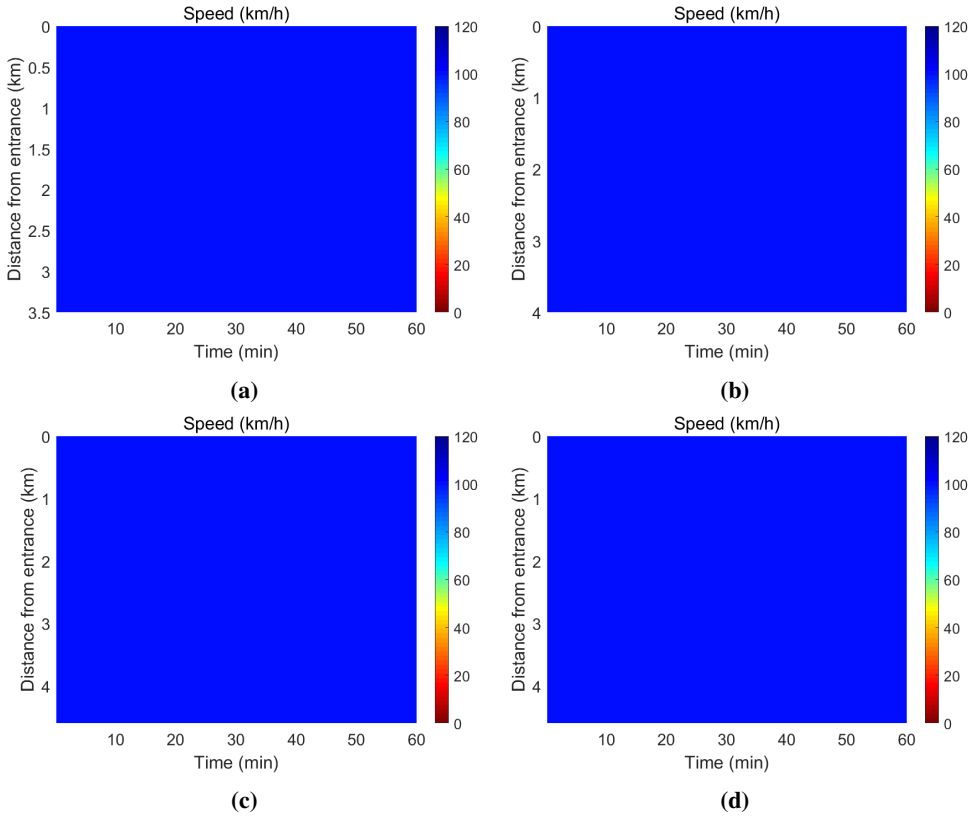

Figure 3.12: Speed contour plots for lane 1 (a), lane 2 (b), lane 3 (c) and lane 4 (d), respectively, for Scenario 2

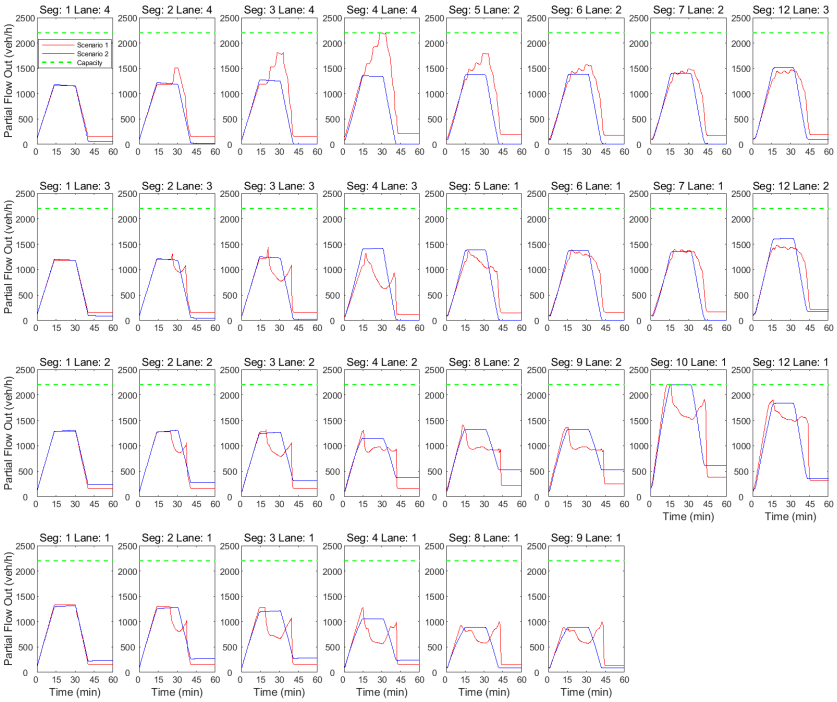

Figure 3.13: Partial flows for all segments of destination 1 for Scenario 1 (red line) and Scenario 2 (blue line)

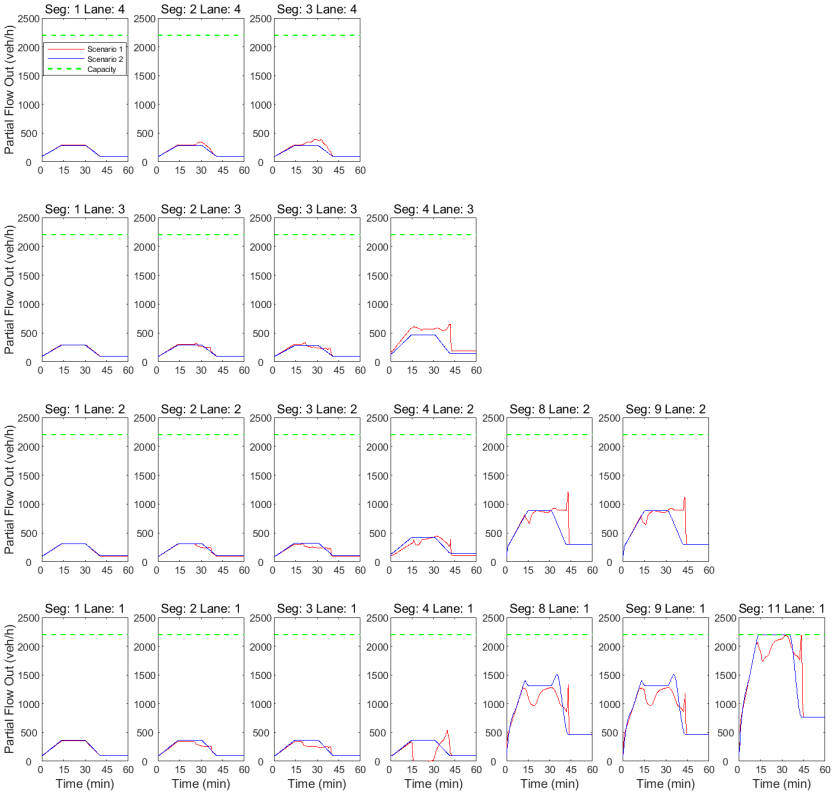

Figure 3.14: Partial flow for all segments of destination 2 for Scenario 1 (red line) and Scenario 2 (blue line)

3.4.4.3 Scenario 3: Results

For Scenario 3 one more destination (D_3) is added with the new trapezoidal traffic demand profiles for all O-D pairs depicted in Fig. 3.15 for a time-horizon equal to 60 min. Following a similar manner as in the previous scenarios, the same demands are also considered in this scenario. As the arriving demand for all destinations exceeds the capacity, congestion initiates at segment 8, where the outflows per lane at segment 8 (see Fig. 3.16), validate that lane 1 (being the right-most lane as presented in Fig. 3.4b) reaches capacity (~2200 veh/h) and lane 2 reaches a value of (~2000 veh/h), after which speed breaks down on both lanes. To this end, a capacity drop of about 18% of the nominal capacity (~2200 veh/h) is observed in Fig. 3.16. For this scenario the average TTS observed a value of 306.7 veh·h and the TD observed a value of 137.3 veh·h.

3.4.4.4 Scenario 4: Results

Using the parameters for Scenario 2 described in Section 3.4.2, the optimisation problem is now applied to the network displayed in Fig. 3.4b. The external demand for all O-D pairs is feeding the mainstream entrance at segment 1 and the on-ramp located at segment 8 for destinations D_1 and D_2. No boundary conditions are specified for the network exits, allowing a fair comparison of the results between Scenario 3 (no-control) and Scenario 4 (control). The performance improvement in terms of TTS and TD compared to Scenario 3, are 42% and 83%, respectively. Due to the increased demand from the on-ramp located at segment 8 lane 1, an integrated use of all the traffic control measures is performed. Specifically, strong lateral movements are performed from lane 1 to lane 2 at segment 8 for the vehicles traveling towards destination D_1 , approaching the maximum value, so as to create the necessary space for those entering from the on-ramp (see Fig. 3.17d). In addition, strong and effective RM actions are performed at segment 8 lane 1 from $t = 15$ min to $t = 40$ min for all vehicles entering, enabling the use of the ramp queues (see Fig. 3.17b). While both control measures try to maintain the density at the merging area below its critical value, strong MTFC actions are performed in the upstream segment 4. In fact, as demonstrated in Fig. 3.17c, at segment 4 lane 1, the VSL values ordered are gradually decreasing close to the value of 80 km/h. As a

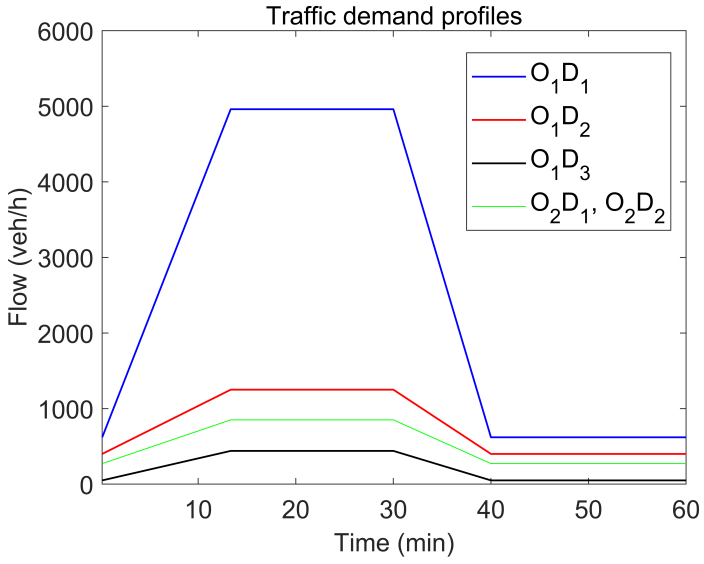

Figure 3.15: Average traffic demand profiles for origin 1 destination 1 (blue line), origin 1 destination 2 (red line), origin 1 destination 3 (black line), on-ramp origin 2 destination 1, 2 (green line) for scenarios 3,4

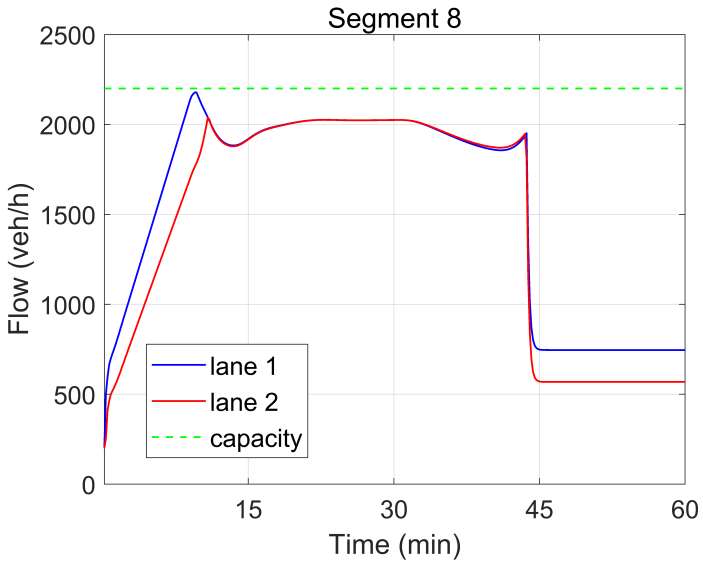

Figure 3.16: Per lane outflow trajectories at segment 8 (on-ramp merge) for lane 1 (blue line) and lane 2 (red line), respectively, for Scenario 3

result, the flow entering the merging area is reduced; thus, capacity drop is avoided, obtaining the corresponding critical density value (see Fig. 3.17a).

As mentioned earlier in Section 3.4.4.1, destination D_1 can be reached using the alternative routes $R1$, $R2$ and $R3$ and destination D_2 using the routes $R4$ and $R5$. For the added destination D_3, there is only one route noted as $R6$: $S1 \rightarrow S2$. The respective results for this scenario are quite similar to the ones presented in scenario 1 (3.4.4.1). The utilized shortest route for destination D_1 is $R2$ and for destination D_2 is $R4$. Fig. 3.18 confirms that the

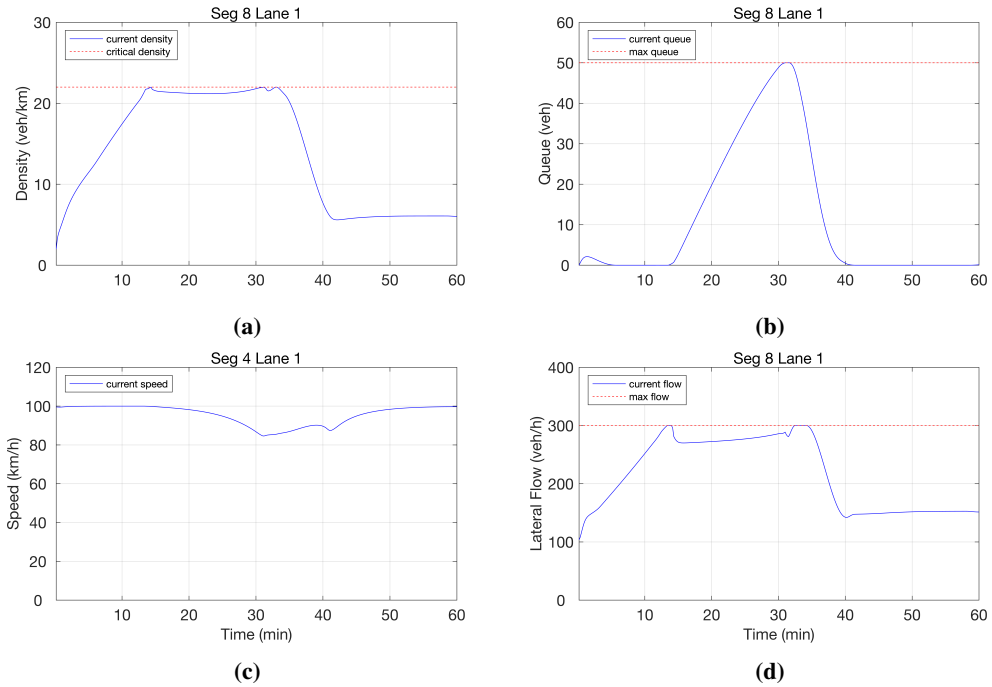

Figure 3.17: Total density value (in blue) (a), ramp queue (in blue) (b), speed value (in blue) (c), lateral flow of destination 1 (in blue) (d); and the corresponding critical, maximum, and speed limit values (in dashed red) for Scenario 4

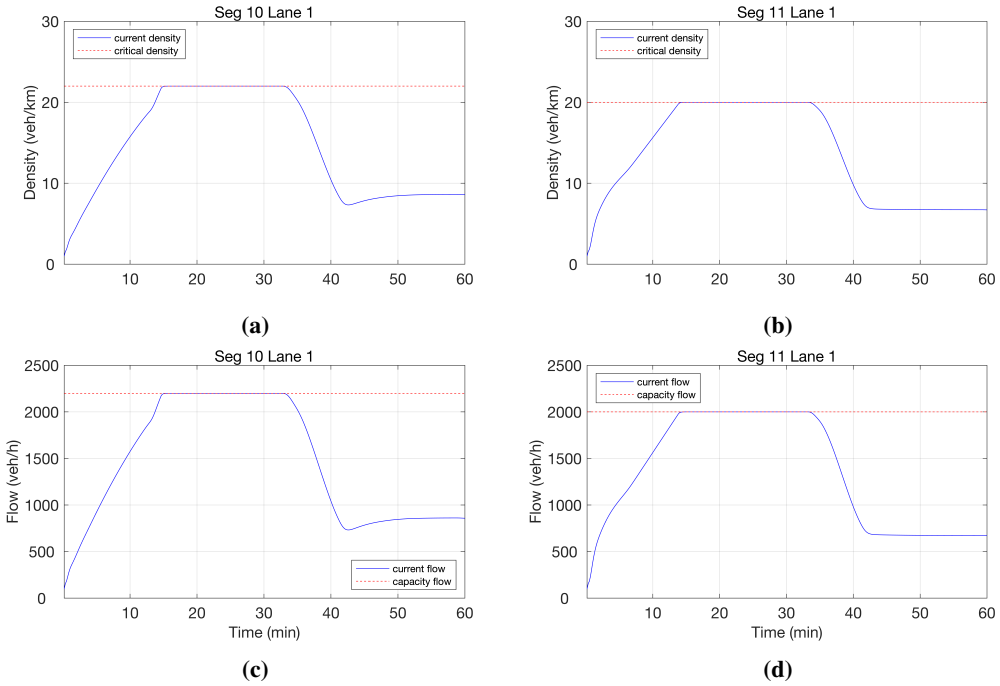

Figure 3.18: Density values (in blue) of destination 1 (a) and destination 2 (b); flow values (in blue) of destination 1 (c) and destination 2 (d); and the corresponding critical, and capacity values (in dashed red) of segments 10 and 11 for Scenario 4

optimizer utilizes the maximum capacity of the shortest routes of the network for all destinations, so as to reduce the total travel time of the system. This implies that the densities (Fig. 3.18a, 3.18b) are always equal or lower than the respective critical densities at both segments 10 and 11; hence, the outflows (Fig. 3.18c, 3.18d) are always close to the nominal capacity (2200 veh/h) for segment 10 and (2000 veh/h) for segment 11. It is worth noting that a lower critical density value (lower capacity) for segment 11 is selected, under the assumption that destination D_2 with a single lane exits to an urban network. During the high-demand period between $t = 15$ min and $t = 40$ min, the remaining vehicles travelling towards destination D_1, are using the longest route $R1$ with the densities (as depicted in Fig. 3.19a, 3.19b) at segment 5 (immediate segment after the routing diversion) never reach the respective critical values; hence, the outflows (as depicted in Fig. 3.19c, 3.19d) are always lower than the nominal capacity per lane (2200 veh/h). Furthermore, looking at the speed contour plots per lane in Fig. 3.20, one can easily observe that the speed reductions are totally avoided; hence, congestion is eliminated.

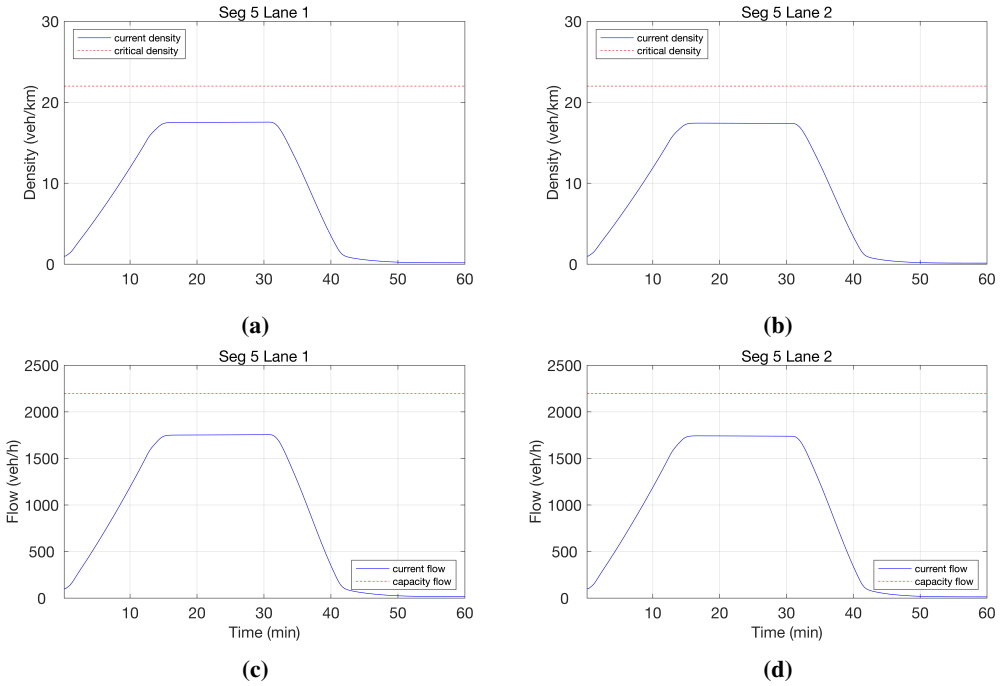

Figure 3.19: Density values (in blue) of destination 1 (a, b); flow values (in blue) of destination 1 (c, d); and the corresponding critical, and capacity values (in dashed red) of segment 5 lane 1 and lane 2 for Scenario 4

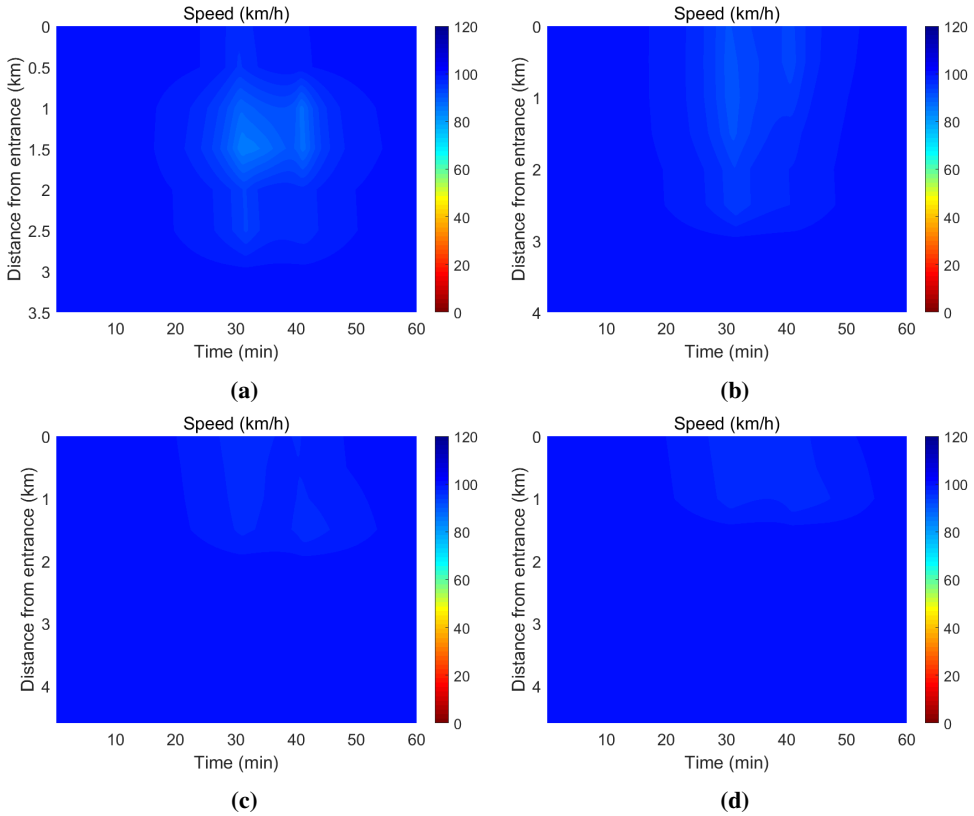

Figure 3.20: Speed contour plots for lane 1 (a), lane 2 (b), lane 3 (c) and lane 4 (d), respectively, for Scenario 4

3.5 Model predictive control

The investigations conducted in Sections 3.4.4.1, 3.4.4.2, 3.4.4.3 and 3.4.4.4 using the traffic control scheme presented in Section 3.3, were based on an open-loop optimization problem. In control theory, an open-loop solution derives control actions that are not updated during the process. As mentioned by Roncoli et al. (2015a,b) this may lead to increasingly diverging process behavior, compared with the predicted one, due to inaccuracies in predicting the external disturbances (mainly the origin demands) or limited model accuracy. For this need, a receding-horizon MPC scheme is employed in this work for evaluating the proposed traffic control scheme. Within an MPC framework such inaccuracies are limited or almost eliminated, since the optimal control problem is solved repeatedly over time. The traffic state measurements and demand predictions are updated before the next optimization horizon and used as an initial prediction for the optimization scheme. The optimization horizon as well as the update period for MPC are appropriately set, so that the discrepancies between the model predictions and the real process output are the lowest possible. The utilized MPC framework follows a multi-layer control structure (see Fig. 3.21). The structure includes the adaptation and prediction layer, the optimization layer, the local layer, and the application layer. After a loop completes a single iteration, the control actions are then passed to the motorway system and dispatched to specific CAVs for their implementation. In the following Section (3.5.1) each MPC layer is explained in more details.

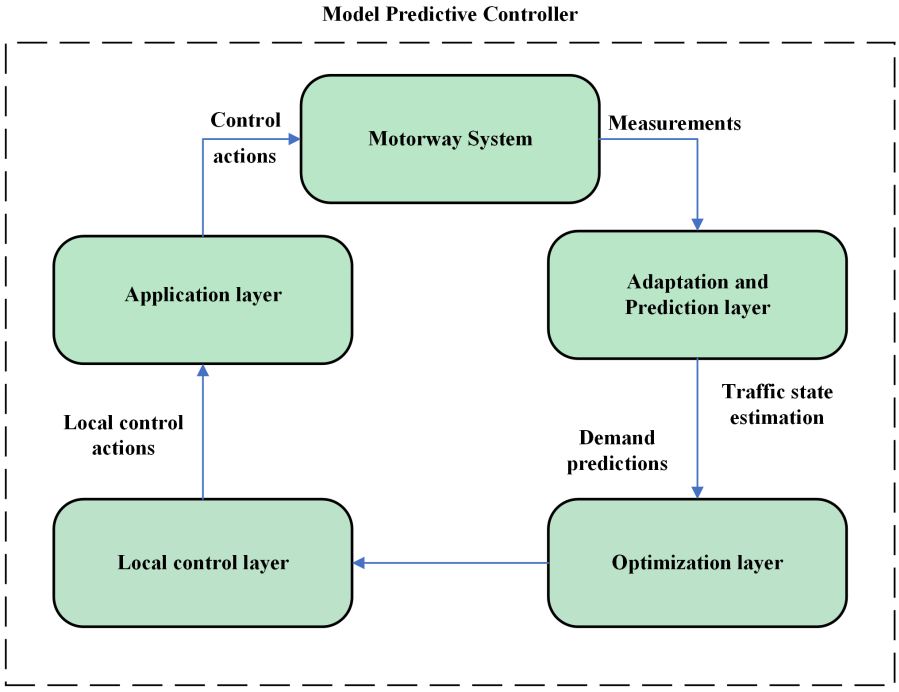

Figure 3.21: Model predictive controller framework

3.5.1 Multi-layer control framework

3.5.1.1 Adaptation and prediction layer

The first layer includes all the processes that are necessary to collect data from the motorway system at predefined measurement intervals in order to be used by the lower layers of the MPC framework. In fact, measurements are retrieved from fixed flow-sensors placed across the motorway network as well as at all origins of the network, in order to derive the necessary predicted demand for the optimization layer. In addition, all the processes required to obtain an estimate of the traffic state are also addressed within this layer, which is used as the initial state for the optimization problem. Finally, before being fed to the optimization layer, the input is processed, aggregated and filtered to remove any unrealistic values (errors).

3.5.1.2 Optimization layer

In this layer the numerical solution of the QP optimization problem is obtained, which is solved real-time in predefined control intervals. Since the objective function (3.28) is convex, it makes the problem easy to solve even for large-scale networks, like the one used in this study.

3.5.1.3 Local control layer

As soon as the optimization layer derives the optimal control solution, the local layer is introduced, which has as a purpose to ensure that the optimal control solutions are actually implemented. To fulfill this task, appropriate local-feedback controllers are utilized, that make use of the values resulting from the optimization problem as set-points. The local controllers used act on RM and MTFC using VSLs. For RM an I-type controller is used, as applied in the well-known ALINEA control strategy proposed by Papageorgiou et al. (1991). In this strategy the set-point to be used is the optimal density derived from the optimization problem for the segment-lane where the on-ramp exists. The following equation describes the controller:

$$r_{i,j}(k) = r_{i,j}(k-1) + K_r\left[\hat{\rho}_{i,j}(k^*) - \overline{\rho}_{i,j}(k)\right] \tag{3.47}$$

where, $r_{i,j}(k)$ is the ramp-flow applied, $\hat{\rho}_{i,j}(k^*)$ and $\overline{\rho}_{i,j}(k)$ are the density set-point (lower bounded by the critical density) and measured density at segment-lane (i, j) respectively and K_r is the integral gain. At the end, the computed ramp flow values, $r_{i,j}(k)$ are bounded within a range of min, max values.

Following a similar manner, the VSL feedback regulator also uses a simple I-type controller introduced by Müller et al. (2015), whose set-point is also in this case the optimal density of segment-lane (i, j). The following equation describes the employed I-type feedback controller:

$$v_{i,j}(k) = v_{i,j}(k-1) + K_v\left[\hat{\rho}_{i+1,j}(k) - \overline{\rho}_{i+1,j}(k)\right] \tag{3.48}$$

where, $v_{i,j}(k)$ is the speed limit applied at segment-lane (i, j), $\hat{\rho}_{i,j}(k)$ and $\overline{\rho}_{i,j}(k)$ are the density set-point and measured density at segment-lane (i, j) respectively and K_v is the integral gain.

3.5.1.4 Application layer

Since the optimal control solutions are not directly applicable to the motorway system, they have to be modified appropriately so as to be implemented within this layer. The outcome of the local layer is converted to actual control actions to be applied to the motorway system. In this layer direct measures (such as RM) make use of traffic signals and indirect measures

(such as LCC, DTA, MTFC) that make use of V2V, V2I and V2X communication protocols, ensure fast and accurate traffic control tasks e.g., lane changing commands and speed limits. In this work, we assume full compliance to the suggested LCC, DTA, MTFC orders and no V2V, V2I and V2X communication delays.

3.5.2 Microscopic investigations for the FRONTIER Project

The microscopic investigations were carried out using the AIMSUN microscopic simulator Aimsun (2023). AIMSUN is a commercial high-detail traffic forecasting solution software, widely used for its high customization capabilities. A part of its modelling features, including traffic network development, different vehicle types and classes, spot detectors etc., are provided using a user-friendly graphical interface (GUI), that allows the user to model anything from a single intersection to an entire network region, using all the up-to-date equipment present in a real traffic network. The default setup of the software is based on car-following and lane-changing models proposed by Gipps (1981, 1986).

3.5.2.1 Network description

A part of a motorway network located in Athens, Greece was utilized for our set of experiments. The motorway network has been imported to AIMSUN from an open-source geographic database, which involves the network graph made of nodes and sections. The model development as well as the model calibration was part of the modelling task, concluded in the framework of the European project FRONTIER (2022). During the calibration process, real traffic data from inductive loop detectors placed across the network were first collected and used for defining the traffic demands in the form of traffic states. Subsequently, the traffic states were transformed in the form of O-Ds, feeding the network origins (where the on-ramps are located). Nevertheless, calibrating and validating a network model with real traffic data is a non-trivial challenging task which requires microscopic data in high-resolution; and is certainly beyond the scope of this work. The motorway network illustrated in (Fig. 3.22) consists of 22 homogeneous segments, each one of them composed of a number of lanes and unique length. The biggest part of the network is composed of three lanes whereas a small part of it is composed of four lanes. The network covers both directions, from Metamorphosi to the Airport (Eastbound) and vice versa. It also features two mainstream origins denoted by O_1 and O_2, several on/off-ramps and four main destinations denoted by D_1, D_2, D_3 and D_4. For destination D_1, only the drivers heading towards the Olympic stadium are considered, since it is the main target of this case study to apply dynamic traffic assignment policies when a sports event takes place at the Olympic stadium.

According to FRONTIER (2022), the model for the Athens test-bed has been calibrated to match the real-life traffic conditions as close as possible. However, congestion phenomena were not observed; hence, the use of traffic control measures would have no major impact on the motorway network. Therefore, it was necessary to increase the traffic demand for the vehicles heading towards D_1 (Olympic Stadium) assuming that a sports event takes place, so as to apply the necessary traffic control measures when congestion phenomena are observed.

Starting from origin O_1, two alternative routes of 3.2 km and 5.0 km in length exist to reach the exit for D_1, another two alternative routes of 1.8 km and 3.2 km in length exist to reach the exit for D_2 and a unique route of 5.0 km exists for D_3. On the other hand, starting from origin O_2, two alternative routes of 1.8 km and 4.2 km in length exist to reach the exit for D_1, while a unique route of 1.8 km exists for D_3 and another unique one of 3.8 km exists for D_4.

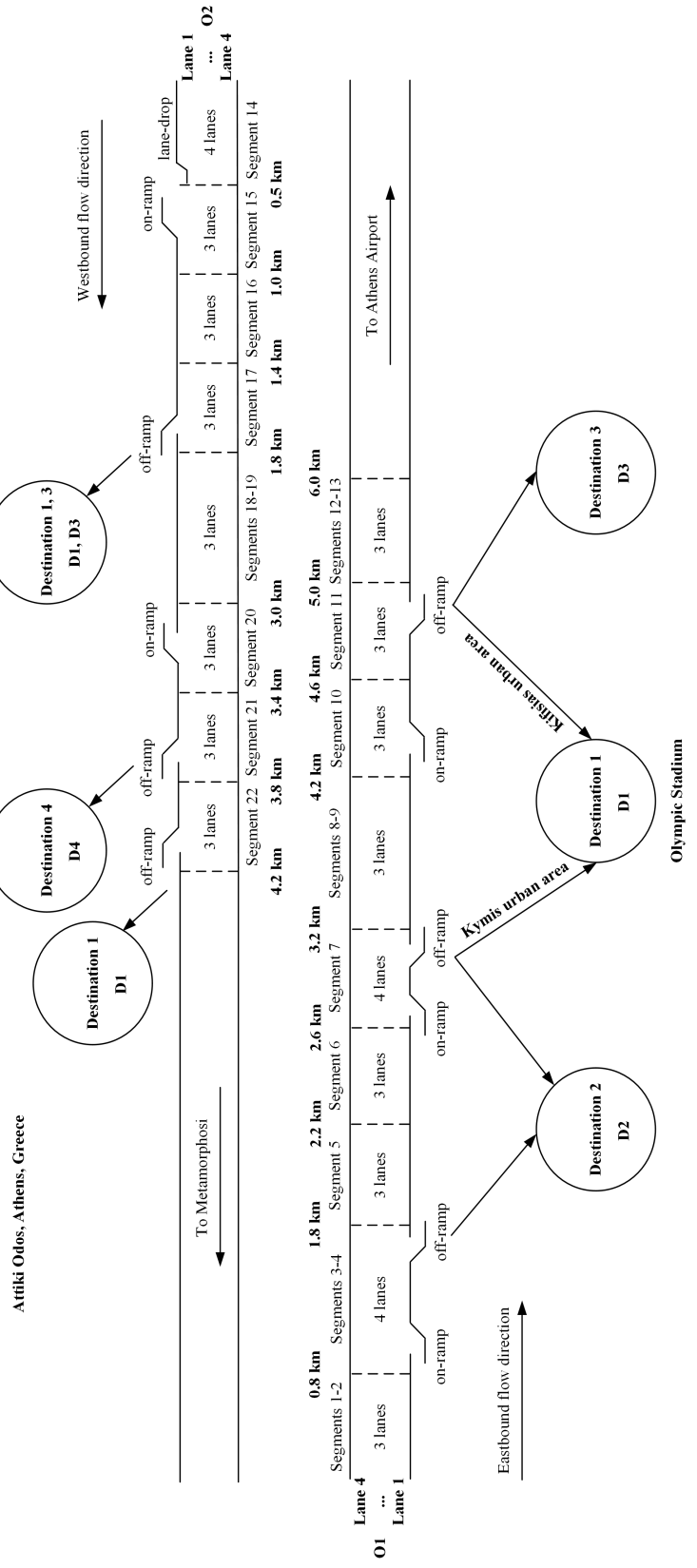

Figure 3.22: Athens network sketch.

3.5.2.2 Configuration of the macroscopic traffic flow model, QP problem and feedback regulators

The utilized CTM parameters are $v_{i,j}^{free} = 100$ km/h, $\rho_{i,j}^{cr} = 22$ veh/km, $\rho_{i,j}^{jam} = 150$ veh/km and $w_{ij}^{s} = 17.2$ km/h for each (i, j) segment-lane. The choice of the simulation step T is a crucial aspect that must be carefully taken into account. In fact, a too long simulation step could allow vehicles to travel in more than one cell during its duration, causing numerical instability of the mathematical model; on the other hand, the size of the optimization problem is also affected by this choice. In this case, a value $T = 10$ s is set, that satisfies the CFL condition (3.2) for model stability. Once the simulation step is chosen, the control steps are defined as a multiple of the simulation step. In our case, the control step for MTFC, LCC, DTA is set equal to the simulation step, that is $T^Q = T^D = 10$ sec and for RM is set equal to $T^R = 20$ sec.

The weighting parameters used in the objective function of the QP problem for the respective terms have been tuned and are $\beta_1 = 10^4$, $\beta_2 = 10^{-5}$, $\beta_3 = 10^{-5}$, $\beta_4 = 10^{-5}$, $\beta_5 = 10^{-2}$, $\beta_6 = 10^1$, $\beta_7 = 10^{-5}$ and $\beta_8 = 10^{-5}$. For the linear penalty terms related to the partial lateral flows, the weight $\alpha_{i,j,\bar{j}}^{d}$ is set either equal to zero, to encourage vehicles to change lane if necessary, or equal to 10^2, when no lane changing movement is allowed. As a result, the QP problem is a convex optimization problem and has a unique solution. In addition, upper bounds are provided for the lateral movements ($f^{\max} = 1000$ veh/h), for the on-ramp queues at the origins ($w^{\max} = 40$ veh) and for the maximum flow that is allowed to enter from the origins, ($r^{\max} = 1200$ veh/h). Furthermore, the parameters for suppressing oscillations of the control variables have been chosen as $v_{i,j}^{*} = v_{i,j}^{free}$, $\rho_{i,j}^{*} = \rho_{i,j}^{cr}$, $\delta_{i,j}^{*} = 10^2$, $\varepsilon_{i,j}^{*} = 10^2$, $w_{i,j}^{*} = w^{\max}$, $W_{i,j}^{*} = w^{\max}$ for each (i, j) segment-lane.

For the feedback controllers a control step of 20 sec is utilized, meaning that the density set-points extracted from the optimal state trajectories (densities) are changing every 20 sec. The integral gain K_v for the VSL feedback regulator is set to 0.8 km^2/(veh·h) and the integral gain K_r for RM is set to 25 km/h. Finally, the MPC optimization horizon is set equal to 10 min, whereas the update period for MPC is set to 1 min.

3.5.2.3 Project integration with AIMSUN APIs

The optimal control solutions, derived from the network level optimization problem, are cast in a MPC mode for testing via application of control actions for various penetration rates of CAVs. An algorithm based on the barrier method (Dikin, 1967) implemented in GUROBI, Gurobi Optimization, L.L.C (2023) provides a fast solution of the QP problem in a reasonable time. More precisely, the tool uses the C++ programming language, making it fast enough when cast in a MPC framework. The optimal control problem formulation was integrated with GUROBI and AIMSUN using the Application Programming Interface (API) and used in the current investigations. Fig. 3.23 illustrates the integrated approach for a single iteration using request and response functions. The API module transfers traffic data from the simulated model upon request to the interface API, using the AIMSUN Next API functions. Subsequently, the external application (GUROBI optimizer) requests the appropriate traffic data from the interface API when and to the extent needed, in order to start the optimization process. As soon as the optimization process is completed, the external library where the local-level controllers are stored, make use of the optimal control solutions derived from the QP optimization problem to derive the appropriate local-level control actions. These actions are then transferred upon request to the simulation model of AIMSUN using the AIMSUN Next API functions for proper application on CAVs.

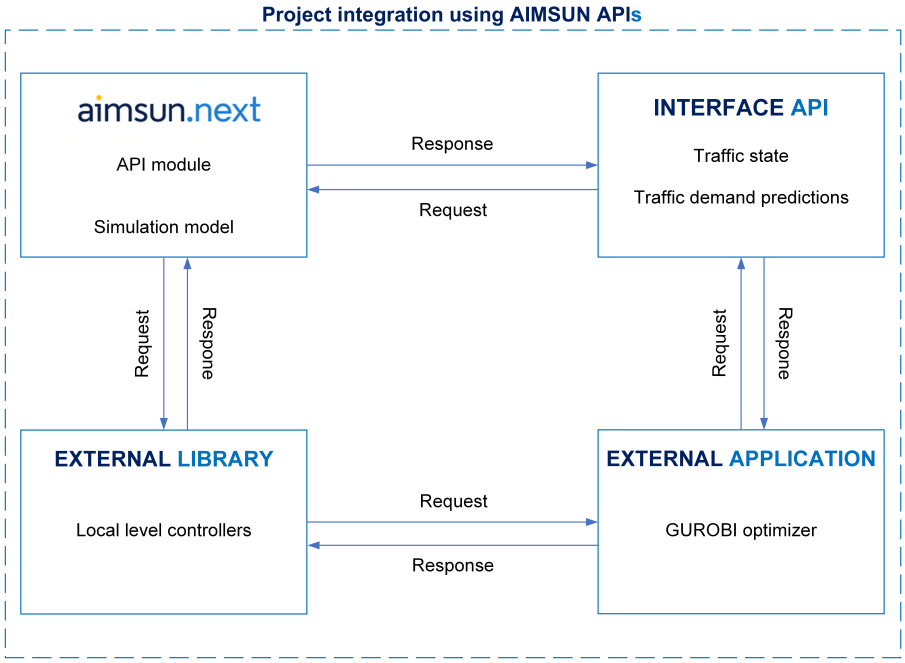

Figure 3.23: The integrated approach adopted using the C++ programming language.

3.5.2.4 Results

A comprehensive analysis and testing, to derive useful conclusions for the proposed optimal control strategy, is presented in the following sections. For a fair comparison between the work previously presented by Roncoli et al. (2015a,b) and the current one (which is an extension of the aforementioned one), experiments without the use of DTA actions were also performed. Moreover, in order to highlight the contributions of this work, we choose to present some key features that are missing from (Roncoli et al., 2015a,b) and included in this work:

1. **Entering/exiting flows of a segment-lane also consider diagonal lateral movement:** It is very common on motorway networks to have changes in the geometry e.g. lane drops, lane additions or even strong bifurcations. To this end, the modelling of the inflows and outflows of a segment-lane (i, j), is enriched with diagonal left/right lateral flows that act as additional longitudinal inflow to the downstream segment-lane (i, j).

2. **An additional traffic control measure for dynamic traffic assignment policies:** One of the major contributions of this work relies on the fact that the same variable used in the optimal control problem formulation for lane changing is also used for dynamic traffic assignment. The lane changing actions ordered by the optimizer are at the same time redirecting the traffic heading to a specific destination from another existing (alternative) route. Hence, the goal of the strategy to create a desired distribution of vehicles across all lanes and at the same time utilize all the alternatives routes of a specific destination in an optimal way, is totally achieved.

Our set of experiments replicate congestion phenomena as they appear in most real infrastructures. Each scenario has been tested on a set of 20 replications, where in the control case different penetration rates 20%, 50%, 100% of CAVs were examined. Each replication utilises the same values for the stochastic parameters, using however a different random seed that differentiates it from the others. The simulation horizon is equal to 90 minutes while the

mainstream and on-ramp (segment 15, Fig. 3.22) demand profiles for a single replication are depicted in (Fig. 3.24). The remaining on-ramps at segments 3, 7, 10 and 20 are also assumed controllable within the optimization problem but since their flows are quite low, they have no major impact on the motorway. Hence, no RM actions are applied from the local control layer.

The results obtained in case no control actions are applied are presented in Section 3.5.2.5, Section 3.5.2.6 presents the results without the use of DTA actions, while Sections 3.5.2.7, 3.5.2.8, 3.5.2.9 and 3.5.2.10 describe the results obtained when an integrated exploitation of all the available traffic control measures are applied to the motorway system. In particular, the combined use of the optimization and local control layer demonstrates the efficiency of the employed MPC control scheme.

3.5.2.5 No-control scenario

The simulation results presented in this case are derived where no control actions are applied to the motorway system. This case will be the main reference for comparison to the proposed traffic control strategy. Two KPIs will be used for the evaluation. The first is TTS, which is the actual time spent by vehicles to travel along the network and the waiting time at the queues (origins), and the second is the TD, which is the respective average value of delay encountered by the vehicles when travelling along the network.

The resulting speed plots for the eastbound direction of the motorway and the southbound direction of the Kymis urban area are presented in (Fig. 3.25). A strong congestion is formed at the 3.0 km of the motorway (Fig. 3.25a) that spills back covering a couple of kilometers on the motorway and lasts for almost 30 min. At this part of the motorway there is an offramp (segment 7, Fig. 3.22) connected to the urban area of Kymis avenue located at the southwestern part of the Olympic stadium. At the 1.0 km of the urban area (Fig. 3.25b), traffic lights are installed with fixed red and green phases. Fig. 3.25a indicates that a congestion is formed at the urban area that spills back to the motorway. Since there are no control actions, all vehicles are using the shortest route to reach their desired destination, which is the exit to Kymis avenue for both destinations D_1 and D_2. After a gradual decrease of the demand, at $t = 80$ min, speed is gradually increasing, and free-flow conditions are prevailed

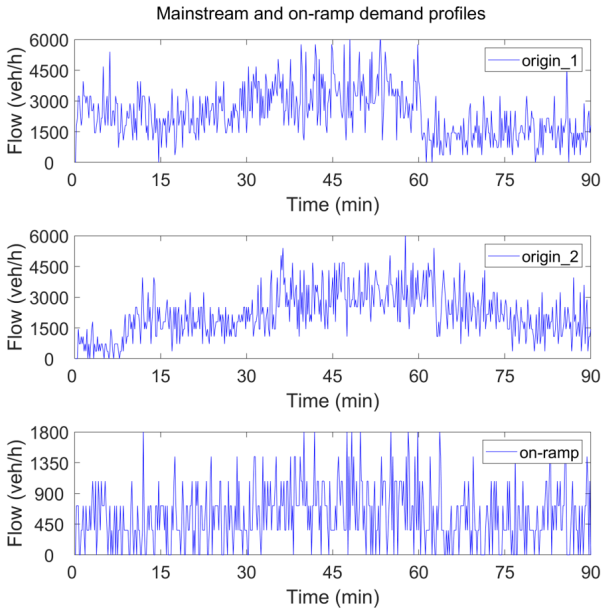

Figure 3.24: Mainstream and on-ramp (segment 15) demand profiles for a single replication.

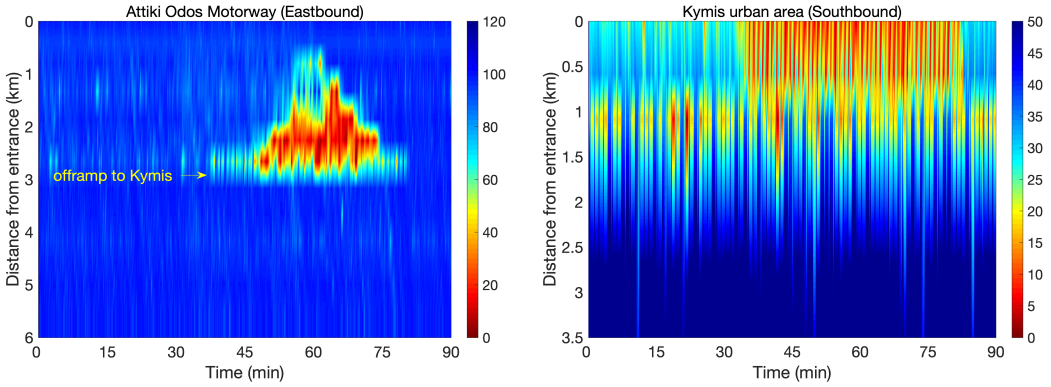

(a) **(b)**

Figure 3.25: Speed (km/h) plots for Attiki Odos eastbound (a) and Kymis southbound (b) direction for the no-control case.

for the remaining time of the simulation horizon on both the motorway and urban areas. For the westbound direction, which is the direction for all vehicles travelling from the Athens airport to Metamorphosi (Fig. 3.26a), weaving phenomena are observed at the 1.0 km where an on-ramp (segment 15, Fig. 3.22) merges to the mainstream motorway. In addition, lower speeds (included in Fig. 3.26a) are observed at the 4.2 km of the motorway, where an off-ramp (segment 22, Fig. 3.22) is connected to the urban area of Kymis. On the other hand, at the urban area of Kifisias avenue which is located at the south-eastern part of the Olympic stadium, speed drops are observed throughout the simulation horizon (Fig. 3.26b). Vehicles are using the off-ramp located at segment 17 to follow the shortest route for reaching their desired destination, D_1, D_3. In this case, the average TTS obtained a value of 2185.6 veh·h and the average TD per vehicle a value of 17.6 sec/km. The average values are obtained from a set of 20 replications with the accompanied results related to one of the replications with KPIs close to the average values.

3.5.2.6 Control scenario without DTA actions

As already mentioned in Chapter 3.5.2.4, the purpose of the experiments presented in this section was to investigate the combined use of the MTFC, LCA and RM actions without considering DTA, as initially proposed by Roncoli et al. (2015a,b). Our optimal control problem formulation was easily adopted to the one presented by Roncoli et al. (2015a,b), considering a unique route (the shortest route) for each one of the destinations included in the optimization problem. This implies that the optimizer does not have the option to redirect

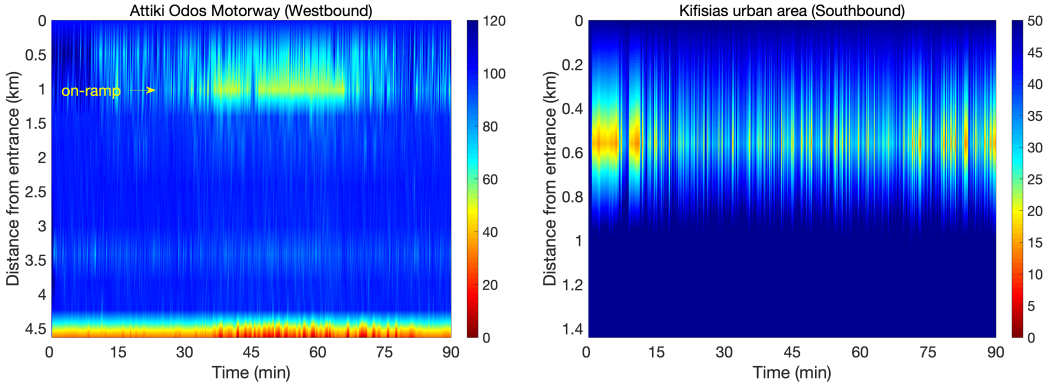

(a) **(b)**

Figure 3.26: Speed (km/h) plots for Attiki Odos westbound (a) and Kifisias southbound (b) direction for the no-control case.

the traffic using alternative routes; hence, the DTA control actions were deactivated in this manner and the lane changing actions were only used to create a desired distribution of vehicles across all lanes. The upcoming investigations as well as the ones presented in Sections 3.5.2.7, 3.5.2.8 and 3.5.2.9 use the same network with the same traffic demand profiles that generate the no-control scenario presented previously in Section 3.5.2.5; thus, allowing for a fair comparison between both optimal control problem approaches. For the sake of brevity and completeness of this work, we discuss part of the results conducted from the experiments without using DTA as an additional control action.

The effect on speed from the combined use of the control actions is presented in Fig. 3.27. For all penetration rates of CAVs investigated, an improvement on both KPIs is observed. In detail, for the lowest PR of CAVs, the average TTS obtained a percentage of improvement

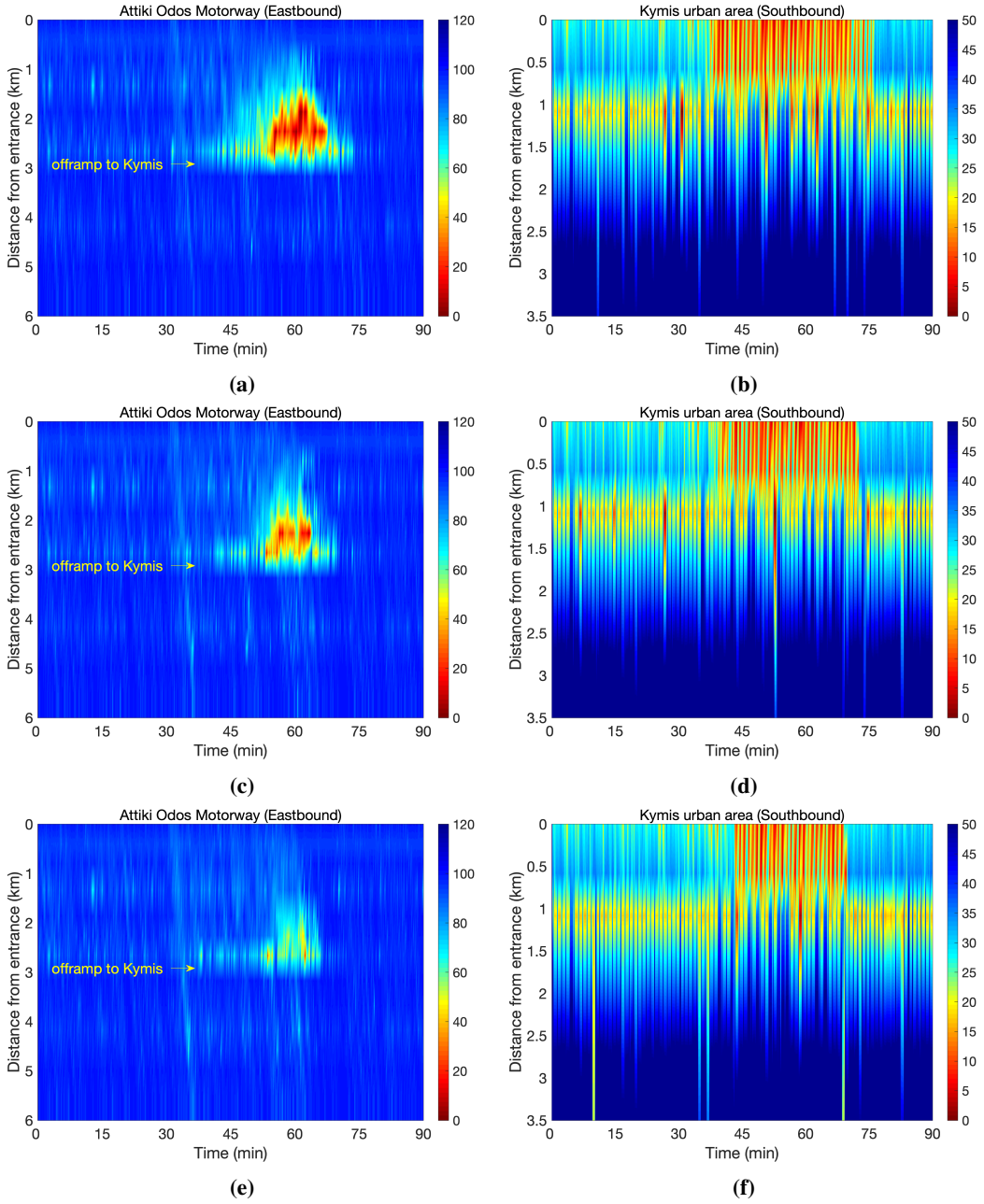

Figure 3.27: Speed (km/h) plots for Attiki Odos eastbound (a), (c), (e) and Kymis southbound (b), (d), (f) direction for the control case and 20% (top), 50% (middle) and 100% (bottom) of CAVs without DTA actions

over the no-control case of 5.4% and for the average TD per vehicle a value of 31.2%. For a higher PR of 50% CAVs, the average TTS obtained a value of 2001.1 veh·h and the average TD obtained a value of 9.4 sec/km. As a percentage of improvement over the no-control case, this is translated to 8.4% for TTS and 46.7% for TD. In a fully connected environment of 100% CAVs, both KPIs were further improved reaching the values of 1947.1 veh·h and 7.1 sec/km. As a percentage of improvement over the no-control case, this is translated to 10.9% for the average TTS and 59.7% for the average TD. Even though the percentages of improvement over the no-control case for all PRs of CAVs investigated are non-negligible, congestion is not totally eliminated.

Looking at Fig. 3.28 for the case of 50% CAVs, the speed limits requested from the local-level control layer (in red) are not in fully agreement with the ones derived from the optimization problem (in blue). In fact, at segment 6 lane 1 the local-level control actions indicate that the selected lower bound for the MTFC control actions (i.e. 40 km/h) is not enough. The congestion created at the urban area of Kymis (see Fig. 3.27d) is spilling back to the motorway (see Fig. 3.27c) with speed at the congested area reaching values close to 20 km/h.

Effective RM actions are performed at segment 15 (see Fig. 3.22, where an on-ramp merges to the mainstream motorway) especially during the high demand period between $t = 35$ min and $t = 65$ min. Fig. 3.29 displays the corresponding flow values entering from the on-ramp truncated to remain within the minimum and maximum values of 400 veh/h and 1200 veh/h, respectively. Fig. 3.29 indicates that when the density at the merging area is close or partially exceeding the selected set-point, appropriate ramp metering actions to reduce the ramp outflow are observed to avoid the steep rise of density at the merging area.

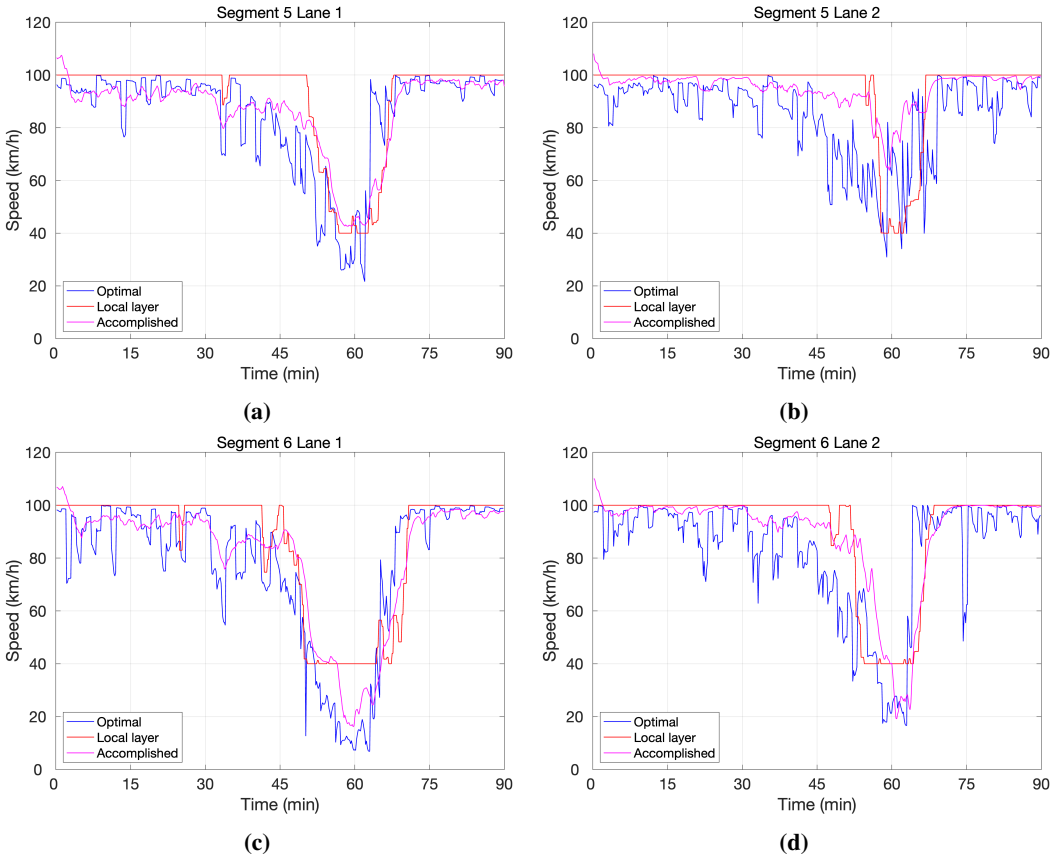

Figure 3.28: Speed limits applied at segment 5 lane 1 (a), lane 2 (b) and segment 6 lane 1 (c), lane 2 (d) for 50% of CAVs.

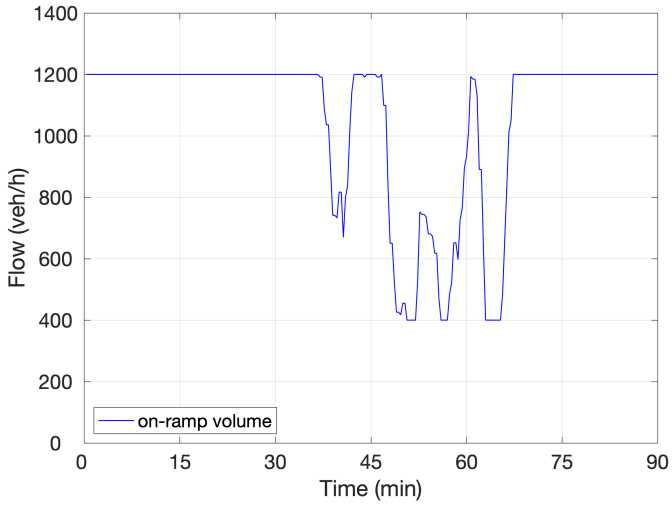

Figure 3.29: Ramp flow values at segment 15 for 100% of CAVs.

3.5.2.7 Control scenario using 20% of CAVs

In this case, the combined use of the optimization and local control layer decisions are applied to the motorway system. As mentioned previously, our optimization problem is a QP problem whose optimal control solutions are cast in an MPC mode for testing via application of control actions on CAVs. For this need, different penetration rates of CAVs were tested, so as to demonstrate the robustness of the MPC framework.

For the case of 20% CAVs, the average TTS obtained a value of 1938.6 veh·h and the average TD per vehicle a value of 7.1 sec/km. The percentages of improvement over the no-control case for both KPIs are 11.3% and 59.9%, respectively. Looking at Fig. 3.30 it is evident from the plots that a percentage of 20% CAVs is sufficient for the optimizer to redirect the traffic from the east and passing through the bottleneck at the urban area of Kymis through the motorway network (segment 8, Fig. 3.22). As a result, vehicles are using the longest route through the urban area of Kifisias avenue. Congestion is significantly reduced in space and time on the motorway (Fig. 3.30a) and at the urban area of Kymis but not completely avoided due to high demand (Fig. 3.30b).

In order to demonstrate the effectiveness of the control actions applied, Figs. 3.31 and 3.32 illustrate the outcome of the related LCC-DTA control actions whereas Fig. 3.33 the MTFC control actions derived from the local-level control layer every 20 sec. Specifically, Fig. 3.31 presents the accumulated exit flows for the eastbound part of the motorway and the southbound part of the Kymis urban area of the network for both the no-control and control scenarios.

Looking at Fig. 3.31, it is obvious that for the case of 20% of CAVs, the optimizer tackles the DTA problem effectively utilizing the alternative route for the vehicles heading towards destination D_1. Comparing the temporal aspects between the no-control (blue line) and control case (red line), one can easily observe that the accumulated flows for the control case especially during the high-demand period, are higher to the motorway and lower to the urban area, respectively. As it is shown in (Fig. 3.30b), the onset of congestion that is created to the urban area is partially avoided for $t < 42$ min and $t > 70$ min.

Fig. 3.33 illustrates the optimal speed limits derived from the optimization problem (in blue), the speed limits requested from the local-level control layer (in red), and the measured speeds (accomplished) (in magenta) for segments 5 (Fig. 3.33a) and 6 (Fig. 3.33b) and lanes 1 and 2. The measured speeds at all segment-lanes demonstrate that a penetration rate of 20% CAVs is sufficient to drive the average speed of all vehicles close to the ordered values of the local control layer, which are those applied on the motorway system. Because of the

VSL actions, a controlled congestion is formed further upstream of segment 7 which is the connection to the urban area of Kymis avenue, reduced in space and time compared to the reference case (no-control case). It is worth noting that the optimal speed limits (Fig. 3.33, blue) derived from the optimization problem are close to the ones ordered from the local-level controller (Fig. 3.33, red). But in order to ensure that the optimal state trajectories are actually implemented in the best possible way, the local control layer actions are applied. For lane 3 of segments 5 and 6, no MTFC actions are necessary.

Strong RM actions are performed at segment 15 (where an on-ramp merges to the mainstream motorway) especially during the high demand period between $t = 35$ min and $t = 65$ min. Fig. 3.34 displays the corresponding measurements of density per lane for the no-control (Fig. 3.34a) and control (Fig. 3.34b) cases. In the no-control case, a steep rise of density is observed reaching values close to 50 veh/km. In the control case, density at the merging area is maintained around the set-point, which is set as the density resulting from the optimization problem lower bounded by the critical density. This can be easily observed from Fig. 3.34b where for $t < 40$ min and $t > 70$ min the set-point is set to 20 veh/km/lane.

3.5.2.8 Control scenario using 50% of CAVs

The MPC control scheme is evaluated in this section under the assumption of 50% CAVs. For this case the average TTS obtained a value of 1921.8 veh·h and the average TD per vehicle a value of 5.9 sec/km. The percentages of improvement over the no-control case for both KPIs are 12.1% and 66.7%, respectively. Similar conclusions are derived in this case for both the eastbound and the westbound directions of the motorway. As demonstrated in Fig. 3.35, a higher penetration rate of CAVs results in greater improvement than in the previous case of 20% CAVs. Congestion on the mainstream motorway (Fig. 3.35a) is almost eliminated in space and time with free-flow conditions prevailing. On the other hand, (Fig. 3.35b), congestion has been reduced to the urban area, avoiding the onset of congestion for almost 15 minutes. Since the optimizer chooses to redirect the traffic to the motorway, higher flows are expected to reach the east-southern part of the Olympic stadium, for vehicles heading towards destination D_1. Fig. 3.31 confirms the aforementioned, since the case of 50% of CAVs influences the overall throughput for the eastbound direction during the simulation horizon on both the motorway and urban area. In comparison to the reference case (no-control case) and the previous case of 20% CAVs, the accumulated flows are further increased to the motorway and decreased to the urban area.

For the vehicles heading west, Fig. 3.36 illustrates the traffic conditions prevailing on both the motorway and the urban area of Kifisias. Compared to the reference case (Fig. 3.26a),

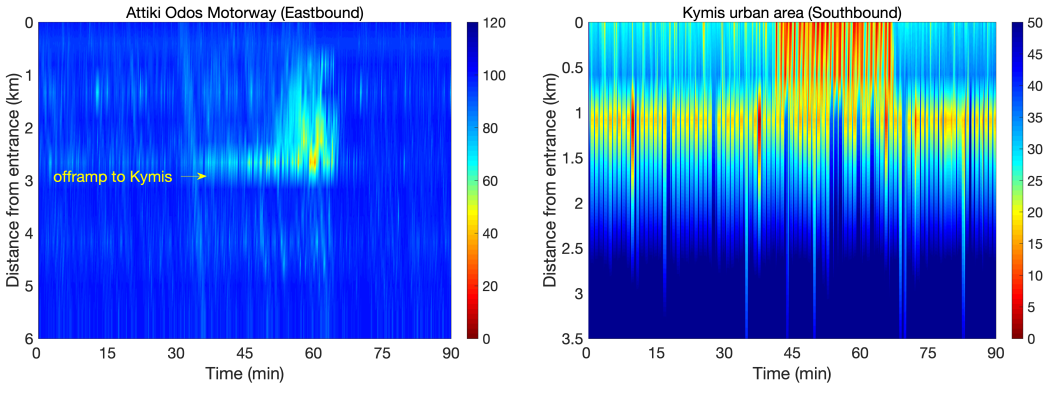

(a) **(b)**

Figure 3.30: Speed (km/h) plots for Attiki Odos eastbound (a) and Kymis southbound (b) direction for the control case and 20% of CAVs.

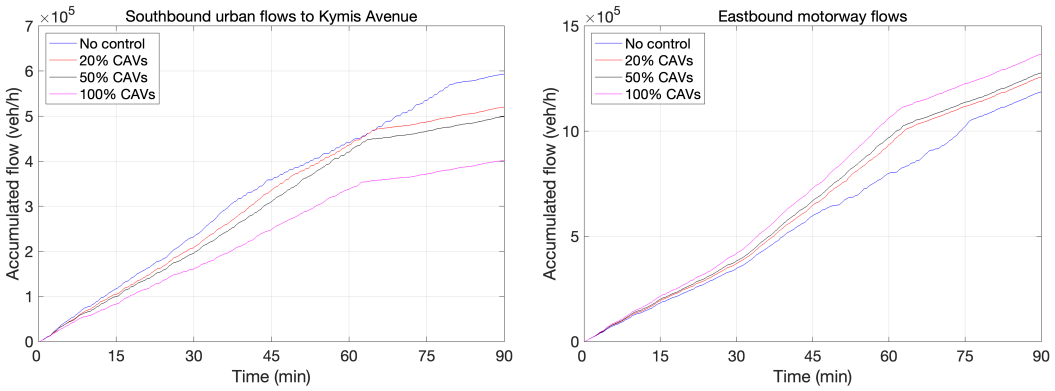

(a) **(b)**

Figure 3.31: The time-accumulated flows for the urban exit to Kymis Avenue (a) and eastbound motorway exit (b) for all penetration rates of CAVs.

lower speeds are still observed at the 4.2 km of the motorway for about 15min (Fig. 3.36a). The Kifisias urban area (Fig. 3.36b) is becoming denser in comparison to the no-control case since on both directions more vehicles are using the alternative routes to reach their desired destinations D_1, D_2 and D_1, D_3 respectively. Fig. 3.31 confirms the increase and decrease of the accumulated flow rates on the urban and motorway area, respectively.

In order to control the inflow from the on-ramp located at segment 15 (Fig. 3.22), similar RM actions are performed also in this case, especially during the high demand period between $t = 35$ min and $t = 65$ min. As in the previous case, some aspects of practical implementation for the set-point are taken into account for proper RM application. Fig. 3.36a, illustrates that at the point where the on-ramp merges to the motorway (1.0 km), a weaving effect is observed that lasts almost 30 minutes and covers 0.5 km of the motorway upstream of the merging area.

3.5.2.9 Control scenario using 100% of CAVs

The MPC control scheme is evaluated in this section under the assumption of 100% CAVs. For this case the average TTS obtained a value of 1898.1 veh·h and the average TD per vehicle a value of 4.6 sec/km. The percentages of improvement over the no-control case for both key performance indicators are 13.2% and 74.1%, respectively. As displayed in Fig. 3.37 and Fig. 3.38, in case of a fully connected environment, the proposed optimal control strategy prevents the appearance of any congestion phenomena. Fig. 3.37 depicts the eastbound direction, where free-flow conditions prevail on the motorway (Fig. 3.37a), whereas at the urban area

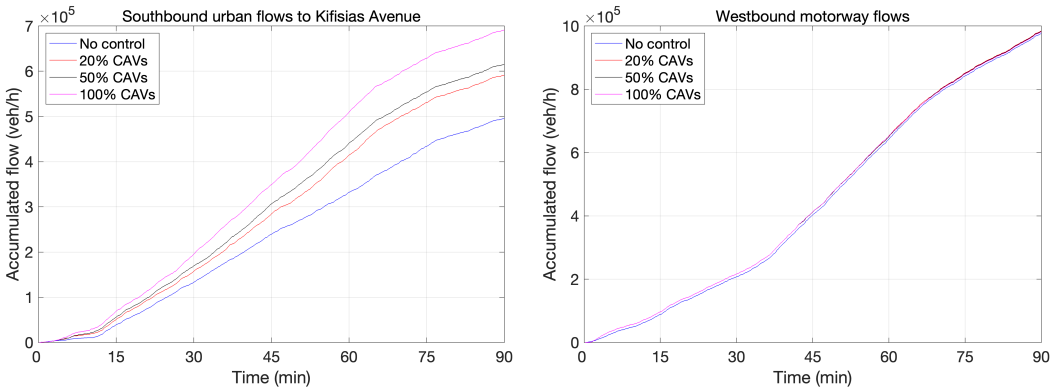

(a) **(b)**

Figure 3.32: The time-accumulated flows for the urban exit to Kifisias Avenue (a) and westbound motorway exit (b) for all penetration rates of CAVs.

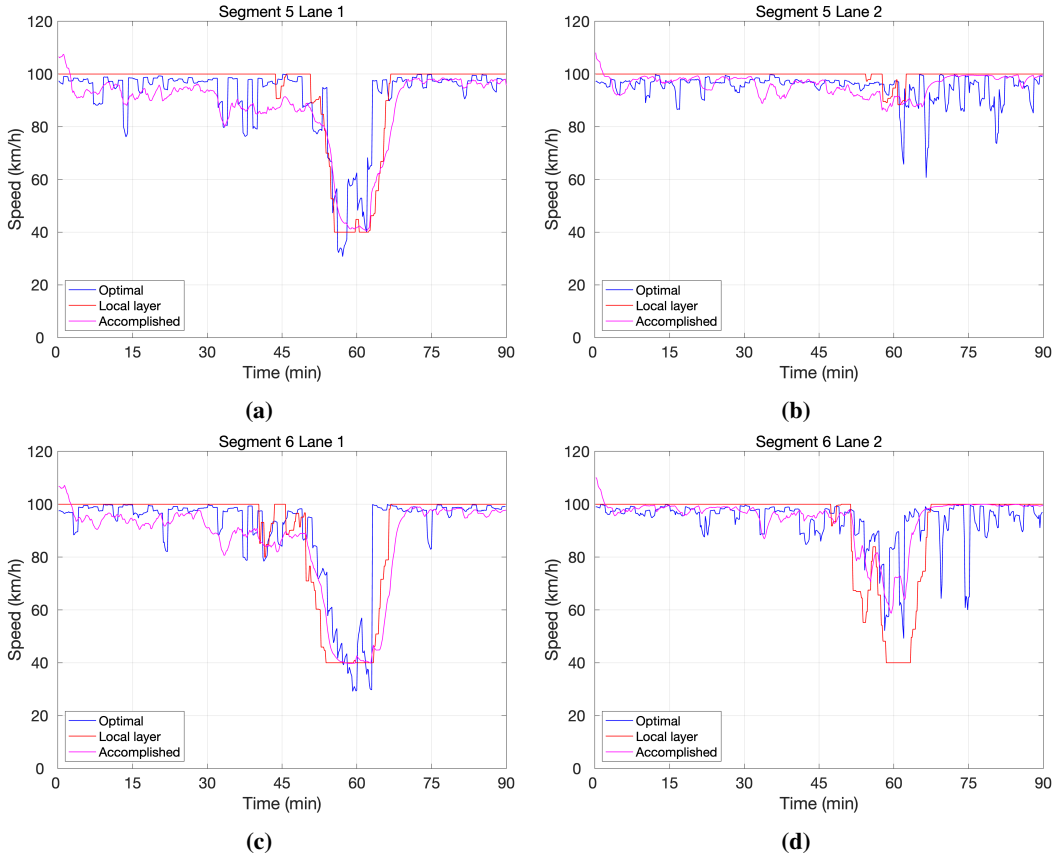

Figure 3.33: Speed limits applied at segment 5 lane 1 (a), lane 2 (b) and segment 6 lane 1 (c), lane 2 (d) for 20% of CAVs.

(Fig. 3.37b) the congestion appearing in all previous cases is totally eliminated. Similarly, for the westbound direction, lower speeds are no longer obtained at the 4.2 km of the motorway (Fig. 3.38a) and the Kifisias urban area (Fig. 3.38b) is becoming even denser compared to all previous cases. This is still normal since the decisions taken from the optimizer to redirect the traffic on both directions using alternative routes, are fully realized given a 100% penetration rate of CAVs.

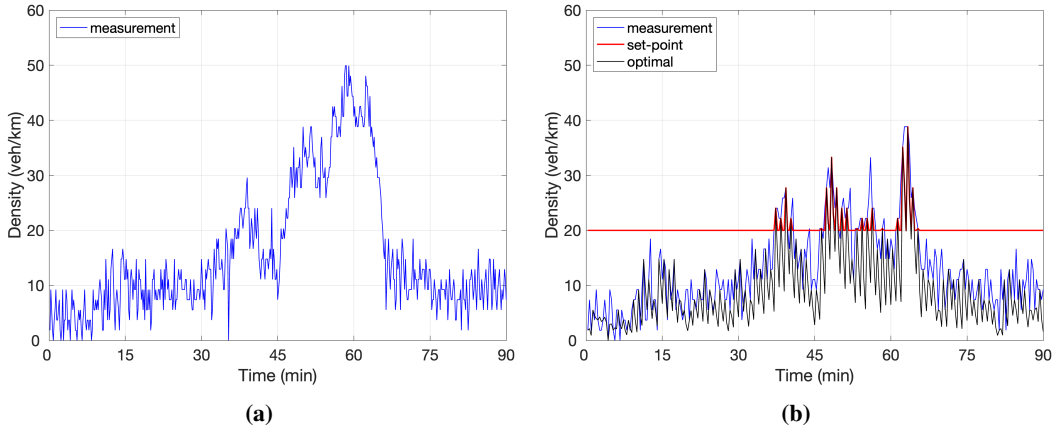

Figure 3.34: Density measurements at segment 15 lane 1 (blue) for the no-control case (a), control case (b), set-point (red), optimal (black) for 20% of CAVs.

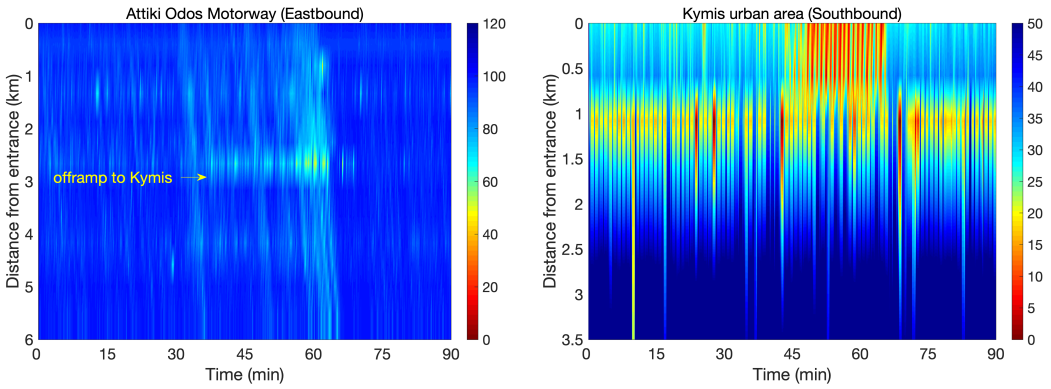

(a) **(b)**

Figure 3.35: Speed (km/h) plots for Attiki Odos eastbound (a) and Kymis southbound (b) direction for the control case and 50% of CAVs.

As expected, Fig. 3.31 and Fig. 3.32 validate that for the case of 100% of CAVs the time-accumulated flow rates behave in a similar manner as in the lower penetration rates. Specifically, for the eastbound direction (Fig. 3.31) even higher flows are accommodated on the urban area rather than on the motorway. For the westbound direction (Fig. 3.32), similar conclusions can be drawn. Analyzing again the case of 100% of CAVs, the RM control actions appear quite similar to all previous cases. Therefore, we choose to omit these results for the sake of brevity.

3.5.2.10 Aggregated results

Averaged results for all penetration rates of CAVs and for both optimal control (OC) approaches adopted are presented in Tables 3.1 and 3.2. Specifically, on both tables the average values of TTS and TD compared with the ones derived from the reference case (no-control case) are presented. As expected, an increased penetration rate of CAVs leads to a decreased value for both TTS and TD with respect to the reference case i.e. the no-control case. For all penetration rates and OC approaches, the integrated use of all the available traffic control measures led to an increased overall improvement on the average KPIs with the highest improvement observed when DTA control actions were added to the optimal control problem formulation. Looking at both Tables 3.1 and 3.2 one can easily observe that for the lower percentage of CAVs examined (20%), there is significant improvement, supporting the fact that in the case of a reduced penetration rate of CAVs, the proposed optimal control strategy when cast in an MPC framework can be effective and bring to a consistent amelioration of

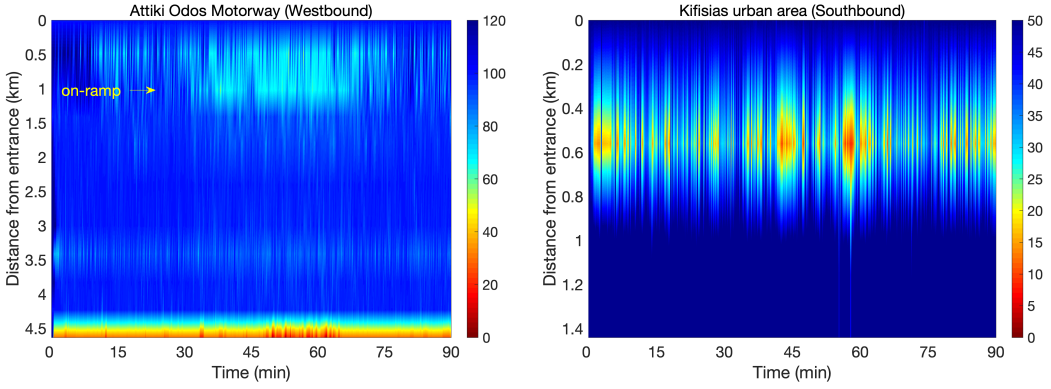

(a) **(b)**

Figure 3.36: Speed (km/h) plots for Attiki Odos westbound (a) and Kifisias southbound (b) direction for the control case and 50% of CAVs.

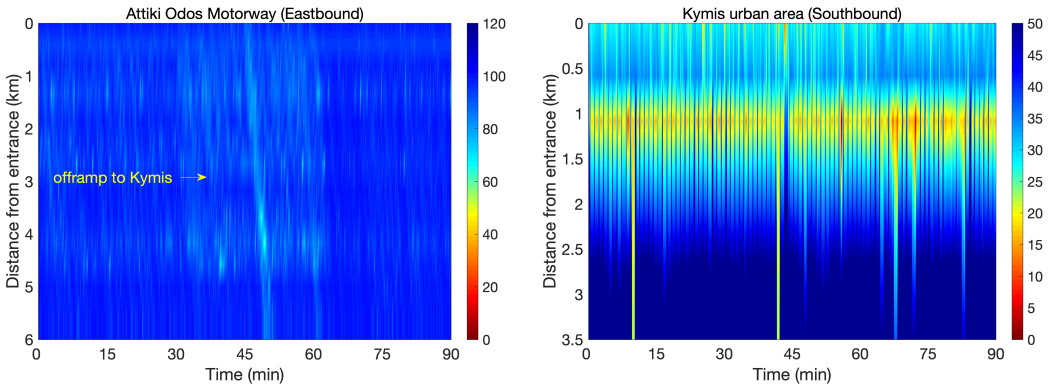

(a) **(b)**

Figure 3.37: Speed (km/h) plots for Attiki Odos eastbound (a) and Kymis southbound (b) direction for the control case and 100% of CAVs.

the traffic conditions. Additional figures related to all the control scenarios can be found in Appendix F.

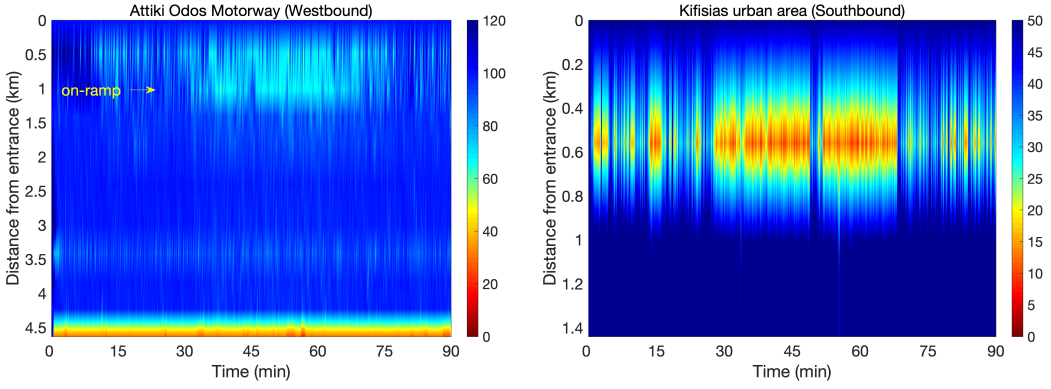

(a) **(b)**

Figure 3.38: Speed (km/h) plots for Attiki Odos westbound (a) and Kifisias southbound (b) direction for the control case and 100% of CAVs.

Table 3.1: Average Total Time Spent for all PRs and OC approaches

Total Time Spent (veh·h)							
		Without DTA			With DTA		
Penetration rate	No Control	20%	50%	100%	20%	50%	100%
Average	2185.6	2067.7	2001.1	1947.1	1938.6	1921.8	1898.1
Improvement (%)	-	5.4	8.4	10.9	11.3	12.1	13.2

Table 3.2: Average Total Delay per vehicle for all PRs and OC approaches

Total Delay (sec/km)							
		Without DTA			With DTA		
Penetration rate	No Control	20%	50%	100%	20%	50%	100%
Average	17.6	12.1	9.4	7.1	7.1	5.9	4.6
Improvement (%)	-	31.2	46.7	59.7	59.9	66.7	74.1

Chapter 4

Conclusions and future work

4.1 Conclusions

The era of CAVs is already with us, changing the role played by the traffic management center. It is expected that within the following years the conributions of CAVs will grow exponentially reshaping the future of travel on motorways and urban areas. The ability of acting as sensors and as control actuators break new ground in the way traffc information is shared and received. In the meantime, CAVs have not yet reached full maturity due to low market penetration rates. This situation creates diffculties in exploiting novel control oppotrunities that have the potential to improve the performance of traffic management and ITS. This uncertainty calls for the development of modelling and control approaches that are robust, to the extent possible, to evolving CAVs and corresponding penetration rates. This work contributes by applying novel control approaches regarding local and network level control utilizing CAVs on motorways. The local level control contributions explore the possible impact of CAVs on maximising throughput at bottleneck locations. On the other hand, the network level control conributions take into account the potential use of CAVs on centralised algorithms that include route guidance as well as strategies for mitigating congestion phenomena at motorway bottlenecks.

The development, testing and evaluation of the local level control algorithms and tools is addressed in Chapter 2. The local level traffic flow control strategies discussed involved: (a) variable speed limits for CAVs; (b) lane change advice for CAVs; (c) control of vehicle ACC time-gap for maximum throughput at bottleneck locations; and (d) dynamic lane advice for CAVs. These developments include feedback-control as well as real-time adaptive control strategies utilizing lane-based as well as aggregated over all lanes measurements of flow, density and speed. In order to get a better understanding of the behaviour of CAVs under mixed traffic conditions (explicitly on motorways), and how mixed traffic can be improved using these novel control techniques, extensive evaluations have been performed utilizing microscopic traffic simulations on two real motorway test-beds, one from Spain and one from Greece. The investigations for the Spanish test site were conducted using the SUMO software for the calibrated microscopic model of the AP7 motorway in Girona. Similarly, the investigations for the Greek test site were conducted using the AIMSUN software, for the calibrated microscopic model of Attiki Odos motorway in Athens. A variety of automation and connectivity capabilities (e.g. V2X messages) were also tested on both microscopic testing grounds.

A novel control concept that influences the mainstream traffic flow using VSLs as actuators is investigated for the case of an on-ramp merge bottleneck. The purpose of this strategy is to ensure that the flow approaching the bottleneck area is not exceeding the overall (possibly increased) capacity of the bottleneck. The strategy requires that vehicles (in our case controlled CAVs) receive speed limit/speed advice information information via V2X messages e.g. IVI, changing dynamically according to the decisions/suggestions of the feedback controller. The investigations provided empirical evidence that sending advices to a limited

number of CAVs is sufficient, due to their fast speed adaptation. This implies that a few equally distributed CAVs at all lanes may influence the whole traffic significantly; hence, the need for immediate PR maturity is not a prerequisite for the MTFC controller.

A lane changing manoeuvre is a complicated process under which a vehicle decides to change its lane in order to achieve a desirable new traffic state. In conventional traffic, these manoeuvres have a significant impact (i.e. normally negative) on traffic flow due to the limited information a driver is provided before completing a lane-changing decision. In a mixed traffic environment, the presence of CAVs has the potential to improve traffic safety and efficiency, since the exploiation of the available traffic information derives informed and safer lane-changing decisions. To this end, a lane changing novelty for the proper lane assignment of vehicles upstream of a bottleneck location utilizing CAVs is investigated in detail in this work. For a percentage of CAVs less than or equal to the half of the vehicle population, solely relying on lane changing actions was not sufficient in preventing a breakdown, in case of increased demand. On the other hand, for a fleet of CAVs more than half of the vehicle population, the formation of congestion was avoided; thus, the expected outcome of increasing the overall bottleneck capacity was also achieved.

Demonstrations concerning the ACC time-gap adaptation strategy, which reduces the time-gaps of ACC vehicles in critical areas of the motorway (e.g. bottleneck areas) for a short period of time, have shown that the suggested strategy can resolve the issue of congestion occurring at a motorway bottleneck (on-ramp merge) and increase the bottleneck throughput (capacity) significantly. In order to explore different aspects of the strategy (i.e. effects of different time-gap settings on traffic flow, sensitivity of the strategy), future market PR of CAVs were examined for two different modes of operation. Mode 1 accounts only for capacity increase using time-gap adaptation and Mode 2 accounts for capacity increase and discharge flow increase at the location of active bottlenecks using time-gap adaptation. The main observations from both test-beds investigated, conclude that even for low PR of CAVs, traffic flow efficiency over the no-control case has been improved in terms of average vehicle delays and average total travel time for both modes examined with the highest improvements observed in Mode 2.

A case study was undertaken in order to test the impact of introducing dedicated lanes for CAVs on traffic flow. The main idea behind the DLA strategy is to distribute in real-time the road traffic over road space in order to improve the overall performance and efficiency of the motorway system. The experimental settings of the scenarios tested, demonstrate the potential of the strategy to dynamically activate or deactivate a dedicated lane in real time according to the prevailing traffic conditions, while balancing the mixed traffic and maintaining its throughput at a level comparable to current traffic throughput for conventional vehicles. The aforementioned scenarios were tested on a normal multi-lane motorway, including lane-drop areas as well as pairs of on/off-ramps. Simulation evidence supports the fact that setting a CAV dedicated lane, not only benefits from the density level but also from the performance of CAVs.

From the network level control perspective, Chapter 3 introduces the combined use of four traffic control measures utilized in an optimal control problem formulation. An MPC approach was adopted taking into account the use of CAV fleets, in order demonstrate the potetial benefits that the use of CAVs on executing appropriate traffic control tasks bring to various traffic conditions. The strategies adopted within the problem formulation include: MTFC, LCC, RM and DTA. It is worth mentioning that each one of the strategies mentioned above, include different aspects of traffic management which are all essential to control the road traffic; thus, optimize traffic flow, reduce congestion phenomena and improve the overall traffic conditions both is space and time. Some of the aspects covered within this work focus on: 1) avoiding the use of the same route, especially during high-demand periods; 2) reducing the inappropriate lane-changing movement to avoid the creation of weaving, especially close

to merging (bottleneck) areas; 3) lowering the speed limit to avoid the onset of congestion and improve traffic flow on the mainstream; 4) delaying the onset of congestion by regulating the volume of vehicles entering the motorway network entrances. Two sets of microscopic simulation experiments were conducted. The first one uses MTFC, LCC and RM control actions while the second one uses additionally DTA control actions. It is worth mentioning that the first set was used as an evaluation metric to be compared to the latter one, since it is an extension of it. The combined use of all traffic control measures played a pivotal role in such a large-scale network highlighting the significant benefits of e.g. reducing the overall TTS and the per vehicle TD.

Our set of experiments were performed on the extended calibrated microscopic model of Attiki Odos corridor in Athens, Greece that includes the area of the Olympic Stadium. The geometry of the network proved beneficial for a series of tests to derive useful conclusions to all of the strategies involved in the optimal control problem formulation. Specifically, it allowed for an examination of the impact of an event-based scenario e.g. a sports event taking place in the Olympic Stadium. The MPC approach adopted to solve the integral optimal control problem, was proven beneficial at all future market PRs examined. The main goal of each one of the traffic control strategies involved, was totally achieved. The lane changing advices ordered by the optimal control strategy and implemented within the MPC framework, were used to redirect the traffic using alternative routes, and thus apply dynamic traffic assignment control. Furthermore, appropriate MTFC actions were necessary to create a controlled congestion upstream of bottleneck locations and avoid the formation of congestion on the mainstream. Lastly, appropriate RM actions were applied at an on-ramp merges so as to avoid the steep rise of density at the merging area and the formation of congestion at all lanes.

4.2 Future work

A few ideas that need further investigations in order to have a better understanding on their validity are presented here below. These ideas include different network topologies, controller configurations and experiments to be tested on both local and network level control applications using the control strategies presented in Chapters 2 and 3.

1. It is of great interest to fully analyze the behavior of the DLA control strategy presented in Section 2.5 in a more challenging motorway network with multiple pairs of on/off-ramps and for motorway stretches that have multiple lanes (i.e. more than 4 lanes) in order to test the strategy for higher penetration rates of CAVs. This implies that more than one lane will be used in the assignment logic; hence, fully utilize the presence of dedicated lanes to accomodate more CAVs in mixed traffic conditions.

2. A proper assessment of communication delays on CAVs is one of the issues that need to be further investigated in order to ensure a safe and effective operation of different local and network level control strategies. In Chapters 2 and 3, we assume full compliance and no communication delays except from the investigations conducted for the ACC time-gap adaptation strategy and which are presented in Sections 2.6.4, 2.6.4.1 and 2.6.4.2. To this end, the idea of constructing a conceptual framework that will allow us to investigate in detail different communication-related scenarios when CAVs act both as sensors and as actuators and infer conclusions on the possible negative effects of limited connectivity remains to be investigated in the near future.

3. Traffic data stemming from CAVs is considered a huge advancement in ITS. One of the ideas that was not investigated in this PhD thesis, is the use of CAVs as traffic sensors. Their ability to sense, collect and deliver in real-time useful information about

the current traffic state, demonstrate the benefits to overall road traffic management. Hence, it is of great interest to investigate in the near future the dynamic behavior of the feedback control strategies presented in Chapter 2, utilizing information from CAVs. This information can be directly provided from CAVs or from a traffic state estimation scheme like the ones presented by Bekiaris-Liberis et al. (2016), Bekiaris-Liberis et al. (2017), Fountoulakis et al. (2017), Papadopoulou et al. (2018). Such schemes, employ a Kalman filtering approach (Anderson and Moore, 1979) utilizing speed measurements stemming from CAV reports to estimate density or flow, that may then serve as the reference input to feedback control strategies. A first attempt was made during the INFRAMIX project, at which two traffic state estimation schemes (i.e. a cross-lane and a per-lane) were employed. The results reported in deliverable D5.3 (INFRAMIX, 2020) support the aforementioned.

4. A real-time traffic control strategy is considered fast enough before a radical change in traffic conditions can be observed. The network-level traffic control strategy presented in Chapter 3 has the potential to run in real-time utilizing a set of measurements already available in modern traffic systems. The strategy is formulated as a QP optimal control problem presented in Section 3.3 providing an extremely fast solution to the problem, especially at low dimensions. The network used for the microscopic investigations presented in Section 3.5.2 is considered as a large-scale network, thus it increases the dimensionality of the problem. However, a fast solution of the problem was observed in less than a minute, providing a fast application of the MPC scheme adopted. In the distant future, one can explore the potential benefits of the strategy to smaller-scale networks when the penetration rate of CAVs is sufficient and able to support the implementation of the control actions included in the OC formulation.

Bibliography

Aimsun (2023). *Aimsun Next 23 User's Manual*. Aimsun Next 23.0.0. Barcelona, Spain. URL: https://docs.aimsun.com/next/23.0.0/.

Anderson, B. D. and Moore, J. B. (1979). *Optimal filtering*. Englewood Cliffs, NJ, USA: Prentice-Hall.

Arnold, E. et al. (1988). *Congestion on Virginia's urban highways*. Tech. rep. Virginia Transportation Research Council (VTRC).

Baskar, L. D., De Schutter, B. and Hellendoorn, H. (2012). "Traffic management for automated highway systems using model-based predictive control". *IEEE Transactions on Intelligent Transportation Systems* 13.2, pp. 838–847.

Bekiaris-Liberis, N., Roncoli, C. and Papageorgiou, M. (2016). "Highway traffic state estimation with mixed connected and conventional vehicles". *IEEE Transactions on Intelligent Transportation Systems* 17.12, pp. 3484–3497.

— (2017). "Highway traffic state estimation per lane in the presence of connected vehicles". *Transportation research part B: methodological* 106, pp. 1–28.

Burger, M, Van Den Berg, M, Hegyi, A., De Schutter, B and Hellendoorn, J (2013). "Considerations for model-based traffic control". *Transportation Research Part C: Emerging Technologies* 35, pp. 1–19.

Carlson, R. C., Papamichail, I. and Papageorgiou, M. (2013). "Comparison of local feedback controllers for the mainstream traffic flow on freeways using variable speed limits". *Journal of Intelligent Transportation Systems* 17.4, pp. 268–281.

Carlson, R. C., Papamichail, I., Papageorgiou, M. and Messmer, A. (2010a). "Optimal mainstream traffic flow control of large-scale motorway networks". *Transportation Research Part C: Emerging Technologies* 18.2, pp. 193–212.

— (2010b). "Optimal motorway traffic flow control involving variable speed limits and ramp metering". *Transportation Science* 44.2, pp. 238–253.

Carlson, R. C., Papamichail, I. and Papageorgiou, M. (2011). "Local feedback-based mainstream traffic flow control on motorways using variable speed limits". *IEEE Transactions on intelligent transportation systems* 12.4, pp. 1261–1276.

Chakraborty, S., Rey, D., Levin, M. W. and Waller, S. T. (2021). "Freeway network design with exclusive lanes for automated vehicles under endogenous mobility demand". *Transportation Research Part C: Emerging Technologies* 133, p. 103440.

Chen, T., Wang, M., Gong, S., Zhou, Y. and Ran, B. (2021). "Connected and automated vehicle distributed control for on-ramp merging scenario: A virtual rotation approach". *Transportation Research Part C: Emerging Technologies* 133, p. 103451.

Chevallier, E. and Leclercq, L. (2009). "Do microscopic merging models reproduce the observed priority sharing ratio in congestion?" *Transportation Research Part C: Emerging Technologies* 17.3, pp. 328–336.

Cohen, S. (2011). "Impact of a dedicated lane on the capacity and the level of service of an urban motorway". *Procedia-Social and Behavioral Sciences* 16, pp. 196–206.

Como, G., Lovisari, E. and Savla, K. (2016). "Convexity and robustness of dynamic traffic assignment and freeway network control". *Transportation Research Part B: Methodological* 91, pp. 446–465.

Daganzo, C. F. (1994). "The cell transmission model: A dynamic representation of highway traffic consistent with the hydrodynamic theory". *Transportation Research Part B: methodological* 28.4, pp. 269–287.

— (1995). "The cell transmission model, part II: network traffic". *Transportation Research Part B: Methodological* 29.2, pp. 79–93.

Delis, A. I., Nikolos, I. K. and Papageorgiou, M. (2016). "Simulation of the penetration rate effects of ACC and CACC on macroscopic traffic dynamics". *2016 IEEE 19th International Conference on Intelligent Transportation Systems (ITSC)*. IEEE, pp. 336–341.

Diakaki, C., Papageorgiou, M. and McLean, T. (2000). "Integrated traffic-responsive urban corridor control strategy in Glasgow, Scotland: Application and evaluation". *Transportation Research Record* 1727.1, pp. 101–111.

Diakaki, C., Papageorgiou, M., Papamichail, I. and Nikolos, I. (2015). "Overview and analysis of vehicle automation and communication systems from a motorway traffic management perspective". *Transportation Research Part A: Policy and Practice* 75, pp. 147–165.

Dikin, I. (1967). "Iterative solution of problems of linear and quadratic programming". *Doklady Akademii Nauk*. Vol. 174. 4. Russian Academy of Sciences, pp. 747–748.

European Commission, E. (2018). *Motorways 2018*. Tech. rep. European Commission, Brussels, Belgium.

— (2024). *2023 figures show stalling progress in reducing road fatalities in too many countries*. Tech. rep. European Commission, Brussels, Belgium.

European Court, E. (2019). *Urban mobility in the EU*. Tech. rep. European Union, Luxembourg City, Luxembourg.

Fakhrmoosavi, F., Kamjoo, E., Zockaie, A., Mittal, A. and Fishelson, J. (2023). "Assessing the Network-Wide Impacts of Dedicated Lanes for Connected Autonomous Vehicles". *Transportation Research Record* 2677.3, pp. 371–388.

Falcocchio, J. C., Levinson, H. S., Falcocchio, J. C. and Levinson, H. S. (2015). "Managing nonrecurring congestion". *Road Traffic Congestion: A Concise Guide*, pp. 197–211.

Fellendorf, M. and Vortisch, P. (2010). "Microscopic traffic flow simulator VISSIM". *Fundamentals of traffic simulation*, pp. 63–93.

Fountoulakis, M., Bekiaris-Liberis, N., Roncoli, C., Papamichail, I. and Papageorgiou, M. (2017). "Highway traffic state estimation with mixed connected and conventional vehicles: Microscopic simulation-based testing". *Transportation Research Part C: Emerging Technologies* 78, pp. 13–33.

FRONTIER (2022). *D2.3: Network models, Report of Project FRONTIER (H2020-955317)*. Brussels, Belgium. URL: https://www.frontier-project.eu/deliverables.

Gipps, P. G. (1981). "A behavioural car-following model for computer simulation". *Transportation Research Part B: methodological* 15.2, pp. 105–111.

— (1986). "A model for the structure of lane-changing decisions". *Transportation Research Part B: Methodological* 20.5, pp. 403–414.

Gomes, G. and Horowitz, R. (2006). "Optimal freeway ramp metering using the asymmetric cell transmission model". *Transportation Research Part C: Emerging Technologies* 14.4, pp. 244–262.

Grumert, E., Ma, X. and Tapani, A. (2015). "Analysis of a cooperative variable speed limit system using microscopic traffic simulation". *Transportation Research Part C: Emerging Technologies* 52, pp. 173–186.

Guo, J., Chen, X., Pang, Y., Wang, Y. and Zheng, P. (2019). "Bottlenecks, shockwave, and off-ramp blockage on freeways". *Sustainability* 11.18, p. 4991.

GUROBI, Gurobi Optimization, L.L.C (2023). *Gurobi Optimizer Reference Manual*. version 9.0. URL: https://www.gurobi.com.

Han, Y., Chen, D. and Ahn, S. (2017). "Variable speed limit control at fixed freeway bottlenecks using connected vehicles". *Transportation Research Part B: Methodological* 98, pp. 113–134.

Han, Y., Yuan, Y., Hegyi, A. and Hoogendoorn, S. P. (2015). "Linear quadratic MPC for integrated route guidance and ramp metering". *2015 IEEE 18th International Conference on Intelligent Transportation Systems*. IEEE, pp. 1150–1155.

He, S., Ding, F., Lu, C. and Qi, Y. (2022). "Impact of connected and autonomous vehicle dedicated lane on the freeway traffic efficiency". *European Transport Research Review* 14.1, p. 12.

INFRAMIX (2018). *D2.2: Architecture and Interface Specification of the Co-Simulation Environment, Report of Project INFRAMIX (H2020-723016)*. Brussels, Belgium. URL: https://www.inframix.eu/public-deliverables/.

— (2020). *D5.3: Evaluation, impact analysis and new safety performance criteria, Report of Project INFRAMIX (H2020-723016)*. Brussels, Belgium. URL: https://www.inframix.eu/public-deliverables/.

Ioannou, P. A. and Stefanovic, M. (2005). "Evaluation of ACC vehicles in mixed traffic: Lane change effects and sensitivity analysis". *IEEE Transactions on Intelligent Transportation Systems* 6.1, pp. 79–89.

Iordanidou, G.-R., Roncoli, C., Papamichail, I. and Papageorgiou, M. (2014). "Feedback-based mainstream traffic flow control for multiple bottlenecks on motorways". *IEEE Transactions on Intelligent Transportation Systems* 16.2, pp. 610–621.

Ivanchev, J., Knoll, A., Zehe, D., Nair, S. and Eckhoff, D. (2017). "Potentials and implications of dedicated highway lanes for autonomous vehicles". *arXiv preprint arXiv:1709.07658*.

Khondaker, B. and Kattan, L. (2015). "Variable speed limit: A microscopic analysis in a connected vehicle environment". *Transportation Research Part C: Emerging Technologies* 58, pp. 146–159.

Kim, S., Kim, Y., Kim, Y. and Lee, C. (2024). "PID-Based Freeway Work Zone Merge Control with Traffic State Prediction under Mixed Traffic Flow of Connected Automated Vehicles and Manual Vehicles". *Journal of Advanced Transportation* 2024.1, p. 5554608.

Kim, Y., Ka, D. and Lee, C. (2023). "Lane-changing control with balancing lane flow at freeway merge bottlenecks in a connected vehicle environment: Application of a PID controller". *IET Intelligent Transport Systems* 17.11, pp. 2313–2332.

Knoop, V. L., Duret, A., Buisson, C. and Van Arem, B. (2010). "Lane distribution of traffic near merging zones influence of variable speed limits". *13th International IEEE Conference on Intelligent Transportation Systems*. IEEE, pp. 485–490.

Kontorinaki, M., Spiliopoulou, A., Roncoli, C. and Papageorgiou, M. (2017). "First-order traffic flow models incorporating capacity drop: Overview and real-data validation". *Transportation Research Part B: Methodological* 106, pp. 52–75.

Kotsialos, A and Papageorgiou, M (2001). "Efficiency versus fairness in network-wide ramp metering". *ITSC 2001. 2001 IEEE Intelligent Transportation Systems. Proceedings (Cat. No. 01TH8585)*. IEEE, pp. 1189–1194.

Kotsialos, A., Papageorgiou, M., Diakaki, C., Pavlis, Y. and Middelham, F. (2002). "Traffic flow modeling of large-scale motorway networks using the macroscopic modeling tool METANET". *IEEE Transactions on Intelligent Transportation Systems* 3.4, pp. 282–292.

Kotsialos, A., Papageorgiou, M. and Middelham, F. (2005). "Local and optimal coordinated ramp metering for freeway networks". *Journal of Intelligent Transportation Systems* 9.4, pp. 187–203.

Kwoczek, S., Di Martino, S. and Nejdl, W. (2014). "Predicting and visualizing traffic congestion in the presence of planned special events". *Journal of Visual Languages & Computing* 25.6, pp. 973–980.

Leclercq, L., Laval, J. A. and Chiabaut, N. (2011). "Capacity drops at merges: An endogenous model". *Procedia-Social and Behavioral Sciences* 17, pp. 12–26.

Li, Y., Li, K., Cai, L., Zhu, H. and Sun, F. (2016). "Feedback-based platoon control for connected autonomous vehicles under different communication network topologies". *2016 35th Chinese Control Conference (CCC)*. IEEE, pp. 8806–8811.

Li, Y., Waller, S. T. and Ziliaskopoulos, T. (2003). "A decomposition scheme for system optimal dynamic traffic assignment models". *Networks and Spatial Economics* 3, pp. 441–455.

Lighthill, M. J. and Whitham, G. B. (1955). "On kinematic waves II. A theory of traffic flow on long crowded roads". *Proceedings of the Royal Society of London. Series A. Mathematical and Physical Sciences* 229.1178, pp. 317–345.

Lopez, P.-A., Behrisch, M., Bieker-Walz, L., Erdmann, J., Flötteröd, Y.-P., Hilbrich, R., Lücken, L., Rummel, J., Wagner, P. and Wießner, E. (2018). "Microscopic Traffic Simulation using SUMO". *The 21st IEEE International Conference on Intelligent Transportation Systems*. IEEE. URL: https://elib.dlr.de/124092/.

Manolis, D., Spiliopoulou, A., Vandorou, F. and Papageorgiou, M. (2020). "Real time adaptive cruise control strategy for motorways". *Transportation Research Part C: Emerging Technologies* 115, p. 102617.

Markantonakis, V. (2018). *Integrated Traffic Control for Motorways using Variable Speed Limits and Lane Change Control Actions*. Master's thesis. Available at https://dias.library.tuc.gr/view/78756. Chania.

Markantonakis, V. and Papamichail, I. (2023). "Integrated optimal control for multi-lane motorway networks". *2023 31st Mediterranean Conference on Control and Automation (MED)*. IEEE, pp. 464–471.

Markantonakis, V., Skoufoulas, D. I., Papamichail, I. and Papageorgiou, M. (2019). "Integrated traffic control for freeways using variable speed limits and lane change control actions". *Transportation Research Record* 2673.9, pp. 602–613.

Messmer, A. and Papageorgiou, M. (1990). "METANET: A macroscopic simulation program for motorway networks". *Traffic Engineering & Control* 31.8-9, pp. 466–470.

Müller, E. R., Carlson, R. C., Kraus, W. and Papageorgiou, M. (2015). "Microsimulation analysis of practical aspects of traffic control with variable speed limits". *IEEE Transactions on Intelligent Transportation Systems* 16.1, pp. 512–523.

Ngoduy, D. (2013). "Instability of cooperative adaptive cruise control traffic flow: A macroscopic approach". *Communications in Nonlinear Science and Numerical Simulation* 18.10, pp. 2838–2851.

Papadopoulou, S., Roncoli, C., Bekiaris-Liberis, N., Papamichail, I. and Papageorgiou, M. (2018). "Microscopic simulation-based validation of a per-lane traffic state estimation scheme for highways with connected vehicles". *Transportation Research Part C: Emerging Technologies* 86, pp. 441–452.

Papageorgiou, M., Ben-Akiva, M., Bottom, J., Bovy, P. H., Hoogendoorn, S. P., Hounsell, N. B., Kotsialos, A. and McDonald, M. (2007). "ITS and traffic management". *Handbooks in Operations Research and Management Science* 14, pp. 715–774.

Papageorgiou, M., Diakaki, C., Dinopoulou, V., Kotsialos, A. and Wang, Y. (2003). "Review of road traffic control strategies". *Proceedings of the IEEE* 91.12, pp. 2043–2067.

Papageorgiou, M., Hadj-Salem, H., Blosseville, J.-M., et al. (1991). "ALINEA: A local feedback control law for on-ramp metering". *Transportation Research Record* 1320.1, pp. 58–67.

Papageorgiou, M., Kosmatopoulos, E. and Papamichail, I. (2008). "Effects of variable speed limits on motorway traffic flow". *Transportation Research Record* 2047.1, pp. 37–48.

Papageorgiou, M. and Papamichail, I. (2008). "Overview of traffic signal operation policies for ramp metering". *Transportation Research Record* 2047.1, pp. 28–36.

Papamichail, I., Bekiaris-Liberis, N., Delis, A. I., Manolis, D., Mountakis, K.-S., Nikolos, I. K., Roncoli, C. and Papageorgiou, M. (2019). "Motorway traffic flow modelling, estimation and control with vehicle automation and communication systems". *Annual Reviews in Control* 48, pp. 325–346.

Pavlis, Y. and Papageorgiou, M. (1999). "Simple decentralized feedback strategies for route guidance in traffic networks". *Transportation Science* 33.3, pp. 264–278.

Protzmann, R., Schuenemann, B. and Radusch, I. (2017a). "Simulation of Convergent Networks for Intelligent Transport Systems with VSimRTI: High Mobile Wireless Nodes".

Protzmann, R., Schünemann, B. and Radusch, I. (2017b). "Simulation of convergent networks for Intelligent Transport Systems with VSimRTI". *Networking Simulation for Intelligent Transportation Systems: High Mobile Wireless Nodes*, pp. 1–28.

Rad, S. R., Farah, H., Taale, H., Arem, B. van and Hoogendoorn, S. P. (2020). "Design and operation of dedicated lanes for connected and automated vehicles on motorways: A conceptual framework and research agenda". *Transportation research part C: emerging technologies* 117, p. 102664.

Roncoli, C., Bekiaris-Liberis, N. and Papageorgiou, M. (2016). "Optimal lane-changing control at motorway bottlenecks". *2016 IEEE 19th International Conference on Intelligent Transportation Systems (ITSC)*. IEEE, pp. 1785–1791.

— (2017). "Lane-changing feedback control for efficient lane assignment at motorway bottlenecks". *Transportation Research Record* 2625.1, pp. 20–31.

Roncoli, C., Papageorgiou, M. and Papamichail, I. (2015a). "Traffic flow optimisation in presence of vehicle automation and communication systems–Part I: A first-order multi-lane model for motorway traffic". *Transportation Research Part C: Emerging Technologies* 57, pp. 241–259.

— (2015b). "Traffic flow optimisation in presence of vehicle automation and communication systems–Part II: Optimal control for multi-lane motorways". *Transportation Research Part C: Emerging Technologies* 57, pp. 260–275.

Roncoli, C., Papamichail, I. and Papageorgiou, M. (2014). "Model predictive control for multi-lane motorways in presence of VACS". *17th International IEEE Conference on Intelligent Transportation Systems (ITSC)*. IEEE, pp. 501–507.

Sha, H., Singh, M. K., Haouari, R., Papazikou, E., Quddus, M., Quigley, C., Chaudhry, A., Thomas, P., Weijermars, W. and Morris, A. (2024). "Network-wide safety impacts of dedicated lanes for connected and autonomous vehicles". *Accident Analysis & Prevention* 195, p. 107424.

Shinskey, F. G. (1996). *Process control systems: application, design, and tuning*. McGraw-Hill.

Shladover, S. E., Su, D. and Lu, X.-Y. (2012). "Impacts of cooperative adaptive cruise control on freeway traffic flow". *Transportation Research Record* 2324.1, pp. 63–70.

Skabardonis, A., Varaiya, P. and Petty, K. F. (2003). "Measuring recurrent and nonrecurrent traffic congestion". *Transportation Research Record* 1856.1, pp. 118–124.

Spiliopoulou, A, Kontorinaki, M, Papamichail, I and Papageorgiou, M (2014a). "Real-time route diversion control at congested off-ramp areas-Part II: route guidance versus off-ramp closure". *Procedia-Social and Behavioral Sciences* 111, pp. 1102–1111.

Spiliopoulou, A., Kontorinaki, M., Papageorgiou, M. and Kopelias, P. (2014b). "Macroscopic traffic flow model validation at congested freeway off-ramp areas". *Transportation Research Part C: Emerging Technologies* 41, pp. 18–29.

Spiliopoulou, A., Kontorinaki, M., Papamichail, I. and Papageorgiou, M. (2013). "Real-time route diversion control at congested motorway off-ramp areas-Part I: User-optimum route guidance". *16th International IEEE Conference on Intelligent Transportation Systems (ITSC 2013)*. IEEE, pp. 2119–2125.

Spiliopoulou, A., Manolis, D., Vandorou, F. and Papageorgiou, M. (2018). "Adaptive cruise control operation for improved motorway traffic flow". *Transportation Research Record* 2672.22, pp. 24–35.

Srivastava, A. and Geroliminis, N. (2013). "Empirical observations of capacity drop in freeway merges with ramp control and integration in a first-order model". *Transportation Research Part C: Emerging Technologies* 30, pp. 161–177.

Tajdari, F., Ramezanian, H., Paydarfar, S., Lashgari, A. and Maghrebi, S. (2022). "Flow metering and lane-changing optimal control with ramp-metering saturation". *2022 CPSSI 4th International Symposium on Real-Time and Embedded Systems and Technologies (RTEST)*. IEEE, pp. 1–6.

Tajdari, F., Roncoli, C., Bekiaris-Liberis, N. and Papageorgiou, M. (2019). "Integrated ramp metering and lane-changing feedback control at motorway bottlenecks". *2019 18th European Control Conference (ECC)*. IEEE, pp. 3179–3184.

Treiber, M. and Helbing, D. (2003). "Memory effects in microscopic traffic models and wide scattering in flow-density data". *Physical Review E* 68.4, p. 046119.

Treiber, M., Hennecke, A. and Helbing, D. (2000). "Congested traffic states in empirical observations and microscopic simulations". *Physical review E* 62.2, p. 1805.

Tympakianaki, A., Spiliopoulou, A, Kouvelas, A., Papamichail, I., Papageorgiou, M. and Wang, Y. (2014). "Real-time merging traffic control for throughput maximization at motorway work zones". *Transportation Research Part C: Emerging Technologies* 44, pp. 242–252.

Vander Laan, Z. and Sadabadi, K. F. (2017). "Operational performance of a congested corridor with lanes dedicated to autonomous vehicle traffic". *International Journal of Transportation Science and Technology* 6.1, pp. 42–52.

Wang, J., Liu, R. and Montgomery, F. (2005). "Car-following model for motorway traffic". *Transportation Research Record* 1934.1, pp. 33–42.

Wang, J., Li, X., Liao, S. S. and Hua, Z. (2013). "A hybrid approach for automatic incident detection". *IEEE Transactions on Intelligent Transportation Systems* 14.3, pp. 1176–1185.

Wang, Y., Kosmatopoulos, E. B., Papageorgiou, M. and Papamichail, I. (2014). "Local ramp metering in the presence of a distant downstream bottleneck: Theoretical analysis and simulation study". *IEEE Transactions on Intelligent Transportation Systems* 15.5, pp. 2024–2039.

Wang, Y., Messmer, A. and Papageorgiou, M. (2001). "Freeway network simulation and dynamic traffic assignment with METANET tools". *Transportation Research Record* 1776.1, pp. 178–188.

Wang, Y., Pang, Y., Chen, X. and Kan, Y. (2016). "Off-Ramp Blockage on Freeways". *IFAC-PapersOnLine* 49.3, pp. 159–164.

Wang, Y., Yu, X., Zhang, S., Zheng, P., Guo, J., Zhang, L., Hu, S., Cheng, S. and Wei, H. (2020). "Freeway traffic control in presence of capacity drop". *IEEE Transactions on Intelligent Transportation Systems* 22.3, pp. 1497–1516.

Wardrop, J. G. (1952). "Road paper. some theoretical aspects of road traffic research." *Proceedings of the Institution of Civil Engineers* 1.3, pp. 325–362.

Wei, S., Zou, Y., Zhang, X., Zhang, T. and Li, X. (2019). "An integrated longitudinal and lateral vehicle following control system with radar and vehicle-to-vehicle communication". *IEEE Transactions on Vehicular Technology* 68.2, pp. 1116–1127.

Weng, J. and Meng, Q. (2013). "Estimating capacity and traffic delay in work zones: An overview". *Transportation Research Part C: Emerging Technologies* 35, pp. 34–45.

Wu, Y., Abdel-Aty, M., Wang, L. and Rahman, M. S. (2020). "Combined connected vehicles and variable speed limit strategies to reduce rear-end crash risk under fog conditions". *Journal of Intelligent Transportation Systems* 24.5, pp. 494–513.

Yao, Z., Ren, T., Wang, Y., Xu, Z. and Jiang, Y. (2023). "Fundamental diagram of mixed traffic flow considering dedicated and shared lanes management policies for CAVs". *IEEE Transactions on Transportation Electrification*.

Ye, L. and Yamamoto, T. (2018). "Impact of dedicated lanes for connected and autonomous vehicle on traffic flow throughput". *Physica A: Statistical Mechanics and its Applications* 512, pp. 588–597.

Yperman, I. (2007). "The link transmission model for dynamic network loading". PhD thesis. Katholieke Universiteit Leuven.

Yuan, K., Knoop, V. L. and Hoogendoorn, S. P. (2015). "Capacity drop: Relationship between speed in congestion and the queue discharge rate". *Transportation Research Record* 2491.1, pp. 72–80.

Zhang, Y. and Ioannou, P. A. (2016). "Combined variable speed limit and lane change control for highway traffic". *IEEE Transactions on Intelligent Transportation Systems* 18.7, pp. 1812–1823.

— (2017). "Coordinated variable speed limit, ramp metering and lane change control of highway traffic". *IFAC-PapersOnLine* 50.1, pp. 5307–5312.

Zhao, X and Gao, Z (2005). "Controlling traffic jams by a feedback signal". *The European Physical Journal B-Condensed Matter and Complex Systems* 43, pp. 565–572.

Zheng, H. and Chiu, Y.-C. (2011). "A network flow algorithm for the cell-based single-destination system optimal dynamic traffic assignment problem". *Transportation Science* 45.1, pp. 121–137.

Zheng, H., Chiu, Y.-C. and Mirchandani, P. B. (2015). "On the system optimum dynamic traffic assignment and earliest arrival flow problems". *Transportation Science* 49.1, pp. 13–27.

Zhu, F. and Ukkusuri, S. V. (2015). "A linear programming formulation for autonomous intersection control within a dynamic traffic assignment and connected vehicle environment". *Transportation Research Part C: Emerging Technologies* 55, pp. 363–378.

Ziebinski, A., Cupek, R., Grzechca, D. and Chruszczyk, L. (2017). "Review of advanced driver assistance systems (ADAS)". *AIP Conference Proceedings*. Vol. 1906. 1. AIP Publishing.

Ziliaskopoulos, A. K. (2000). "A linear programming model for the single destination system optimum dynamic traffic assignment problem". *Transportation Science* 34.1, pp. 37–49.

Appendix A

ACC concept: Additional figures related to the results

A.1 Flow, speed, density trajectories and fundamental diagrams for the Spanish test-bed

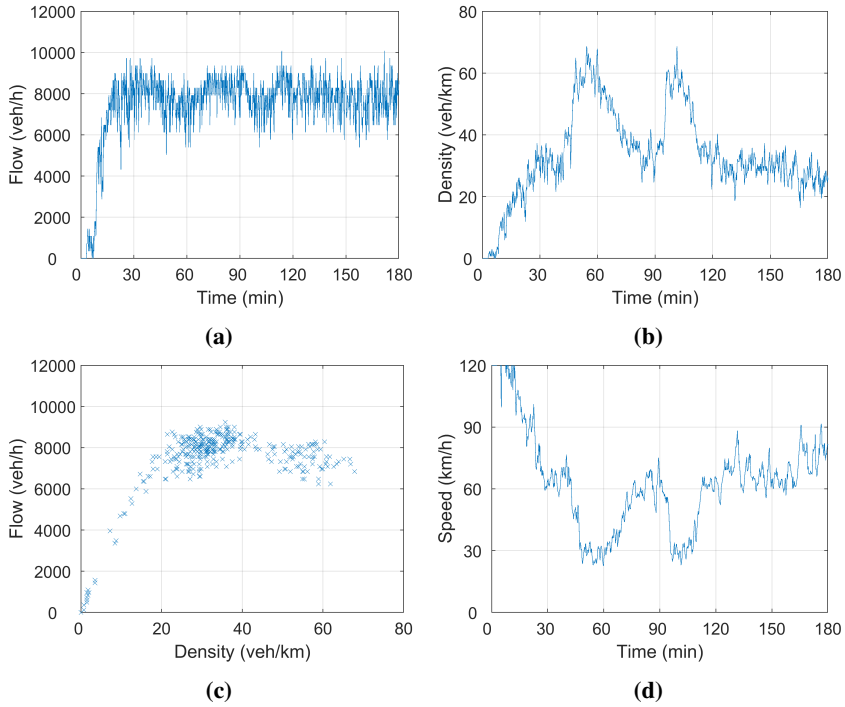

Figure A.1: ACC – Flow (a), density (b), FD (c) and speed (d) values for the no-control case and for the 30-45-25 CV-CCV-CAV configuration at the bottleneck area (segment 31).

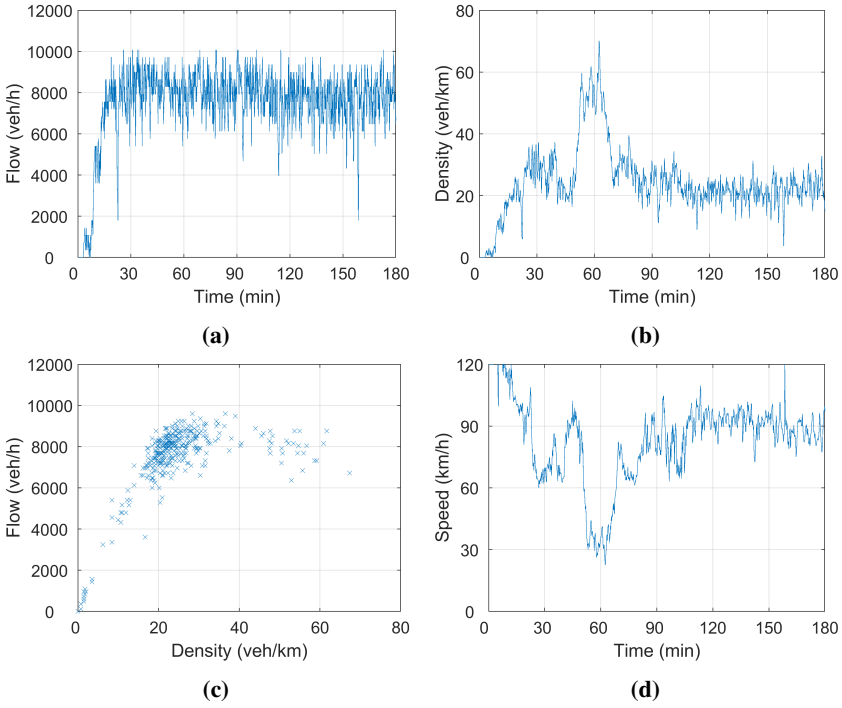

Figure A.2: ACC – Flow (a), density (b), FD (c) and speed (d) values for the control case with Full RSU coverage and $T_{min} = 1.2$ sec, for the 30-45-25 CV-CCV-AV configuration at the bottleneck area (segment 31).

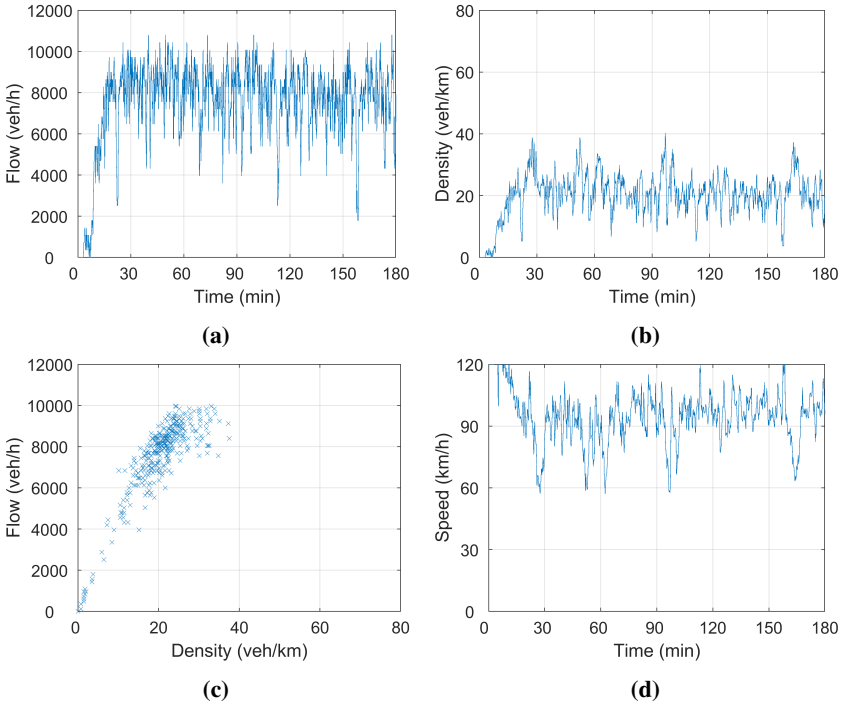

Figure A.3: ACC – Flow (a), density (b), FD (c) and speed (d) values for the control case with Full RSU coverage and $T_{min} = 1.0$ sec, for the 30-45-25 CV-CCV-AV configuration at the bottleneck area (segment 31).

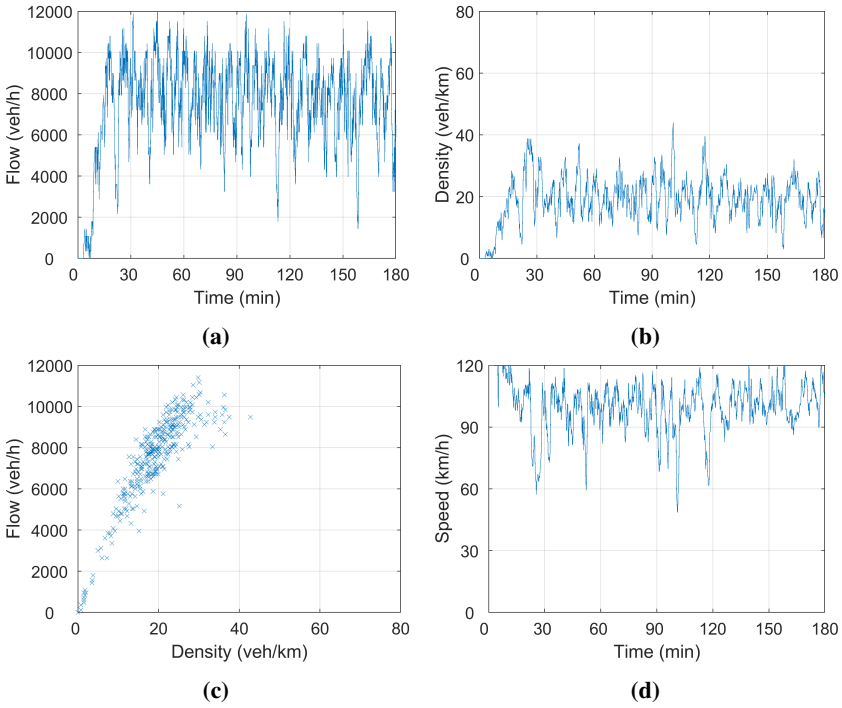

Figure A.4: ACC – Flow (a), density (b), FD (c) and speed (d) values for the control case with Full RSU coverage and $T_{min} = 0.8$ sec, for the 30-45-25 CV-CCV-AV configuration at the bottleneck area (segment 31).

A.2 Time-gap values in relation to flow values for the Spanish test-bed

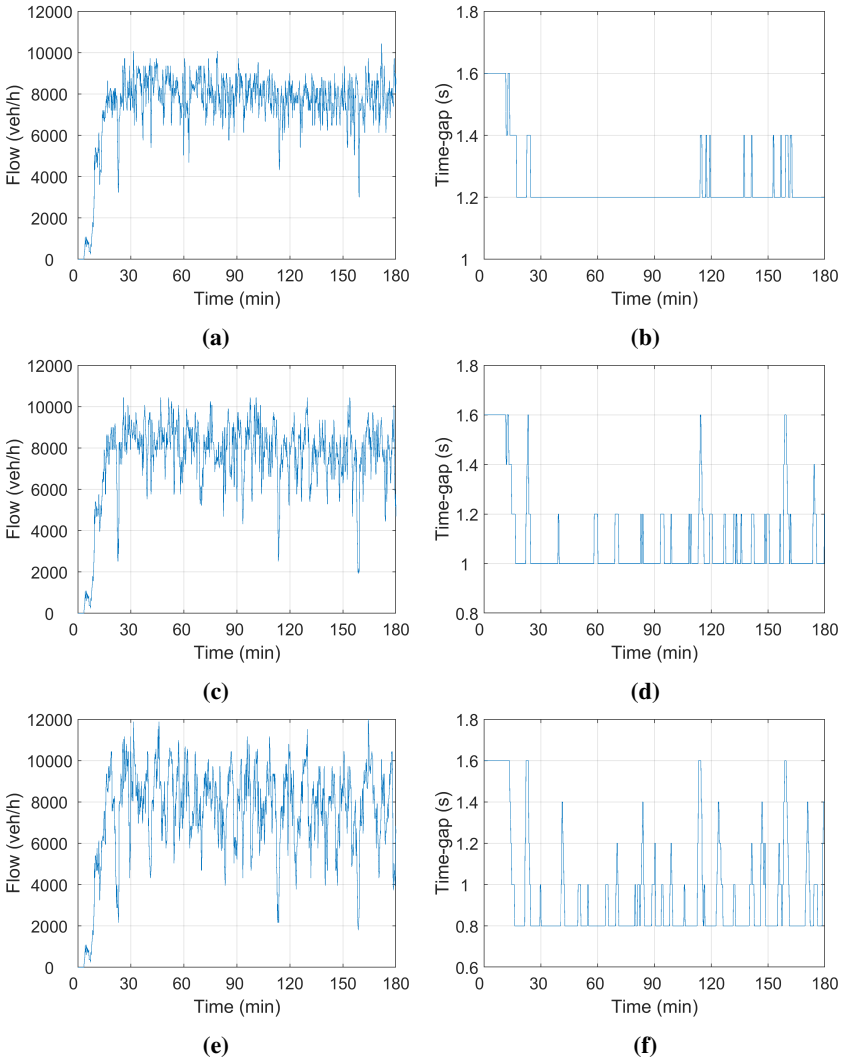

Figure A.5: ACC – Flow and time-gap values for the control case with Full RSU coverage and $T_{min} = 1.2$ sec (a), (b), $T_{min} = 1.0$ sec (c),(d) and $T_{min} = 0.8$ sec (e),(f) for the 30-45-25 CV-CCV-AV configuration at the bottleneck area (segment 31).

A.3 Flow, speed, density trajectories and fundamental diagrams for the Greek test-bed

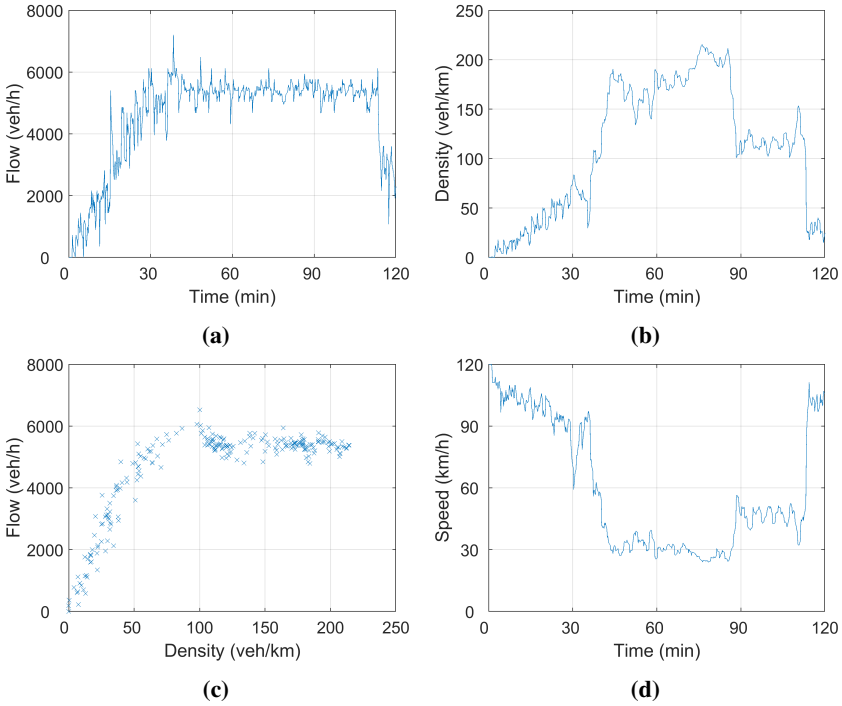

Figure A.6: ACC – Scenario 1: Flow (a), density (b), FD (c) and speed (d) values for the eastbound direction and for 100% CAVs at the bottleneck area.

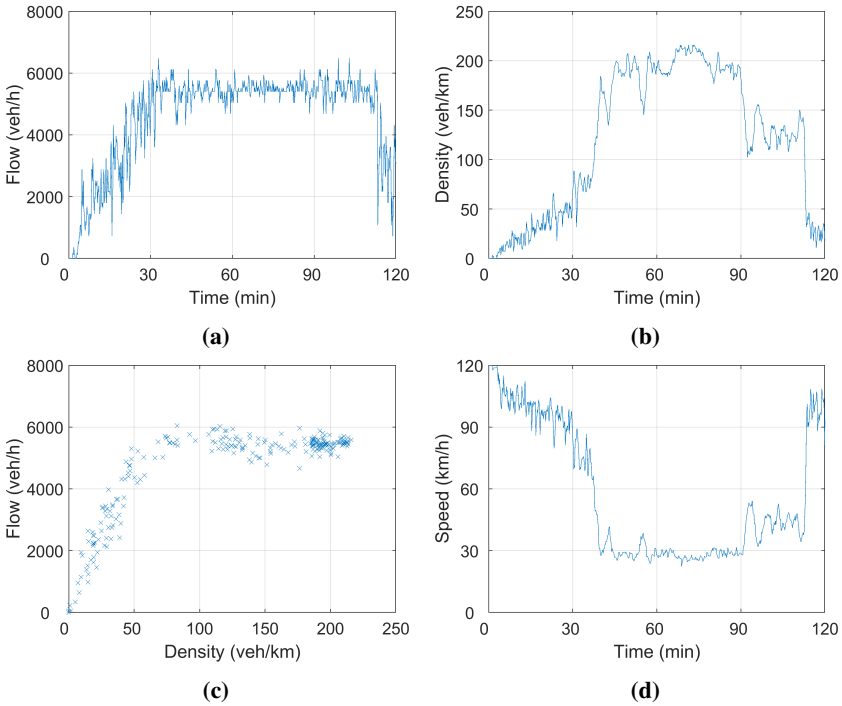

Figure A.7: ACC – Scenario 1: Flow (a), density (b), FD (c) and speed (d) values for the westbound direction and for 100% CAVs at the bottleneck area.

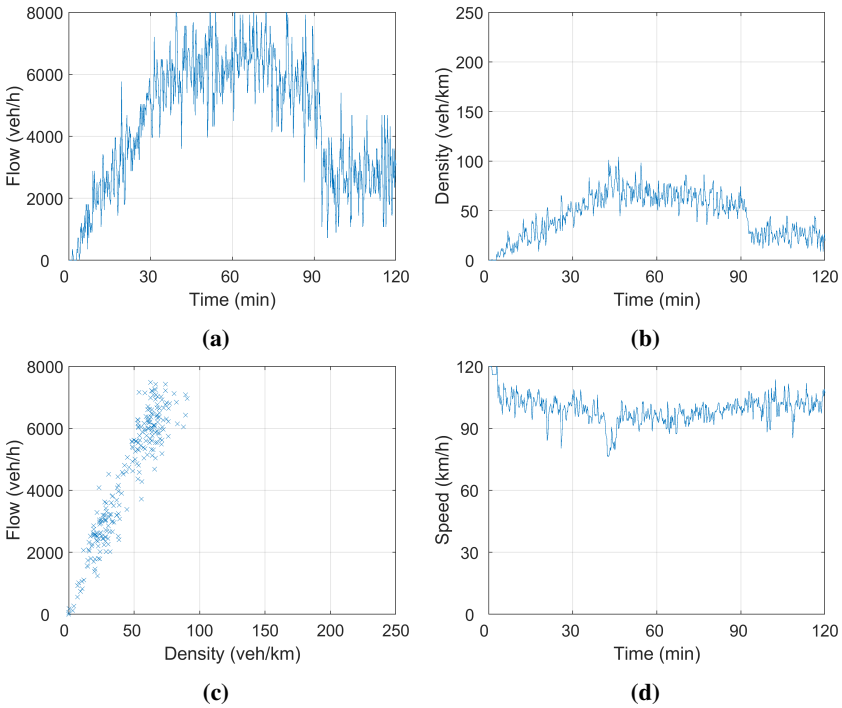

Figure A.8: ACC – Scenario 2: Flow (a), density (b), FD (c) and speed (d) values for the eastbound direction and for 80% CAVs at the bottleneck area.

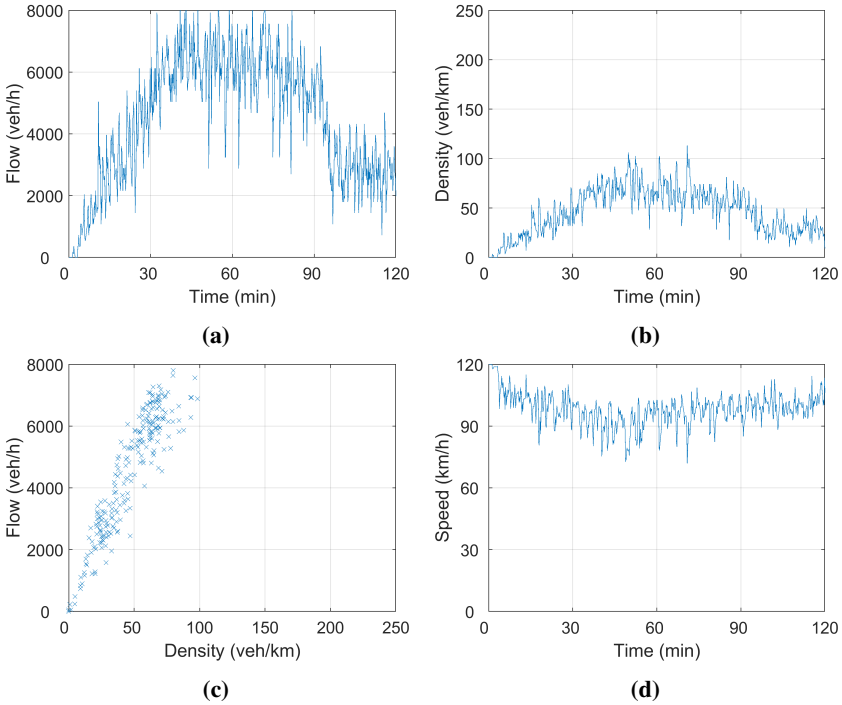

Figure A.9: ACC – Scenario 2: Flow (a), density (b), FD (c) and speed (d) values for the westbound direction and for 80% CAVs at the bottleneck area.

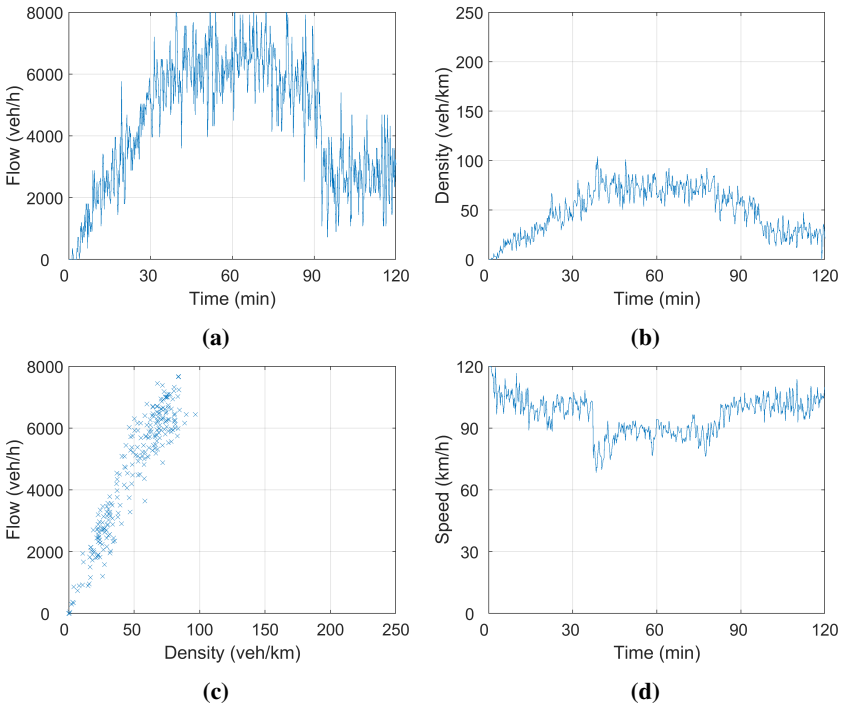

Figure A.10: ACC – Scenario 3: Flow (a), density (b), FD (c) and speed (d) values for the eastbound direction and for 100% CAVs at the bottleneck area.

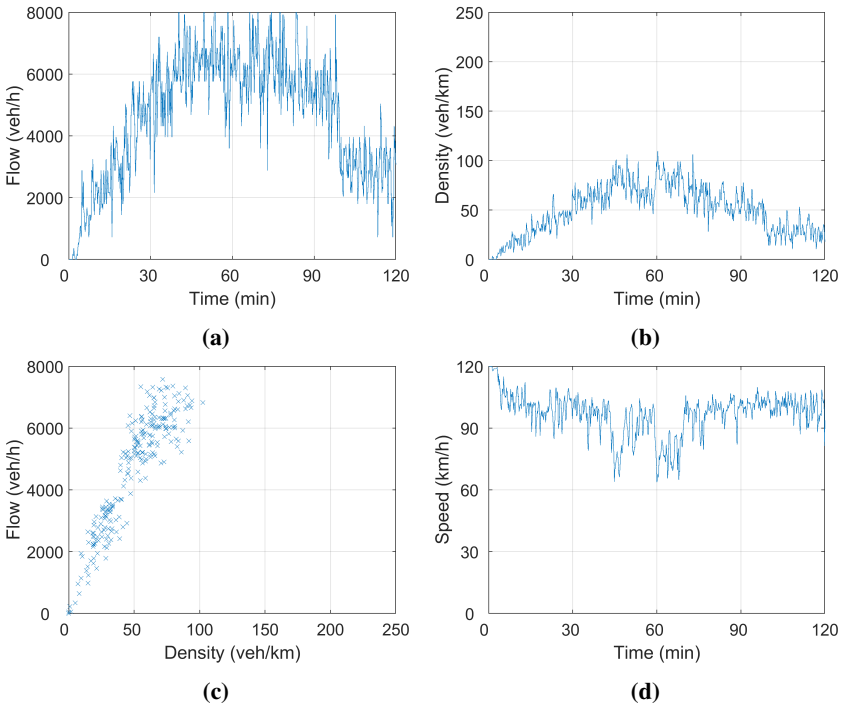

Figure A.11: ACC – Scenario 3: Flow (a), density (b), FD (c) and speed (d) values for the westbound direction and for 100% CAVs at the bottleneck area.

A.4 Time-gap values in relation to flow values for the Greek test-bed

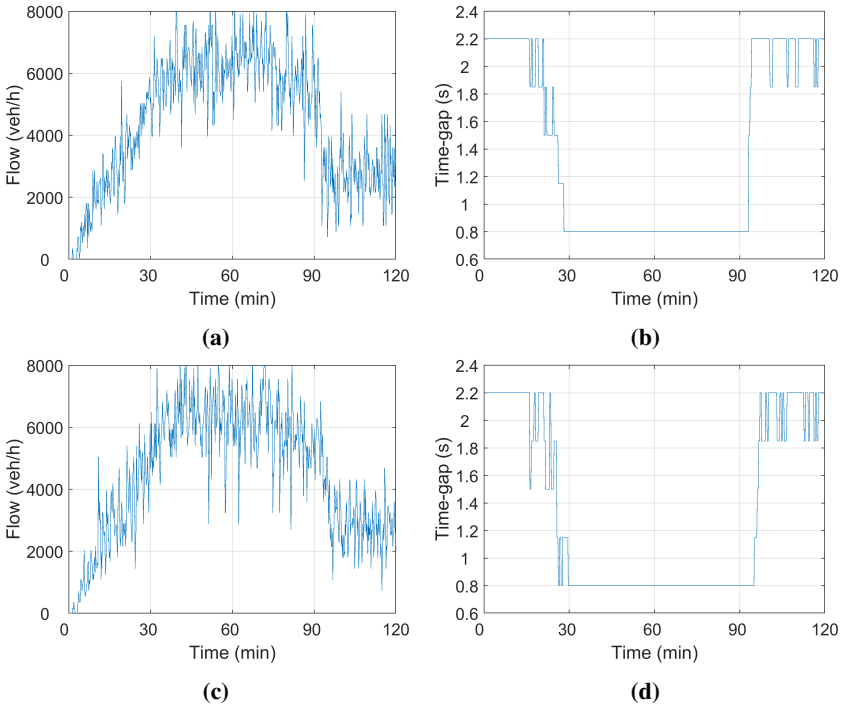

Figure A.12: ACC – Scenario 2: Flow and time-gap values for 80% CAVs for the eastbound (a), (b) and westbound (c), (d) direction at the bottleneck.

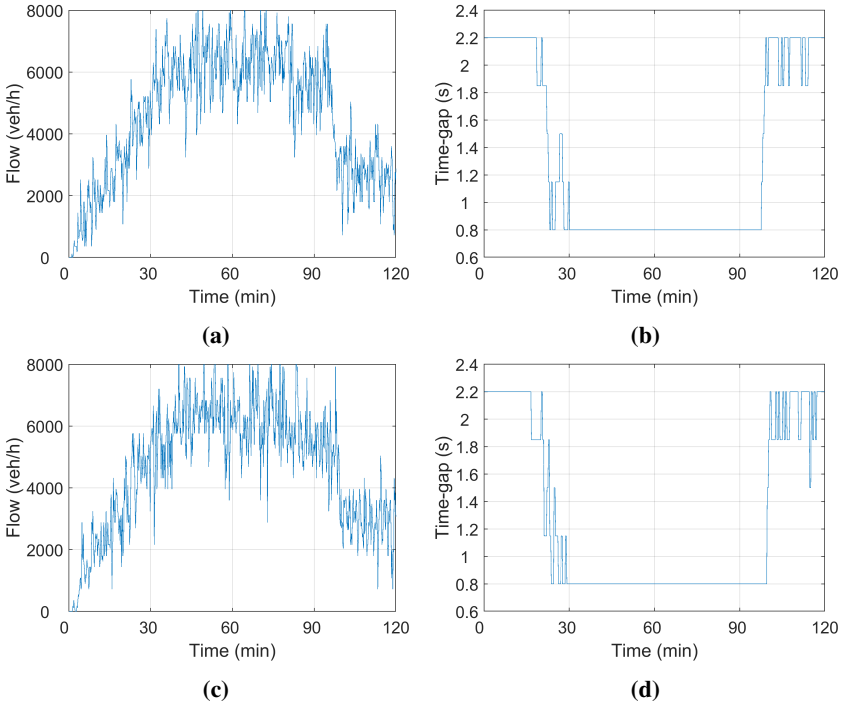

Figure A.13: ACC – Scenario 3: Flow and time-gap values for 100% CAVs for the eastbound (a), (b) and westbound (c), (d) direction at the bottleneck.

Appendix B

MTFC concept: Additional figures related to the results

B.1 Density and speed measurements for the Greek test-bed

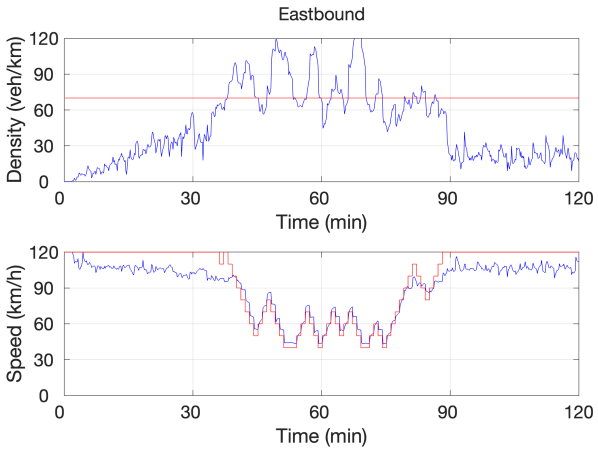

Figure B.1: MTFC – VSLs communicated to 80% of CAVs for the eastbound direction – Density (blue line) at the lane-drop area with the corresponding critical density (red line) (a); and measured speed (blue line) at the MTFC application area with the corresponding speed limits (red line) (b).

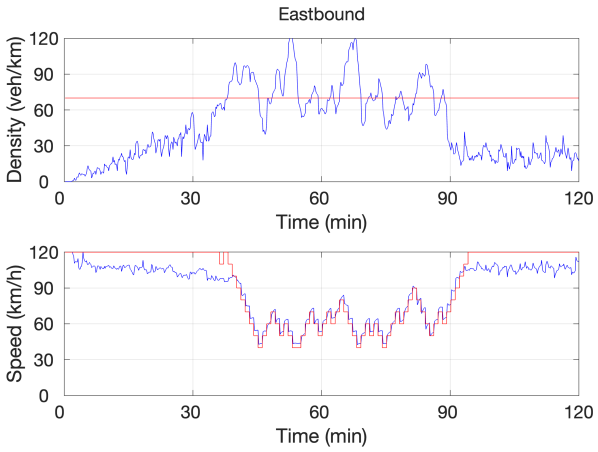

Figure B.2: MTFC – VSLs communicated to 100% of CAVs for the eastbound direction – Density (blue line) at the lane-drop area with the corresponding critical density (red line) (a); and measured speed (blue line) at the MTFC application area with the corresponding speed limits (red line) (b).

Appendix C

LCA concept: Additional figures related to the results

C.1 Speed plots for the eastbound direction of the Greek test-bed

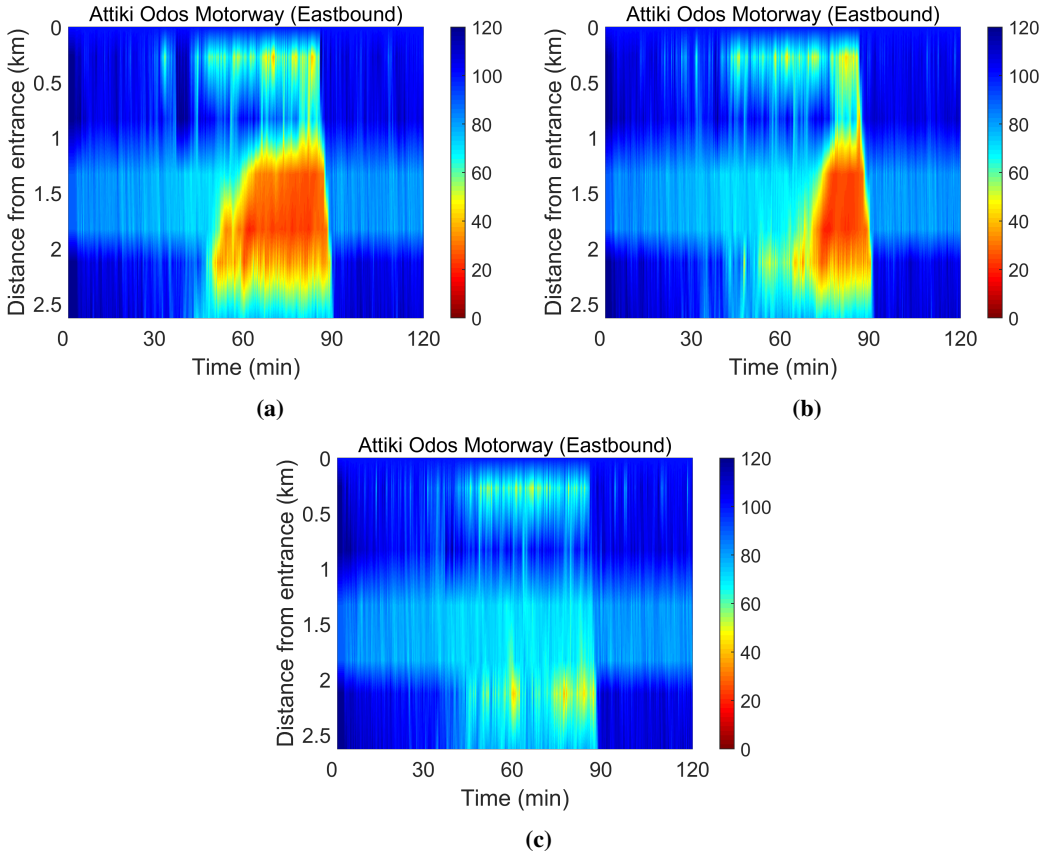

Figure C.1: LCA – Speed contour plots for the eastbound direction and for 20% of CAVs (a), 60% of CAVs (b) and 100% of CAVs (c).

C.2 Speed plots for the westbound direction of the Greek test-bed

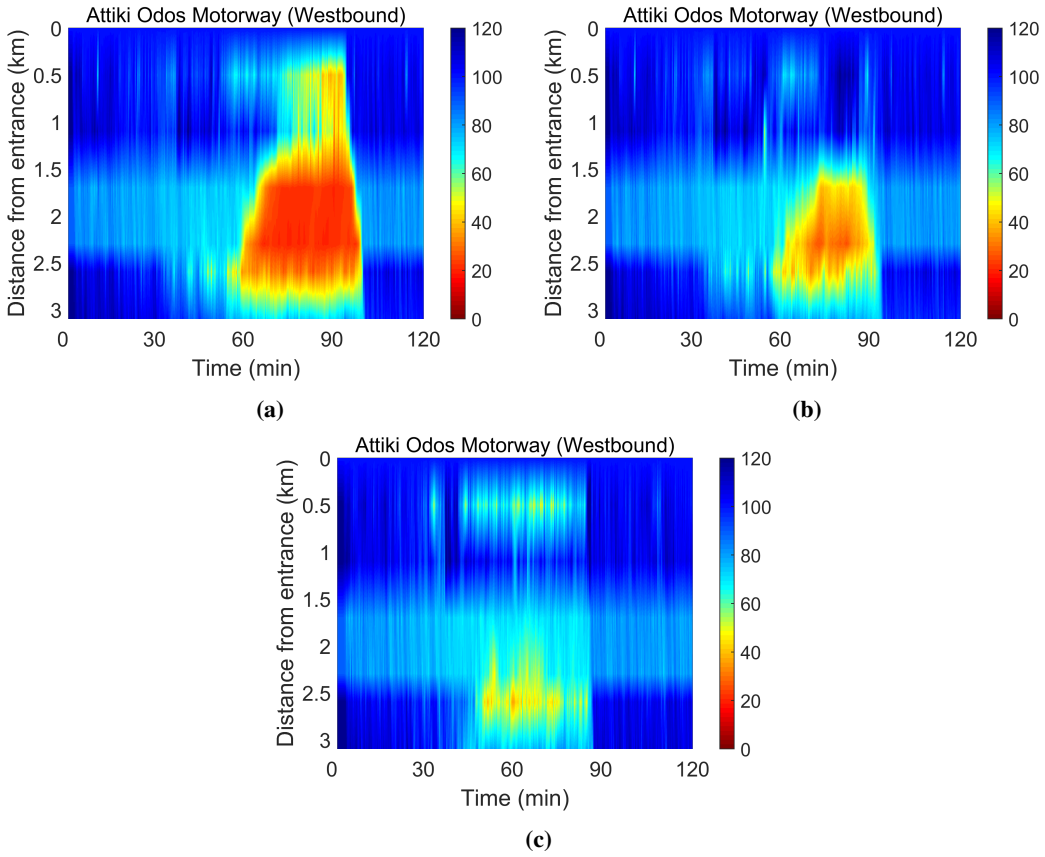

Figure C.2: LCA – Speed contour plots for the westbound direction and for 20% of CAVs (a), 60% of CAVs (b) and 100% of CAVs (c).

Appendix D

Integrated concept: Additional figures related to the results

D.1 Speed plots for the eastbound direction of the Greek test-bed

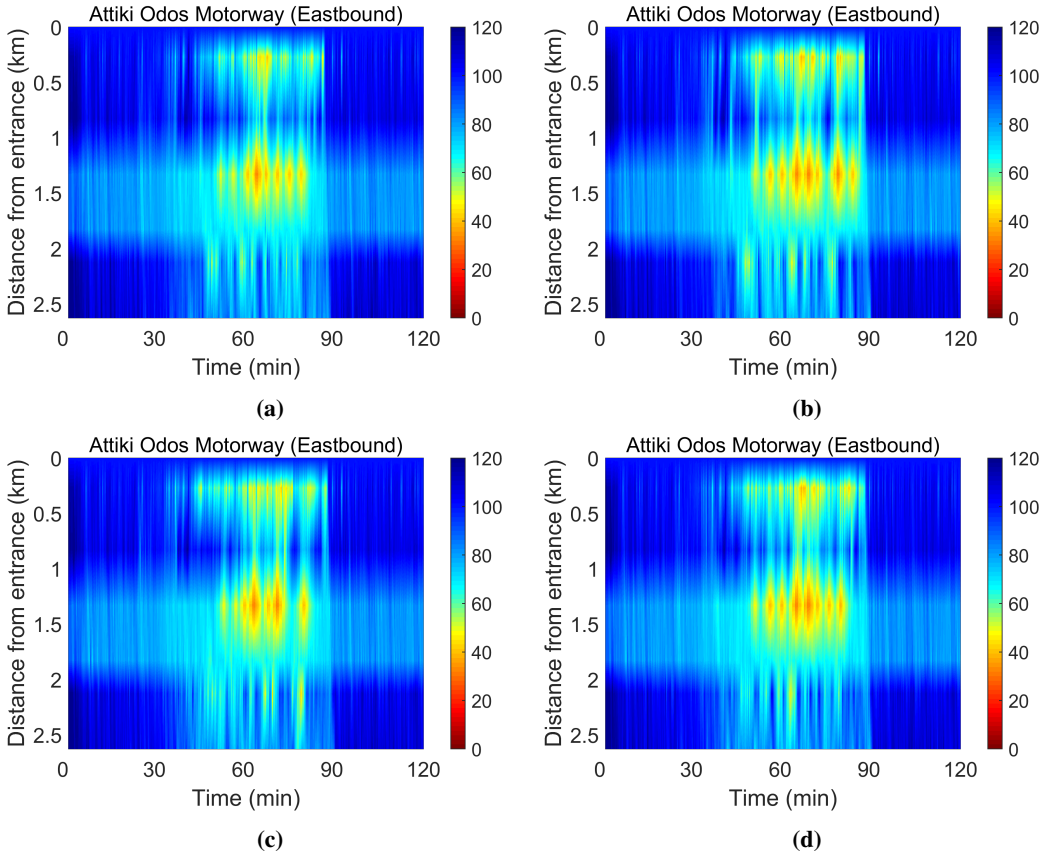

Figure D.1: Integrated – Speed contour plots for the eastbound direction and for 40% of CAVs (a), 60% of CAVs (b), 80% of CAVs (c) and 100% of CAVs (d).

D.2 Density and speed measurements for the eastbound direction of the Greek test-bed

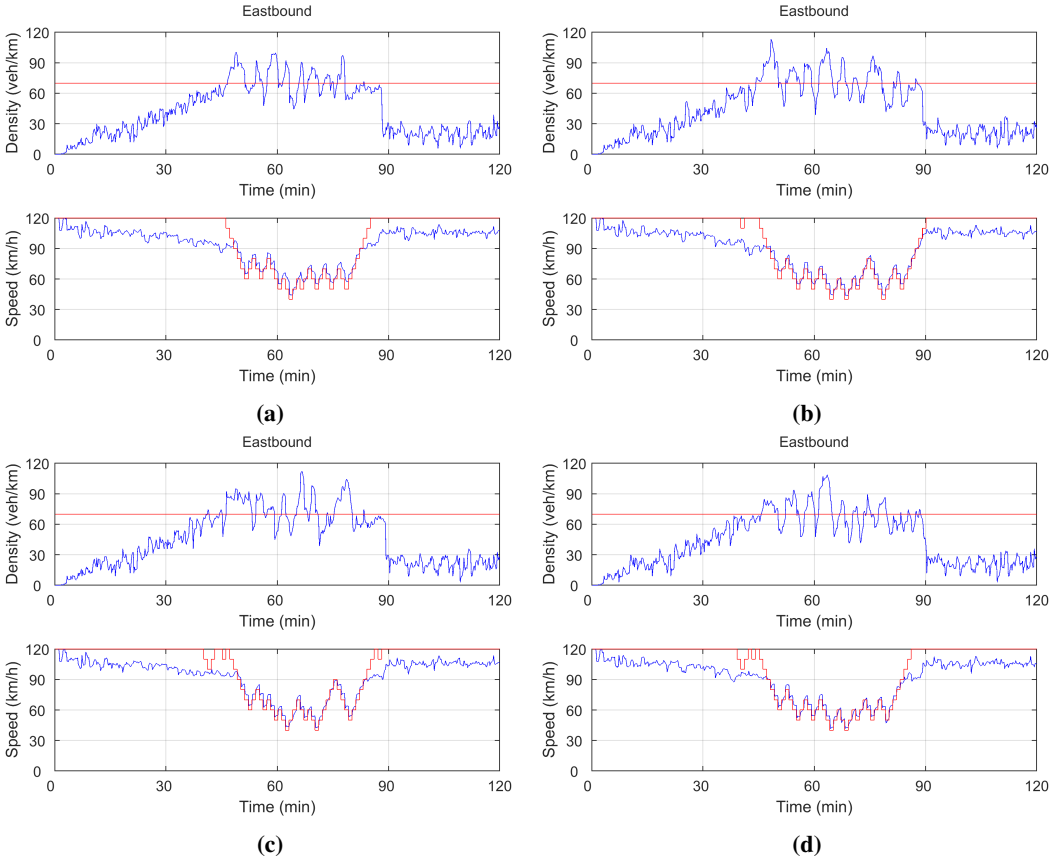

Figure D.2: Integrated – VSLs communicated to 40% of CAVs (a), 60% of CAVs (b), 80% of CAVs (c) and 100% of CAVs (d) for the eastbound direction – Density (blue line) at the lane-drop area with the corresponding critical density (red line) and measured speed (blue line) at the MTFC application area with the corresponding speed limits (red line)

Appendix E

MTFC, LCA and Integrated concept comparison of the average TTS and TD values

E.1 Tables for TTS and TD

Table E.1: Total Delay per penetration rate of CAVs for the no-control case and control cases

Total Delay (sec/km)				
PR (%)	No Control	MTFC	LCA	Integrated
0	22.6	22.6	22.6	22.6
20	22.6	20.6	21.6	17.4
40	22.6	19.2	20.0	17.1
60	22.6	19.0	18.7	17.3
80	22.6	18.3	18.1	17.3
100	22.6	18.4	18.1	17.3

Table E.2: Total Time Spent per penetration rate of CAVs for the no-control case and control cases

Total Time Spent (veh·h)				
PR (%)	No Control	MTFC	LCA	Integrated
0	2225.5	2225.5	2225.5	2225.5
20	2225.5	2144.0	2167.8	2048.2
40	2225.5	2098.1	2098.0	2025.2
60	2225.5	2109.5	2042.0	2018.6
80	2225.5	2095.5	2019.6	2008.5
100	2225.5	2117.5	2018.2	1997.7

E.2 Average values of TTS and TD along with min-max bars

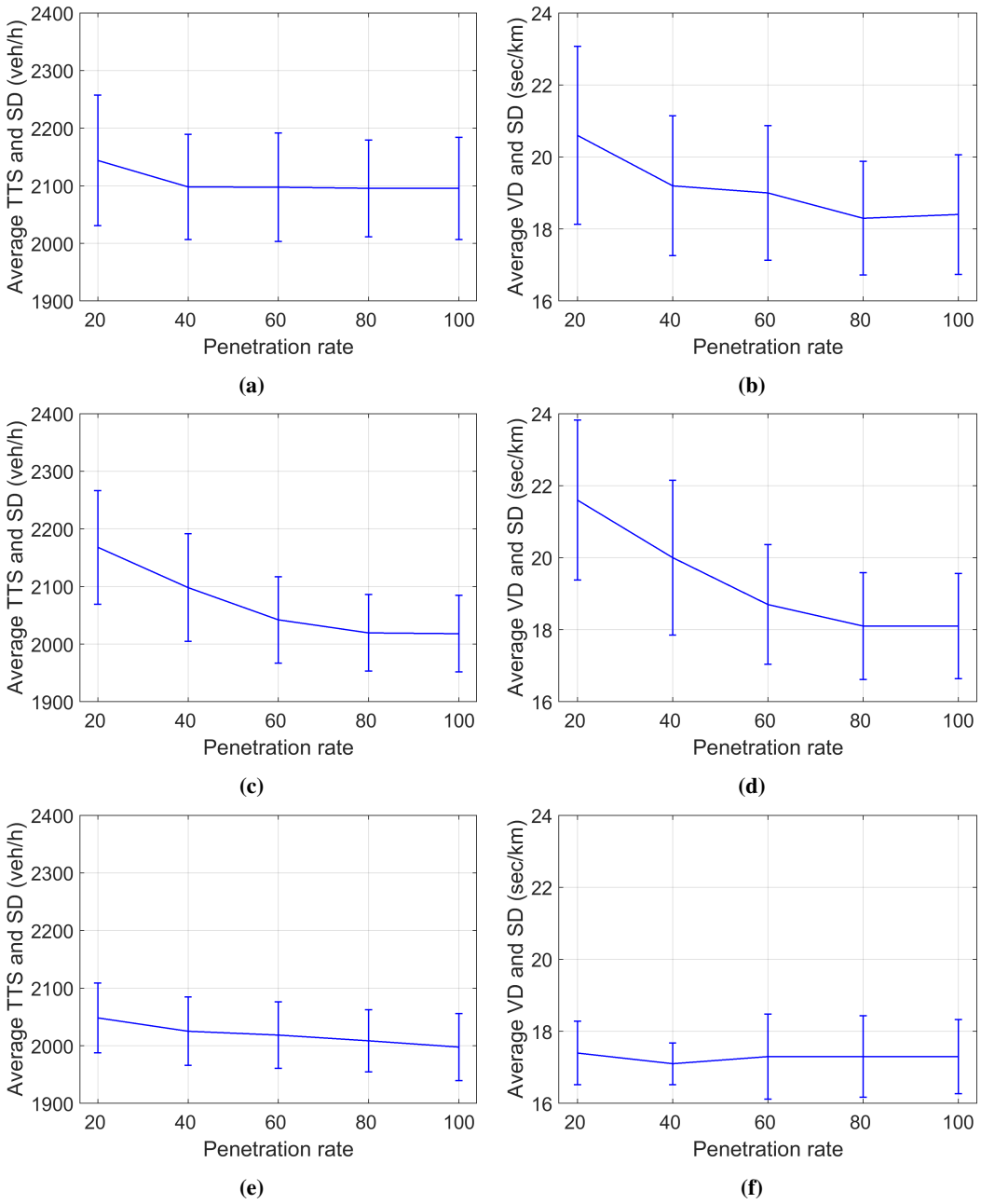

Figure E.1: Average TTS, TD and min-max bars for all penetration rates investigated for the MTFC concept (a), (b), for the LCA concept (c), (d) and for the Integrated concept (e), (f).

Appendix F

Network level optimization: Additional figures related to the results

F.1 Flow, speed, density and fundamental diagrams for the Greek test-bed

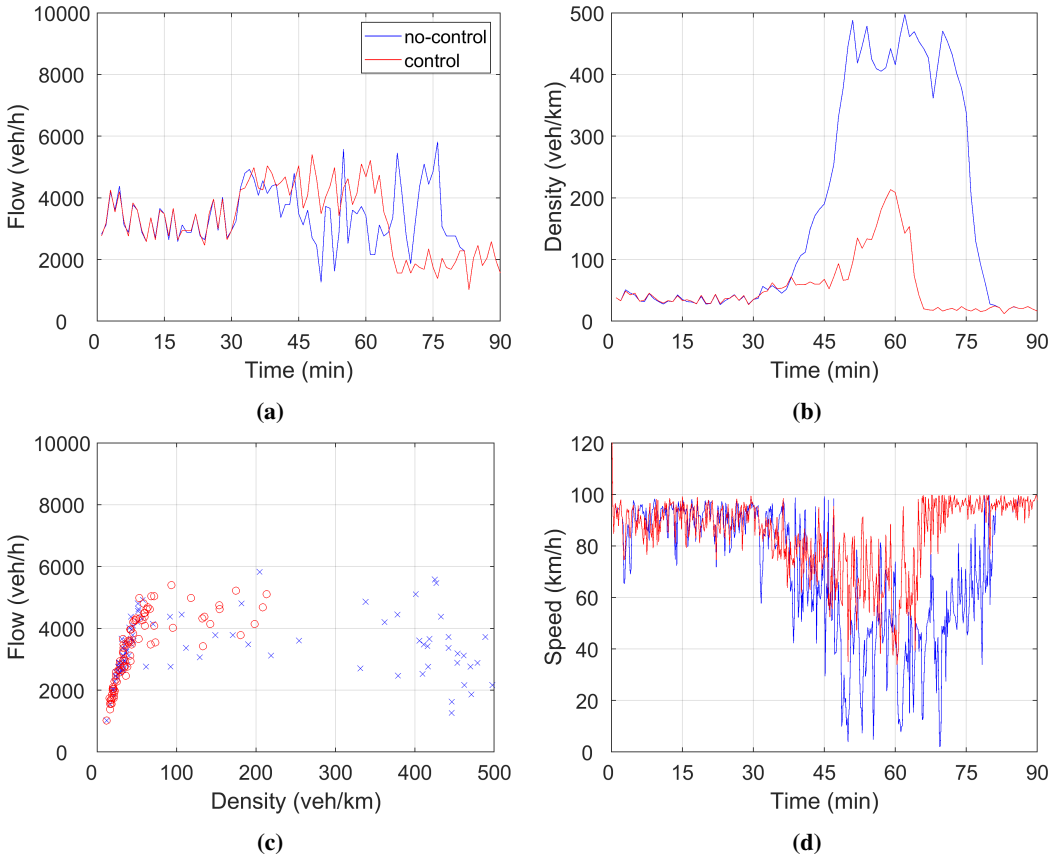

Figure F.1: Flow (a), density (b), FD (c) and speed (d) measurements for the no-control (blue line) and control (red line) scenario for 20% of CAVs at segment 7.

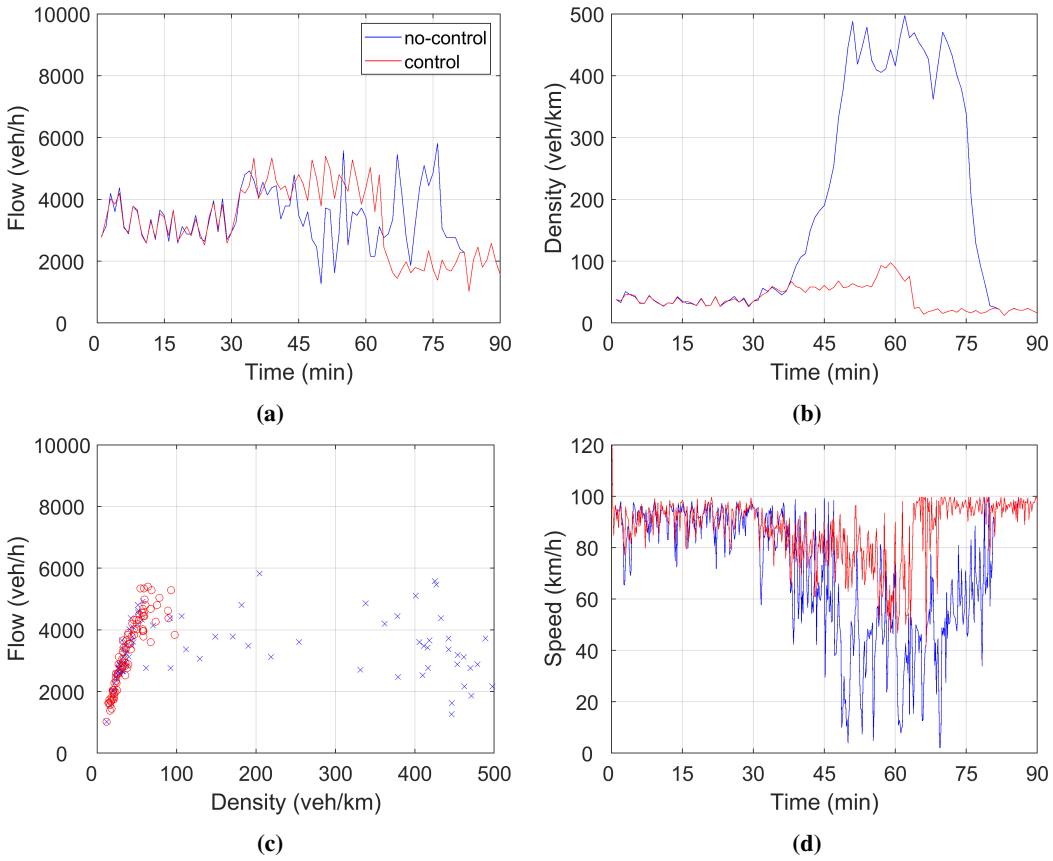

Figure F.2: Flow (a), density (b), FD (c) and speed (d) measurements for the no-control (blue line) and control (red line) scenario for 50% of CAVs at segment 7.

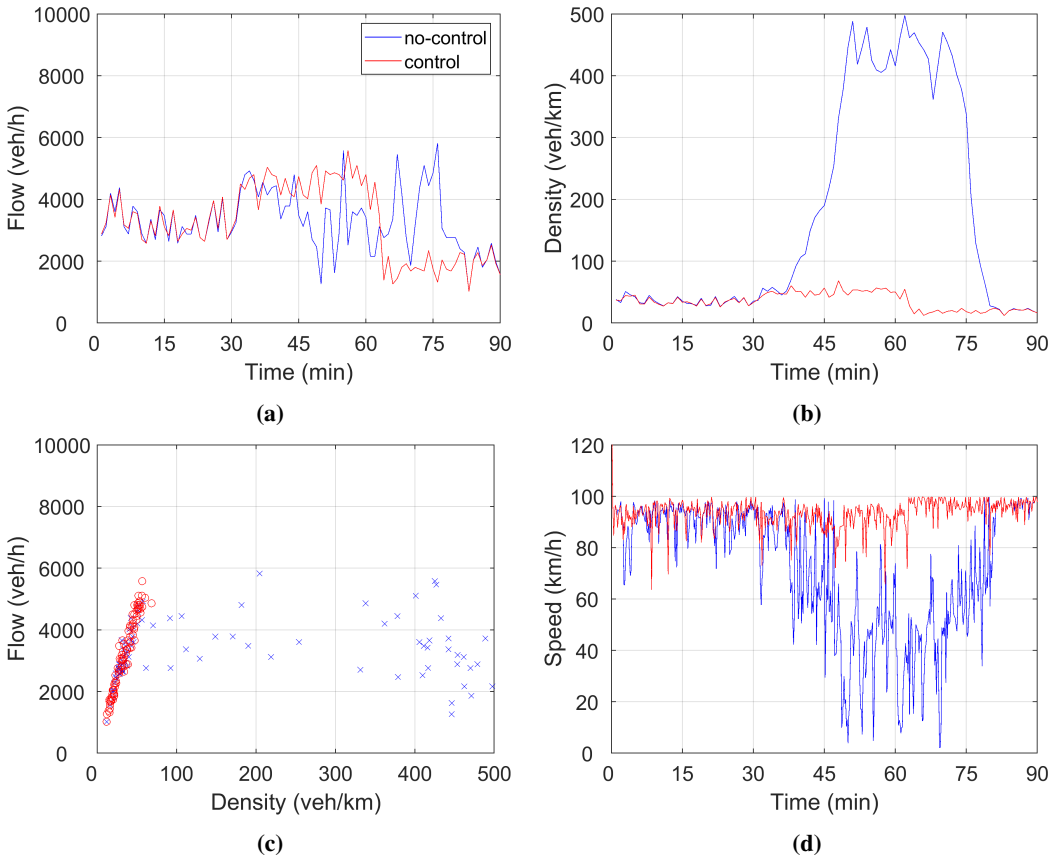

Figure F.3: Flow (a), density (b), FD (c) and speed (d) measurements for the no-control (blue line) and control (red line) scenario for 100% of CAVs at segment 7.